Natural Resources Canada | Ressources naturelles Canada

GEOLOGICAL SURVEY OF CANADA
OPEN FILE 7791

Targeted Geoscience Initiative 4: unconformity-related uranium systems

E.G. Potter and D.M. Wright (ed.)

2015

Canada

GEOLOGICAL SURVEY OF CANADA
OPEN FILE 7791

Targeted Geoscience Initiative 4: unconformity-related uranium systems

E.G. Potter[1] and D.M. Wright[2] (ed.)

[1] Geological Survey of Canada, 601 Booth Street, Ottawa, Ontario
[2] Peridot Geoscience Ltd., 19 Rein Terrace, Kanata, Ontario

2015

© Her Majesty the Queen in Right of Canada, as represented by the Minister of Natural Resources Canada, 2015

doi:10.4095/295776

This publication is available for free download through GEOSCAN (http://geoscan.nrcan.gc.ca/).

Recommended citation
Potter, E.G., and Wright, D.M. (ed.), 2015. Targeted Geoscience Initiative 4: unconformity-related uranium systems; Geological Survey of Canada, Open File 7791, 126 p. doi:10.4095/295776

Publications in this series have not been edited; they are released as submitted by the author.

Targeted Geoscience Initiative 4: unconformity-related uranium systems

Edited by
Eric G. Potter and Donald M. Wright

TGI-4 Unconformity-related Uranium Deposits Synthesis: Tools to Aid Deep Exploration and Refine the Genetic Model

Eric G. Potter[1] and Donald M. Wright[2]

1. Geological Survey of Canada, 601 Booth Street, Ottawa, Ontario, K1A 0E8, epotter@NRCan.gc.ca

2. Peridot Geoscience Ltd., 19 Rein Terrace, Kanata, Ontario, K2M 2A9

Abstract

This report summarizes the key activities completed under the uranium ore systems project of the Targeted Geoscience Initiative Four (TGI-4) program operated by the Geological Survey of Canada. This collaborative project between government, academia and industry examined unconformity-related uranium systems in the Proterozoic Athabasca (Phoenix, Millennium and McArthur River deposits and Dufferin Lake zone), Thelon (Bong deposit) and Otish (Camie River deposit) basins in order to refine genetic models and exploration techniques for the deposits. Significant to the Canadian economy, high-grade unconformity-related uranium deposits remain prime exploration targets given their potential for large tonnage, high-grade ore. As the depths of discoveries increase in the established Athabasca Basin and geological settings hosting the ore diversify, a variety of new exploration methods are required to allow for efficient target identification and successful discovery of deeply buried ore deposits. The results of the project clearly illustrate that deeply buried ore, ore-forming fluids, structural-fluid controls and precipitation mechanisms produce diagnostic signatures that can be identified and modelled over the entire fluid pathway through fertile fault systems, including post-mineralization dispersal of elements into subsurface and surficial environments.

Introduction

The Targeted Geoscience Initiative (TGI-4) uranium ore systems project has been a five-year collaborative federal geoscience program focussed on providing industry with the next generation of geoscience knowledge and innovative techniques, to guide more effective targeting of deeply-buried uranium deposits. Building on the successful EXTECH IV program (Jefferson et al., 2007a), TGI-4 was tasked with addressing industry interest in refining uranium exploration tools and techniques in light of renewed uranium exploration at depth and technological advancements. Specifically, the hypothesis explored under the TGI-4 project is that the properties of the ore, ore-forming fluids, structural controls and precipitation mechanisms produce diagnostic signatures that can be identified and modelled over the entire fluid pathway through fertile fault systems, including dispersal of exotic radionuclides into subsurface and surficial environments. In order to refine methods of defining these signatures, TGI-4 activities focussed on geochemistry, fluid flow-structural modelling and genetic studies using several deposits in concert to develop a system-wide understanding of the basement-to-surface expressions of deep mineralization, and to refine critical factors favourable for the genesis of the unconformity-related uranium deposits.

Uranium in Canada

Uranium continues to rank amongst Canada's top 10 metal commodities. The nuclear energy industry is an integral part of the Canadian economy, with the mining, refining and electrical energy production components supporting more than 60, 000 direct and indirect full-time jobs (Calvert, 2013; Canadian Nuclear Assoc., 2013). All of Canada's current (2014) uranium production, which in 2013 accounted for about 16 % of the world production (World Nuclear Assoc., 2014), is from three high-grade deposits located in the eastern Athabasca Basin of Saskatchewan: Cigar Lake, Eagle Point and McArthur River. Despite containing the world's highest grade deposits and contributing significantly to the Canadian economy, Canadian resources currently account for only 8% of known recoverable resources of uranium globally (in the <130USD/kg U cost category; OECD, 2014). Nevertheless these high-grade unconformity-related uranium deposits remain prime exploration targets globally given the continued trend toward lower grades and higher production costs. A recent global synthesis of uranium resources noted significant decreases in identified and reasonably assured resources within the <80 USD /kg U cost category (36.4% and 39.9%, respectively). Furthermore, inferred resources were reduced by 6.1% in the <40USD /kg U cost category and 30% in the <80USD /kg U cost category. With their high-grade ore, existing infrastructure and modern mining methods, Athabasca Basin uranium resources comprise 47% of the global <40USD /kg U cost category (OECD, 2014).

One of several Proterozoic basins prospective for uranium in Canada (Fig. 1), the Athabasca Basin covers more than 85,000 km^2, but approximately 96% of its known uranium resources are located along a limited corridor near the shallow, eastern margin of the basin (Jefferson et al., 2007a). Situated along this trend, the McArthur River and Cigar Lake deposits represent the last of the 'first generation' of deposits mined in the basin. These deposits were discovered using the classic Rabbit Lake unconformity-related model of Hoeve and Sibbald (1978). However, exploration in recent years has discovered deposits in deeper areas of the basin and in different geological settings, such as the basement-hosted Patterson Lake South deposit located south of the basin (50–250 m below the surface; Armitage, 2013; Fisson Uranium Corp., 2015), Eagle Point mine (100–300 m below the surface in basement rocks; Lemaitre 2006; Cloutier et al., 2011), Millennium deposit (650–750 m below surface; Roy et al., 2005; Cloutier et al., 2009) and the non-graphitic con-

Potter, E.G., and Wright, D.M., 2015. TGI-4 Unconformity-related Uranium Deposits Synthesis: Tools to Aid Deep Exploration and Refine the Genetic Model, *in* Targeted Geoscience Initiative 4: unconformity-related uranium systems, (ed.) E.G. Potter and D.M. Wright; Geological Survey of Canada, Open File 7791, p. 1–13. doi:10.4095/295776

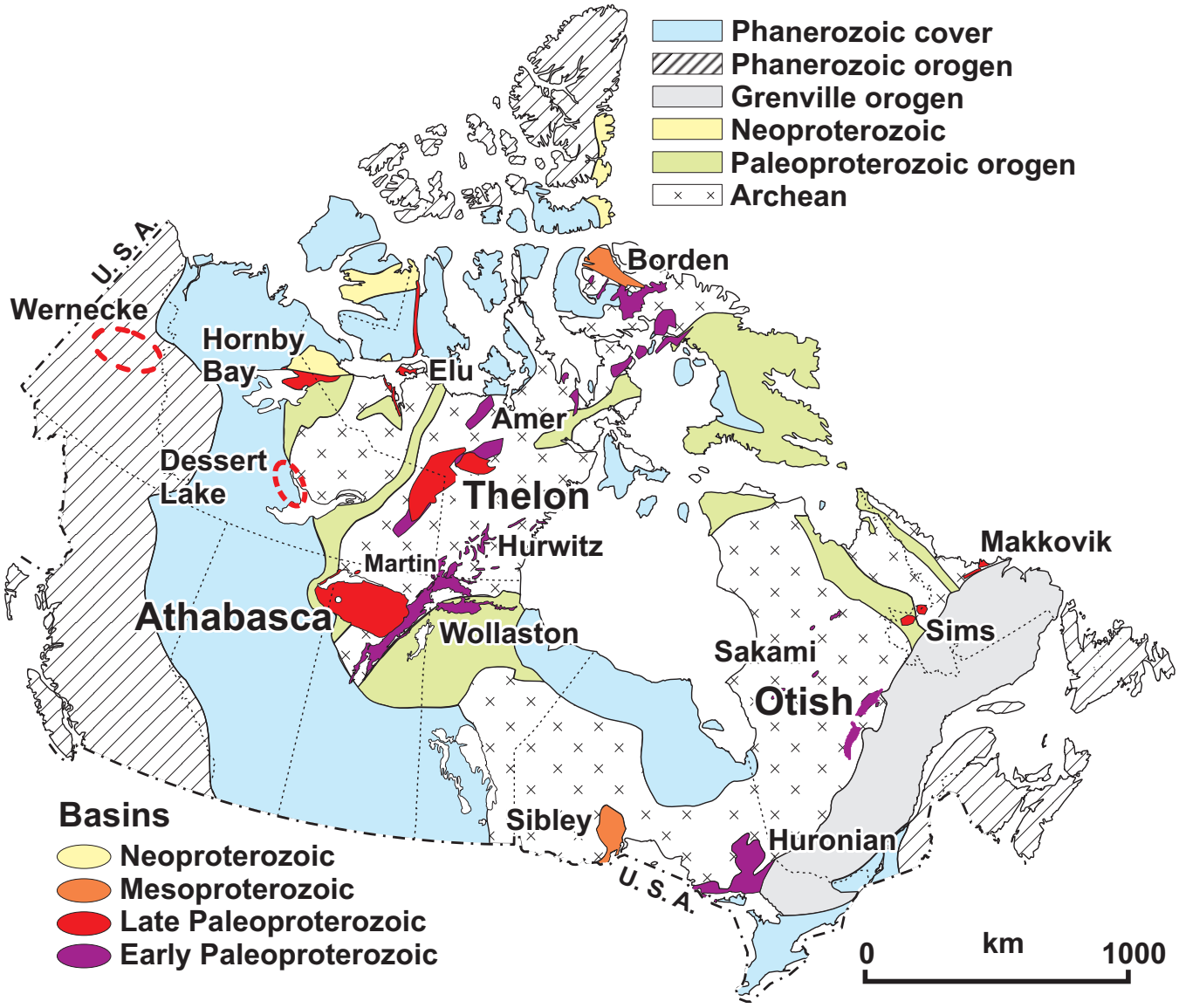

Figure 1. Known Proterozoic basins and sedimentary sequences in Canada, after Jefferson et al., (2007a).

ductor associated Centennial deposit (800–830 m below present-day surface; Jiricka, 2010; Alexandre et al., 2012; Reid et al., 2014). The basement-hosted systems can also extend up to 400 m below the unconformity along structures (Thomas et al., 1998). Additional Proterozoic basins in Canada with known uranium deposits include the: Thelon, Otish, Martin, Hornby Bay and Huronian. Prospective Proterozoic basins with potential to host uranium occurrences include: Sibley, Borden, Aston, Elu, and Dessert Lake. As the depths of discoveries increase and geological settings diversify, a variety of new exploration methods are required to allow for efficient target identification and successful discovery of deeply buried deposits. Furthermore, discovery of significant basement-hosted mineralization as an end-member of the unconformity-related systems has expanded the exploration potential beyond the present basin limits (e.g. Patterson Lake South). These basement-hosted deposits are challenging exploration targets because the diagnostic low temperature clay alteration is superimposed on metamorphic basement-rocks and is much smaller in size than that of the deposits hosted right at the unconformity or perched in the sandstone (Alexandre et al., 2005; Jefferson et al., 2007a). This volume summarizes research activities completed under the TGI-4 unconformity-related uranium systems project that focussed on deposits located in the Athabasca, Thelon and Otish Basins of northern Saskatchewan, Nunavut and Quebec, respectively, to develop a system-wide understanding of the basement to surface expressions of deep mineralization and refinement of critical factors leading to the genesis of the unconformity-related uranium deposits.

Unconformity-related uranium deposits: important characteristics

Unconformity-related uranium deposits contain high-grade uranium ore in pods, veins, breccia zones and semi-massive concentrations above, straddling or below the

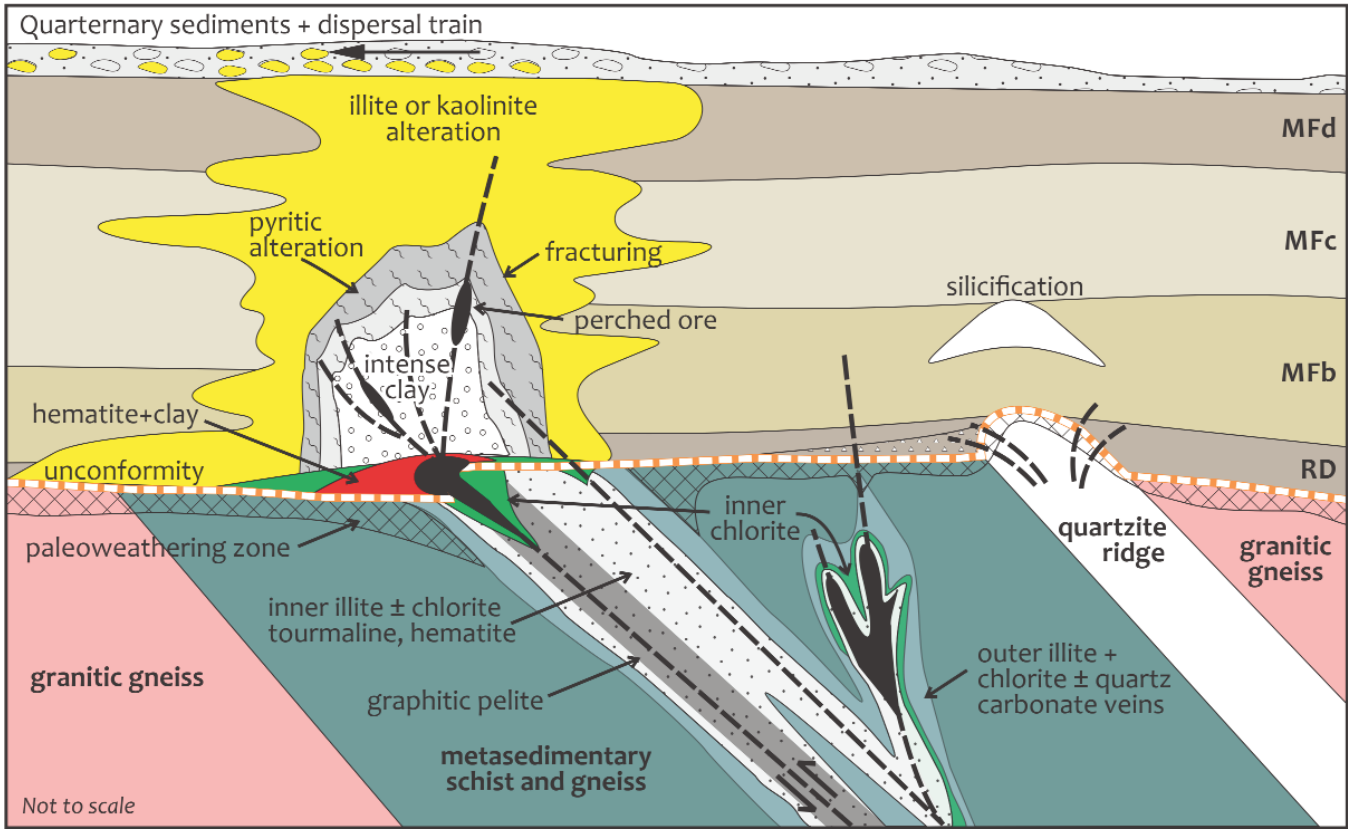

Figure 2. Simplified Athabasca Basin unconformity-related uranium deposit models, after Kyser and Cuney (2009) and Jefferson et al., (2007a). Abbreviations: RD = Read Formation, Members of the Manitou Fall Formation: MFb = Bird, MFc = Collins and MFd = Dunlop.

regional unconformity between Proterozoic conglomeratic sandstones and Archean to Paleoproterozoic metamorphosed basement rocks where intersected by reactivated fault systems (Jefferson et al., 2007b; Fig. 2). Alteration halos are characterized by the presence of illite, kaolinite, tourmaline, chlorite, euhedral quartz, and locally, by concentrations of Fe-Ni-Co-As-Cu sulphide minerals (Hoeve and Quirt, 1984; Wallis et al., 1985; Kotzer and Kyser, 1995; Jefferson et al., 2007b; Kyser and Cuney, 2009; Fig. 2). Exploration for these highly economic yet elusive deposits is dependent upon understanding the inter-relationships between: 1) ore fluids; 2) structure; 3) alteration and mineralization chemistry; and 4) the history of these deposits, encompassing pre-, syn-, and post-ore events. The products of these inter-relationships can be explored using a variety of tools (Fig. 3), with TGI-4 focusing on tracking fluid compositions and pathways in time and space through geochemical signatures, mineral assemblages and chemistry, and modelling the relationships between fluid flow and structural pathway development (tectonism and faults).

Fluids

Most conventional genetic models invoke circulation of oxidizing, basinal brines, heated to 160–250°C, reacting with reducing media in, or fluids in or permeating out of, reactivated basement shear zones (Pagel et al., 1980; Kyser et al., 2000; Derome et al., 2005), producing either egress- (dominantly sandstone-hosted) or ingress-type (basement-hosted) deposit end-members depending on the physical position of fluid interaction relative to the unconformity (Jefferson et al., 2007a and references therein). As uranium mobility is largely governed by oxidation state (Grandstaff, 1976; Romberger, 1984), uranium precipitation is inferred to occur in reactivated fault zones where the uranium-bearing, oxidized fluids were reduced. Critical to this model are the characteristics of the fluids, efficiency of metal precipitation and length of time in which the fluids were focussed along key structural intersections.

Fluid compositions

Although debate continues as to the source of the uranium in unconformity-related deposits (c.f. Kyser and Cuney, 2009), uranium transport is generally considered best achieved using warm (160–250°C), oxidized, acidic brine (Jefferson et al., 2007b). Variations on the chemistry of these fluids have been proposed, including multiple brines with differing compositions (NaCl-rich, $CaCl_2$-rich; Kotzer and Kyser, 1995; Kyser et al., 2000; Derome et al., 2005; Richard et al., 2010), halogen contents (Fayek and Kyser, 1997), gas contents (CO_2, CH_4, H_2S; Derome et al., 2003) and pH (weakly to highly acidic, i.e. pH = 5 or 2.5–4.5; Kotzer and Kyser, 1995; Richard et al. 2012; Sharpe, 2013).

From the Dufferin Lake zone, Pascal et al. (2015; Fig. 4) document the presence of CH_4- and N_2-rich fluids in fluid inclusions within quartz veins from graphitic pelitic schists, which support interaction of multiple fluids with the base-

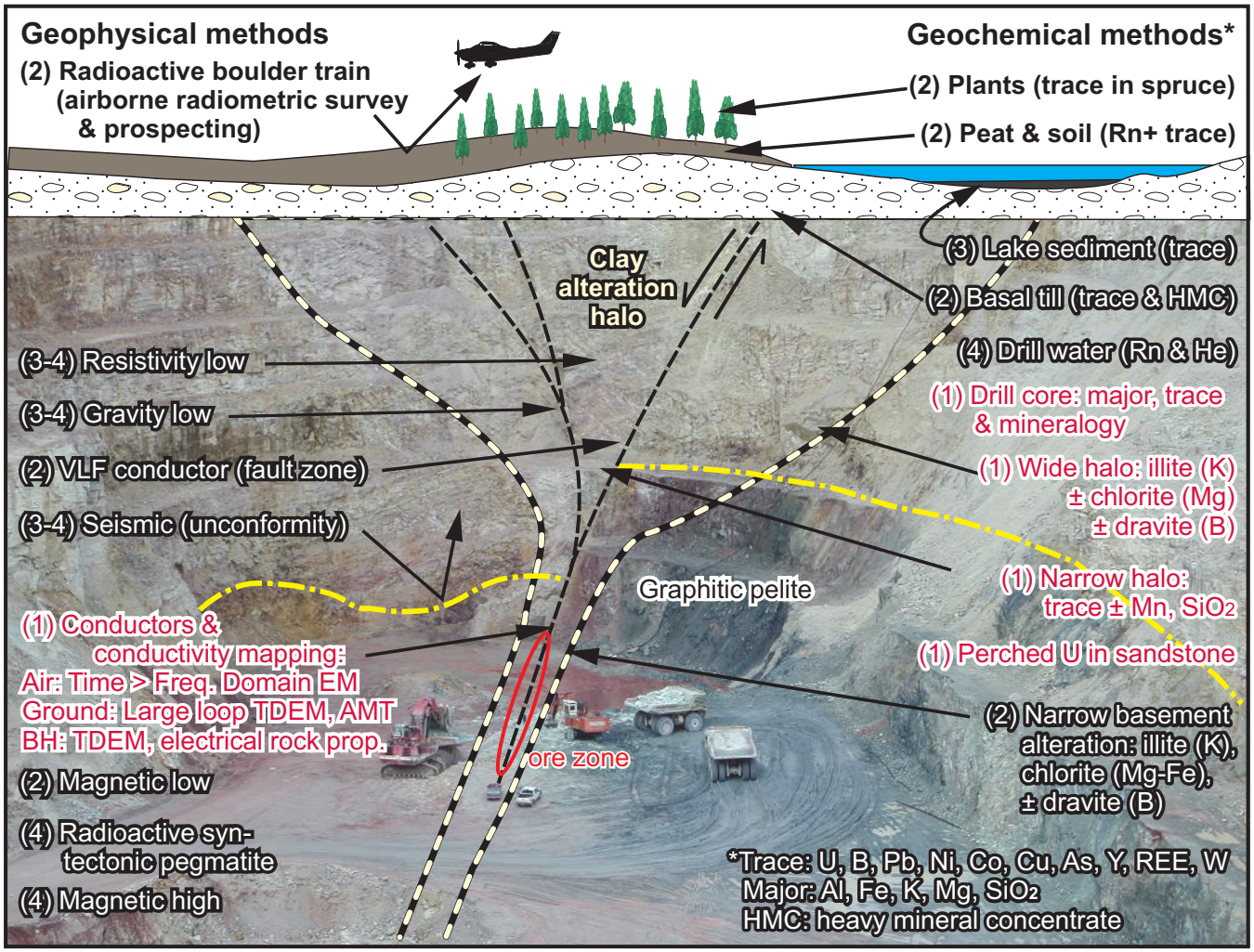

Figure 3. Synopsis of tools for exploration of unconformity-related deposits, divided by geochemical and geophysical techniques and ranked in order of importance (numbers in brackets). Modified from Jefferson et al. (2007b) and Tourigny et al. (2002, 2007). Photograph of Sue C Pit by C.W. Jefferson, 2002, courtesy of AREVA Resources Canada.

ment rocks underlying the mineralization. As proposed by the authors, retrograde metamorphism and diagenetic processes are the dominant processes that led to graphite depletion. During retrograde metamorphism, methane (CH_4) can be generated by the breakdown of graphite during hydration reactions and/or cooling of C-O-H fluids (Huizenga, 2010; Annesley and Wheatley, 2011; Card and Annesley, 2012), and N_2 by the breakdown of micas and feldspar (Duit et al., 1986; Bebout et al., 1999; Hurai et al., 2000; Sadofsky and Bebout, 2000). In the altered paleoregolith (Fig. 3) that is depleted in graphite at the Dufferin Lake zone, evidence of both NaCl- and $CaCl_2$-rich brines has been identified similar to the results from Derome et al. (2005) and Richard et al. (2010). By having circulated in the upper part of the basement, where graphite and sulphides are depleted, the $CaCl_2$-rich fluids may have reacted with graphite leading to the formation of methane. If the timing of these reactions was appropriate, the upward migration of gases (and associated fluids) could have reduced hexavalent uranium in oxidized basinal brines above the unconformity.

Fluid reduction mechanisms

In the original unconformity-related uranium model, Hoeve and Sibbald (1978) invoked reaction between graphite and oxidizing diagenetic brines to produce carbon dioxide and methane that reduced hexavalent uranium to the immobile tetravalent state. Alexandre et al. (2005) also proposed direct reduction of U^{6+} by radiolysis of graphite. Graphitic basement rocks, however are not spatially associated with ore at the Raven-Horseshoe, Cluff Lake, Maurice Bay and Centennial deposits in the Athabasca Basin nor at the Nabarlek deposit in the McArthur Basin of Australia (Cloutier et al., 2011; Rhys et al., 2008; Koning and Robbins, 2006; Alexandre et al., 2009; Reid et al., 2014) while at other deposits (e.g. Gartner-Key Lake and Shea Creek), uranium can be more strongly associated with other basement rocks (Yeo and Potter, 2010). This has led to the examination of alternative mechanisms such as: fluid hydrocarbons (Alexandre and Kyser, 2006); generation of H_2S from the breakdown of pyrite (Cheney, 1985; Ruzicka, 1993; Beyer et al., 2012); redox reactions involving Fe^{2+} liberated from pyrite oxidation, chloritization of biotite or illitization of hornblende (Wallis et al., 1985; Alexandre et al., 2005); or

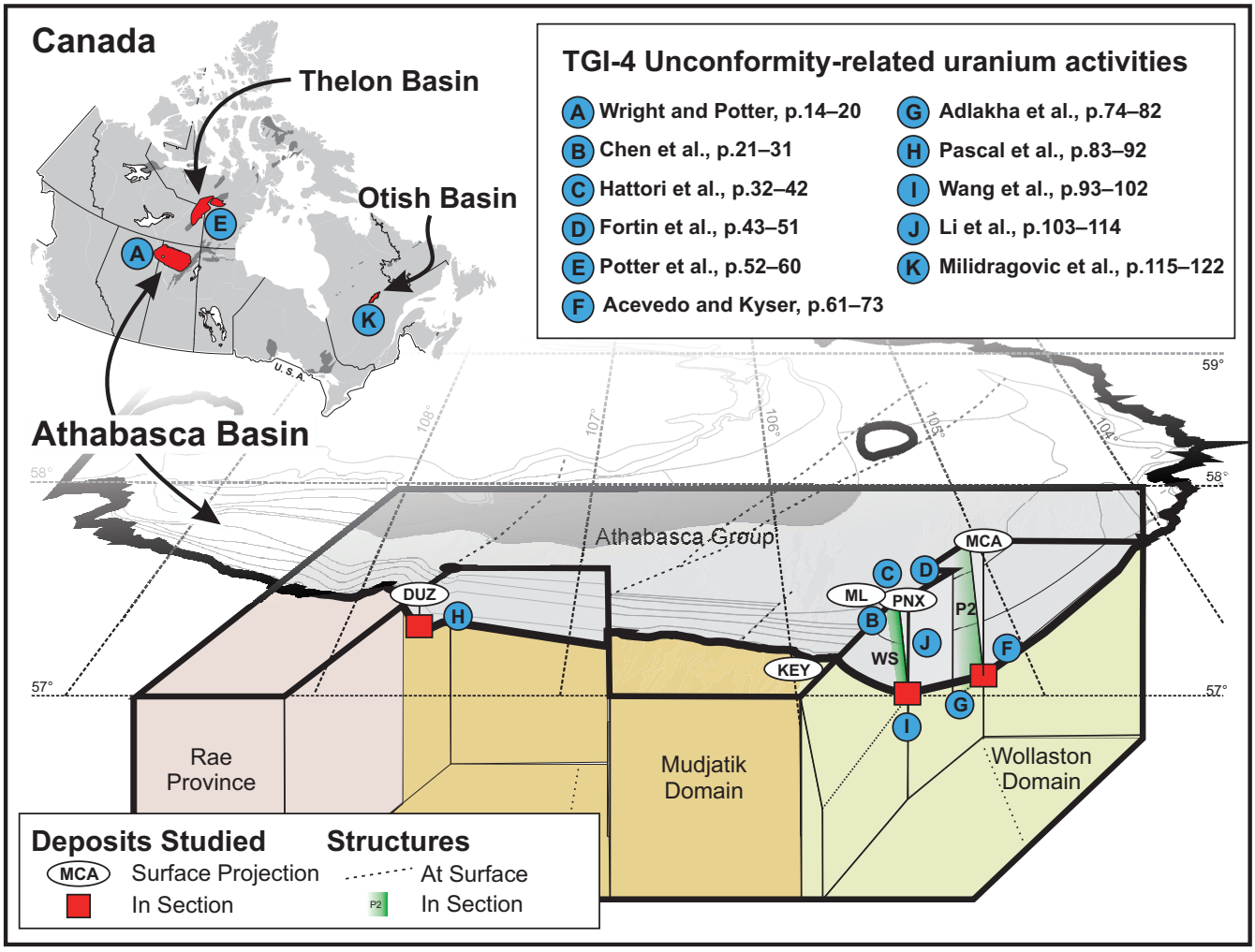

Figure 4. Location of TGI-4 uranium activities in three-dimensions. Abbreviations: DUZ = Dufferin Lake zone, ML = Millennium deposit, PNX = Phoenix deposits, KEY = Key Lake mine, MCA = McArthur River mine. P2 = P2 fault, WS = WS shear zone.

mixing of geochemically distinct NaCl-rich and $CaCl_2$-rich brines (Derome et al., 2005; Richard et al., 2010).

Research supported under TGI-4 by Pascal et al. (2015) and Wang et al. (2015) support graphite disaggregation as an indicator of hydrothermal fluid alteration. In addition to evaluating the role of graphite as a potential reductant, Pascal et al. (2015) also sought to investigate the petrogenetic disaggregation of graphite relative to P-T-t conditions within the Dufferin Lake Zone (Fig. 4). The authors propose that graphite and sulphide depletion proximal to mineralization reflects the final and most significant stage of graphite depletion associated with hydrothermal alteration of the basement, after deposition of the lower Athabasca Group sediments (e.g. associated with pre-/syn-ore alteration). Wang et al. (2015) also report a disordering of graphite with proximity to mineralization at the Phoenix deposit (Fig.4); investigation of this relationship continues. Wang et al., (2015) also present evidence supporting boiling in quartz veins during the waning stages of the systems while the stress regime transitioned from ductile to brittle deformation in the sandstones that would have facilitated precipitation of metals in solution.

The role of iron in unconformity-related systems, including as a potential reductant, is investigated by Potter et al. (2015) and Acevedo and Kyser (2015) by examining iron and magnesium isotope systematics in the alteration assemblages at the Bong and McArthur River deposits, respectively (Fig. 4). While Potter et al. (2015) note significant iron and magnesium isotope fractionations driven by leaching of iron during incursion of acidic, oxidized brines in the ore-forming alteration, Acevedo and Kyser (2015) were able to define a population of iron isotopic values ($\delta^{56}Fe_{IRMM-014}$ values >0.5‰) reflecting oxidation-reduction reactions related to uranium precipitation.

Fluid flow geometry

A primary classification of unconformity-related uranium deposits is based on their location relative to the unconformity and basement shear structures, with “egress”-type (sandstone-hosted) deposits primarily straddling or situated above the unconformity surface, and “ingress”-type deposits occurring underneath the unconformity, hosted entirely with-

in Paleo-Proterozoic to Archean basement material. Li et al. (2015) specifically model regional fluid flow and structural relationships for the eastern Athabasca Basin (Fig. 4) to examine what physical and chemical conditions focussed the high flux of fluids required to form the large deposits at specific sites within the basin, especially along fault zones and within wider structural zones, and why some faults are more economically prospective than others. The regional-scale modelling results illustrate that widths of individual thermal convection cells are less than 2 km and are controlled by the location of faults. Deposit-scale studies within the regional fluid flow modelling study area complement these studies, providing a more detailed examination of the structural-fluid interactions and related fluid regimes (Wang et al., 2015). As mentioned above, it has been suggested that high fluid flux along key structural intersections is a potentially important component of the fluid dynamics of these systems, perhaps complemented by sharp decreases in fluid pressure under brittle deformation conditions, as recorded in drusy quartz veins in the sandstones (e.g. Wang et al., 2015).

Structures

Basement structures with displacement pre-, syn- and post-deposition of the Proterozoic sediments are considered integral parts of both genetic and applied exploration models of unconformity-related uranium deposits (Jefferson et al., 2007a, b). Specific structural orientation directions and intersections critical to unconformity-related uranium deposits have been defined from brittle overprints on basement shear zones (e.g. D_3 structures of Portella and Annesley, 2000; Annesley et al., 2005). Post-mineralization reactivation of pre-existing structures and magmatic intrusions (e.g. Mackenzie Dyke swarm in the Athabasca and Thelon Basins, Otish Gabbro sills and lamprohyric dykes in Otish Basin, Martin Group mafic sills and dikes in the Martin Basin and Nipissing Diabase in the Huronian (Morelli et al., 2009; Potter and Taylor, 2010; Reid et al., 2014; Milidragovic et al., 2015) offset earlier structures and may have also remobilized primary mineralization. A popular and effective method of identifying structural corridors for unconformity-related uranium deposits has been through the use of geophysical, and more specifically, electromagnetic (EM), techniques (Jefferson et al., 2007b). The EM techniques identify conductive material in the basement, typically inferred to represent pre-ore graphite. Ongoing application of EM geophysical techniques to unconformity-related uranium deposits has identified two important observations: 1) the targeting of prospective zones along conductive corridors is dependent on the disruption of the EM signature due to alteration (including disaggregation of graphite); and 2) not all structures or deposits are hosted by altered graphitic rocks or contain enough graphite contents to produce a conductive signature.

The TGI-4 uranium project did not undertake geophysical research to evaluate better methods of identifying structures, but several projects investigated graphite disaggregation as an exploration vector or identified alternate methods of prioritizing conductor trends and intersections through geochemistry. Graphite disaggregation was specifically examined by both Pascal et al. (2015) and Wang et al. (2015) as part of TGI-4 supported research. Both authors confirm graphite depletion and visible graphite disordering with proximity to mineralization at the Dufferin Lake zone (Pascal et al., 2015) and at the Phoenix deposits (Wang et al., 2015).

Wright and Potter (2015) highlight the distribution and ranking of key geochemical signatures using exploratory data analysis techniques (Tukey, 1977), including scatterplots, boxplot analysis, and multivariate correlation analyses to identify distinct element patterns associated with the ore-forming alteration. For instance, a combined signature of both elevated U^2/Th and Y^2/Th values display a spatial association with known deposits at depth and reflect structural trends and intersections in the uppermost sandstones of the Athabasca Basin, providing a method of prioritizing prospective structural intersections and emphasizing relative geochemical-structural relationships. The physical distribution of geochemical and radiometric signatures in soils also support the identification and ranking of prospective structural intersections (Hattori et al., 2015; Fortin et al., 2015; Wright, 2014)

Building on the recognition and classification of local to regional alteration systems along key structural corridors (Earle and Sopuck, 1989; Earle et al., 1999; Wasyliuk, 2002), Adlakha et al., (2015) examine subtle changes in mineral chemistry as vectors to ore in basement rocks along the 12 km long P2 fault that hosts the McArthur River deposit (Fig. 4). Within larger clay alteration systems, the presence of florencitic aluminum phosphate-sulphate (APS) minerals (building on earlier work by Gaboreau et al., 2005, 2007) and magnesio-foitite are proposed as additional mineralogical indicators of fertile structures.

Geochemical signatures

The geochemistry of unconformity-related uranium ores are categorized broadly into “simple” and “complex” suites corresponding respectively with basement-hosted and sandstone hosted end-members (Jefferson et al., 2007a, b). While individual deposits can exhibit combinations of both end-members, simple or ingress deposits tend to be basement-hosted and essentially monometallic. Complex or egress deposits occur at the unconformity or within sandstones and can contain significant concentrations of Co, Cu, Ni, As, S, Pb, Fe, Au, Ag and REE (Ruzicka, 1996; Fryer and Taylor, 1987; Jefferson et al., 2007a). Jefferson et al. (2007a, b) also identified REE relationships as a discriminating feature of ingress versus egress deposit types. The widespread adoption by industry of lower cost, more sensitive and precise multi-element analytical techniques (i.e. ICP-OES and ICP-MS) has rapidly expanded the geochemical dataset available to model unconformity-related chemical processes since publication of the EXTECH IV volume that was released in 2007 (e.g. Card et al., 2011). Much of this data has become available publicly due to mineral assessment filings, which were used to compile a large uranium exploration-specific geochemical dataset under TGI-4 to support further geochemical research in the basin (Athabasca Basin Uranium Geochemistry database (AUG); Wright et al., 2014,

in press). The AUG database permitted TGI-4-supported research by Wright and Potter (2015) and Ramaekers et al. (in press) to undertake regional examination and integration of geochemical data with components of the uranium exploration model and basin geology.

Cuney (2010) emphasized the importance of modeling uranium content relative to thorium, which reflects the primary association of these elements under igneous conditions, and the preferred mobility of hexavalent uranium (U^{6+}) under hydrothermal, oxidizing conditions (Grandstaff, 1976; Romberger, 1984). In response to this relationship, chemical analyses for uranium have focussed on partial digestion techniques to favour more mobile uranium. TGI-4 supported research by Ramaekers et al. (in press) note that uranium released by the partial dissolution of the sample accounts for less than a third of the total uranium in the non-mineralized sandstones – stressing that uranium in resistate minerals is the dominant source of uranium in the surface outcrops and till. However, through application of Principal Component Analysis (PCA), the authors illustrate that the signal of hydrothermal uranium can be recognized.

As part of TGI-4, projects by Wright and Potter (2015) and Chen et al. (2015) demonstrate the relationship of uranium to other high field strength elements, including thorium, yttrium, and the rare earth elements within a sample suite of the Athabasca Group. Fryer and Taylor (1987), Quirt et al. (1991) and Fayek and Kyser (1997) were amongst the first to discuss the rare earth elements as important components of uranium mineralization in the Athabasca Basin, including the potential implications for required fluid composition (e.g. fluorine contents). Wright and Potter (2015) specifically identify and rank important uranium-thorium (U^2/Th) and yttrium-thorium (Y^2/Th) relationships that categorize types of uranium enrichments relative to an inferred genetic-temporal association between uranium mineralization and the Wolverine Point and Locker Lake Formations of the Athabasca Group. Spatially, a population of elevated U^2/Th and Y^2/Th values are significant as they consistently occur over known zones of mineralization in the uppermost sandstones. Wright and Potter (2015) also identify MgO-B-Li and Cu-Co relationships that display enhanced chemical relationships with tourmaline and base metal alteration relative to gross lithogeochemistry (e.g. McGill et al., 1993; Jefferson et al., 2007b). Distinct signatures within these groups also show important spatial relationships to known zones of mineralization, including within range of the present day surface.

At property-scales, access to industry geochemistry datasets and analysis of surficial media permitted documentation of the geochemical and mineralogical signatures from basement rocks into the surficial environment overlying the Phoenix uranium deposit and the uranium-poor, REE-rich Maw zone (Hattori et al., 2015, Chen et al., 2015). Principal Component Analysis (PCA) by Chen et al. (2015) highlights distinct elemental associations and geochemical variations in the sandstone units over the Phoenix uranium deposit, reflecting subtle changes in lithology and alteration related to ore-forming processes. When compared to the uranium-poor, REE-rich Maw zone, sandstones overlying the Phoenix deposit exhibit distinct element associations (e.g. U-HREE-Y, LREE-Pb) that can be used to recognize subtle geochemical expressions of ore-forming processes in exploration (Chen et al., 2015).

Based on the strong statistical and spatial geochemical inter-element relationships between uranium, thorium, yttrium, and the rare earth elements discussed by Wright and Potter, (2015), Chen et al. (2015), Hattori et al. (2015), and Adlakha et al. (2015), Chi et al. (2014) suggest an increased fluid flux to partially account for the strong element relationships and concentrations observed. This difference in flux may complement the fluorine-bearing brines proposed by Fayek and Kyser (1997) to explain elevated contents of typically immobile elements in the massive uranium ore.

Surficial techniques were also examined in several TGI-4 activities, linking metal, gas, and radiometric responses to better contrast potential mineralization and alteration signatures from background (Hattori et al., 2015; Fortin et al., 2015). Hattori et al. (2015) assess the expression of refined geochemical signatures within soils associated with deeply buried mineralization at the Phoenix and Millennium deposits and the presence of radon and helium dissolved in ground water as exploration vectoring tools. The authors highlight that both humus and B-horizon soil show elevated concentrations of U, Pb, ± Mo, Cu, Ag, Co, Ni, W and As directly above the deposits and/or structural zones. Elevated yet variable concentrations of radon and helium in groundwater over the deposits highlight the need for careful sampling and understanding of the local glacio-fluvial history, soil development and hydrological conditions. Fortin et al. (2015) discuss integration of quantitative analysis of the airborne data with surficial geological knowledge to differentiate between the complex patchwork of background signals and deposit-related surficial geochemical anomalies, based on focussed ground-truthing of airborne gamma-ray signatures along the McArthur River – Key Lake corridor (Fig. 4).

Alteration mineralogy

As with geophysical techniques, mineralogical evaluation of alteration relative to unconformity-related uranium deposits in the Athabasca Basin has seen widespread use (Jefferson et al., 2007a, b). Techniques applied have evolved from petrographic and X-ray diffraction methods (Hoeve and Quirt, 1984), through clay normative calculations (Earle and Sopuck, 1989), to the widespread use of short-wave infrared (SWIR or PIMA; e.g. Wasyliuk, 2002) clay identification techniques. Clay alteration phase proportions, primarily amongst illite, kaolinite, tourmaline (magnesio-foitite) and chlorite (sudoite), have been shown repeatedly to display spatial associations with known mineralized systems, although local variations in actual clay contents and clay species proportions illustrate complexities in the clay alteration systems.

In TGI-4 supported research, Adlakha et al. (2015) investigate the presence and distinct mineral chemistry amongst syn-ore minerals magnesio-foitite (MgF), APS (florencite) and sudoite along the P2 fault which hosts the McArthur River uranium deposits (Fig. 4). Building on previous work (e.g. Gaboreau et al., 2005, 2007), changes in APS mineral

chemistry and relative changes in sudoite and MgF abundances in the alteration assemblage provide vectors to ore along fertile basement structures, with enrichment in REE and uranium in APS and increased sudoite and MgF proximal to ore (Adlkaha et al., 2015). These changes in APS and MgF chemistry also mimic the lithogeochemical patterns described by Wright and Potter (2015), Chen et al. (2015), and Hattori et al. (2015).

Potentially linked to precipitation mechanisms, recognition of graphite depletion and visible graphite disordering may also provide property-scale indications of fertile alteration along prospective structures (Pascal et al., 2015; Wang et al., 2015).

Iron, often as brick-red hematite, is commonly associated with uranium at most examples of unconformity-related mineralization within the Athabasca Basin (Jefferson et al., 2007a), and has been inferred to reflect a direct or sympathetic response to oxidation-reduction processes responsible for ore genesis (Wallis et al.,1985). The isotopes of iron and magnesium were investigated by Potter et al. (2015) and Acevedo and Kyser (2015) to assess actual iron and magnesium mobility in relation to uranium precipitation in the Thelon and Athabasca Basins (Fig. 4). Potter et al., (2015) propose that significant leaching of iron from the Bong deposit in the Thelon basin suggests that enrichment in whole-rock iron contents with low $\delta^{57}Fe$ values along faults may be a distal indicator of mineralization. In a similar manner, distinct $\delta^{56}Fe$ values indicative of reduction-oxidation reactions occur up to 300 m from the ore zone and above the projection of the P2 fault at McArthur River (Acevedo and Kyser, 2015), and thus provide an indication on the fertility of an alteration assemblage, particularly along ore-hosting faults. Acevedo and Kyser (2015) do emphasize a complex iron system at McArthur River, and assign the most distinct example of iron fractionation to a late, post-mineralization fluid event. Due to the sensitivity of iron to oxidation-reduction conditions, combined with evidence for multiple resetting events within the Athabasca Basin (and likely other prospective Proterozoic basins; Fig. 1), iron enrichment/depletion signatures can represent evidence for distal alteration associated with unconformity-related uranium deposits in the absence of detailed isotopic analysis.

Basin evolution and uranium deposits

The current physical expressions of any ore system, including unconformity-related uranium deposits, are products of multiple events spanning the pre- to post-history of each ore deposit. Multiple paragenetic stages and remobilization of ore elements during primary and secondary dispersal within unconformity-related uranium deposits of the Athabasca and Thelon Basins of Canada have been defined by authors such as Kyser et al. (2000), Cameron et al. (2004) and summarized in Jefferson et al. (2007a). Post-mineralization dispersion of ore and alteration elements have the potential to increase the physical expression of such deposits, but also produce diluted and complicated signatures. As a result, understanding the role of individual components and events affecting the deposit can be critical to their effective use in exploration.

The formation of primary unconformity-related uranium mineralization in the Proterozoic basins has been shown to be intimately linked to basin diagenesis (Kyser et al., 2000, and references therein). However, due to the chemically active nature of uraninite, its ability to recrystallize under low temperature conditions causes disruption of the U-Pb isotopic system through loss of radiogenic Pb (Finch and Murakami 1999; Fayek and Kyser 2000; Alexandre and Kyser 2005). Uraninite geochronology from the Athabasca, Otish and Thelon basins has revealed significant remobilization and precipitation of ore post-diagenesis, in relation to tectonic and intrusive events (Farkas, 1984; Alexandre et al., 2009 and references therein; Sharpe, 2013; Shabaga et al., in press; Milidragovic et al., 2015). While most unconformity-related deposits do not have syn-ore minerals amendable to age dating, molybdenite-bearing samples from Camie River in the Otish Basin presented a unique opportunity to apply Re-Os techniques and develop a better chronology of basin evolution and deposit formation (Milidragovic et al., 2015). This study produced an age date of 1724 ± 4.9 for the Camie River deposit, within error of uraninite U-Pb ages of 1723 ± 16 Ma and 1721 ± 20 Ma; from the Camie River (Höhndorf et al., 1987; Beyer et al., 2012) and 1717 ± 20 Ma from the Lorenz Gully occurrence (Höhndorf et al., 1987). These results, when coupled with an age of the basin defined by intrusion of the Otish Gabbros at 2165–2170 Ma (Hamilton and Bucham, 2007; submitted; Milidragovic et al., 2015), indicate that mineralization post-dated the deposition of the Otish Basin by ca. 450 Ma — clearly post-peak diagenesis.

The numerical modelling results of Chi et al., (2014) indicate that migration of hydrocarbons to the sites of uranium precipitation may be a factor in the formation and preservation of the high-grade ore characteristic of the Athabasca Basin (c.f. Jefferson et al., 2007a). For example, the authors were able to hydrodynamically model migration of oil and gas developed in the ca. 1541 Ma Douglas Formation to the base of the basin and the sites of the unconformity-related uranium deposits that formed at ca. 1600–1500 Ma and 1460–1350 Ma, with significant remobilization events at ca. 1176 Ma, 900 Ma, and 300 Ma (Hoeve and Quirt, 1984; Cumming and Krstic 1992; McGill et al., 1993; Fayek et al., 2002; Alexandre et al., 2003; Jefferson et al., 2007a; Creaser and Stasiuk, 2007). While Wilson et al. (2007) proposed that some of the hydrocarbons in the uranium deposits postdate the ore, biomarker results indicate they were derived from the Douglas Formation.

The importance of relative paragenesis is also emphasized by spatial-temporal relationships observed by other TGI-4 activities. Wright and Potter (2015) highlight that anomalous yttrium signatures associated with high-grade uranium mineralization and chemo-stratigraphically with the Wolverine Point and Locker Lake Formations suggest a temporal and possible genetic association. As Jefferson et al. (2007a) note, early diagenetic xenotime rimming zircon grains in the Wolverine Point Formation contain little to no uranium, but other generations of xenotime and diagenetic apatite contain locally abundant uranium (Rainbird et al., 2003). Age dates from the Wolverine Point Formation (ca. 1644 Ma; Rainbird et al., 2007) and fluorapatite cements in

the Athabasca Group (1640–1620 Ma; Davis et al., 2008) overlap with those for pre-ore alteration (1730–1590 Ma, Alexandre et al., 2009). The association of elevated yttrium is also reflected in U-Y-REE-bearing florencite rims in APS minerals along the P2 fault (Adlakha et al., 2015), and early xenotime associated with zircon observed by Chen et al. (2015) at the Phoenix deposit.

Summary

Building on historical research, several primary exploration techniques and knowledge to guide application of these tools have been refined and/or identified by TGI-4 research activities including:

Exploration techniques

- *Geochemical signatures*
  - Geochemical expressions of deeply-buried mineralization and alteration in uppermost sandstones, soils and ground waters (Wright and Potter, 2015; Chen et al., 2015; Hattori et al., 2015; Ramaekers et al., in press)
  - Modelling of helium and radon dispersion from the ore zones (Hattori et al., 2015)
  - Deposit-related geochemical signatures spatially associated with lineaments produced from the intersection of brittle structures (Wright and Potter, 2015; Hattori et al., 2015)
  - Reconciliation of Quaternary geology with gamma-ray signatures to enhance application of regional airborne radiometric surveys to detected geochemical anomalies (Fortin et al., 2015)
  - Distinct iron and magnesium isotopic signatures in the alteration assemblages related to alteration and uranium precipitation mechanisms (Potter et al., 2015; Acevedo and Kyser., 2015)

- *Mineral assemblages and mineral chemistry:*
  - Relative proportions of APS, magnesio-foitite and sudoite and changes in APS and tourmaline chemistry related to alteration and ore-forming processes along fertile basement structures (Adlakha et al., 2015)
  - Graphite depletion and disordering proximal to ore along ore-hosting structures rooted in graphitic basement rocks (Pascal et al., 2015; Wang et al., 2015)

- *Fluid flow - structural relationships*
  - Intimate relationship between deposits, unconformity-surface offsets associated with NE-SW trending, fault-related quartzite ridges and later NW-SE trending cross structures (Li et al., 2015; Wang et al., 2015).
  - Fluid flow modelling relative to unconformity and structure intersections, highlighting possible structure distribution patterns required to produce ingress-egress fluid movement (Li et al., 2015).
  - Fault control on hydrothermal fluid convection which ultimately control the extent of geochemical signatures in the overlying sandstones (Li et al., 2015)
  - Numerical modelling supporting hydrocarbon migration from uppermost units to sites of uranium precipitation (Chi et al., 2014; Li et al., 2015).

Genetic Implications

Research supported by TGI-4 has influenced our understanding of the genesis of unconformity-related uranium deposits in several ways:

- *Brine-fluid compositions*
  - Re-emphasis on the need for the efficient transport and spatially restricted precipitation of uranium, thorium, yttrium, and the rare earth element-enriched source fluids (Adlakha et al., 2015; Chen et al., 2015; Wright and Potter, 2015)
  - Incursion of highly acidic brines into the basement rocks, neutralized or buffered through fluid-rock interactions (Potter et al., 2015)

- *Reduction mechanisms*
  - Potential for multiple reduction mechanisms in the high-grade deposits with:
    - Reduction-oxidation reactions recorded in iron isotopic values in clay alteration minerals linked to uranium precipitation at the McArthur River deposit (Acevedo and Kyser, 2015).
    - Reduction and neutralization of acidic fluids through fluid-rock interactions (Potter et al., 2015)
    - Graphite and sulphide depletion proximal to ore during pre- to syn-ore alteration (Pascal et al., 2015; Wang et al., 2015).

- *Fluid flow –structural relations*
  - Basement fluid flow was focussed along key structures over long distances (i.e. 12 km along the P2 fault; Adlakha et al., 2015).
  - Strong structural control on these uranium ore systems with the position and size of the hydrothermal convections cells controlled by the location of fault zones and estimated to be on the order of 2 km (Li et al., 2015).

Basin evolution

  - Potential for primary ore precipitation post-peak diagenesis, related to regional tectono-magmatic events (Mildragovic et al., 2015).
  - Hydrocarbon migration to the base of the basin syn- to post-ore formation (Li et al., 2015).

Acknowledgments

The TGI-4 unconformity-related uranium project was a five-year collaborative project funded by the Geological Survey of Canada from 2010-2014, with support from Cameco Corporation, Denison Mines Corporation, AREVA Resources Canada and the Saskatchewan Geological Survey. Targeted funding for activities was primarily through research grants administered by the Geological Survey of Canada with the universities of Regina, Saskatchewan, Ottawa, and Queen's. Funding for some graduate students

was through the Research Affiliate Program (RAP) bursaries. Mentors and facilitators not included as co-authors in this volume include: Alexandre Aubin, Eric Bort, Dan Brisbin, Aaron Brown, Gary Delaney, Claude Dion, Charlie Jefferson, Dan Jiricka, Tyler Mathieson, Brian McGill, Scott Rogers, Vlad Sopuck, Bill Slimmon, David Thomas, Gary Witt, and Garnet Wood. A draft of this review benefitted from highly constructive comments from Sean Bosman, Colin Card and Charlie Jefferson.

Delivery of the TGI-4 uranium program was facilitated through supportive mentorship, guidance and managerial oversights by Michael Villeneuve, Cathryn Bjerkelund, Dan Richardson and Christine Hutton. Angèle Miron is thanked for the timely execution and coordination of the human resource and finance procedures. Prompt and professional technical layout editing was completed by Beverly Strickland with guidance from Bruce Blair and Eleanor Everett at the Scientific and Technical Publishing Services unit.

Contributions to this volume were significantly improved by peer-reviews by the following: Anonymous, Steve Beyer, Sean Bosman, Janet Campbell, Colin Card, Paul Gammon, Eric Grunsky, Tom Kotzer, Kurt Kyser, Christopher Lawley, Julien Mercadier, Antonin Richard, David Thomas, Victoria Tschirhart, Jianweng Yang, and Gerard Zaluski.

References

Acevedo, A. and Kyser, T.K., 2015. Fe isotopic composition of alteration minerals from McArthur River zone 4 deposit, Athabasca Basin, Saskatchewan; *in* Targeted Geoscience Initiative 4: unconformity-related uranium systems, (ed.), E.G. Potter and D.M. Wright; Geological Survey of Canada, Open File 7791, p. 61–73. doi:10.4095/295776

Adlakha, E.E., Hattori, K., Zaluski, G., Kotzer, T.G., Davis, W.J., and Potter, E.G., 2015. Mineralogy of a fertile fluid conduit related to unconformity-type uranium deposits in the Athabasca Basin, Saskatchewan; *in* Targeted Geoscience Initiative 4: unconformity-related uranium systems, (ed.), E.G. Potter and D.M. Wright; Geological Survey of Canada, Open File 7791, p. 74–82. doi:10.4095/295776

Alexandre, P., and Kyser, T.K., 2005. Effects of cationic substitutions and alteration of uraninite, and implications for the dating of uranium deposits; The Canadian Mineralogist, v. 43, p. 1005–1017

Alexandre, P., Kyser, T.K., Jiricka, D., and Witt, G., 2012. Formation and Evolution of the Centennial Unconformity-Related Uranium Deposit in the South-Central Athabasca Basin, Canada; Economic Geology, v. 107, p. 385–400.

Alexandre, P., and Kyser, T.K., 2006. Geochemistry of uraniferous bitumen in the southwest Athabasca Basin, Saskatchewan, Canada; Econonic Geology, v.101, p. 1605–1612.

Alexandre, P., Kyser, K., and Polito, P., 2003, Geochronology of the Paleoproterozoic basement-hosted unconformity-type uranium deposits in northern Saskatchewan, Canada: Uranium Geochemistry 2003, International Conference, Université Henri Poincaré, Nancy, France, Proceedings, p. 37–40.

Alexandre, P., Kyser, K., Polito, P., Thomas, D., 2005, Alteration mineralogy and stable isotope geochemistry of Paleoproterozoic basement-hosted unconformity- type uranium deposits in the Athabasca Basin, Canada: Economic Geology, v. 100, p. 1547–1563.

Alexandre, P., Kyser, T.K., Thomas, D., Polito, P., and Marlat, J., 2009. Geochronology of unconformity-related uranium deposits in the Athabasca Basin, Saskatchewan, Canada and their integration in the evolution of the basin; Mineralium Deposita, v. 44, p. 41–59.

Annesley, I.R., Madore, C., and Portella, P., 2005. Geology and thermotectonic evolution of the western margin of the Trans-Hudson Orogen: Evidence from the eastern sub-Athabasca basement, Saskatchewan: Canadian Journal of Earth Sciences, v. 42, p. 573–597.

Annesley, I.R., and Wheatley, K., 2011. Insights into understanding the carbon-uranium (± sulfur and boron) geochemical system along a retrograde P-T-t path from 600°C to 250°C: New constraints with implications for U/C-type uranium deposits; Joint annual meeting of the Geological Association of Canada – Mineralogical Association of Canada, Abstracts, v. 34, p. 4–5.

Armitage, A., 2013. Technical report on the Patterson Lake, Patterson lake South and Clearwater West Properties; N.I. 43-101 technical report prepared for Fission Uranium Corp. and Fission Energy Corp., 132 p.

Bebout, G.E., Cooper, D.C., Bradley, A.D., and Sadofsky, S.J., 1999. Nitrogen-isotope record of fluid-rock interactions in the Skiddaw aureole and granite, English Lake District; American Mineralogist, v. 84, p. 1495–1505.

Beyer, S.R., Kyser, K., Hiatt, E.E., Polito, P.A., Alexandre, P., and Hoksbergen, K., 2012. Basin evolution and unconformity-related uranium mineralization: The Camie River U prospect, Paleoproterozic Otish Basin, Quebec; Economic Geology, v. 107, p. 401–425.

Calvert, H.T., 2013. Uranium – 2012 Annual Review; 2012 Canadian Minerals Yearbook, Minerals and Metals Sector, Natural Resources Canada, 9 p. http://www.nrcan.gc.ca/mining-materials/markets/commodity-reviews/8360

Cameron, E.M., Hamilton, S.M., Leybourne, M.I., Hall, G.E.M., McClenaghan, M.B., 2004. Finding deeply buried deposits using geochemistry; Geochemistry: Exploration, Environments and Analysis, v. 4, p. 7–32

Canadian Nuclear Association, 2013. Canadian Nuclear Factbook; Canadian Nuclear Association, 64 p. https://cna.ca/wp-content/uploads/2014/07/CNA-Factbook-2013.pdf

Card, C.D., and Annesley, I.R., 2012. The origin(s) of graphite-rich rocks in the Wollaston-Mudjatik Transition Zone: syngenetic versus epigenetic?; Saskatchewan Geological Survey, Open House 2012, Abstract volume, p. 6.

Card, C.D., Bosman, S.A., Slimmon, W.L., Zmetana, D.J. and Delaney, G.D., 2011. Geochemical Analyses of Athabasca Group Outcrops in Saskatchewan (NTS 64L, 74F to 74K, and 74N to 74P); Saskatchewan Ministry of Energy and Resources Data File Report 29 (digital).

Chen, S., Hattori, K., Grunsky, E.C., and Liu, Y., 2015. Geomathematical study of sandstones overlying the Phoenix uranium deposits and the REE-rich Maw Zone, Athabasca Basin, Saskatchewan; *in* Targeted Geoscience Initiative 4: unconformity-related uranium systems, (ed.) E.G. Potter and D.M. Wright; Geological Survey of Canada, Open File 7791, p. 21–31. doi:10.4095/295776

Cheney, E.S., 1985. Similarities between roll-front and Athabasca unconformity-type uranium deposits and the possible role of sulphides in their origin; in Geology of Uranium Deposits, T.I.I. Sibbald and W. Petruk; Canadian Institute of Mining, Metallurgy and Petroleum, v. 32, p. 159–163.

Chi, G., Li, Z., and Bethune, K.M., 2014. Numerical modeling of hydrocarbon generation in the Douglas Formation of the Athabasca Basin (Canada) and implications for unconformity-related uranium mineralization; Journal of Geochemical Exploration, v. 144, p. 37–48

Cloutier, J., Kyser, T.K., Olivo, G.R., Alexandre, R., and Halaburda, J., 2009. The Millennium uranium deposit, Athabasca Basin, Saskatchewan, Canada: an atypical basement-hosted unconformity-related uranium deposit; Economic Geology, v.104, p. 815–840

Cloutier, J., Kyser, T.K., Olivo, G.R., and Brisbin, D., 2011. Geochemical, isotopic, and geochronologic constraints on the formation of the Eagle Point basement-hosted uranium deposit, Athabasca Basin, Saskatchewan, Canada and recent remobilization of primary uraninite in secondary structures; Mineralium Deposita, v. 46, p. 35–56.

Creaser, R.A., and Stasiuk, L.D., 2007. Depositional age of the Douglas Formation, northern Saskatchewan, determined by Re-Os geochronology; in EXTECH IV: Geology and Uranium EXploration TECHnology of the Proterozoic Athabasca Basin, Saskatchewan and Alberta, (ed.) C.W. Jefferson and G. Delaney; Geological Survey of Canada, Bulletin 588, p. 341–346.

Cumming, G.L., and Krstic, D., 1992. The age of unconformity-associated uranium mineralization in the Athabasca Basin, northern Saskatchewan; Canadian Journal of Earth Sciences, v. 29, p. 1623-1639.

Cuney, M., 2010. Evolution of uranium fractionation processes through time: driving the secular variation of uranium deposit types; Economic Geology, v. 105, p. 553–569.

Davis, W.J., Rainbird, R.H., Gall, Q., and Jefferson, C.W., 2008. In situ U-Pb dating of diagenetic apatite and xenotime: paleofluid flow history within the Thelon, Athabasca, and Hornby Bay basins; Goldschmidt 2008 Conference Abstracts, Geochimica Cosmochimica Acta, v. 74, no. 12S, p. A203.

Derome, D., Cathelineau, M., Cuney, M., Fabre, C., Lhomme, T., and Banks, D.A., 2005. Mixing of sodic and calcic brines and uranium deposition at McArthur River, Saskatchewan, Canada: a Raman and laser-induced breakdown spectroscopic study of fluid inclusions; Economic Geology, v. 100, p. 1529-1545.

Derome, D., Cuney M., Cathelineau, M., Dubessy, J., and Bruneton, P., 2003. A detailed fluid inclusion study in silicified breccias from the Kombolgie sandstones (Northern Territory, Australia): Application to the genesis of Middle-Proterozoic unconformity-type uranium deposits; Journal of Geochemical Exploration, v. 80, p. 259–275.

Duit, W., Jansen, J.B.H., Van Breemen, A., and Bos, A., 1986. Ammonium micas in metamorphic rocks as exemplified by Dome de l'Agout (France); American Journal of Science, v. 286, p. 702–732

Earle, S., and Sopuck, V., 1989. Regional lithogeochemistry of the eastern part of the Athabasca Basin uranium province, Saskatchewan; in Uranium Resources and Geology of North America, (ed.) E. Muller-Kahle; International Atomic Energy Agency, TECDOC-500, p. 263–269.

Earle, S., Wheatley, K., and Wasyliuk, K., 1999. Application of reflectance spectroscopy to assessment of alteration mineralogy in the Key Lake area; MinExpo '96 Symposium - Advances in Saskatchewan geology and mineral exploration, Proceedings, p. 109–123.

Farkas, A., 1984. Mineralogy and host rock alteration of the Lone Gull deposit; Internal Report prepared for Urangesellschaft.

Fayek, M., and Kyser, T.K., 1997. Characterization of multiple fluid-flow events and rare-earth element mobility associated with formation of unconformity-type uranium deposits in the Athabasca Basin, Saskatchewan; The Canadian Mineralogist, v. 35, p. 627–658.

Fayek, M., and Kyser, T.K., 2000. Low temperature oxygen isotopic fractionation in the uraninite-UO_3-CO_2-H_2O system; Geochimica et Cosmochimica Acta, 64, p. 2185–2197

Fayek, M., Kyser, T.K., and Riciputi, L.R., 2002. U and Pb isotope analysis of uranium minerals by ion microprobe and the geochronology of the McArthur River and Sue Zone uranium deposits, Saskatchewan, Canada; The Canadian Mineralogist, v. 40, p. 1553–1569.

Finch, R.J., and Murakami, T., 1999. Systematics and paragenesis of uranium minerals; in Uranium: mineralogy, geochemistry, and the environment, (ed.) P.C. Burns and R.J. Finch; Mineralogical Society of America, Reviews in Mineralogy v. 38, p. 91–179

Fission Uranium Corp., 2015. Fission's initial resource totals at PLS: 79.6M lbs and 25.9M lbs inferred; Fission Uranium Corporation press release dated January 9, 2015, www.fissionuranium.com

Fortin, R., Campbell, J.E., Harvey, B.J.A., McCurdy, M.W., Sinclair, L.E., Hanson, M.A., Potter, E.G., and Jefferson, C.W., 2015. Ground-truthing of the 'Eastern Athabasca Basin' regional airborne gamma-ray survey: Context for exploration of deeply buried unconformity-related uranium deposits in the Athabasca Basin of northern Saskatchewan; *in* Targeted Geoscience Initiative 4: unconformity-related uranium systems, (ed.), E.G. Potter and D.M. Wright; Geological Survey of Canada, Open File 7791, p. 43–51. doi:10.4095/295776

Fryer, B., and Taylor, R.P., 1987. Rare-earth element distribution in uraninites: implications for ore genesis; Chemical Geology, v.63, p. 101–108.

Gaboreau, S., Beaufort, D., Vieillard, P., Patrier, P., and Bruneton, P., 2005. Aluminum phosphate–sulfate minerals associated with Proterozoic unconformity-type uranium deposits in the East Alligator River Uranium Field, Northern Territories, Australia; The Canadian Mineralogist, v. 43, p. 813–827.

Gaboreau, S., Cuney, M., Quirt, D., Beaufort, D., Patrier, P., and Mathieu, R., 2007. Significance of aluminum phosphate-sulfate minerals associated with U unconformity-type deposits: The Athabasca Basin, Canada; American Mineralogist, v. 92, p. 267–280

Grandstaff, D.E., 1976. A kinetc study of the dissolution of uraninite; Economic Geology, v.71, p. 1493–1506.

Hamilton, M.A. and Buchan, K.L., 2007. U-Pb baddeleyite age for Otish Gabbro: Implications for correlation of Proterozoic sedimentary sequences and magmatic events in the eastern Superior Province; Joint Annual Meeting of the Geological Association of Canada – Mineralogical Association of Canada, Abstracts, v. 32, p. 35.

Hattori, K., Power, M.J., Krahenbil, A., Sorba, C., Kotzer, T.G., and Potter, E.G., 2015. Surficial geochemical surveys over concealed uranium ore of the Phoenix and Millennium deposits in the Athabasca Basin, Saskatchewan; *in* Targeted Geoscience Initiative 4: unconformity-related uranium systems, (ed.), E.G. Potter and D.M. Wright; Geological Survey of Canada, Open File 7791, p. 32–42. doi:10.4095/295776

Hoeve, J., and Quirt, D.H., 1984. Mineralization and Host Rock Alteration in Relation to Clay Mineral Diagenesis and Evolution of the Middle-Proterozoic, Athabasca Basin, northern Saskatchewan, Canada; Saskatchewan Research Council, SRC Technical Report 187.

Hoeve, J., and Sibbald, T.I.I., 1978. On the genesis of Rabbit Lake and other unconformity-type uranium deposits in northern Saskatchewan, Canada; Economic Geology, v. 73, p. 1450–1473.

Höhndorf, A., Bianconi, F., and Von Pechmann, E., 1987. Geochronology and metallogeny of vein-type uranium occurrences in the Otish Basin area, Quebec, Canada; in Metallogenesis of Uranium Deposits: Proceedings of a Technical Committee Meeting on Metallogenesis of Uranium Deposits, Vienna, IAEA, p. 233–260.

Huizenga, J.M., 2010. hermodynamic modelling of a cooling C–O–H fluid–graphite system: implications for hydrothermal graphite precipitation; Mineralium Deposita, v. 46, p. 23–33.

Hurai, V., Janak, M., Ludhova, L., Horn, E.E., Thomas, R., and Majzlan, J., 2000. Nitrogen-bearing fluids, brines and carbonate liquids in Variscan migmatites of the Tatra Mountains, Western Carpathians; heritage of high-pressure metamorphism; European Journal of Mineralogy, v. 12, p. 1283–1300.

Jefferson, C.W., Thomas, D.J., Gandhi, S.S., Ramaekers, P., Delaney, G., Brisbin, D., Cutts, C., Portella, P., and Olson, R.A. 2007a. Unconformity-associated uranium deposits of the Athabasca Basin, Saskatchewan and Alberta; in EXTECH IV: geology and uranium EXploration TECHnology of the Proterozoic Athabasca Basin, Saskatchewan and Alberta, (ed.) C.W. Jefferson and G. Delaney; Geological Survey of Canada Bulletin, v.588, p. 23–68

Jefferson, C.W., Thomas, D., Quirt, D., Mwenifumbo, C.J., and Brisbin, D., 2007b. Empirical Models for Canadian Unconformity-Associated Uranium Deposits; in Proceedings of Exploration 07: Fifth Decennial International Conference on Mineral Exploration, (ed.) B. Milkereit; p. 741–769

Jiricka, D., 2010. The Centennial deposit—an atypical unconformity-related uranium deposit—an update; International Association on the Genesis of Ore Deposits (IAGOD), 13th Quadrennial IAGOD Symposium, Adelaide, Australia, Proceedings.

Koning, E., and Robbins, J., 2006. The Cluff Lake deposits, west Athabasca Basin, Saskatchewan, Canada; in Uranium: Athabasca Deposits and Analogues, Uranium Field Conference, (ed.) D. Quirt; Canadian Institute of Mining, Metallurgy and Petroleum, Saskatoon, Abstract Volume, C1, 13p.

Kotzer, T.G., and Kyser, T.K., 1995. Petrogenesis of the Proterozoic Athabasca Basin, northern Saskatchewan, Canada, and its relation to diagenesis, hydrothermal uranium mineralization and paleohydrogeology; Chemical Geology, v. 120, p. 45–89.

Kyser, T.K., Cuney, M., 2009. Unconformity-related uranium deposits; in Recent and Not-So-Recent Developments in Uranium Deposits and Implications for Exploration, (ed.) M. Cuney and T.K. Kyser; Mineralogical Association of Canada Short Course Series, v. 39, p. 161–220.

Kyser, T.K., Hiatt, E., Renac, C., Durocher, K., Holk, G., Deckart, K., 2000. Diagenetic fluids in paleo– and meso–Proterozoic sedimentary basins and their implications for long protracted fluid histories; in Fluid and Basin Evolution, (ed.) T.K. Kyser; Mineralogical Association of Canada Short Course, v.28, p. 225–262.

Lemaitre, R., 2006. The Eagle Point Mine. Old Fashioned geological interpretation is the key to exploration success in basement rocks; Prospectors and Developers Association of Canada Meeting, Proceedings

Li, Z., Chi, G., Bethune, K.M., Bosman, S.A., and Card, C.D., 2015. Geo-

metric and hydrodynamic modelling and fluid-structural relationships in the southeastern Athabasca Basin and significance for uranium mineralization; *in* Targeted Geoscience Initiative 4: unconformity-related uranium systems, (ed.), E.G. Potter and D.M. Wright; Geological Survey of Canada, Open File 7791, p. 103–114. doi:10.4095/295776

McGill, B.D., Marlatt, J.L., Matthews, R.B., Sopuk, V.J., Homeniuk, L.A., and Hubregtse, J.J., 1993. The P2 North uranium deposit, Saskatchewan, Canada; Exploration and Mining Geology, v. 2, p. 321–331.

Milidragovic, D., Lesbros-Piat-Desvial, M., King, J.J., Beaudoin, G., Hamilton, M.A., and Creaser, R.A., 2015. The Otish Basin: basin evolution and formation of the Camie River uranium deposit, Quebec; *in* Targeted Geoscience Initiative 4: unconformity-related uranium systems, (ed.), E.G. Potter and D.M. Wright; Geological Survey of Canada, Open File 7791, p. 115–122. doi:10.4095/295776

Morelli, R.M., Hartlaub, R.P., Ashton, K.E., and Ansdell, K.M., 2009. Evidence for enrichment of subcontinental lithospheric mantle from Paleoproterozoic intracratonic magmas: Geochemistry and U–Pb geochronology of Martin Group igneous rocks, western Rae Craton, Canada; Precambrian Research, v. 175, p. 1–15.

OECD, 2014. Uranium 2014: Resources, production and demand; A Joint Report by the OECD Nuclear Energy Agency and the International Atomic Energy Agency, 508 p.

Pagel, M., Poty, B., and Sheppard, S.M.F., 1980. Contributions to some Saskatchewan uranium deposits mainly from fluid inclusions and isotopic data; in Uranium in the Pine Creek geosynclines, (ed.) S. Ferguson and A. Goleby; International Atomic Energy Agency, Vienna, Austria p. 639−654.

Pascal, M., Ansdell, K.M., and Annesley, I.R., 2015 Graphite-bearing and graphite-depleted basement rocks in the Dufferin Lake zone, south-central Athabasca Basin, Saskatchewan; *in* Targeted Geoscience Initiative 4: unconformity-related uranium systems, (ed.), E.G. Potter and D.M. Wright; Geological Survey of Canada, Open File 7791, p. 83–92. doi:10.4095/295776

Portella, P., and Annesley, I.R., 2000. Paleoproterozoic tectonic evolution of the eastern sub-Athabasca basement, northern Saskatchewan: Integrated magnetic, gravity, and geological data; in GeoCanada: The Millennium Geoscience Summit: Joint meeting of the Canadian Geophysical Union, Canadian Society of Exploration Geophysicists, Canadian Society of Petroleum Geologists, Canadian Well Logging Society, Geological Association of Canada and the Mineralogical Association of Canada, Calgary, Alberta, Canada, 4 p.

Potter, E.G., Sharpe, R., Girard, I., Fayek, M., Gammon, P., Quirt, D., and Robbins, J., 2015. Fe and Mg Signatures of the Bong Uranium Deposit, Thelon Basin, Nunavut; *in* Targeted Geoscience Initiative 4: unconformity-related uranium systems, (ed.), E.G. Potter and D.M. Wright; Geological Survey of Canada, Open File 7791, p. 52–60. doi:10.4095/295776

Potter, E.G. and Taylor, R. P., 2010. The stable and radiogenic isotopic atributes of precious-metal-bearing polymetallic veins from the Cobalt Embayment, Northern Ontario, Canada: genetic and exploration implications; The Canadian Mineralogist, v. 48, p. 391–414.

Quirt, D., Kotzer, T., and Kyser, T.K., 1991. Tourmaline, phosphate minerals, zircon and pitchblende in the Athabasca Group: Maw Zone and McArthur River areas; in Summary of Investigations 1991; Saskatchewan Geological Survey, Saskatchewan Energy and Mines, Report 91-4, p. 181–191.

Rainbird, R.H., Rayner, N., and Stern, R.A., 2003. SHRIMP U-Pb geochronology of apatite cements and zircon bearing tuff clasts in sandstones from the Athabasca Group, Athabasca Basin, northern Saskatchewan and Alberta; Saskatchewan Industry Resources, Open House, December 1-3, 2003, Saskatoon, Proceedings, p. 6

Rainbird, R.H., Stern, R.A., Rayner, N., and Jefferson, C.W., 2007. Age, provenance, and regional correlation of the Athabasca Group, Saskatchewan and Alberta, constrained by igneous and detrital zircon geochronology; in EXTECH IV: geology and uranium EXploration TECHnology of the Proterozoic Athabasca Basin, Saskatchewan and Alberta, (ed.) C.W. Jefferson and G. Delaney; Geological Survey of Canada Bulletin, v.588, p. 193–210.

Ramaekers, P., Bosman, S.A., and Card, C.D., in press. Lithogeochemical facies of Athabasca Basin strata, Saskatchewan – results of a reconnaissance PCA study; Geological Survey of Canada, Open File 7790.

Reid, K.D., Ansdell, K., Jiricka, D., Witt, G., and Card, C., 2014. Regional Setting, Geology, and Paragenesis of the Centennial Unconformity-Related Uranium Deposit, Athabasca Basin, Saskatchewan, Canada; Economic Geology, v. 109, p. 539–566

Rhys, D.A., Horn, L., Baldwin, D., and Eriks, R.S., 2008. Technical Report of the Geology of, and Drilling Results from, the Horseshoe and Raven Uranium Deposits, Hidden Bay Property, Northern Saskatchewan; NI 43-101 Report for UEX Corporation, 206 p.

Richard, A., Pettke, T., Cathelineau, M., Boiron, M. C., Mercadier, J., Cuney, M., and Derome, D., 2010. Brine–rock interaction in the Athabasca basement (McArthur River U deposit, Canada): consequences for fluid chemistry and uranium uptake; Terra Nova, v. 22, p. 303–308.

Richard, A., Rozsypal, C., Mercadier, J., Banks, D.A., Cuney, M., Boiron, M.C., and Cathelineau, M., 2012. Giant uranium deposits formed from exceptionally uranium-rich acidic brines; Nature Geoscience, v. 5 p. 142–146.

Romberger, S.B., 1984. Transport and deposition of uranium in hydrothermal systems of temperatures up to 300°C: geological implications; in Uranium Geochemistry, Resources, (ed.) B. de Vivo, F. Ippolito, G. Capaldi and P.R. Simpson; The Institution of Mining and Metallurgy, London, UK, p. 12–17.

Roy, C., Halarburda, J., Thomas, D., and Hirsekorn, D., 2005, Millennium deposit—basement-hosted derivative of the unconformity uranium model: Uranium production and raw materials for the nuclear fuel cycle—supply and demand, economics, the environment and energy security: International Atomic Energy Agency Proceedings Series, p. 111–121.

Ruzicka, V., 1993. Unconformity-type uranium deposits; in Mineral Deposit Modelling, (ed.) R.V. Kirkham, W.D. Sinclair, R.I . Thorpe, and J.M. Duke; Geological Survey of Canada, Special Paper 40, p. 125–149.

Ruzicka, V.R., 1996. Unconformity-associated uranium, in Geology of Canadian mineral deposit types, (ed.) O.R. Eckstrand, W.D. Sinclair, and R.I. Thorpe; Geological Survey of Canada, Geology of Canada v. 8, p. 197–210.

Sadofsky, S.J., and Bebout, G.E., 2000. Ammonium partitioning and nitrogen-isotope fractionation among coexisting micas during high-temperature fluid-rock interactions; examples from the New England Appalachians; Geochimica et Cosmochimica Acta, v. 64, p. 2835–2849

Shabaga, B.M., Fayek, M., Quirt, D., Davis, W.J., Pestaj, T., and Jefferson, C.W., in press. Geochemistry and Geochronology of the Andrew Lake Deposit, Thelon Basin, Nunavut, Canada; Joint annual meeting of the Geological Association of Canada – Mineralogical Association of Canada, Abstracts, v. 38.

Sharpe, R., 2013. The geochemistry and geochronology of the Bong uranium deposit, Thelon Basin, Nunavut Canada; M.Sc. thesis, University of Manitoba, Winnipeg, 213 p.

Shives, R.B.K., Wasyliuk, K., and Zaluski, G., 2000. Detection of K enrichment, illite chimneys using ground gamma ray spectrometry, McArthur River area, northern Saskatchewan; in Summary of Investigations 2000, Volume 2; Saskatchewan Geological Survey, Sask. Energy Mines, Misc. Rep. 2000-4.2, p. 160–169.

Thomas, D., 2003. Preliminary observations on the structural setting of uranium mineralization and alteration - Eagle Point deposit; Unpublished report by Cameco Corporation

Thomas, D.J., Matthews, R.B., and Sopuck, V.J., 1998. Athabasca Basin unconformity-type uranium deposits: a synopsis of the empirical model and review of exploration and production trends; in Canadian Institute of Mining, Metallurgy an Petroleum meeting, Montreal, Proceedings.

Tourigny, G., Quirt, D.H., Wilson, N., Wilson, S., Breton, G., and Portella, P., 2007. Basement geology of the Sue C uranium deposit, McClean Lake area, Saskatchewan; in EXTECH IV: geology and uranium EXploration TECHnology of the Proterozoic Athabasca Basin, Saskatchewan and Alberta, (ed.) C.W. Jefferson and G. Delaney; Geological Survey of Canada Bulletin, v.588, p. 229–248.

Tourigny, G., Wilson, G., Breton, G., and Portella, P., 2002. Geology of the Sue C uranium deposit, McClean Lake area, northern Saskatchewan; in

The Eastern Athabasca Basin and its Uranium Deposits, (ed.) G.B. Andrade, C.W. Jefferson, D.J. Thomas, G. Tourigny, S. Wilson and G.M. Yeo; Geological Association of Canada - Mineralogical Association of Canada, Field Trip Guidebook, Trip A1, p. 35–51.

Tukey, J.W., 1977. Exploratory Data Analysis, Addison-Wesley, Reading, Massachusetts, 688 p.

Wallis, R.H., Saracoglu, N., Brummer, J.J., and Golighltly, J.P., 1985. The geology of the McClean uranium deposits, northern Saskatchewan; in Geology of Uranium Deposits, (ed.) T.I.I. Sibbald, and W. and Petruk, Canadian Institute of Mining, Metallurgy and Petroleum, v. 32, p. 101–131.

Wang, K., Chi, G., Bethune, K.M., Card, C.D., 2015. Fluid composition, thermal conditions, fluid-structural relationships and graphite alteration of the Phoenix uranium deposit, Athabasca Basin, Saskatchewan; *in* Targeted Geoscience Initiative 4: unconformity-related uranium systems, (ed.), E.G. Potter and D.M. Wright; Geological Survey of Canada, Open File 7791, p. 93–102. doi:10.4095/295776

Wasyliuk, K., 2002. Petrogenesis of the kaolinite-group minerals in the eastern Athabasca basin of northern Saskatchewan: applications to uranium mineralization; unpublished M.Sc. Thesis, University of Saskatchewan. 140 p.

Wilson, N.S.F., Stasiuk, L.D., and Fowler, M.G., 2007. Origin of organic matter in the Proterozoic Athabasca Basin of Saskatchewan and Alberta, and significance to unconformity uranium deposits; in EXTECH IV: Geology and Uranium Exploration TECHnology of the Proterozoic Athabasca Basin, Saskatchewan and Alberta, (ed.) C.W. Jefferson and G. Delaney; Geological Survey of Canada, Bulletin 588, p. 325–339.

World Nuclear Association, 2014. World uranium mining production; World Nuclear Association, press release dated October 2014, http://www.world-nuclear.org/info/Nuclear-Fuel-Cycle/Mining-of-Uranium/World-Uranium-Mining-Production/?ekmensel=c580fa7b_702_744_430_1

Wright, D.M., 2014. Why think about unique uranium? emphasizing uranium mineralization patterns using geochemistry and radiometrics, Athabasca Basin, Saskatchewan; Saskatchewan Geological Survey, Open House 2014, Abstract Volume, p. 7.

Wright, D.M. and Potter, E.G., 2015. Application of regional geochemical datasets to uranium exploration in the Athabasca Basin, Saskatchewan; *in* Targeted Geoscience Initiative 4: unconformity-related uranium systems, (ed.) E.G. Potter and D.M. Wright; Geological Survey of Canada, Open File 7791, p. 14–20. doi:10.4095/295776

Wright, D.M., Potter, E.G., and Comeau, J-S., 2014. Athabasca Basin Uranium Geochemistry database; Geological Survey of Canada, Open File 7495. doi:10.4095/293345

Wright, D.M., Potter, E.G., and Comeau, J-S., in press. Athabasca Basin Uranium Geochemistry database v.2; Geological Survey of Canada, Open File 7792.

Yeo, G., and Potter, E.G., 2010. Review of reductants potentially involved in the formation of “basin-related” uranium deposits and their relevance in the Athabasca Basin; Saskatchewan Geological Survey Open House 2010, Abstract Volume, p. 16.

Application of Regional Geochemical Datasets to Uranium Exploration in the Athabasca Basin, Saskatchewan

Donald M. Wright[1] and Eric G. Potter[2]

1. *Peridot Geoscience Ltd., 19 Rein Terrace, Kanata, Ontario, K2M 2A9, don@peridotgeo.com*
2. *Geological Survey of Canada, 601 Booth Street, Ottawa, Ontario, K1A 0E8, epotter@NRCan-RNCan.gc.ca*

Abstract

Regional examination and integration of geochemical data with other components of the uranium exploration model can influence mineral exploration. This approach was applied to regional geochemical data for the Athabasca Basin, northern Saskatchewan, which is host to some of the world's most significant high-grade unconformity-associated uranium deposits.

Composite geochemical features based on components of four lithogeochemical signatures highlight specific chemical-spatial relationships important to ongoing exploration for unconformity-associated uranium in the Athabasca Basin. Geospatial integration of these geochemical signatures with regional lineaments and the exploration model highlights that they: 1) correspond with known uranium occurrences and deposits; 2) occur in the exposed and near-surface rocks, including locations overlying ore at significant depths; and 3) correspond with lineament traces and highlight lineament intersections that are fertile for uranium enrichment.

Geochemical Signature 1 illustrates uranium enrichment relative to thorium, emphasizing two distinct types of uranium anomalism. Geochemical Signature 2 illustrates yttrium enrichment relative to phosphorous, which reflects chemo-stratigraphic signatures in the upper Athabasca Group and also displays a spatial (and perhaps temporal) association with known zones of uranium mineralization. Geochemical Signatures 3 and 4, represented by magnesium behaviour relative to lithium, and copper behaviour relative to cobalt, respectively, provide further refinement of the proximal to distal alteration signatures around known deposits.

Introduction

The analysis of large, public datasets can provide important context for deposit-focussed studies that define and refine techniques used to identify mineral exploration targets. The regional lithogeochemistry of the Athabasca Group of northern Saskatchewan was examined to define inter-element relationships that are significant to unconformity-associated uranium mineralization. Taking advantage of the continual advances in analytical techniques that permit accurate determination of lower concentrations and broader suites of elements, this study builds on earlier work such as Sopuck et al. (1983) and Clark (1987). Using only near-total digestion, multi-element data, inter-element behaviour patterns were primarily identified using statistical and spatial Exploratory Data Analysis techniques. The spatial distribution of multi-element signatures in the upper 50 m of bedrock were plotted relative to Athabasca Group stratigraphy, structural features, and known uranium occurrences in order to highlight key relationships. Several geochemical signatures are defined herein and are cumulatively significant in that: 1) they are present in the exposed and near-surface rocks of the Athabasca Basin; 2) correspond with inferred and/or known structures, and highlight structural intersections that are the loci for uranium mineralization; and 3) record potential linkages between diagenetic-hydrothermal alteration in certain sedimentary formations and uranium deposition.

Data and Methodology

The lithogeochemical data for the Athabasca Group used in this study were taken from the Athabasca Uranium Geochemistry (AUG) database (Wright et al., 2014; in press), a regional compilation of lithogeochemical data for the Athabasca Basin based on public and assessment file sources. The element relationships within the Athabasca Group data discussed in this report were identified primarily through: 1) the identification of elements currently important to the uranium exploration model (e.g. Jefferson et al., 2007), and/or 2) the application of Exploratory Data Analysis techniques (Tukey, 1977), including scatterplots, boxplot analysis, and multivariate correlation analyses to identify distinct element patterns. Numerous inter-element relationship groups were identified but only a select group were chosen for further discussion in this report. The definition of thresholds for each of the parameters discussed in this report is based primarily on statistical differences in sample populations related to Athabasca Group stratigraphy, where defined within the AUG Database. Additional and/or alternate criteria for threshold definition are described below for each element system. To emphasize the regional significance and application of the signatures identified, only those samples within 50 metres of surface were modeled spatially relative to the stratigraphy, structure, and known areas of uranium mineralization within the Athabasca Basin (Annesley et al., 2005; Jefferson et al., 2007; Ramaekers et al., 2007; Bosman et al., 2012; Sask. Geol. Atlas, 2013).

Geochemical Signature 1: Uranium – Thorium Behaviour

Cuney (2010) emphasized the importance of modeling uranium content relative to thorium, which reflects the primary association of these elements under igneous conditions, and the preferred mobility of hexavalent uranium (U^{6+}) under hydrothermal, oxidizing conditions (Grandstaff, 1976; Romberger, 1984). Uranium-thorium relationships within the Athabasca Group are defined in Figure 1, illustrating dif-

Wright, D.M. and Potter, E.G., 2015. Application of regional geochemical datasets to uranium exploration in the Athabasca Basin, Saskatchewan, *in* Targeted Geoscience Initiative 4: unconformity-related uranium systems, (ed.) E.G. Potter and D.M. Wright; Geological Survey of Canada, Open File 7791, p. 14–20. doi:10.4095/295776

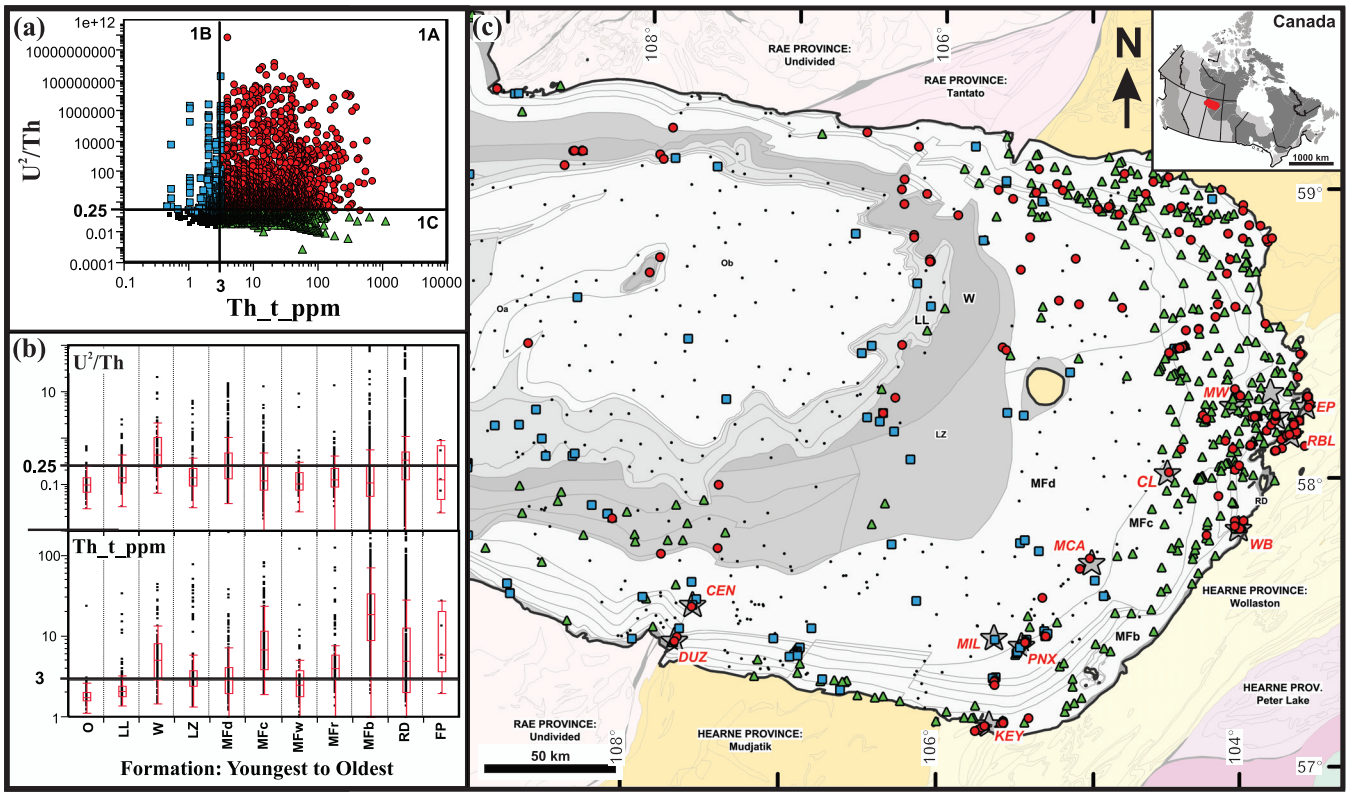

Figure 1: Statistical and spatial associations of Geochemical Signature 1 (U^2/Th vs. Th) features: a) feature scatterplot, b) Athabasca Group Formation boxplots, and c) spatial distribution in surfaces samples (depth < 50 m). Grey stars represent deposits and occurrences (CEN = Centennial, CLF = Cluff Lake, EP = Eagle Point, DUZ = Dufferin Lake Zone, KEY = Key Lake, PNX = Phoenix, MIL = Millennium, MCA = McArthur River, CL = Cigar Lake, WB = West Bear, MW = Midwest, RBL = Rabbit Lake). Athabasca Group (youngest to oldest): Ob – Otherside Fm, Birkbeck Member; Oa – Otherside Fm, Archibald Member; LL – Locker Lake; W - Wolverine Point Fm; LZ – Lazenby Lake Fm; Manitou Falls Formations: MFd –Dunlop Member; MFc – Collins Member; MFb –Bird Member; and RD – Read Formation.

ferences in composite ratio **U^2/Th** [gross uranium multiplied by the ratio of uranium to thorium (U/Th)] versus gross thorium content. A basic threshold for both **U^2/Th** and **Th** are based on distinct differences in statistical populations (Fig. 1b) between the Wolverine Point Formation (X = 25th percentile) and other formations of the Athabasca Group (X = 75th percentile), emphasizing a lithogeochemical boundary within the Athabasca Group. The threshold for **Th** is based solely on the 25th percentile for the Wolverine Point Formation. Uranium enrichment from most known deposits represented in the AUG display both elevated **U^2/Th** ratios and elevated gross thorium contents (Fig. 1: Sub-suite 1A). Subsuite 1A signatures at surface display a clear spatial association with several known uranium deposits located at depth. A second type of uranium enrichment is characterized by elevated **U^2/Th** ratio values, yet lack significant thorium concentrations (Fig. 1: Sub-suite 1B), interpreted to represent uranium mobilized under lower temperature, oxidizing conditions. The distribution of suite 1B samples at surface displays a distal association with known uranium occurrences. Thorium enrichment in the absence of distinct **U^2/Th** enrichment (Fig. 1: Sub-suite 1C) is characteristic of lower Manitou Falls and Read Formations, consistent with the presence of thorium-bearing aluminum phosphate-sulphate (APS) minerals in altered, heavy mineral-rich layers (Mwenifumbo and Bernius, 2007; Yeo et al., 2007; Carson et al., 2002; and references therein).

Geochemical Signature 2: Yttrium – Phosphorous Oxide Behaviour

Fluorapatite or apatite-(CaF) [$Ca_5(PO_4)_3(OH,F,Cl)$] and xenotime [YPO_4] have been identified in several locations in the Athabasca Basin, including the uranium deposits and occurrences (Fayek and Kyser, 1997), the uranium-poor, REE-rich Maw Zone (MacDougall, 1990; Quirt et al., 1991), and the Wolverine Point Formation (Rainbird et al., 2003, 2007; Davis et al., 2008). Aluminum phosphate-sulphate minerals have also been noted throughout the basin and associated with several ore deposits (Wilson, 1985; Gaboreau et al., 2007). The inter-element behaviour of yttrium and phosphorous were examined relative to select immobile elements to model mineralogy associated with hydrothermal alteration (xenotime, fluorapatite and other immobile element-bearing minerals) from mineralogy associated with predominantly diagenetic alteration (e.g. APS minerals). Yttrium-phosphorous relationships within the Athabasca Group are defined in Figure 2, illustrating differences in the composite ratio **Y^2/Th** [gross yttrium (Y) multiplied by the ratio of yttrium to thorium (Y/Th] versus the composite ratio **$P_2O_5^2/TiO_2$** [gross phosphorous oxide (P_2O_5) multiplied by the ratio of phos-

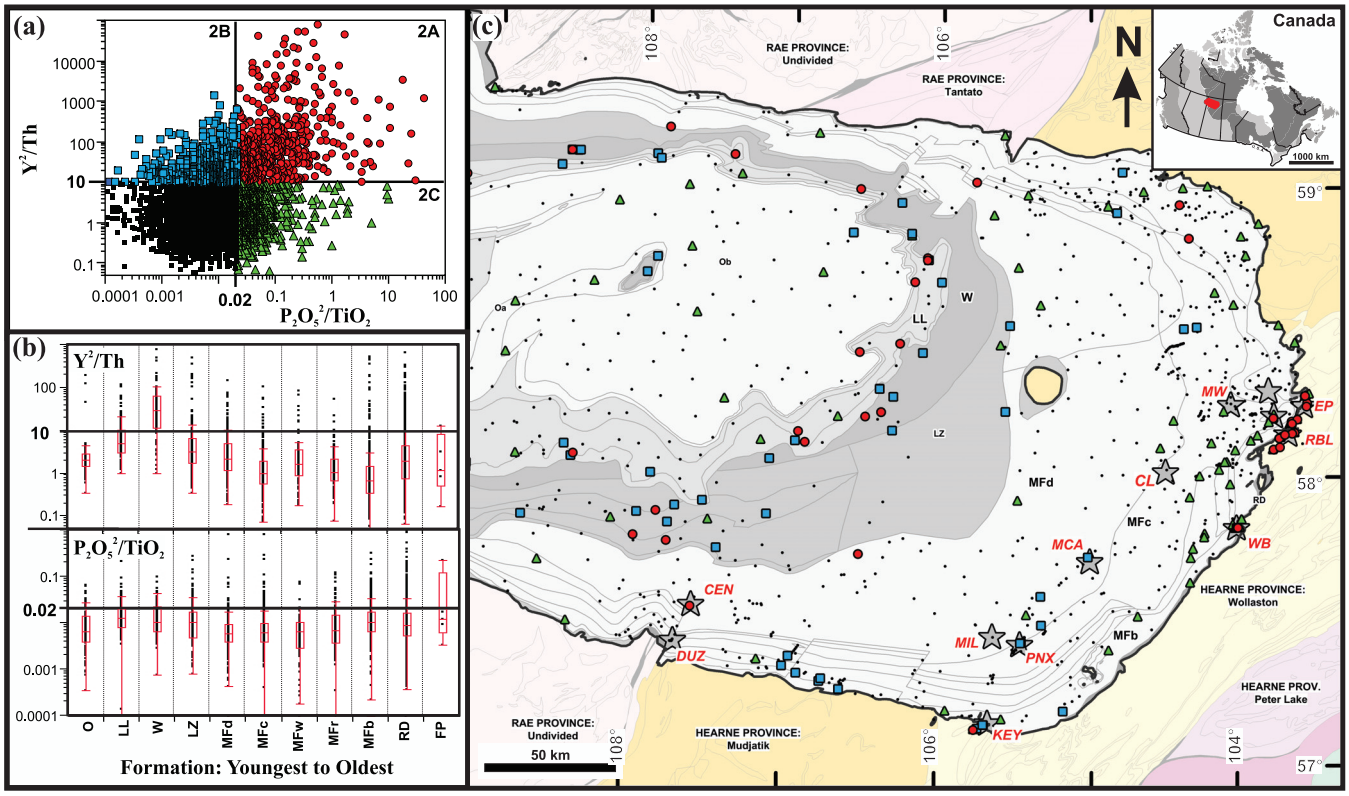

Figure 2: Statistical and spatial associations of Geochemical Signature 2: (Y^2/Th vs. $P_2O_5^2/TiO_2$) features: a) feature scatterplot, b) Athabasca Group Formation boxplots, and c) spatial distribution in surface samples (depth < 50 m). Deposit, occurrence, and stratigraphic labels as per Fig. 1.

phorous oxide to titanium oxide (P_2O_5/TiO_2)]. Basic thresholds for **Y^2/Th** is based on a distinct difference in statistical populations (Fig. 2b) between the Wolverine Point Formation (X = 25th percentile) and other formations of the Athabasca Group (X = 75th percentile), emphasizing a lithogeochemical boundary within the Athabasca Group. The basic threshold for **$P_2O_5^2/TiO_2$** (Fig. 2b) approximates the 75th percentile of most formations of the Athabasca Group, and is intended to represent a more general enrichment of phosphorous independent of lithogeochemical stratigraphy. Relative enrichment of both yttrium and phosphorous (Fig. 2: Sub-suite 2A) perhaps indicate evidence for a strong hydrothermal signature including the presence of xenotime and fluorapatite. This signature is observed in portions of the Wolverine Point Formation and areas of known uranium occurrences. Elevated concentrations of trace elements (including yttrium) have also been observed in sandstones above the Phoenix deposit (Power et al., 2012; Dann et al., 2014). Enrichment of yttrium relative to thorium and phosphorous (Fig. 2: Sub-suite 2B), is perhaps indicative of relict xenotime signatures subjected to later alteration, or overall lower xenotime contents. This signature is more widely spatially associated with the Wolverine Point and Locker Lake Formations, and with areas of known uranium mineralization. Phosphorous enrichment in the absence of yttrium enrichment (Fig. 2: Sub-suite 2C) is interpreted to reflect the genesis and or modification of APS minerals during lower temperature alteration. A wide spatial association with areas of known uranium occurrences is observed in the eastern Athabasca Basin. This feature is observed in all formations, with some linear trends crosscutting stratigraphy (presumably along late structure).

Geochemical Signature 3: Magnesium Oxide – Lithium Behaviour

The inter-element behaviour of magnesium and lithium was primarily examined to model chemical anomalism possibly related to dravite, magnesiofoitite, and chlorite alteration often associated with uranium occurrences in the Athabasca Basin (Jefferson et al., 2007 and references therein). The relationship of boron to magnesium and lithium was also reviewed, but was not presented due to fewer boron analyses in the AUG dataset. Magnesium-lithium relationships within the Athabasca Group are defined in Figure 3, illustrating differences in the composite ratio **MgO^2/Li** [gross magnesium oxide (MgO) multiplied by the ratio of magnesium oxide to lithium (MgO/ Li)] versus gross lithium (**Li**) content. Basic thresholds for both **MgO^2/Li** and **Li** are based on distinct differences in statistical populations (Fig. 1b) between the Wolverine Point Formation (X = 25th percentile) and other formations of the Athabasca Group (X = 75th percentile), emphasizing primarily a lithogeochemical boundary within the Athabasca Group. Relatively elevated magnesium with high lithium concentrations (Fig. 3: Subsuite 3A) display a proximal spatial association with known uranium occurrences (e.g. Phoenix Deposit, Centennial, West Bear). These signatures also reflect enrichment of MgO relative to boron (not shown), likely indicative of a

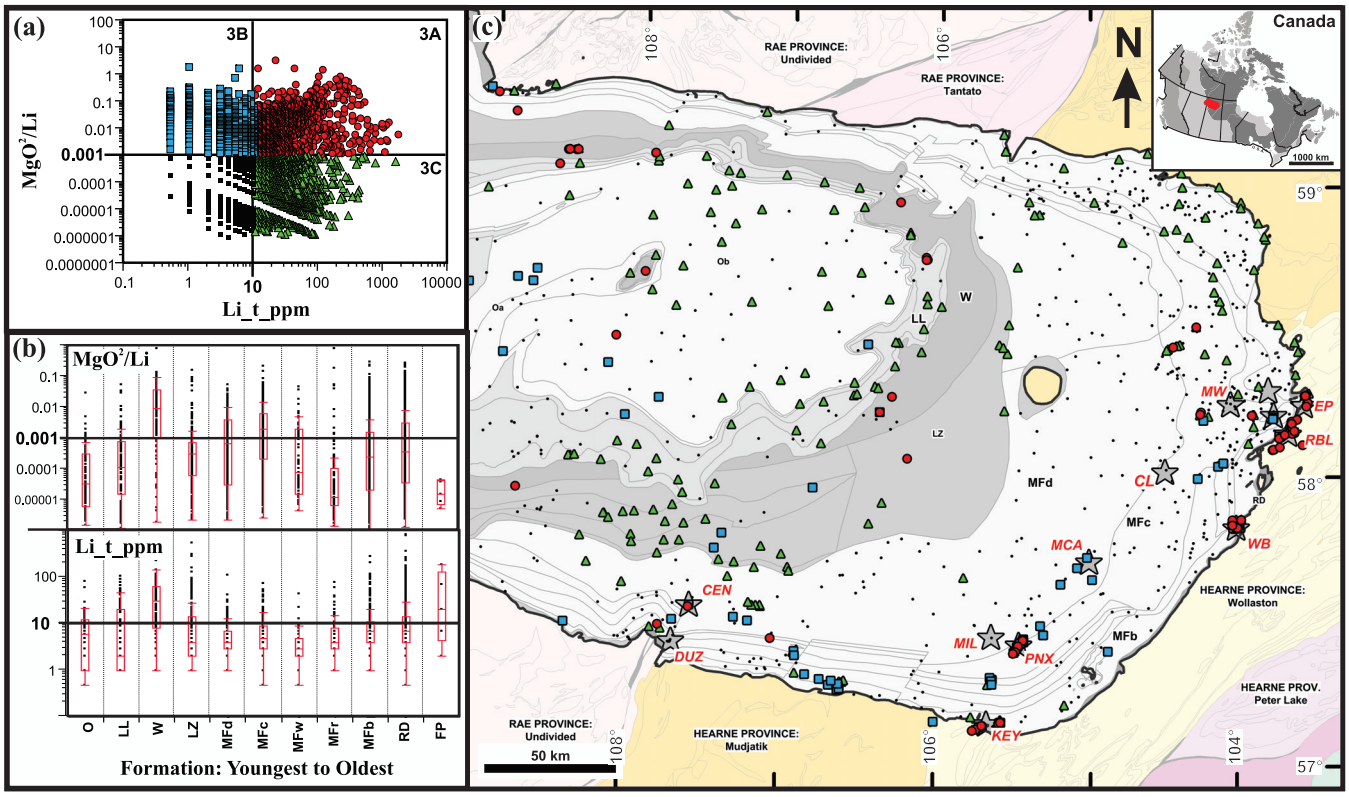

Figure 3: Statistical and spatial associations of Geochemical Signature 3 (MgO^2/Li vs. Li) features: a) feature scatterplot, b) Athabasca Group Formation boxplots, and c) spatial distribution in surface samples (depth < 50 m). Deposit, occurrence, and stratigraphic labels as per Fig. 1.

magnesium-enriched chlorite (c.f. Adlakha et al., 2013). Elevated relative magnesium with *low* lithium contents (Fig. 3: Sub-suite 3B) appear to represent a distal alteration signature, with broad spatial associations with known uranium occurrences that mimics the distribution of dravite in the southeast Athabasca Basin (Earle and Sopuck, 1989; Adlakha et al., 2013). A more direct positive association between magnesium and boron is also observed for the 3B suite (not shown). Gross lithium enrichment in the absence of relative magnesium enrichment (Fig. 3: Sub-suite 3C) is interpreted to represent a possible proxy for late hydrothermal alteration, inferred primarily from the wide spatial distribution of this signature within the upper stratigraphy of the Athabasca Group (excluding the Douglas and Carswell Formations. A distinct and consistent association between lithium, magnesium, and boron is also observed within the Sub-suite 3C samples, and may reflect an important background mineralogical relationship, such as detrital tourmaline within the Athabasca Group (c.f. Sopuck et al., 1983).

Geochemical Signature 4: Copper – Cobalt Behaviour

Base metal enrichment is commonly associated with uranium occurrences in the Athabasca Basin (Jefferson et al., 2007). The inter-element behaviour of copper and cobalt was examined to model the relationships between copper mobility and subtle uranium enrichment. The diagram **Cu^2/Co** vs. **U^2/Th** (Fig. 4) defines three distinct suites in terms of copper-cobalt versus uranium-thorium behaviour within the Athabasca Group. Copper-cobalt relationships within the Athabasca Group are defined in Figure 4, illustrating differences in the composite ratio **Cu^2/Co** [gross copper (Cu) multiplied by the ratio of copper to cobalt (Cu/Co)] versus the composite ratio **U^2/Th** [gross uranium (U) multiplied by the ratio of uranium to thorium (U/Th)]. A basic threshold for **Cu^2/Co** (Fig. 4b) approximates the 75th percentile of most formations of the Athabasca Group, and is intended to represent a more general enrichment of copper, independent of lithogeochemical stratigraphy. The basic threshold for **U^2/Th** is identical to that defined above. Elevated relative copper *with* sympathetic uranium enrichment (Fig. 4: Sub-suite 4A) suggests that some copper enrichment may be directly related to uranium enrichment processes (e.g. Geochemical Signature 1). Elevated copper contents have been reported in soils above the Cigar Lake and Phoenix deposits (Bonham-Carter and Hall, 2010; Power et al., 2012). Elevated relative copper without sympathetic weak uranium enrichment (Fig. 4: Sub-suite 4B) may represent more distal copper alteration related to uranium ore-forming processes, or localized copper enrichment related to the alteration of other copper-bearing features. Weak uranium enrichment in the absence of relative copper enrichment (Fig. 4: Sub-suite 4C) is interpreted to represent a lower temperature, perhaps diagenetic or remobilization phase, inferred primarily from the wide spatial distribution of this signature.

Spatial and Temporal Geochemical Associations

Composite geochemical features based on the inter-element signatures described above display broad temporal and

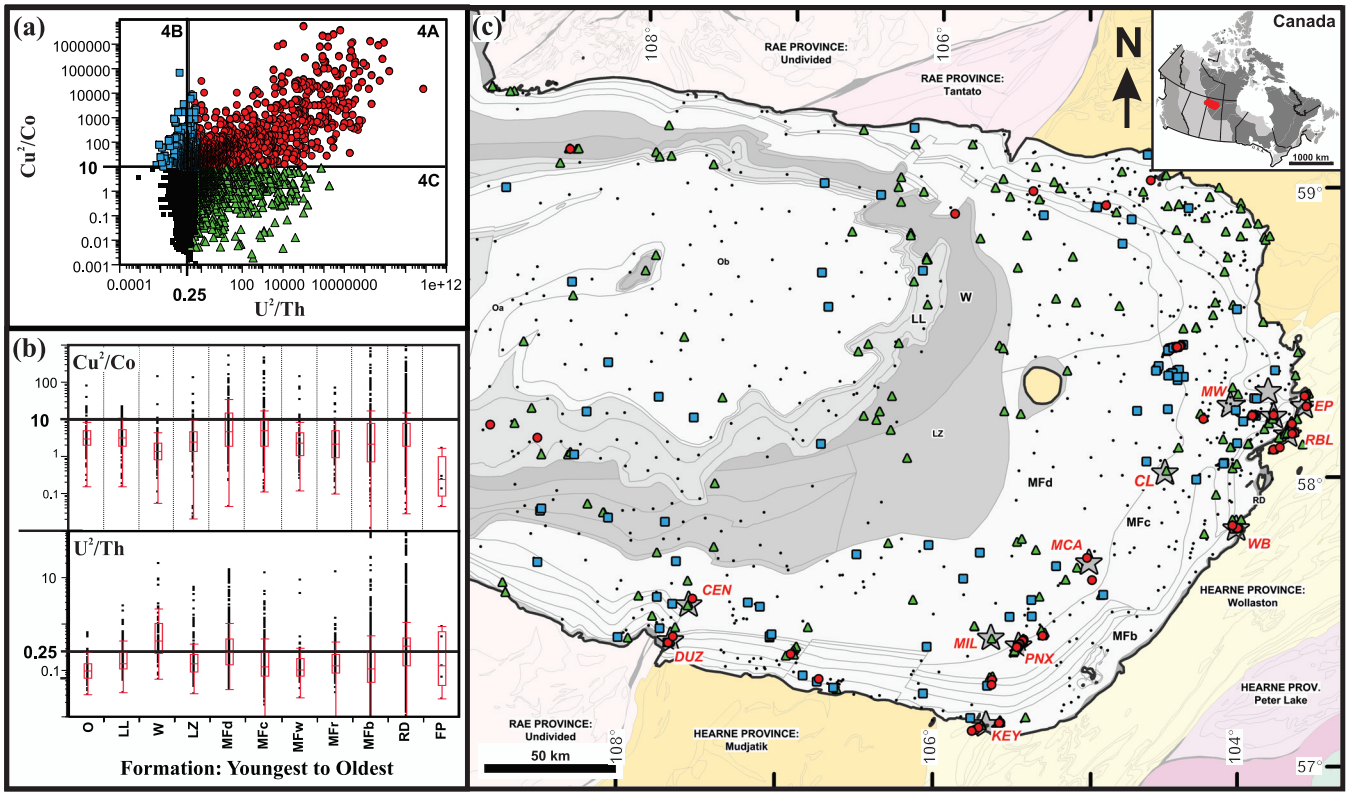

Figure 4: Statistical and spatial associations of Geochemical Signature 4 (Cu^2/Co vs. U^2/Th) features: a) feature Scatterplot, b) Athabasca Group Formation boxplots, c) spatial distribution in surface samples (depth < 50 m). Deposit, occurrence, and stratigraphic labels as per Fig. 1.

spatial associations with known uranium occurrences, stratigraphy, and structure within the Athabasca Basin (Fig. 5). These associations are important to applying these geochemical signatures to active exploration projects, evaluating the intensity and concentrations of these signatures relative to potential uranium deposits. In addition, elevated Y^2/Th signatures suggest a genetic and temporal relationship between high-grade uranium mineralization and the Wolverine Point and Locker Lake Formations of the Athabasca Group.

Most high-grade occurrences captured in the AUG dataset display a combined signature of both elevated U^2/Th and elevated Y^2/Th values (Fig.5; Geochemical Feature 1). Samples of the Read and Manitou Falls Formations at surface with this combined signature display a spatial association with known deposits at depth (Fig. 5). Elevated U^2/Th and Y^2Th also occur within the Wolverine Point and Locker Lake Formations (Signature 1a), but are considered more likely a coincidental feature than indicative of higher-grade uranium mineralization (discussed in more detail below).

A more distal pattern of uranium enrichment in the absence of relative yttrium enrichment (Fig. 5: Geochemical Feature 2) is interpreted to represent the higher mobility of hexavalent uranium relative to thorium and associated high field strength elements (such as yttrium) under low temperature, oxidizing conditions (i.e. remobilizing fluids). At surface, the spatial distribution of this type of uranium enrichment signature is observed distal to known deposits along known and inferred structural conduits at surface (Fig. 5; Geochemical Feature 2). The occurrence of elevated U^2/Th ratios within the Wolverine Point and Locker Lake formations is considered to be probably more associated with this group (Fig.5; Signature 2a), where remobilized uranium has overprinted the chemostratigraphic Y^2/Th signature.

A distal composite alteration feature is represented by relative phosphorous, magnesium oxide, and copper enrichment (Fig. 5; Geochemical Feature 3). A spatial association of this composite alteration feature correspond to late structures, consistent with 070°- and 110–120°-trending lineament features (e.g. Portella and Annesley, 2000; Annesley et al., 2005). This distal alteration crosscuts all units of the Athabasca Group, suggesting that they represent a later alteration event that has been mobilized along pre-existing structures.

A temporal and genetic relationship is implied by an elevated yttrium signature common to the Wolverine Point Formation, Locker Lake Formation, and zones of higher-grade uranium mineralization (Fig. 5: Geochemical Features 1 and 4). Elevated Y^2/Th signatures observed in the Wolverine Point and Locker Lake Formations, are suggested to be associated with xenotime and fluorapatite cements in these units (Jefferson et al., 2007) providing a chemo-stratigraphic marker. This chemo-stratigraphic signature may share a genetic association with the enrichment of Y, Th, and other high field strength/incompatible elements observed with high-grade uranium mineralization (Jefferson et al., 2007). Within the Wolverine Point Formation, intraclast zircon grains (1644 ± 13 Ma; Rainbird et al., 2007) are broadly con-

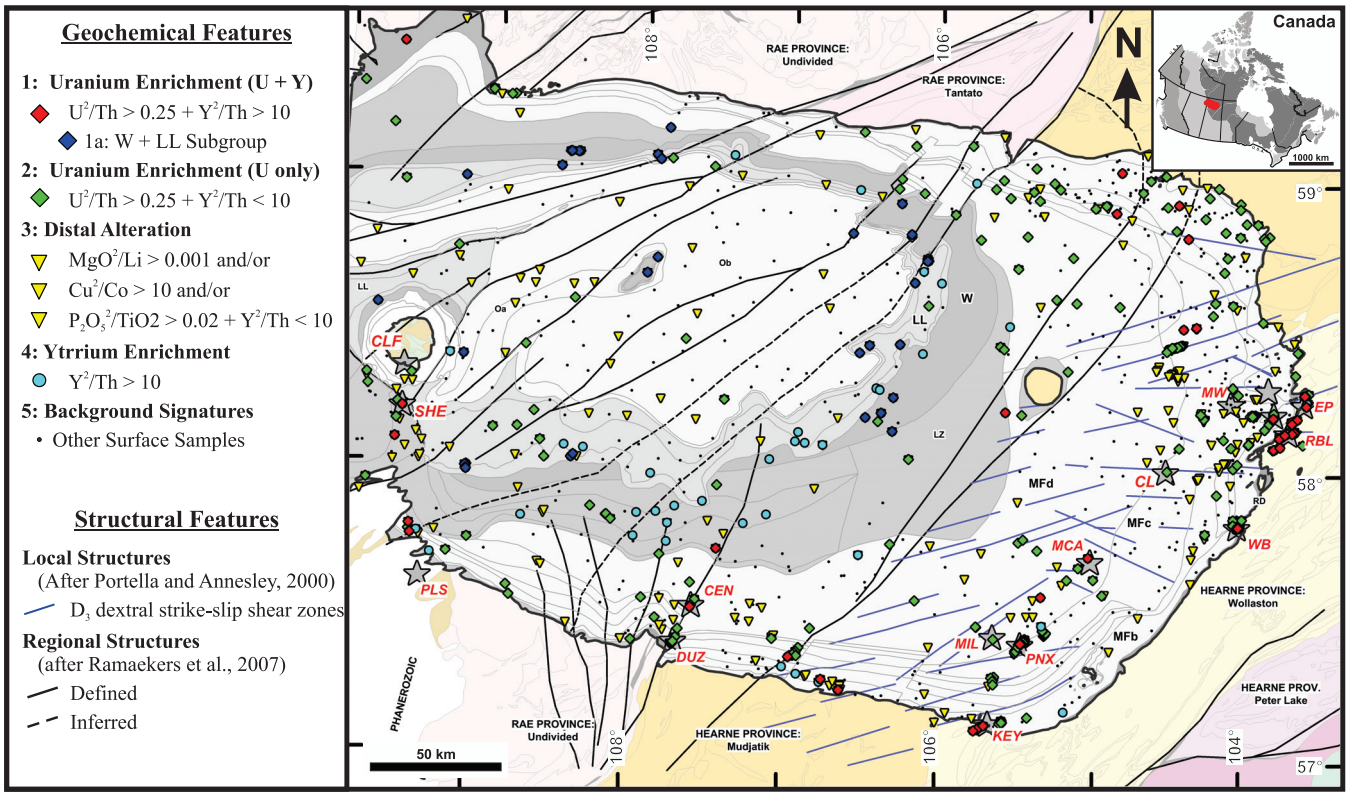

Figure 5: Spatial synthesis of composite geochemical features relative to lithology, structure, and known mineral deposit locations in the Athabasca Basin. Deposit, occurrence, and stratigraphic labels as per Fig.1.

current with diagenetic fluorapatite cements (1640–1620 Ma; Rainbird et al., 2003; Davis et al., 2008), both of which are broadly contemporaneous with the timing of pre-ore alteration (1730–1590 Ma; Alexandre et al. 2009) around major uranium deposits in the Athabasca Basin. The unconformable contact at the top of the Locker Lake Formation, demarcated by the 1544 ± 13 Ma Douglas Formation (Creaser and Stasiuk, 2007), indicates a significant hiatus prior to deposition of the Otherside Formation, which may explain the absence of elevated Y^2/Th ratio values in this later unit.

Acknowledgments

Funding for this research was provided by the Targeted Geoscience Initiative 4 (TGI-4), uranium ore systems project and benefitted from discussions with C.W. Jefferson, J.E. Campbell, S.A. Bosman and C.D. Card. Constructive reviews by C.J.M. Lawley and E.C. Grunsky improved the final submission.

References

Adlakha, E.E., Hattori, K., and Potter, E.G., 2013. Fluid evolution recorded by alteration minerals along the P2 reverse fault and associated with the McArthur River U deposit; Mineralogical Magazine, v. 77, p. 558.

Alexandre, P., Kyser, K., Thomas, D., Polito, P. and Marlatt, J., 2009. Geochronology of unconformity-related uranium deposits in the Athabasca Basin, Saskatchewan, Canada and their integration in the evolution of the basin; Mineralium Deposita, v. 44, p. 41–59

Annesley, I.R., Madore, C., and Portella, P., 2005. Geology and thermotectonic evolution of the western margin of the Trans-Hudson Orogen: evidence from the eastern sub-Athabasca basement, Saskatchewan; Canadian Journal of Earth Sciences, v. 42, p. 573–597.

Bonham-Carter, G., and Hall, G., 2010. Multi-media techniques for direct detection of covered unconformity uranium deposits in the Athabasca Basin, Phase III, Final report of results of soil geochemistry using selective leaches; Canadian Mining Industry Research Organization (CAMIRO) Exploration Division, 280 p. <https://www.appliedgeochemists.org/index.php/publications/other-publications/2-uncategorised/116-camiro-project-08e01>

Bosman. S.A., Card, C.D., MacKnight, S.G., and Boulanger, S., 2012. The Athabasca Basin ore-systems project: an update on geochemistry, spectral data, and core logging; in Summary of Investigations 2012, Volume 2, Saskatchewan Geological Survey, Sask. Ministry of the Economy, Misc. Rep. 2012-4.2, Paper A-5, 10p, <http://economy.gov.sk.ca/SOI2012V2_A5>

Carson, J.M., Holman, P.B., Ford, K.L., Grant, J.A., and Shives, R.B.K., 2002. Airborne Gamma Ray Spectrometry Compilation Series, Wollaston Lake, Saskatchewan; Geological Survey of Canada, Open File 4253, scale: 1:1 000 000.

Clark, L.A.C., 1987. Near surface lithogeochemical halos as an aid to discovery of deeply buried unconformity-type deposits, Athabasca Basin, Canada; Journal of Geochemical Exploration, v. 28, p. 71–84.

Creaser, R.A. and Stasiuk, L.D., 2007. Depositional age of the Douglas Formation, northern Saskatchewan, determined by Re–Os geochronology; in EXTECH IV: geology and uranium EXploration TECHnology of the Proterozoic Athabasca Basin, Saskatchewan and Alberta, (ed.) C.W. Jefferson and G. Delaney; Geological Survey of Canada Bulletin, v.588, p. 341–346.

Cuney, M., 2010. Evolution of uranium fractionation processes through time: driving the secular variation of uranium deposit types; Economic Geology, v. 105, p. 553–569.

Dann, J., Hattori, K., Potter, E.G., and Sorba, C., 2014. Discrimination of Elemental Assemblages in the Alteration Halo of the Phoenix Deposit, Saskatchewan, Through Applied GIS; Geological Survey of Canada, Open File 7463. doi:10.4095/293122

Davis, W.J., Rainbird, R.H., Gall, Q., and Jefferson, C.W., 2008. In situ U-

Pb dating of diagenetic apatite and xenotime: Paleofluid flow history within the Thelon, Athabasca, and Hornby Bay basins; Goldschmidt Conference Abstract.

Earle, S. and Sopuck, V., 1989. Regional lithogeochemistry of the eastern part of the Athabasca Basin uranium province, Saskatchewan, in Uranium resources and geology of North America, (ed.) E. Muller-Kahle; International Atomic Energy Agency, TECDOC-500, p. 263–269.

Fayek, M., and Kyser, T.K., 1997. Characterization of multiple fluid-flow events and rare-earth-element mobility associated with formation of unconformity-type uranium deposits in the Athabasca Basin, Saskatchewan; The Canadian Mineralogist, v.35, p. 627–658.

Gaboreau, S., Cuney, M., Quirt, D., Beaufort, D., Patrier, P., and Mathieu, R., 2007. Significance of aluminum phosphate-sulfate minerals associated with U unconformity-type deposits: the Athabasca basin, Canada; American Mineralogist, v. 92, p. 267–280.

Geological Atlas of Saskatchewan. Saskatchewan Geological Survey, Sask. Ministry of Energy and Resources, Misc. Rep. 2013-7 <http://economy.gov.sk.ca/geological_atlas>.

Grandstaff, D.E., 1976. A kinetc study of the dissolution of uraninite; Economic Geology, v.71, p. 1493–1506.

Jefferson, C.W., Thomas, D.J., Gandhi, S.S., Ramaekers, P., Delaney, G., Brisbin, D., Cutts, C., Portella, P., and Olson, R.A. 2007. Unconformity-associated uranium deposits of the Athabasca Basin, Saskatchewan and Alberta; in EXTECH IV: geology and uranium EXploration TECHnology of the Proterozoic Athabasca Basin, Saskatchewan and Alberta, (ed.) C.W. Jefferson and G. Delaney; Geological Survey of Canada Bulletin, v.588, p. 23–68.

MacDougall, D.G., 1990. Rare earth mineralization in the Athabasca Group – Maw Zone, in Summary of Investigations 1990: Saskatchewan Geological Survey, Saskatchewan Energy and Mines; Miscellaneous Report 90-4, p. 103–105.

Mwenifumbo, C.J., and Bernius, G., 2007. A Th rich crandallite group mineral: a source of thorium enrichment in the Athabasca Group, Saskatchewan; in EXTECH IV: geology and uranium EXploration TECHnology of the Proterozoic Athabasca Basin, Saskatchewan and Alberta, (ed.) C.W. Jefferson and G. Delaney; Geological Survey of Canada Bulletin, v.588, p. 521–532.

Portella, P., and Annesley, I.R., 2000. Paleoproterozoic tectonic evolution of the eastern sub-Athabasca basement, northern Saskatchewan: Integrated magnetic, gravity, and geological data; in GeoCanada: The Millennium Geoscience Summit: Joint meeting of the Canadian Geophysical Union, Canadian Society of Exploration Geophysicists, Canadian Society of Petroleum Geologists, Canadian Well Logging Society, Geological Association of Canada and the Mineralogical Association of Canada, Calgary, Alberta, Canada, 4 p.

Power, M.J., Hattori, K., Sorba, C., and Potter, E.G., 2012. Geochemical anomalies in soils and uppermost siliciclastic units overlying the Phoenix uranium deposit, Athabasca Basin, Saskatchewan; Geological Survey of Canada, Open File 7257. doi:10.4095/291981

Quirt, D., Kotzer, T., and Kyser, T.K., 1991. Tourmaline, phosphate minerals, zircon and pitchblende in the Athabasca Group: Maw Zone and McArthur River areas, in Summary of Investigations 1991; Saskatchewan Geological Survey, Saskatchewan Energy and Mines, Report 91-4, p. 181-191.

Rainbird, R.H., Rayner, N., and Stern, R.A., 2003. SHRIMP U-Pb geochronology of apatite cements and zircon bearing tuff clasts in sandstones from the Athabasca Group, Athabasca Basin, northern Saskatchewan and Alberta; Saskatchewan Industry Resources, Open House, December 1-3, 2003, Saskatoon, Proceedings, p. 6

Rainbird, R.H., Stern, R.A., Rayner, N., and Jefferson, C.W., 2007. Age, provenance, and regional correlation of the Athabasca Group, Saskatchewan and Alberta, constrained by igneous and detrital zircon geochronology; in EXTECH IV: geology and uranium EXploration TECHnology of the Proterozoic Athabasca Basin, Saskatchewan and Alberta, (ed.) C.W. Jefferson and G. Delaney; Geological Survey of Canada Bulletin, v.588, p. 193–210.

Ramaekers, P., Jefferson, C.W., Yeo, G.M., Collier, B., Long, D.G.F., Drever, G., McHardy, S., Jiricka, D., Cutts, C., Wheatley, K., Catuneanu, O., Bernier, S., Kupsch, B. and Post, R.T., 2007. Revised geological map and stratigraphy of the Athabasca Group, Saskatchewan and Alberta; in EXTECH IV: geology and uranium EXploration TECHnology of the Proterozoic Athabasca Basin, Saskatchewan and Alberta, (ed.) C.W. Jefferson and G. Delaney; Geological Survey of Canada Bulletin, v.588, p. 155–191.

Romberger, S.B., 1984. Transport and deposition of uranium in hydrothermal systems of temperatures up to 300°C: geological implications; in Uranium Geochemistry, Resources, (ed.) B. de Vivo, F. Ippolito, G. Capaldi and P.R. Simpson; The Institution of Mining and Metallurgy, London, UK, p. 12–17.

Sopuck, A.J., de Carla, A., Wray, E.M., and Cooper, B., 1983. The application of lithogeochemistry in the search for unconformity-type uranium deposits, northern Saskatchewan, Canada; Journal of Geochemical Exploration, v. 19, p. 77–99.

Tukey, J.W., 1977. Exploratory Data Analysis, Addison-Wesley, Reading, Massachusetts, 688 p.

Wilson, J.A., 1985. Crandallite group minerals in the Helikian Athabasca Group in Alberta, Canada; Canadian Journal of Earth Science, v. 22, p. 637–641.

Wright, D.M., Potter, E.G., and Comeau, J-S., 2014. Athabasca Basin Uranium Geochemistry Database; Geological Survey of Canada, Open File 7495. doi:10.4095/293345

Wright, D.M., Potter, E.G., and Comeau, J-S., in press. Athabasca Basin Uranium Geochemistry Database v.2; Geological Survey of Canada, Open File 7792.

Yeo, G.M., Jefferson, C.W. and Ramaekers, P., 2007. Comparison of lower Athabasca Group stratigraphy among depositional systems, Saskatchewan and Alberta; in EXTECH IV: geology and uranium EXploration TECHnology of the Proterozoic Athabasca Basin, Saskatchewan and Alberta, (ed.) C.W. Jefferson and G. Delaney; Geological Survey of Canada Bulletin, v.588, p.465–488.

Geomathematical Study of Sandstones Overlying the Phoenix Uranium Deposits and the REE-rich Maw Zone, Athabasca Basin, Saskatchewan

Shishi (Chris) Chen[1], Keiko Hattori[1], Eric C. Grunsky[2] and Yongxing Liu[3]

1. Department of Earth Sciences, University of Ottawa, 25 Templeton Street, Ottawa, Ontario, K1N 6N5

2. Geological Survey of Canada, 601 Booth Street, Ottawa, Ontario, K1A 0E8

3. Denison Mines Corporation, 230 22nd Street East, Suite 200, Saskatoon, Saskatchewan, S7K 0E9

Abstract

To evaluate the relationship between the enrichment of REEs and U mineralization, we carried out Principal Component Analysis (PCA) of sandstones above the Phoenix U deposits and in the REE-rich Maw Zone in the eastern Athabasca Basin. The Phoenix deposits, with indicated resources of 70.2 M lbs U_3O_8, occur along the unconformity and a steeply dipping fault in the basement at ca. 400 m depth. The Maw Zone, a breccia pipe with surface exposure of 300 by 200 m, consists of highly silicified, hematitized, dravitic tourmaline-rich rocks with high REE (<8.1 wt. % as total REE oxides). The Maw Zone is ca. 4 km southwest from the south end of Phoenix deposits and does not contain high U (< 7.8 ppm U) contents. PCA of sandstones above the Phoenix deposits shows that U is associated with Heavy REEs (HREE)+Y, Light REEs (LREE) and Pb, and inversely correlated with Ti, Zr, Al, and Th. The Maw Zone displays different element groupings as revealed by PCA: U is strongly correlated with V, Cr, Fe, Ni, Cu, Cd, Na, Li and Ba, but very weakly correlated with HREEs+Y, and inversely with LREEs and P. Relative enrichment of HREEs, Y, and P suggests xenotime is the predominant host of the HREEs. The grouping of LREEs+Sr+Th+P suggests the occurrence of monazite and/or aluminum phosphate-sulphate (APS) minerals. A mineralogical study confirmed xenotime and APS minerals as the major host of HREEs and LREEs, respectively. These REE-bearing minerals precipitated from hydrothermal fluids during the brecciation of hematitized sandstones. The positive association between U and Fe in the PCA plot from the Maw Zone suggests that U was transported by oxidized fluids. The absence of U mineralization in the Maw Zone is explained by low U in the oxidizing fluids, or a lack reducing fluids to precipitate U.

Introduction

The Athabasca Basin is a large Paleo- to Mesoproterozoic sandstone basin that occupies much of the northernmost quarter of Saskatchewan and a smaller portion of northeastern Alberta. The Phoenix deposits are typical of sandstone-hosted unconformity-related U deposits in the basin (e.g. Kerr, 2010) which can host significant concentrations of rare earth elements (REE) due to their ability to substitute for uranium (U) in the ore mineral uraninite (Fayek and Kyser, 1997; Hanly and Hagni, 2002). The rare earth element-enriched Maw Zone is located only 4 km southwest of the Phoenix deposits but lacks high U contents (< 7.8 ppm U; Denison Mines Corp., 2006). Despite some features in common, such as hematite, xenotime, tourmaline and euhedral quartz alteration assemblages in the sandstone host rocks, the relationship between the two types of mineralization is not clear (Quirt et al., 1991). Previous studies have proposed the Maw Zone is a near-surface expression of processes that also resulted in unconformity-related U mineralization (McDougall, 1990; Hanly, 2001). Using the methodology outlined by Grunsky (2010), principal component analysis (PCA) was applied to evaluate the behavior of elements in sandstones overlying the Phoenix U deposits and those in the REE-rich Maw Zone. First introduced by Pearson (1901), PCA can reduce the dimensionality of a dataset with a large number of variables, while retaining as much as possible of the variation in the variables (Jolliffe, 1986). Further refinements in PCA methodology resulted in the creation of the biplot (Gabriel (1971) that combines the loadings of the variables with the scores of the observations on the same diagram. The reduction in the number of variable to describe the variation in the data and the association of the variable facilitates recognition of geological processes responsible for these variables, with several geoscientific applications such as: elemental assemblages associated with geochemical processes, hydrothermal alteration and mineralization (Grunsky, 1986) and evaluation of mineral assemblages in regional stream sediment geochemical data and styles of mineralization (Grunsky et al., 2009; Grunsky, 2010). This paper presents the results of PCA from two deposits located close to each other with different styles of mineralization, compares the elemental assemblages of the two, and discusses the processes important for controlling the U and REE mineralization in each system.

General study area

The study area is located in the eastern Athabasca Basin (Fig. 1). The Maw Zone is located ca. 4 km southwest of the southern end of the Phoenix uranium deposits along the same northeast-trending structure, the WS shear.

Sandstone stratigraphy

In the study area, the Athabasca Basin is comprised of sandstones and conglomeratic sandstones of the Manitou Falls and Read Formations. Three members of the Manitou Falls Formation are recognized, using the parameters of Ramaekers et al. (2007) and are presented in Table 1. The thickness of sandstones overlying the Phoenix deposits is ca. 450 m whereas the total thickness of sandstones at the Maw Zone varies greatly from 202 m in the western part, to over

Chen, S., Hattori, K., Grunsky, E.C., and Liu, Y., 2015. Geomathematical Study of Sandstones Overlying the Phoenix Uranium Deposits and the REE-rich Maw Zone, Athabasca Basin, Saskatchewan, *in* Targeted Geoscience Initiative 4: unconformity-related uranium systems, (ed.) E.G. Potter and D.M. Wright; Geological Survey of Canada, Open File 7791, p. 21–31. doi:10.4095/295776

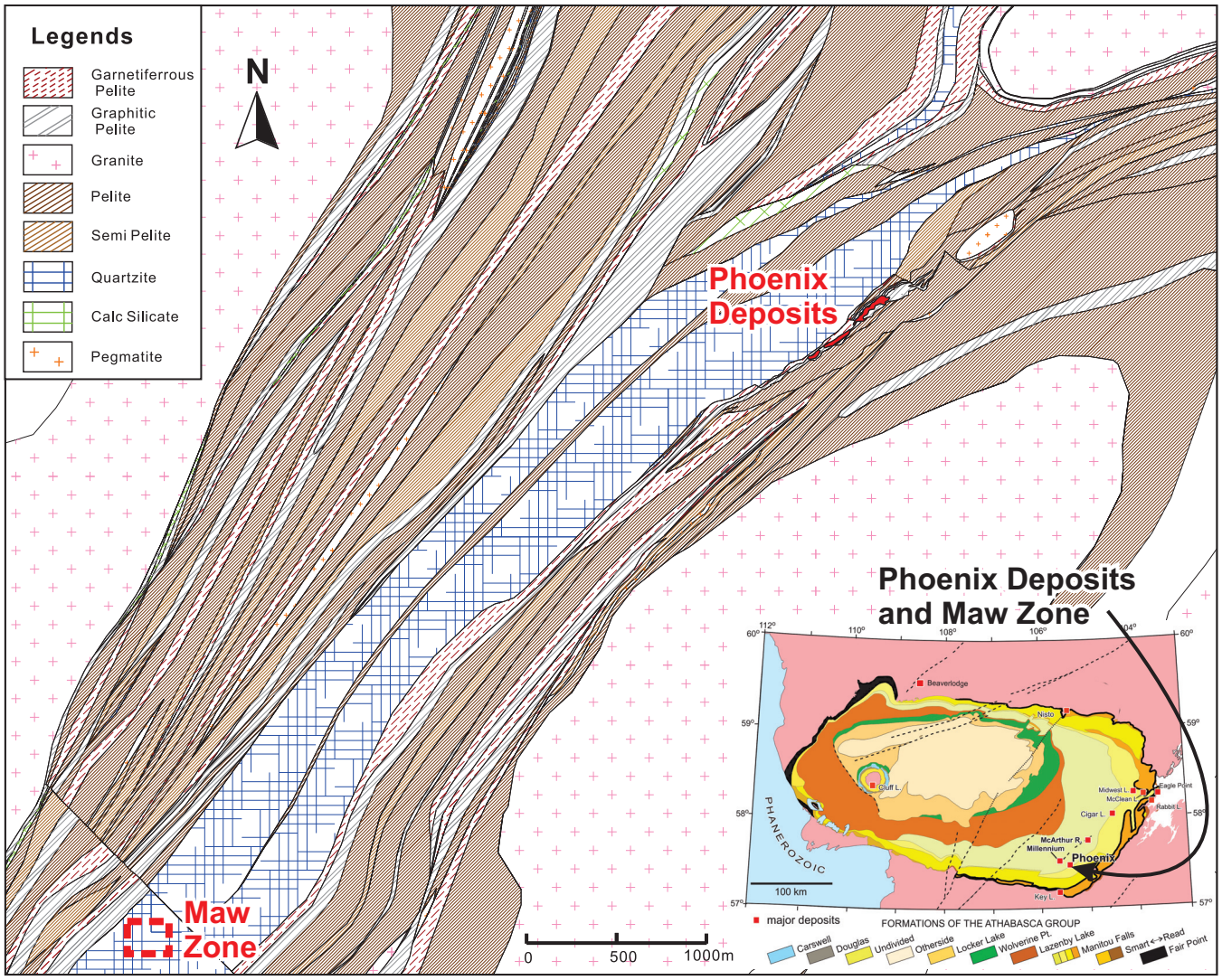

Figure 1. Basement geological map of the Wheeler River Property illustrating the location of the Maw Zone 4 km southwest of the Phoenix Deposit Zone B (Denison Mines Corp., 2014). Inset: Location of the study area within the Athabasca Basin, northern Saskatchewan (after Jefferson et al., 2007).

Table 1. Athabasca Group units in the study area, using classification of Ramaekers et al. (2007).

	Unit (from top to bottom)	Lithology
Manitou Falls Formation	Dunlop Member (MFd)	Fine-grained quartz arenite with abundant (>1 vol. %) clay intraclasts
	Collins Member (MFc)	Quartz arenite with rare (<1 vol. %) clay intraclasts
	Bird Member (MFb)	Interbedded quartz arenite and conglomerate distinguished from the underlying Read Formation and overlying MFc by the presence of at least 1 % to 2 vol. % conglomerate in beds thicker than 2 cm
Read Formation (formerly the MFa Member)		Sequence of poorly sorted quartz arenite and minor conglomerate

300 m in east and north (Denison Mines Corporation, 2006). The large difference in the sandstone thickness is partly due to the presence of a quartzite ridge that was a paleotopographic high prior to deposition of the Athabasca Group but was also displaced by fault reactivation syn- and post-deposition of the sandstones, as noted from the McArthur River and Phoenix deposits (Marlatt et al., 1992; Györfi et al., 2007; Jefferson et al., 2007; Ramaekers et al., 2007; Tourigny et al., 2007; Yeo et al., 2007; Kerr, 2010). A major northeast-trending basement fault directly below the Maw

Zone occurs along a metapelite unit in quartzite, with significant vertical displacement and moderate to steep dip to the east. Sandstones and quartzite close to the fault are brecciated (Barker, 2011).

Phoenix uranium deposits

The Phoenix deposits are unconformity-type uranium deposits lying along the unconformity between the Athabasca Group sandstones and Paleoproterozoic basement rocks at ca. 450 m of depth (Kerr, 2010). Current indicated resources are 70.2 million lbs U_3O_8 at an average grade of 19.13 % U_3O_8 (Roscoe, 2014). Minor amounts of ore also extend from the unconformity into the basement along the WS Shear Zone. Alteration in the sandstones above the deposits is characterized by the formation of kaolinite-group minerals, illite, and dravitic tourmaline (Dann et al., 2014). Basement rocks at the Phoenix deposit are part of the Wollaston Domain and are comprised of metasedimentary and granitoid gneisses. The metasedimentary rocks belong to the Wollaston Supergroup and include graphitic and non-graphitic metapelitic and semipelitic gneisses, meta-quartzite, and rare calcsilicate rocks together with felsic and quartz feldspathic granitoid gneisses (Roscoe, 2014). The basement geology is similar to the Maw Zone and is critical to the unconformity-related U models.

The Maw Zone (REE)

The Maw Zone, with a surface exposure of 300 by 200 m, consists of highly silicified, hematitized, dravitic tourmaline-rich rocks with high REE and Y concentrations (up to 8.1 wt. % as total REE oxides; Agip Canada Ltd, 1985). Despite similar alteration assemblages, host rocks, and proximity to the uranium deposits (Fig. 1), the zone does not contain significantly concentrations of U (< 7.8 ppm U); except for one sample located close to the unconformity at a depth of 320 m (DDH-WR195 with 40.9 ppm U). The most prominent feature of the Maw zone is the intensely brecciated and altered Athabasca sandstones, including large (40 to 90 cm) cross-bedded clasts (McDougall, 1990). The predominant crystalline basement rocks are a succession of variably graphitic, sillimanite-, garnet- and cordierite-bearing, biotite metapelites, semipelites and quartzite (Barker, 2011).

Methodology

Principal Component Analysis

This study applied R (variables or elements in this study)-Q (samples) mode Principal Component Analysis scripts developed by Grunsky (2001) in the R statistical software environment (R Core Team, 2013), and described in detail in Chen et al. (2014). In general, PCA is a multivariate procedure to reduce the dimensionality of a multivariate dataset to a smaller set of summary components, while retaining as much as possible of the variation in the original variables (Jolliffe, 1986). For the Phoenix and Maw Zone datasets, RQ-mode PCA appears to be well-suited for evaluating the elemental association and geological processes associated with the geochemical dataset because it can display the relationships of the samples and elements at the same scale. After a centered log-ratio transformation of the raw data, the elemental assemblages were evaluated using simultaneous RQ-mode PCA. As geochemical data are governed by the stoichiometry of minerals, the elemental assemblages can represent minerals (Grunsky et al., 2008). Geochemical data are compositional in nature and therefore restricted in the positive number space (simplex). Statistics applied to such data are not valid and the use of logratios are required to "open" the data into the real number space in which statistics can be properly applied (Aitchison, 1986). In this study the centred logratio was applied to all of the data prior to any statistical analysis.

Geochemical Datasets

This study uses chemical compositions of sandstones determined at the Saskatchewan Research Council for Denison Mines Corp. using inductively coupled plasma optical emission spectrometry (ICP-MS) and inductively coupled plasma mass spectrometry (ICP-OES) following near total digestion of samples using three acids (HF-HNO_3-HCl). Complete details on the analytical methods can be found in Roscoe (2014). The size of the two datasets and chemical elements used for PCA are listed in Table 2.

Mineralogical Study

Thirty-eight polished thin sections were made from the Maw Zone and 60 from Phoenix site for petrography. They were examined with a petrographic microscope and a JEOL 6610 LV scanning electron microscope (SEM) equipped with an Oxford SDD detector at University of Ottawa.

Results

Sandstones overlying the Phoenix deposits

Sample and variable scores derived from PCA are projected onto the PC1-PC2 axes of Figures 2A and B. The two Principal Components (PC1 and PC2), explain 40.2% of the total variation in the data. The figure shows distinct groupings of elements in four sandstone units. Relative enrichment of U-HREE-Y-Pb occurs along the positive PC1 axis in RD, MFc and MFd units. Relative enrichment of LREE occurs exclusively in the RD, along the positive PC1 and PC2 axes. The enrichments of U and REE are inversely associated with Fe-Mn-Th-Ti-Al-K.

The biplot of PC2-PC3 (accounting for 18.0% of the total variation) shows LREE enrichment along the positive PC2 axis; mostly in the RD and MFb (Figs. 2B, D). The HREEs and Y occur together with high-field strength elements Zr, Hf, Nb, and Th along the negative PC3 axis; mostly in MFc although the element association is weak, with only small number of samples exhibiting this feature (Fig. 2B). This pattern is also expressed weakly for MFb and RD.

Scores of PC1 and PC2 for the data from the RD were plotted in Figure 3. The biplot indicates that there is a relative enrichment of U, Y and HREEs along the positive PC1 axis (Fig. 3A). This enrichment is inversely associated with relative enrichment of K-Fe-Al-Mg-Mn-Ca-Ni-Ga-Zn, which have negative scores of PC1 (Fig.3A). The biplot of PC1-PC2 shows that U is not associated with REEs in the MFb, as relative enrichment of REEs is shown along the

Table 2. Summary of the Phoenix deposits and Maw Zone datasets. Some of the elements were removed from the dataset because concentrations below or close to their detection limits.

	Total number of samples	Number of sandstone samples	Analytical method	Elements used for PCA	Elements removed from dataset	Rare Earth Elements
Phoenix	6718	4630	ICP-OES	Al, Ba, Be, Ca, Cd, Ce, Cr, Cu, Dy, Er, Eu, Fe, Ga, Gd, Hf, Ho, K, La, Li, Mg, mn, na, Nb, Nd, Ni, P, Pb, Pr, Sr, Th, Ti, U, V, Y, Yb, Zn, Zr, B, Sm	Ag, Co, Mo, Sc, Sn, Ta, Tb and W	La, Ce, Pr, Nd, Sm, Eu and Gd (LREE) Dy, Yb, Er and Ho (HREE)
Maw Zone	660	545	ICP-MS	U, Cu, La, Fe, Ni, P, Pb, V, Y, Zn, Al, Ba, Be, Ca, Cd, Ce, Cr, Dy, Er, Eu, Ga, Gd, Hf, K, Li, Mg, Na, Nb, Nd, Pr, Sc, Sm, Sr, Th, Ti, Yb	Ag, Co, Mo, Sn, Ta, Tb, and W	La, Ce, Nd, and Sm (LREE) Dy, Yb, Er, and Gd (HREE)

positive PC1 axis without U (Fig. 3B). There is a positive association of HREE and high-field strength elements (Th-Zr-Ti-Nb). The MFc data shows a weak relative enrichment of U-Pb-Y-HREEs- Hf-Zr and Ni-Na-B-Mg along the positive PC1 axis (Fig. 3C). The biplot of PC1-PC2 for MFd (Fig. 3D) shows relative enrichment of HREEs along the negative PC1 axis and LREEs along the positive PC2 axis. In the MFd, U and Pb are not associated with REEs. Relative U-Pb enrichment is weakly associated with positive PC5 scores (not shown).

Vertical stratigraphic profile of the principal components

When the scores of the first and second principal components are plotted stratigraphically (Fig. 4) , the RD unit generally displays higher PC1 and PC2 scores than upper sandstone units, although there is greater dispersion of RD relative to the other units. Elements in decreasing order of dominance in PC1 are: K, Dy, Er, Fe, Y, Mn, Yb, U, and Th. Elements in decreasing order of dominance in PC2 are: V, Mg, Nd, Sm, P, Sr, Ce, La, Pr, Ni and B. Uranium appears as a dominant element in PC1 together with HREEs and LREEs in PC2. Therefore, PC1 and PC2 represent relative enrichment of U and REEs in the sandstones overlying the Phoenix deposits. Furthermore, U shows positive values in PC1 and PC2 scores, therefore, samples with high positive values of PC1 and PC2 are likely associated with the enrichment of U. The findings may be useful in evaluating the potential for uranium deposits in the area by mapping PC1 and PC2 scores of rocks by interpolation.

Sandstones of the Maw Zone

Relative enrichment of HREEs and Y is observed along the negative PC2 axis in samples from the MFb, MFc and MFd in PC1 vs. PC2 plot (Fig. 5A). These two PCs account for 36.3% of the total information. Figure 5A also shows the separation of HREEs and LREEs, and the fractionation of Eu from the rest of the REE. Sandstones in the Maw Zone show negative Eu anomalies compared to Sm and Gd. LREE enrichment along PC1 and the position of P between HREEs and LREEs suggest that samples contain at least two phosphate phases: HREE-rich xenotime and LREE-rich monazite. The enrichment of Fe is observed in the upper left quadrant in Figure 5A, reflecting hematite which is abundant in all rocks in the Maw Zone. Therefore, the enrichment of Fe is attributed to the presence of an oxidized environment. The PC1 and PC2 loadings for Fe show a distinct location in the upper left quadrant of Figure 5A. This indicates that the concentrations of Fe are relatively higher in rocks plotted towards the upper left quadrant. The sandstone samples plotted towards the upper left are interpreted to be more oxidized.

PC3 and PC4 together account for 18.0% of the total variance. The biplot of PC3 versus PC4 shows that the samples with a relative enrichment in U, LREEs, and P plot along the positive axis of PC3 (Fig. 5B), indicating the likely association of LREEs with monazite or possibly APS minerals. Since U concentrations are low in the Maw Zone, U in monazite may explain this elemental association.

Principal component analysis of the Maw Zone data shows that Sr, Th, Y, the LREEs, Ti, V and U, contribute mostly to the variation of PC1, and the HREEs, P, Y Li, Ni and Ba for PC2. The 3D diagrams of drill holes and scores of PC1 and PC2 of total dataset (Fig. 6) shows negative scores of PC1 and PC2 appear in the upper part of sandstones (MFc and MFd). Since the HREEs and Y show strongly negative scores on PC2, this reflects the occurrence of xenotime in the upper sandstone units.

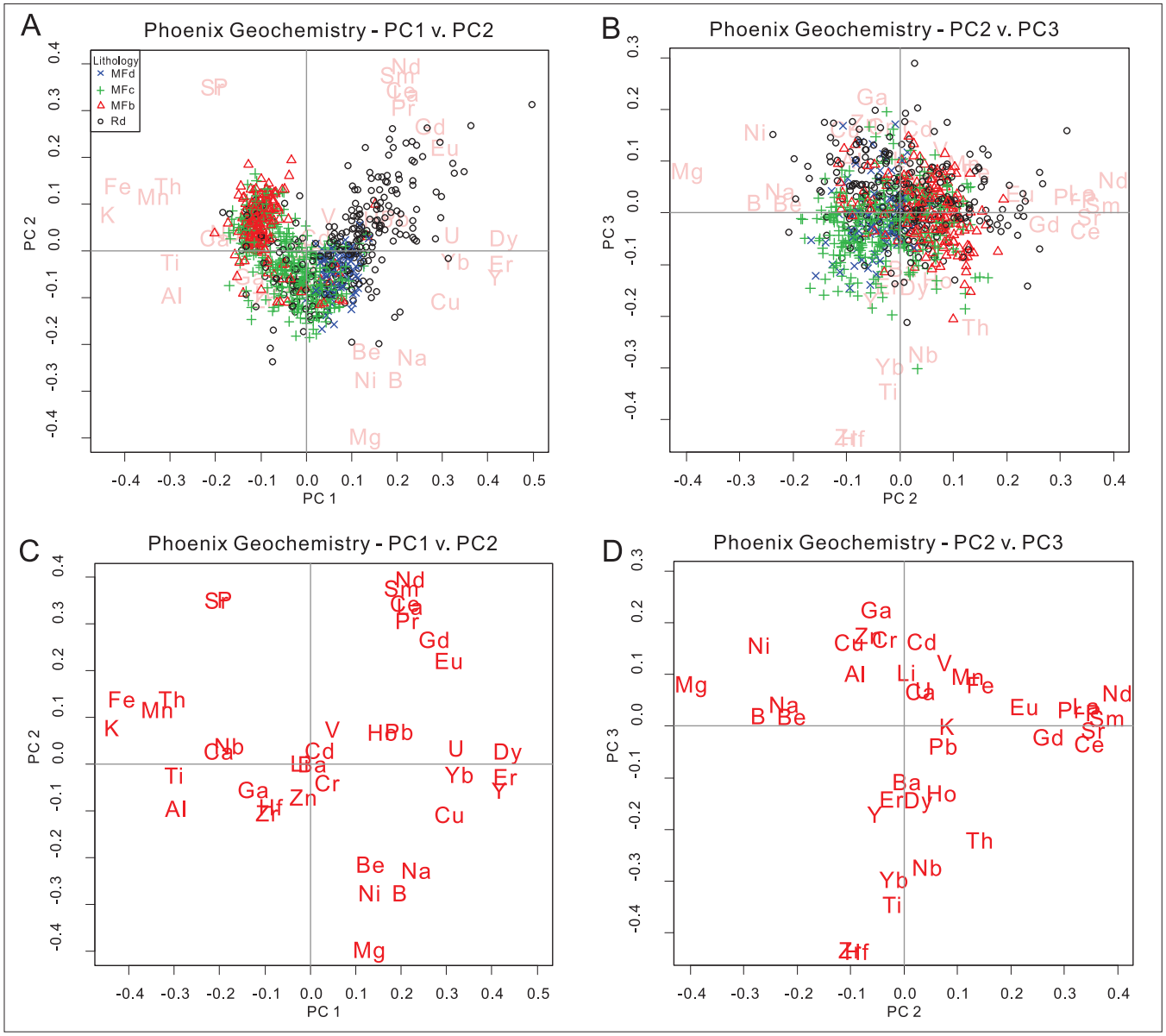

Figure 2. Biplots of PC1 vs. PC2 and PC2 vs. PC3 for the combined sandstones dataset for the Phoenix zone. For the clarity of diagrams, elements are separately shown in C and D. The data were transformed using logcentred ratio.

Minerals containing REE in the Maw Zone

In the Maw Zone, REEs are correlated with P, indicating that monazite, APS and xenotime are the potential carriers of REEs. This is consistent with earlier reports on the occurrence of xenotime and monazite by Quirt et al. (1991) and Hanly (2001). Thin section examination shows REE-bearing minerals are concentrated in buff-colored veinlets that cut hematitized fragments of sandstones. The occurrence suggests that REEs were introduced by reduced fluids that dissolved hematite. Back-scattered electron (BSE) images of xenotime show two different occurrences. Subhedral to euhedral grains of xenotime are spatially associated with detrital zircon grains (Figs. 7A, B, C, F, H). The second type is dissemination in a groundmass of sudoite without any zircon grains (Fig. 7G). The fine-grained xenotime appears to have crystallized late from the hydrothermal fluids. In addition, several small (< 5 μm) grains containing high HREEs and Y were noted. They nucleated on zircon grains and show no P contents in energy-dispersive spectra (EDS) on the SEM. The contents of HREEs and Y are much greater than those of xenotime, suggesting that these grains are most likely the REE carbonate bastnäsite (Figs. 7D, E).

Aluminum phosphate-sulphate minerals were identified as the primary host of LREEs in the Maw Zone. Monazite was not found in our samples. The APS minerals occur as aggregates of small grains in sandstone (Fig. 7A) and in a matrix of magnesio-foitite ± sudoite and illite (Fig 8). Analysis of EDS from the APS minerals indicates that they contain elevated Sr and LREE contents. They also contain SO_4^{2-} and Ca, suggesting that the APS minerals are most likely solid

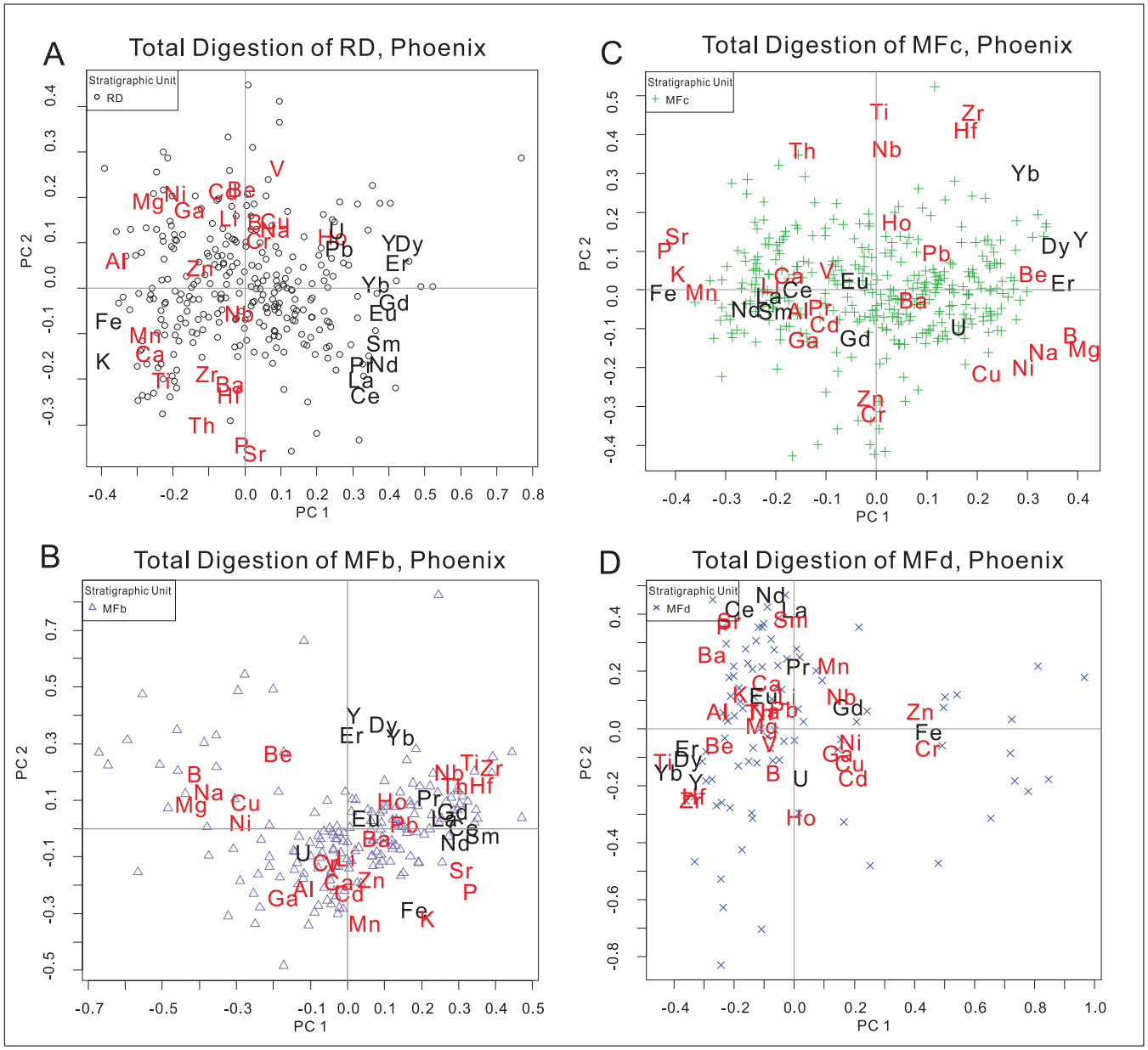

FIGURE 3. Biplots of PC1 vs. PC2 for the RD, MFb, MFc and MFd datasets separately for sandstones overlying the Phoenix deposits. The data were transformed using logcentred ratio.

solutions of svanbergite-florencite. The presence of SO_4^{2-} confirms the oxidized environments for the hydrothermal activity. Core of APS minerals are known to contain high Th (Mwenifumbo and Bernius, 2007). The association of Th and LREE in PCA is consistent with Th hosted by APS minerals.

Discussion and Summary

The PCA shows distinct geochemical signatures in the different sandstone units above the Phoenix deposits: relative enrichment of LREEs, HREEs and Y in RD; P, Sr, Th, Mn, K and Fe in MFb; Ca, Nb, Ti, Al, Zr, and Zn in MFc, Na, B, Ni, Mg and Cr in MFd.

For Maw Zone dataset, most of the relative HREE and Y enrichments occur in MFd and MFc and LREE in RD, MFb and MFc samples. Relative enrichment of HREEs and Y-P occur in the MFb, MFc and MFd samples.

The sandstones above the Phoenix deposits show that U is associated with HREEs+Y, LREEs and Pb, and inversely correlated with Ti, Zr, Hf, Al, and Th. The relative enrichment of K-Fe-Al-Mg-Mn-Ca-Ni-Ga-Zn, which have negative scores of PC1 (Fig.3A), likely reflects the presence of Fe-oxides, sudoite and illite. These minerals are common in altered sandstones overlying the unconformity deposits (Jefferson et al., 2007 and references therein). The location of Ca along the negative PC1 axis may reflect the presence of

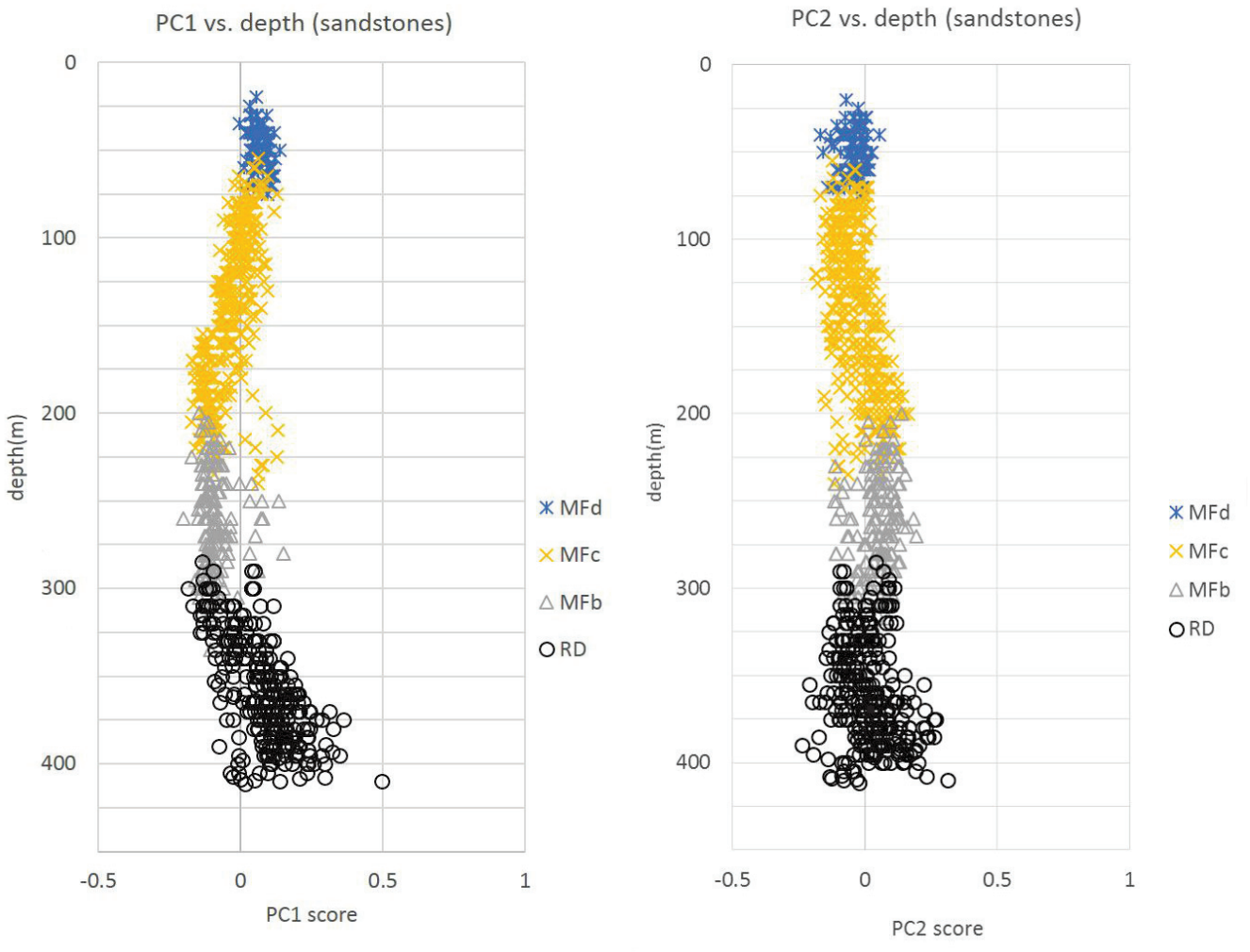

Figure 4. Plots of vertical variations of PC1 and PC2 scores in sandstones over the Phoenix deposit. The data were transformed using logcentred ratio.

unaltered feldspar or calcite-dolomite veins. This will be confirmed in further petrographic studies. The positive association of HREE and high-field strength elements (Th-Zr-Ti-Nb) may reflect the presence of heavy minerals, such as zircon and oxides. This will be confirmed through a mineralogical study of samples. The MFc data shows a weak relative enrichment of U-Pb-Y-HREEs- Hf-Zr and Ni-Na-B-Mg along the positive PC1 axis (Fig. 3C), supporting an association of U and REEs with tourmaline (B-Na-Mg, most likely magnesio-foitite) in the MFc. The tourmaline has high vacancy in the X-site and relatively high Mg, and is classified as magnesiofoitite (O'Connell et al., 2015). Uranium is inversely correlated with Zr, Hf and Th but positively correlated with HREEs. Zircon grains can contain high concentrations of not only HREEs and Y but also Zr, Hf and Th (Föster, 2006). However, the observed elemental association suggests that zircon is not an important host of REEs in the sandstones. Furthermore, P is closely associated with REEs, Al and Sr, therefore APS may be important host. Although REEs are associated with U in the sandstone above the Phoenix deposits, the absolute concentrations are overall low (∑REEs <150 ppm) and it was difficult to identify phases hosting REEs.

Compared with the Phoenix dataset, the Maw Zone has different element groups: U is strongly correlated with V, Cr, Fe, Ni, Cu, Cd, Na, Li and Ba, but very weakly correlated with HREEs+Y, and inversely with LREEs and P. Relative enrichment of HREEs and Y-P suggests that xenotime is the predominant host of the HREEs while the elemental grouping of LREEs-Sr-Th-P in the MFb suggests the occurrence of monazite and/or APS minerals. The mineralogical studies confirmed APS minerals as the major host of LREEs.

The positive correlation between U and Fe and their loadings in the oxidized regions of the biplots suggest that U was transported by oxidized fluids and is associated with Fe-oxides (possibly adsorbed on Fe-oxides/hydroxides and clays). REEs and U have different precipitation mechanisms, with U reduced from relatively soluble U^{6+} to insoluble U^{4+} in a reducing environment (Jefferson et al., 2007). Deposition of REEs is related to increasing pH and decreasing temperature (Williams-Jones et al., 2012)]. Although REEs can be transported by oxidizing brines similar to those which trans-

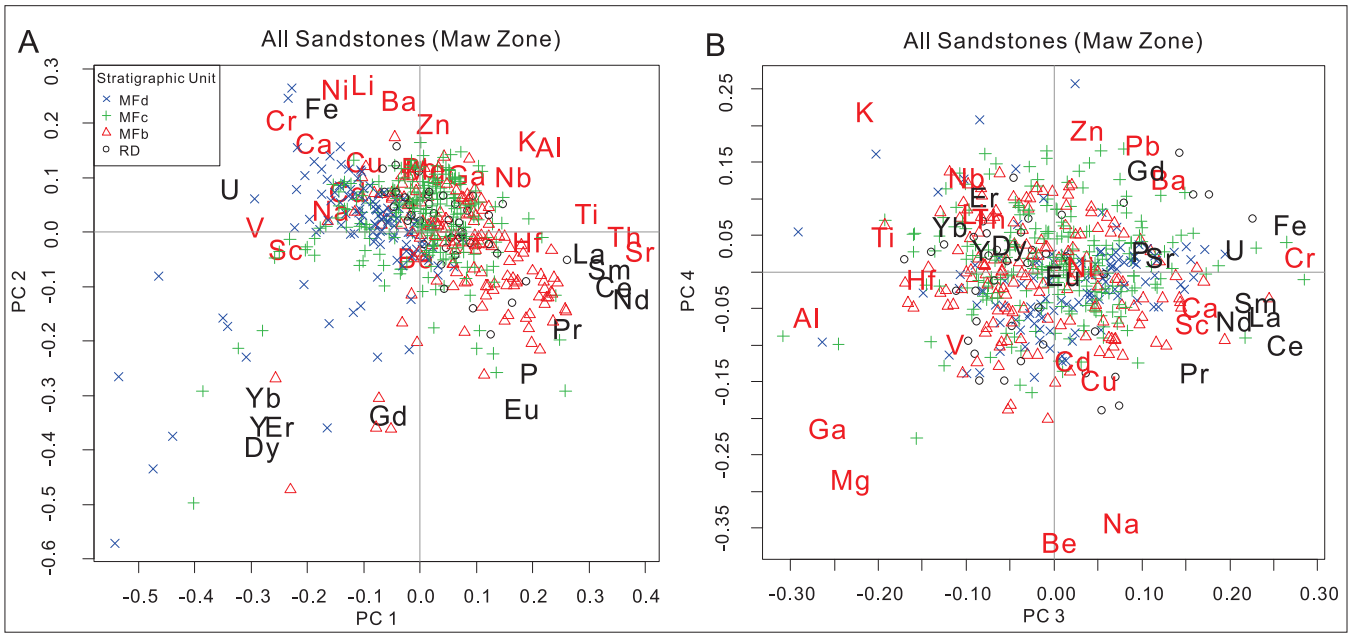

Figure 5. Biplots of PC1 vs. PC2 and PC3 vs. PC4 for all sandstone data from the Maw Zone. The data were transformed using logcentred ratio.

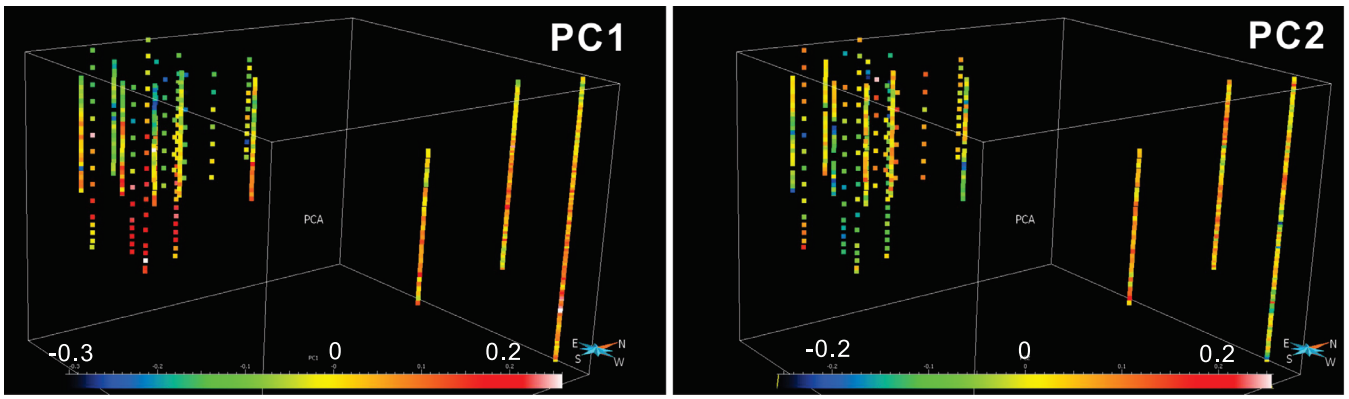

Figure 6. 3D diagrams showing scores of PC1 (Left) and PC2 (Right) in drill cores. The data were transformed using logcentred ratio.

port U (Fayek and Kyser, 1997), if there is no reducing conditions, REEs may precipitate while U remains in the fluids.

Sandstones in the Maw Zone show negative Eu anomalies compared to Sm and Gd, suggesting interaction between hydrothermal fluids and felsic rocks. Ca-rich plagioclase is the major host of Eu^{2+} and mafic igneous rocks commonly show positive Eu anomalies in chondrite-normalized REE patterns, whereas felsic rocks show negative Eu anomalies in normalized patterns because of earlier crystallization of plagioclase in mafic rocks (Henderson, 1984)

Uranium concentrations in the Maw Zone are overall low (< 7.89 ppm U in almost all samples; Denison Mines Corp., 2006), although the values are generally higher than the average crustal concentration of 0.91 ppm U (Taylor and McLennan, 1985). Uranium shows positive correlations with Fe, V and Cr (Fig. 5A), suggesting that relatively high contents of U are associated with Fe oxides (possibly adsorbed on Fe-oxides/hydroxides and clays). The data suggests that small quantities of U precipitated under oxidized conditions. Since rocks of MFd are mostly plotted in the upper left quadrant, it is interpreted that the MFd unit was less reduced or not reduced compared to MFb and MFc. This is reasonable considering that the MFd is the farthest unit from the reduced basement rocks. The occurrence of kaolinite with Fe oxides in the MFd suggests that this oxidation likely took place during the diagenesis of sandstones.

There are three possible explanations for the absence of significant U mineralization in the Maw Zone. The concentrations of U in the oxidizing fluids were low, as suggested by Pan et al. (2013) based on the lack radiation-induced defects in quartz. Alternatively, the oxidizing fluids did not encounter reduced fluids or media in the basement to precipitate U. Finally, introduction of REEs in reduced fluids took place at much later time, as shown by REE-rich veins in the hematite-rich breccia.

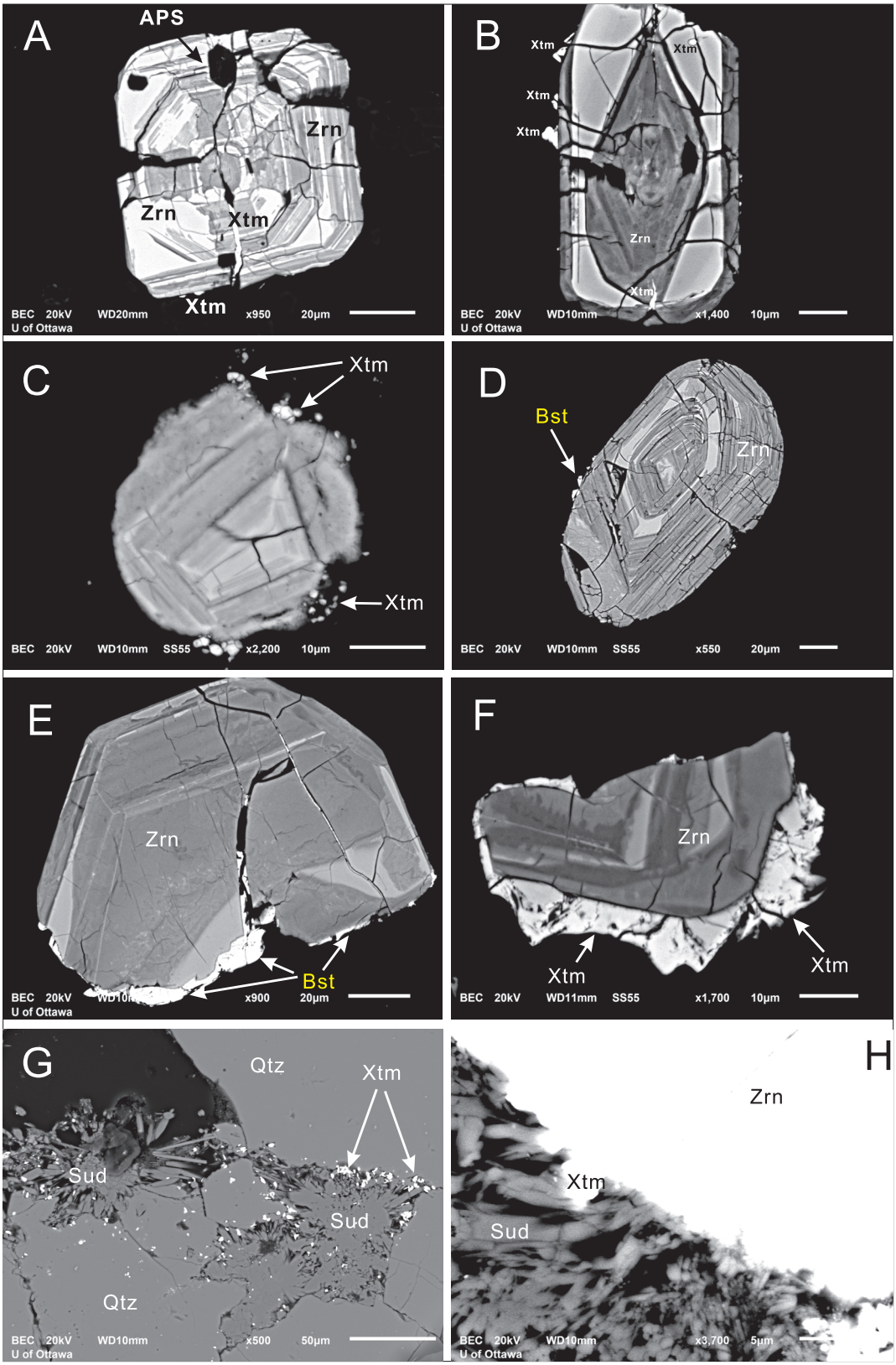

Figure 7. Backscatter electron (BSE) images of xenotime (Xtm) and bastnäsite (Bst) in sandstone samples from MFb (Fig. 7A: DDH 85-3, 102.5m depth, Fig 7B and H: ZQ-09, 215m depth, Fig. 7G: DDH 85-3, 132.5m depth), MFd (Fig 7C: DDH 84-2, 30m depth; Fig 7D: DDH 84-2, 50m depth), the RD (Fig 7E: ZQ-09 225m depth, Fig 7F: DDH WR-194, 357.5m depth). Bst = bastnäsite, Mgf= magnesiofoitite, Qtz = quartz, Sud = Sudoite, Xtm = xenotime, Zrn = zircon.

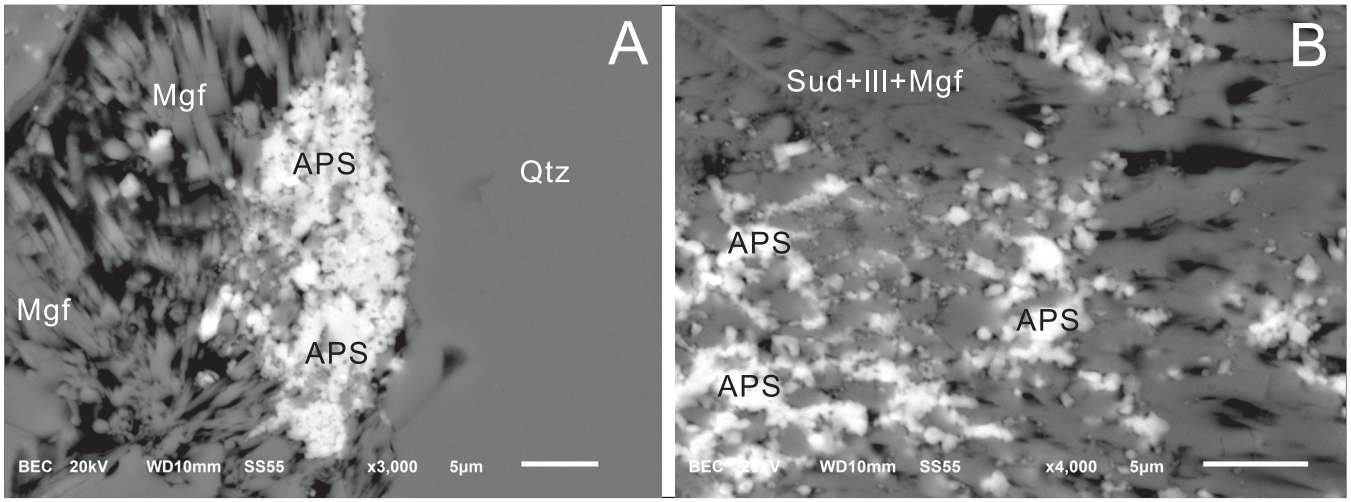

Figure 8. BSE images of APS minerals (bright) in sandstone sample from MFd (DDH ZQ-08, 33 m depth). Ill=illite, Mgf = magnesiofoitite, alkali-deficient Mg-rich tourmaline, Qtz=quartz.

Exploration Implications

The elemental assemblages observed from dominant PCs are likely associated with alteration assemblages. Therefore, these elemental associations can be used to recognize alteration related to unconformity-related uranium deposits. In this study, positive values in PC1 and PC2 scores are associated with the enrichment of U. These findings may be useful in evaluating the potential for U deposits in the area by mapping PC1 and PC2 scores of rocks by interpolation.

Acknowledgments

We thank Denison Mines Ltd for providing the geochemical data and approving the publication of this manuscript. The research project is funded by a grant to K.H. from Natural Resources of Canada through the TGI-4 program. This report benefitted from constructive reviews by Julien Mercadier, Donald Wright and Eric Potter.

References

Agip Canada Ltd., 1985. Assessment File 74H06-NW-0080: Saskatchewan Ministry of Energy and Mines, 113 p.

Aitchison, J., 1986. The statistical analysis of compositional data. Chapman and Hall, New York. 416p.

Barker, M., 2011. The Y and HREE enrichment of the Maw Zone, Wheeler River preliminary Summary; unpublished report prepared for Denison Mines Corporation, 16 p.

Chen, S., Grunsky, E., Hattori, K., and Liu, Y., 2014. Principal component analysis of geochemical data from the REE-rich Maw Zone, Athabasca Basin, Canada; Geological Survey of Canada, Open File 7689, 22 p.

Dann, J., Hattori, K., Potter, E.G., and Sorba, C., 2014. Discrimination of Elemental Assemblages in the Alteration Halo of the Phoenix Deposit, Saskatchewan, Through Applied GIS; Geological Survey of Canada, Open File 7463. 66 p.

Denison Mines Corporation, 2006. [Geochemistry of the REE-enriched Maw Zone]; Unpublished raw data.

Denison Mines Corporation, 2014. Wheeler River Property; <http://www.denisonmines.com/s/Wheeler_River.asp>

Fayek, M., and Kyser, T.K., 1997. Characterization of multiple fluid-flow events and rare earth element mobility associated with formation of unconformity- type uranium deposits in the Athabasca basin, Saskatchewan; The Canadian Mineralogist, v. 35, p. 627–758.

Föster, H.-J., 2006. Composition and origin of intermediate solid solutions in the system thorite–xenotime–zircon–coffinite; Lithos v. 88, p. 35-55.

Gabriel, K.R., 1971. The biplot graphic display of matrices with application to principal component analysis; Biometrika, v. 58, p. 453–467.

Grunsky, E.C., 1986. Recognition of alteration in volcanic rocks using statistical analysis of lithogeochemical data; Journal of Geochemical Exploration, v. 25, p. 157–183.

Grunsky, E.C., 2001. A program for computing RQ-mode principal components analysis for S-plus and R; Computers and Geosciences, v. 27, p. 229–235.

Grunsky, E.C., Drew, L.J., and Sutphin, D.M., 2009. Process recognition in multi-element soil and stream-sediment geochemical data; Applied Geochemistry, v. 24, p. 1602–1616.

Grunsky, E.C., Kjarsgaard, B.A., Egozcue, J.J., Pawlowsky-Glahn, V., and Thió i Fernández de Henestrosa, S., 2008. Studies in Stoichiometry with Compositional Data; in Proceedings of CODAWORK'08, 7 p.

Grunsky, E.C. 2010. The interpretation of geochemical survey data; Geochemistry, Exploration, Environment Analysis, v. 10, p. 27–74.

Györfi, I., Hajnal, Z., White, D.J., Takács, E., Reilkoff, B., Annesley, I.R., Powell, B., and Koch, R., 2007. High-resolution seismic survey from the McArthur River region: contributions to mapping of the complex P2 uranium ore zone, Athabasca Basin, Saskatchewan; in EXTECH IV: Geology and Uranium Exploration TECHnology of the Proterozoic Athabasca Basin, Saskatchewan and Alberta, (ed.) C.W. Jefferson and G. Delaney; Geological Survey of Canada, Bulletin 588, p. 397–412.

Hanly, A.J., 2001. The mineralogy, petrology and rare earth element geochemistry of the Maw Zone, Athabasca Basin, Canada, University of Missouri-Rolla; unpublished M.Sc. thesis, 108 p.

Hanly, A.J., and Hagni, R.D., 2002. The petrology and rare earth element geochemistry of the Maw Zone: an yttrium and heavy rare earth element enriched zone in the Athabasca Basin, Canada; Joint Annual meeting of the Geological Association of Canada – Mineralogical Association of Canada, Abstracts, v. 27, 1 p.

Henderson, P., 1984. Rare earth element geochemistry. Elsevier. 510 p.

Jefferson, C.W., Thomas, D.J., Gandhi, S.S., Ramaekers, P., Delaney, G., Brisbin, D., Cutts, C., Portella, P., and Olson, R.A., 2007. Unconformity-associated uranium deposits of the Athabasca Basin, Saskatchewan and Alberta; in EXTECH IV: Geology and Uranium EXploration TECHnology of the Proterozoic Athabasca Basin, Saskatchewan and Alberta, (ed.) C.W. Jefferson and G. Delaney; Geological Survey of Canada Bulletin 588, p. 23–68

Jolliffe, I.T., 1986. Principal Component Analysis; Encyclopedia of Statistics in Behavioral Science, John Wiley & Sons, Ltd, 487 p.

Kerr, W.C., 2010. The discovery of the Phoenix Deposit; a new high-grade, Athabasca Basin unconformity-type uranium deposit, Saskatchewan, Canada; Society of Economic Geologists Special Publications, v.15, p. 703–728.

Marlatt, J., McGill, B., Matthews, R., Sopuck, V., and Pollock, G., 1992. The discovery of the McArthur River uranium deposit, Saskatchewan, Canada; in New Developments in Uranium Exploration, Resources, Production and Demand; International Atomic Energy Agency and the Nuclear Energy Agency of the Organization for Economic Cooperation Development, IAEA-TECDOC-650, p. 118–127.

McDougall, D.G., 1990. Rare earth element mineralization in the Athabasca Group – Maw Zone; in Summary of Investigations 1990; Saskatchewan Geological Survey, Miscellaneous Report 90-4, 3 p.

Mwenifumbo, C.J., and Bernius, G.R., 2007. Crandallite-group minerals: host of thorium enrichment in the eastern Athabasca Basin, Saskatchewan; in EXTECH IV: Geology and Uranium Exploration TECHnology of the Proterozoic Athabasca Basin, Saskatchewan and Alberta, (ed.) C.W. Jefferson and G. Delaney; Geological Survey of Canada Bulletin 588, p. 521–532.

O'Connell, I., Hattori, K., Chen, S., Adlakha, E.E., and Sorba, C., 2015. Tourmaline in the Maw Zone, uranium ore of the Gryphon Zone and sandstones above the Phoenix uranium deposits, Athabasca Basin, Saskatchewan, Canada; Presentation at Saskatchewan Geological Open House 2014, 1 poster.

Pan, Y., Yeo, G., Rogers, B., Austman, C., and Hu, B., 2013. Application of natural radiation-induced defects in quartz to uranium exploration: A case study on the Maw Zone, Athabasca Basin; in Uranium in Canada: Geological Environments and Exploration Developments, (ed.) E.G. Potter, C.W. Jefferson and D. Quirt; Journal of Exploration and Mining Geology, v. 21, p. 115–128.

Pearson, K., 1901. On lines and planes of closest fit to systems of points in space; Philosophical Magazine, v. 11, p. 559–572.

Quirt, D., Kotzer, T., and Kyser, T.K., 1991. Tourmaline, phosphate minerals, zircon and pitchblende in the Athabasca Group: Maw Zone and McArthur River areas; in Summary of Investigations 1991; Saskatchewan Geological Survey, Saskatchewan Energy and Mines, Report 91-4, p. 181–191.

Ramaekers, P., Jefferson, C.W., Yeo, G.M., Collier, B., Long, D.G.F., Drever, G. and Wheatley, K., 2007. Revised geological map and stratigraphy of the Athabasca Group, Saskatchewan and Alberta; in EXTECH IV: Geology and Uranium Exploration TECHnology of the Proterozoic Athabasca Basin, Saskatchewan and Alberta, (ed.) C.W. Jefferson and G. Delaney; Geological Survey of Canada Bulletin 588, p. 155–190.

R Core Team., 2013. R: A Language and Environment for Statistical Computing; R Foundation for Statistical Computing, Vienna, Austria. <http://www.R-project.org/>.

Roscoe, W., 2014. Technical report on a mineral resource estimate update for the Phoenix uranium deposit, Wheeler River Project, eastern Athabasca Basin, Northern Saskatchewan, Canada; NI 43-101 technical report, 134 p.

Taylor, S.R., and McLennan, S.M., 1985. The Continental Crust: Its Composition and Evolution; Blackwell Scientific Publications, 328 p.

Tourigny, G., Quirt, D.H., Wilson, N.S.F., Wilson, S., Breton, G., and Portella, P., 2007. Geological and structural features of the Sue C uranium deposit, McClean Lake area, Saskatchewan; in EXTECH IV: Geology and Uranium Exploration TECHnology of the Proterozoic Athabasca Basin, Saskatchewan and Alberta, (ed.) C.W. Jefferson and G. Delaney; Geological Survey of Canada, Bulletin 588, p. 229–247.

Williams-Jones, A.E., Migdisov, A.A., and Samson, I.M., (2012). Hydrothermal mobilization of the rare earth elements – a tale of 'ceria' and 'yttria'. Elements, v. 8, p. 355-360

Yeo, G.M., and Delaney, G., 2007. The Wollaston Supergroup, stratigraphy and metallogeny of a Paleoproterozoic Wilson cycle in the Trans-Hudson Orogen, Saskatchewan; in EXTECH IV: Geology and Uranium Exploration TECHnology of the Proterozoic Athabasca Basin, Saskatchewan and Alberta, (ed.) C.W. Jefferson and G. Delaney; Geological Survey of Canada, Bulletin 588, p. 89–118.

Surficial Geochemical Surveys Over Concealed Uranium Ore of the Phoenix and Millennium Deposits in the Athabasca Basin, Saskatchewan

Keiko Hattori[1], Michael J. Power[1,5], Austin Krahenbil[1], Chad Sorba[2], Tom G. Kotzer[3], and Eric G. Potter[4]

1. *Department of Earth Sciences, University of Ottawa, 25 Templeton Street, Ottawa, Ontario, K1N 6N5; khattori@uottawa.ca*
2. *Denison Mines Corporation, 230 22nd Street East, Saskatoon, Saskatchewan, S7K 0E9*
3. *Cameco Corporation, 2121 11th Street West, Saskatoon, Saskatchewan, S7M 1J3*
4. *Geological Survey of Canada, 601 Booth Street, Ottawa, Ontario, K1A 0E8*
5. *current address: Dillon Consulting Limited, 137 Chain Lake Drive, Halifax, Nova Scotia, B3S 1B3*

Abstract

Geochemical surveys of surficial media (soil, water, and gas) have been conducted to evaluate and prioritize methods of detecting the presence of deeply-buried unconformity-related U deposits. The study selected two sites: the Phoenix and Millennium deposits in the eastern Athabasca Basin, Saskatchewan. The Phoenix deposits lie at a depth of ca. 400 m along the unconformity between Athabasca sandstones and the basement rocks, and the Millennium deposit at a depth of ca. 750 m along a major shear deformation zone in the basement. Humus and B-horizon soil samples show elevated metal contents including U directly above the ore bodies and WS Shear Zone at the Phoenix deposits, and broad areas over shear zones at the Millennium property. The elevated values of metals in the soil samples were reproduced in subsequent years of sampling in both properties. Laboratory leach experiments on humus using a variety of acids indicate that the elevated contents of metals are tightly held in organics, not adsorbed on the surface of clays or organic matter.

Examination of sandstone geochemistry over the Phoenix deposits shows a chimney-like distribution of elevated metal contents from the deposits to the upper sandstones. The uppermost sandstones contain elevated metal contents, including U. Principal component analysis reveals high scores of elements associated with U, such as rare earth elements and Pb in the basal Read Formation and the uppermost Dunlop Member of the Manitou Falls Formation. The evidence suggests that metals were dispersed in the sandstones during hydrothermal alteration related to ore-formation but were recently dispersed into the surface media. The proposed interpretation is consistent with low ^{206}Pb and ^{207}Pb in humus samples and high contents of ^{222}Rn in ground waters. With a half-life of 3.8 days, ^{222}Rn cannot be transported from the deeply-seated ore to the surface in several days, and likely originated from U and/or ^{226}Ra (direct parent of ^{222}Rn) present in upper sandstones and soil.

The concentrations of He are extremely high in groundwater close to the surface projection of the Millennium ore body and higher at deeper levels. The data appears to suggest upward diffusion of He from the U ore, but the distribution of high He in two study sites suggests its dispersion both vertically and laterally with groundwater flow. In summary, deeply-buried U deposits produce geochemical anomalies in surface media, but the expression of anomalies and media vary at different sites in response to local glacio-fluvial history, soil development and hydrological conditions.

Introduction

Many large U deposits are located along the eastern margin of the Athabasca Basin, Saskatchewan (Fig. 1), and are associated with the unconformity between the crystalline basement and the overlying Athabasca sandstones (Jefferson et al., 2007). In the eastern margin, the unconformity is relatively shallow compared to the interior of the Basin. However, discoveries of high-grade deposits indicate that U mineralization took place also in deeper sections of the basin and significantly below the unconformity, in some cases up to 400 m along structures (Thomas et al., 1998). They include the Millennium, Centennial, and Eagle Point deposits located ca. 650–750 m, 800–830 m and 50–500 m below the present day surface, respectively (Lemaitre 2006; Cloutier et al., 2009; Jiricka, 2010; Cloutier et al., 2011; Alexandre et al., 2012; Reid et al., 2014). These discoveries expand the possibility of finding more concealed deposits below thick sandstones in the interior of the Athabasca Basin and in basement rocks peripheral to the basin. Since the late 1970s, a variety of surficial geochemical exploration techniques have been employed in the Athabasca region, including lake sediments (Coker and Dunn, 1981; Maurice et al., 1985; Wasyliuk, 2006), and noble gases (Dyck, 1980; Cameron, 1983). A recent CAMIRO project examined soil and plant samples over Cigar Lake and McClean Lake deposits and reported geochemical anomalies close to the surface projection of the deposits (Bonham-Carter and Hall, 2010; Dunn, 2010). Based on these previous studies, we initiated a TGI 4-supported project in the summer of 2011 to identify the best techniques and reliable surface media in detecting concealed U deposits, and evaluate the pathways and trapping mechanisms of elements in the surface media. In order to track the movement of metals through the overlying sandstone column (building on previous studies such as Sopuck et al., 1983 and Clark, 1987), examination of drill core databases were done in conjunction with the surficial media sampling. Two sites were selected for the study (Fig. 1): the Phoenix deposits with indicated resource of 70.2 million lb U_3O_8 (Roscoe, 2014) and the Millennium deposit with indicated resource of 75.9 million lbs U_3O_8 (Cameco Corporation, 2013). Both sites have no apparent surface expression of the buried uranium ore. The Phoenix deposits occur at ca. 400 m

Hattori, K., Power, M.J., Krahenbil, A., Sorba, C., Kotzer, T.G., and Potter, E.G., 2015. Surficial Geochemical Surveys Over Concealed Uranium Ore of the Phoenix and Millennium Deposits in the Athabasca Basin, Saskatchewan, *in* Targeted Geoscience Initiative 4: unconformity-related uranium systems, (ed.) E.G. Potter and D.M. Wright; Geological Survey of Canada, Open File 7791, p. 32–42. doi:10.4095/295776

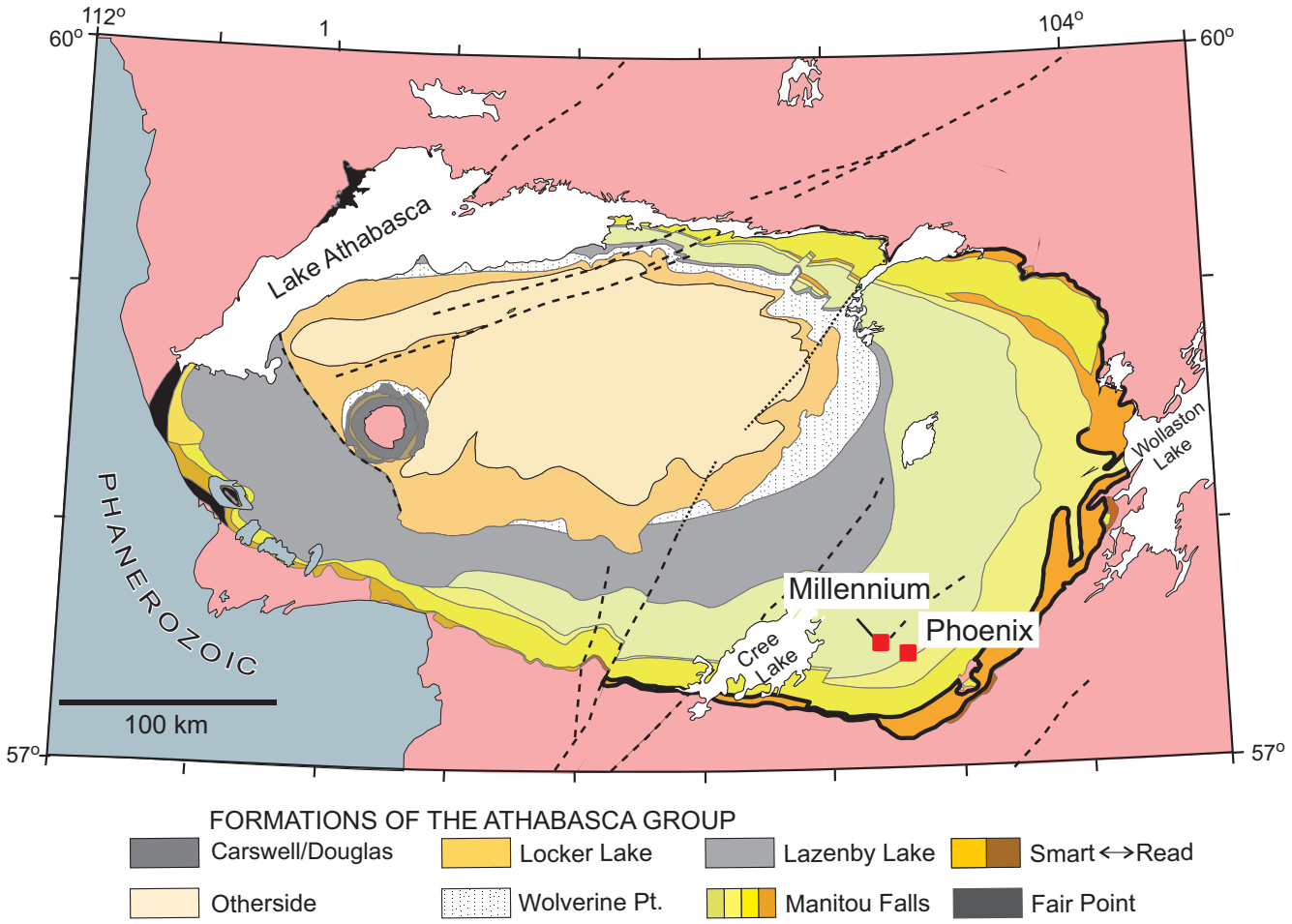

Figure 1. Locations of study areas and simplified geology of the Athabasca Basin (modified after Jefferson et al., 2007)

depth, mostly along the unconformity and at its intersection with the WS Shear (Fig. 2A). The Millennium deposit is a basement-hosted deposit located 650–750 m beneath the surface along the Marker Fault, a major shear deformation zone in the basement (Cloutier et al., 2009; Wood et al., 2012; Fig. 2B). This paper presents a summary of the findings.

Study Areas

The Athabasca Basin is primarily comprised of fluvial sandstones and conglomerates that were deposited over the metamorphosed basement rocks of Archean to Paleoproterozoic granite and gneiss. The sandstones in the study areas in the southeastern margin of the Athabasca Basin (Fig. 1) are about 400 m in thickness and divided into the Read Formation at the base and the overlying Manitou Falls Formation (Jefferson et al., 2007). The Manitou Falls Formation is further divided into Bird Member (MFb), Collins Member (MFc) and Dunlop Member (MFd) in ascending order (Fig. 2B). The Phoenix deposits occur along the unconformity and also a steeply dipping shear deformation zone, WS Shear, in graphitic pelitic gneisses in the basement (Kerr, 2010; Fig. 2A). The basement rocks are metasedimentary rocks and granitic gneisses of the Paleoproterozoic Wollaston Domain of the Trans Hudson orogeny (Yeo and Delaney, 2007). The metasedimentary rocks are graphitic and non-graphitic pelitic gneisses that are intensely altered near the mineralization. The Millennium deposit lies at a depth of ca. 750 m from the surface and 100 m below the unconformity along a major reverse fault, the Marker Fault, in the basement (Fig. 2B). The Marker Fault is rooted in graphite-rich pelitic gneisses. The Paleoproterozoic basement rocks in the area belong to the transition zone between the Wollaston and Mudjatik Domains of the Trans Hudson orogeny (Smith et al., 2010). The rocks of the Mudjatik Domain are similar to those of the Wollaston Domain, but the former is dominated by granitic gneisses.

The study areas are mainly covered by gently rolling hills of well-drained, glacial sediments, that consist of eskers, outwash sand plains, drumlins (Schreiner, 1984; Campbell, 2007). Black spruce is the dominant tree species in the area with minor jack pine. A thin layer of caribou moss covers the forest floor. The Millennium property experienced a forest fire in 2008, which burned much of the vegetation. Therefore, trees are sparse and short (< 2 m). Logging data of exploration drilling shows that glacial sediments are mostly 20–30 m thick, except for the top of eskers. The general ice flow direction in the eastern part of the Athabasca Basin is southwest (Campbell, 2007). This glacial dispersal direction

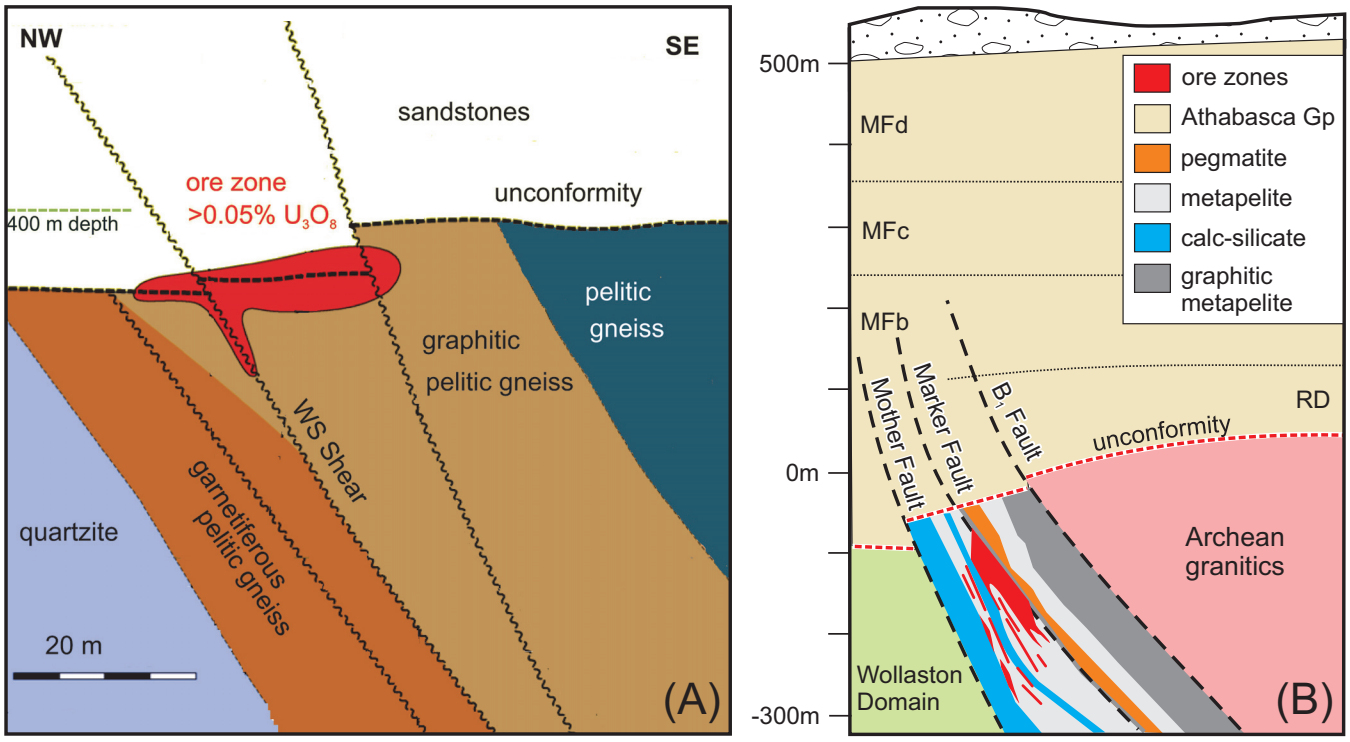

Figure 2. (A) Schematic cross section of the Phoenix deposits (modified from Gamelin et al., 2010). The uranium deposits (dark shaded) lie ca. 400 m beneath the present day surface along the unconformity between the Athabasca sandstone and Paleoproterozoic basement rocks. Minor mineralization extends below the unconformity along the reverse fault of the WS Shear. (B) Cross section of the Millennium deposit (red) at ca. 750 m below the surface along the Marker fault in the basement. Modified after Smith et al. (2010) and Wood et al. (2012).

is consistent with the general morphology of drumlins in the study areas.

The region has a sub-arctic climate with long, cold winters and mild summers with moderately high precipitation, approximately 482 mm of annual precipitation (Dimitrov et al., 2014).

Sampling and Analytical Techniques

Soil sample sampling

Although the last glacier retreated from the study area only ca. 9000 years ago (Campbell, 2007), soil horizons are well developed in both properties partly due to well drained sandy glacial sediments on the surface of the properties (Figs. 3A, B). Boggy areas are only developed around a small swamp close to the north end of the surface projection of the Millennium deposit and close to Slush Lake, in the western part of the study area in the Millennium property (Fig. 4B). The thickness of humus varies up to 5 cm and that of B-horizon soil varies from 20 to greater than 60 cm (Figs. 3A, B). The 2008 forest fire at the Millennium property produced charcoal and fragments common in humus.

Sampling (1–2 kg each) was conducted at 15–20 m interval along traverses covering the surface projections of major faults and ore bodies (Figs. 4A, B). Before the sampling, the topography and surface conditions were carefully examined to select sampling traverses to collect similar media. Considering the southwest directing ice dispersion, the orientation of sampling traverses was set perpendicular to this ice flow so that samples possibly affected by glacial dispersal would not be collected along the entire traverse. At the Millennium property, the traverses only covered the northern tip and southern tip of the surface projection of the deposit (Fig. 4B) because the central area was highly disturbed due to extensive drilling and the presence of a swamp directly above the northern body of the deposit. After removing caribou moss and forest litter including dead leaves and twigs, soil samples were collected using a hand-held Dutch auger. Samples were collected of humus, E-horizon soil, B-horizon soil and C-horizon (till). At several locations, B-horizon soil was well developed and extends down to a depth of 100 cm.

To evaluate the reliability of soil data, a test was conducted by repeated sampling at different times at given sites. The site that was selected from the Phoenix deposit property yielded the highest U content in humus in 2011 (indicated with a triple circle in Fig. 4A). It is directly above the Phoenix Deposit B. The site in the Millennium property was directly above the projection of the Marker Fault, the main ore-hosting structure (indicated with an arrow in Fig. 4B).

Humus samples were digested with aqua regia and B-horizon soil with ammonia acetate leach after drying at temperatures below 60°C and sieving – 80 mesh (0.177 mm) at Acme Labs Ltd., Vancouver. To evaluate different techniques, a suite of B-horizon soil samples was subjected to ammonia acetate and hydroxylamine leaches plus aqua regia digestion. For quality control, one every ten samples was split into two and the two were given different labels for the analysis. The results show reproducibility of greater than 90%.

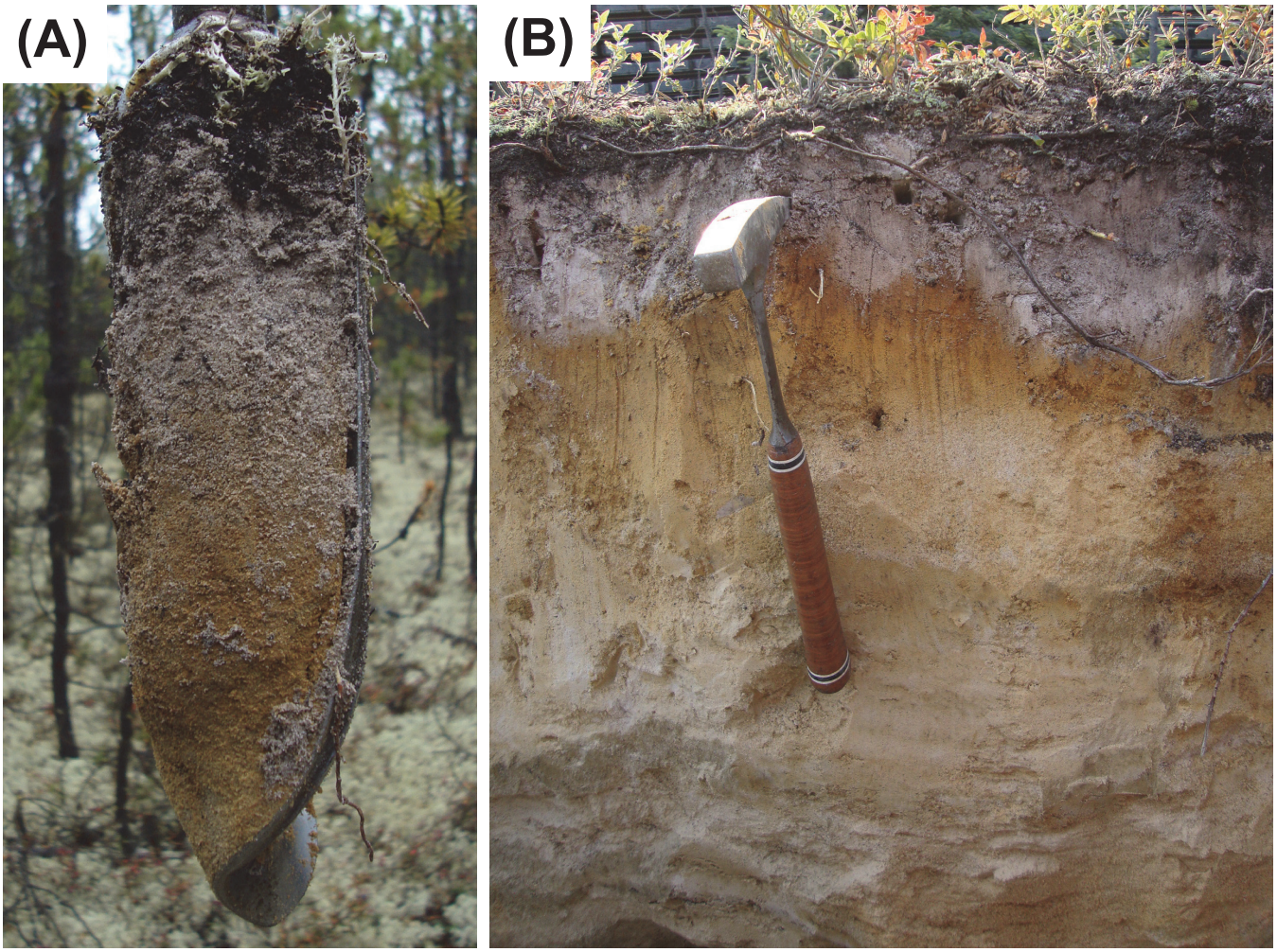

Figure 3. Well-developed soil horizons at the Wheeler River (A) and Millennium properties (B).

Leach test of humus samples

Laboratory tests were conducted at the University of Ottawa to evaluate the leaching of metals in humus with a variety of acids. First, the samples were dried at 60°C, and sieved -80 mesh (0.177 mm) using stainless steel sieves. They were placed in Milli-Q water at 25 ºC, 0.02 N hydrobromic acid (HBr) at 25 ºC, 1 N nitric acid (HNO_3) at 25 ºC, and concentrated mixture of hydrofluoric (HF)-hydrobromic (HBr) (3:2) at 100ºC. The samples in solutions were agitated frequently for the first hour and every hour for over 4 hours. The concentrations of metals (Cu, Ni, Co, As, U, Pb) in the solutions and blank solutions were measured using a Thermo-Agilent HP-7700 inductively coupled plasma mass spectrometer (ICP-MS) at the University of Ottawa. Reagents used for the laboratory analysis were double-distilled at sub-boiling temperatures and purchased from Seastar Chemicals, British Columbia.

Lead isotope analysis of humus samples

Solutions used for the leaching tests of humus were used for Pb isotope analysis. After the solutions were evaporated at low temperatures, they were re-dissolved in HBr solution for the separation and purification of Pb, following a standard procedure using Dowex AG1-8X anion resin (200-400 mesh) and elution using HBr solution at the University of Ottawa (Hinchey and Hattori, 2007). The total procedure blanks for Pb were less than 200 picograms. The isotope compositions of Pb were determined using Thermo-Agilent HP-7700 ICP-MS and also a Thermo-Finnigan Triton thermal ionization mass spectrometer. The mass fractionation was 0.13 % a.m.u. based on the measured values of NBS 981 and the values given by Todt et al. (1995). For the ICP-MS analysis, ^{204}Pb was counted for a long time, 3.0 sec, in each cycle to give the uncertainty of 0.1 % (2σ) of the quoted values. The two instruments yielded similar results.

Till samples

The major and minor element abundance of till samples were determined using a Philips PW 2400 X-ray fluorescent spectrometer at the University of Ottawa after fusing the sample powder with a flux composed of 78.5% $Li_2B_4O_7$ and 21.5 % $LiBO_2$.

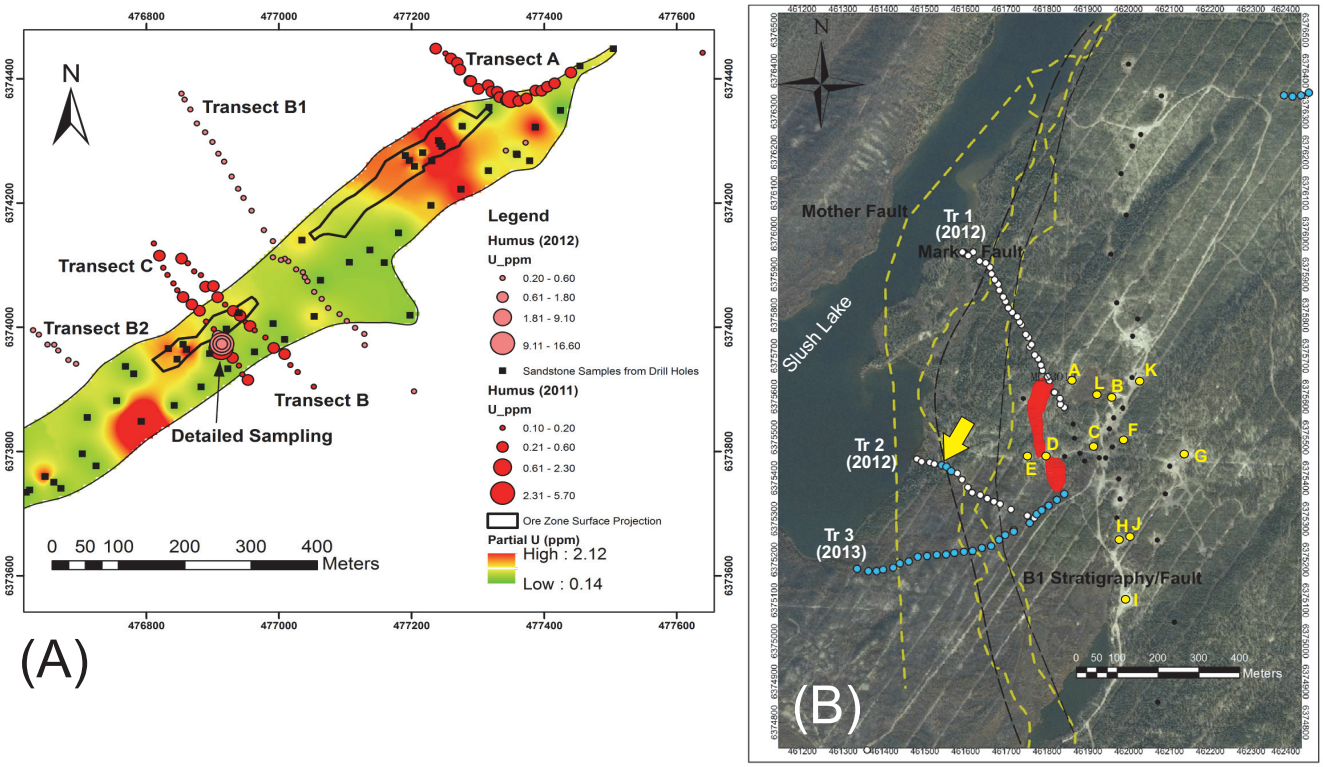

Figure 4. (A) Uranium concentrations in ammonia acetate leach of B-horizon soil (circles) and in aqua regia of the uppermost sandstones above the Phoenix deposits. Reproducibility of soil data was tested at PHX 28 shown with brown triple circle. Modified after Power et al. (2012). (B) Sampling traverses (white and blue circles, Tr 1, Tr2, Tr3) and sites (yellow circles) for helium survey by Power et al. (2012) and Krahenbil et al. (2014). A=DDH CX-86, B=DDH CX52, C=DDH CX98, D=DDH CX40, E=DDH CX43, F=DDH CX45, G=DDH CX63, H=DDH CX58, I=DDH CX49, J=Monitoring well ML 07-02, K=Monitoring well BH127, L = swamp). The surface projection of the Millennium deposit is shown in red. Major shear deformation zones in the basement rocks are extended to the surface (shown in yellow dashed lines). Modified after Krahenbil et al. (2014). The reproducibility of soil sample was collected in 2013 at MLN 145 (shown with a yellow arrow along transect 2 (Tr2))

Water

Groundwater was collected from monitoring wells and exploration drill holes using a bailer made of Cu tube with one end closed. Both groundwater and surface water samples were subjected to analysis of the abundance of cations and anions, tritium, dissolved carbon, and isotope compositions of hydrogen and oxygen. Water samples were also used to determine dissolved Rn contents.

Noble Gases

Radon gas dissolved in groundwater and surface water was measured after extracting Rn gas using mineral oil following the method described by Leaney and Herczeg (2006). Radon gas contents were also measured in soil pore fluids close to drill holes. Helium gas dissolved in water was collected using a diffusion gas sampler, which is made of a Cu tube (¼" OD, ~ 8 cm in length) connected to a ca. 5 cm long silicon tube (e.g. Sanford et al., 1996; Hamilton et al., 2005). The samplers were submerged in a small swamp, shallow environmental monitoring wells and exploration drill holes in the Millennium property, and in exploration drill holes in the Phoenix property.

Results

C-horizon (Till)

The 17 till samples collected from the two properties show remarkably similar major and minor element abundances. They are characterized by high SiO_2 (avg. 89 %), moderate Al_2O_3 (avg. 4.5 %), and low CaO (avg. 0.50 %), Na_2O (avg. 0.83 %), K_2O (avg. 0.93 %), MgO (avg. 0.21 %), and Fe_2O_3 as total Fe (avg. 0.56%) (Power et al., 2014).

Soil

Humus samples show very low concentrations of Al, less than 0.1 %, confirming that humus samples contain very little minerals, such as clays. Both humus and B-horizon soil show elevated concentrations of U, Pb, Mo, Ag, Co, Ni and W directly above the Phoenix deposits and WS Shear (Fig. 2A). Arsenic values are also high in selected samples (Power et al., 2012).

At the Millennium property, elevated contents of U, Pb and Cu were observed in broad areas covering several major deformation zones. B-horizon soil samples indicate that ammonia acetate leaches yield the most relevant results in this study area. Hydroxylamine is designed to target the dis-

solution of Fe and Mn oxides (Cameron et al., 2004), but it dissolves other phases, such as carbonates, and leaches adsorbed metals. Aqua regia dissolves not only sulphides but also carbonates, clays and metal-oxyhydroxides. Higher concentrations of elements in the analytical solutions decreases the detection limits of most elements, but can increase detection limits of trace elements targeted. This obscures the detection of anomalies.

At the Phoenix property, the site that yielded the highest U content in humus in 2011 was resampled in 2012 and 2013 approximately 1m from the original site (Fig. 4A). Both visits reproduced elevated values (Figs. 6A, B). At the Millennium property, two sampling sites above the Marker Fault were revisited in 2013 (Fig. 4B). The subsequent sampling around (< 2 m) the original site reproduced elevated values (Figs. 4B, 6C; Krahenbil et al., 2014). Although the absolute values are different, the data indicates the reliability of soil geochemical anomalies.

Leach testing of humus using a variety of acids shows that metals are released only when the organic material is decomposed (Fig. 5; Power et al., 2013a). The results suggest that metals are not adsorbed on the surface of material in the humus, but they are tightly bound within organic matter.

Lead isotope compositions of various humus leach fractions (water, 0.02N HBr leach, 1 N HNO_3 leach, and concentrated HF-HBr digestion) show $^{206}Pb/^{204}Pb$ values ranging from 17.3 to 1.6 and $^{207}Pb/^{204}Pb$ from 15.4 to 15.6.

Water

Analyses of inorganic carbon dissolved in water yielded low values of $\delta^{13}C$, from -6 to -20 ‰ $_{PDB}$ (Power et al., 2012; Dudek et al., in press). The values are lower than that in equilibrium with the atmospheric CO_2, indicating oxidation of significant amounts of organic carbon in groundwater.

Radon Gas

Radon contents are high and variable in groundwaters above the Phoenix deposits. There is no systematic variation

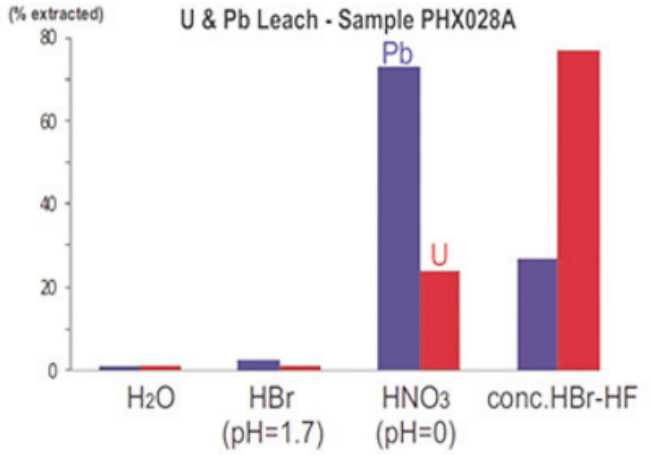

Figure 5. Concentrations of U and Pb in leach tests of a humus sample, after Power et al (2013a). The amounts of metals leached are expressed as percent of the total metals extracted in aqua regia; 5.7 ppm U and 15.2 ppm Pb. H_2O = Milli Q water, HBr = hydrobromic acid, HNO3 = nitric acid, HF=hydrofluoric acid.

of Rn contents with increasing depths; Rn contents increase or decrease with increasing depths. The data suggest a local source of Rn or ^{226}Ra, a direct parent nuclide of ^{222}Rn Radium is highly soluble in water and ^{222}Ra has a relatively long half-life, 1600 yrs. Radon contents in pore fluids of soil were all below the detection limit of 3 Bq/L. Sporadically high values were noted in soil just around recent drill holes, but high values were not reproduced in the second measurement, 15 min after the first data collection.

Helium Gas

Swamp and monitoring wells in the Millennium property show low He concentrations (Power et al., 2013b; Fig. 7A). Deeper water samples show greater concentrations of He (Power et al., 2013b; Krahenbil et al., 2014; Fig. 7B). The sample sites east of the deposit show rather low He values, which suggests He transport by groundwaters that flow

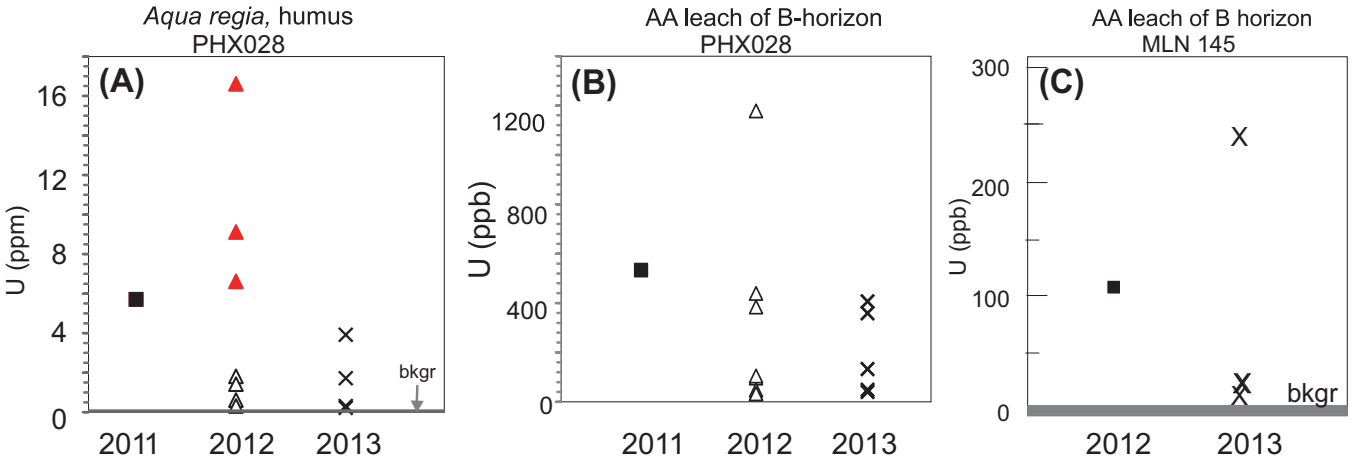

Figure 6. Uranium contents in humus after aqua regia digestion (A) and ammonia acetate leach of B-horizon soil (B) at PHX028 site (shown as a triple circle in Fig. 4A) in 2011 (C) at MLN 145 (shown with an arrow in Fig. 4B). Soil data after Power et al. (2012) and Krahenbil et al (2014). Background values (bkgr) are shown as gray lines. The location of PHX028 and MLN 145 are shown in Figs.4A and 4B.

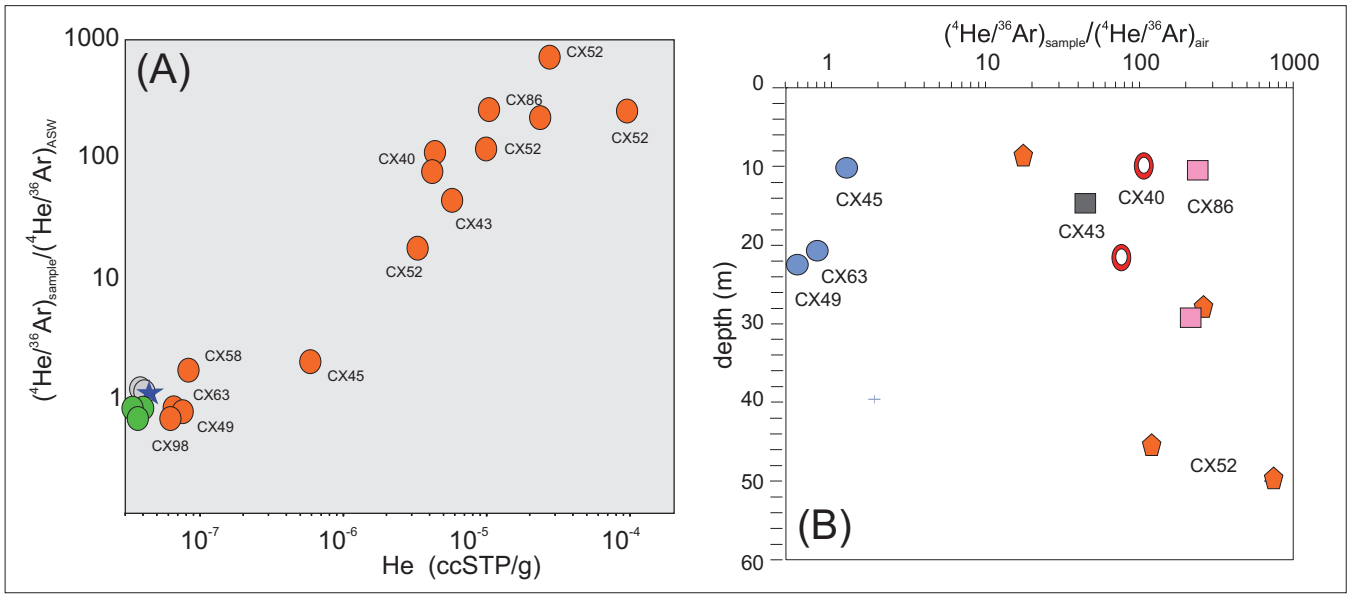

Figure 7. (A) Helium and the ratio of He/Ar in gas dissolved in water and in the Millennium property. The ratio of 1 indicates that He/Ar ratio of sample gas is identical to that in water in equilibrium with the atmosphere. The gray circles are the values from shallow environmental monitoring wells, BH127 and ML0702, and a swamp, and red circles are from exploration drill holes in the Millennium property. The blue star denotes the values of water in equilibrium with the atmosphere after Power et al (2013b), and Krahenbil et al. (2014). (B) Depth profile of He/Ar in gases dissolved in water. Location of sampling sites indicated in Fig. 4B.

westwards toward the lake.

Groundwater in the exploration drill holes above the Phoenix deposits show low He contents, similar to water in equilibrium with the atmosphere (Dudek et al., in press)

C-horizon (Till)

The SiO_2 contents of the C-horizon samples are high, supporting the Athabasca sandstones as the dominant source of glacial sediments. However, the Na_2O contents vary from 0.4 to 1.32 wt. % and are much higher than average contents of Athabasca Group sandstones. For example, the uppermost sandstone unit, MFd, in the Athabasca sandstones contain Na_2O less than 0.05 wt. % (Card et al., 2011; Bosman and Card, 2012). The data suggests the glacial sediments are derived not only from Athabasca Group sandstones but also from granitic basement rocks in the up-ice direction. The finding is consistent with the occurrence of glacial erratics of granitic and gneissic rocks on the surface of the study areas. Furthermore, granitic basement rocks are exposed ca. 150 km to the northeast (Fig. 1).

Sandstones

Sandstones above the Phoenix deposits show chimney-like vertical distribution of elevated metal contents (Dann et al., 2014). The patterns are especially apparent for elements, such as rare earth elements, Y and W (Figs. 8A, B). Furthermore, high metal contents including U are present in the uppermost sandstones on the Phoenix property (Fig. 4A, Power et al., 2012). Principal component analysis of total digestion data of sandstones confirms that the Dunlop Member of the Manitou Falls Formation has high scores of PC1, which includes U, B and rare earth elements (Chen et al., 2014, 2015; Fig. 9).

Discussion

Soil data

This study produced two encouraging results in the use of soil in surficial geochemical exploration for concealed U deposits. First, a variety of acid leach and digestion on humus samples show that metals are tightly held within the organic material, not on the surface of organics or minor clays (Fig. 5). The data rejects a possible incorporation of metals into humus as the result of drilling and other exploration activity. The analytical results of this study suggest that digestions to decompose organic, such as aqua regia, are necessary for the analysis of humus samples in U exploration. This is in accord with the procedure, aqua regia digestion of humus, recommended by the CAMIRO-sponsored project (Bonham-Carter and Hall, 2010). As proposed by (Dunn, 1983), plants may have extracted U from groundwater and soils prior to decomposition into a humus layer.

Repeated sampling tests show reliable nature of elevated metal contents in soil. Samples of humus as well as B-horizon soil collected in the vicinity, ca. 1–2 m, from the original sites of collection both at the Phoenix and Millennium properties yielded elevated values of metals in subsequent years (Fig. 6). The absolute values vary, but they are elevated relative to the surrounding soils. Considering different months of sampling, the data is encouraging for soil geochemical surveys.

Traverse sampling of soil samples shows that elevated metal contents are close to the surface projections of U ore of the Phoenix deposits (Fig. 4A). To evaluate the contribution of glacial dispersion to the metal contents, sampling was conducted along Transect B1, which runs above the barren area between the Phoenix Deposit A and Deposit B (Fig. 4A). Transect B1 did not yield elevated metal contents. The

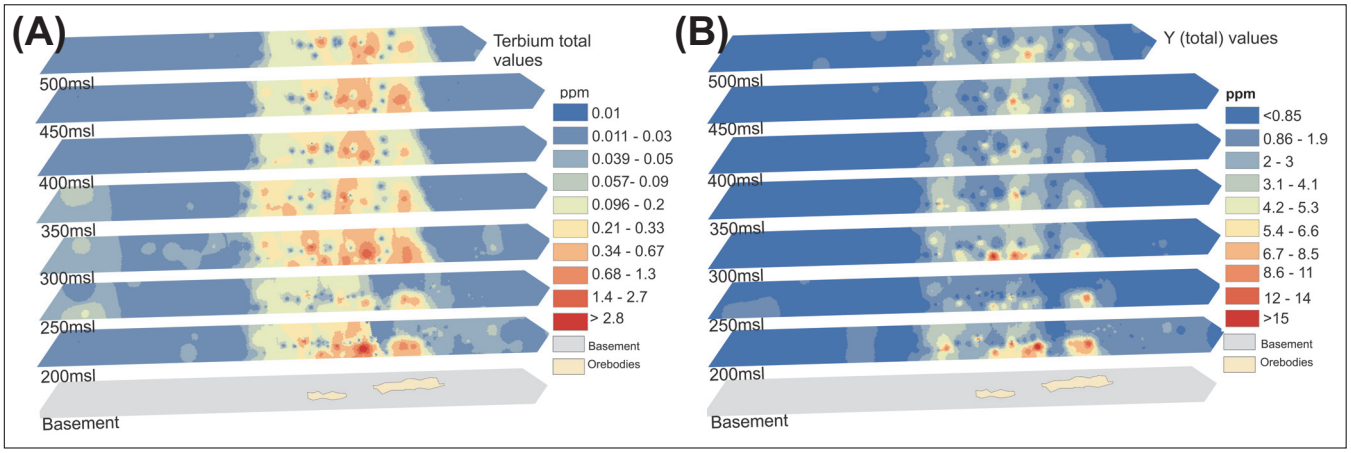

Figure 8. (A) Yttrium and Tb (B) concentrations in sandstones above the Phoenix Deposit A and B, after Dann et al. (2014). MSL = metres above sea level.

data suggest that glacial dispersion is unlikely source for elevated metal contents in soil samples.

Metal Sources

The data from the Phoenix deposit suggest that metals in soils were most likely derived from sandstones. This is supported by chimney-like elevated concentrations of metals in sandstones above U ore (Figs. 8A, B), and relatively high metal contents in the upper sandstones (Figs. 4A; 8). Elevated concentrations of U and W in soil samples are consistent with oxidized conditions of groundwaters where organic carbon is oxidized. These elements are mobile as U^{6+} and $W^{VI}O_4^{2-}$ under oxidized conditions.

At the Millennium site, the composition data is not available for sandstones above the Millennium deposit because their exploration drill holes are all from the east of the deposit. Therefore, it is difficult to evaluate the source of metals whether sandstones or deep-seated U ore. In the Millennium property, reactivation of basement shear deformation zones produced abundant faults in sandstones, which are clearly imaged in seismic surveys (Wood et al., 2012). Elevated metal contents in soil samples directly above such major faults suggest that faults are conducive in transferring elements from deep levels.

Sandstones

Anomalous compositions of sandstones above the Phoenix deposits are consistent with the sandstone compositions above U deposits at the Key Lake, Midwest Lake and Eagle Point (Sopuck et al., 1983) and at the Cigar Lake, Dawn Lake and Wolf Lake deposits (Clark, 1987). The data suggests that sandstones above U deposits commonly show elevated concentrations of elements associated with the deposits. The dispersion of elements in sandstones may have taken place during the U mineralization (primary dispersion) or long after the mineralization (secondary dispersion; c.f. Cameron et al., 2004). The primary dispersion is supported by extensive occurrences of alteration minerals in the overlying sandstones (Jefferson et al., 2007; Gamelin et al., 2010; Kerr, 2010). Furthermore, heavy REE and W are considered to be immobile at low temperatures. The dispersion of such elements in sandstones suggests that elevated metal contents are likely produced during the hydrothermal activity related to the U mineralization.

Noble Gases

Noble gases are chemically inert, which makes them disperse quickly along fractures in rocks and soil. Among noble gases, He and Rn are decay products of U and therefore they are expected to be in higher concentrations around U deposits. Helium is light, stable, and able to diffuse more quickly in water than Rn (Yaws, 2009; Dudek and Hattori, in press). The high diffusivity of He, however, poses a problem. Gas sampled near the surface of water in environmental monitoring holes, exploration drill holes, and swamps yielded low contents of He, identical to the amount expected in water in equilibrium with the atmosphere (Power et al., 2013b). The results suggest that He gas should be collected in water at a depth greater ca. 5 m below the top of the water table.

Although He contents were high in deeper waters in proximity to the surface projection of the Millennium deposit, low contents of He are noted in the eastern part of the property where water is flowing towards the deposit and the lake (Fig. 4B). If He is transported through diffusion process either vertically or radially, it should be detected above U ore. The data suggests that He is not ascending vertically but rather transported laterally by groundwater flow. This is also consistent with low He contents in waters above the Phoenix deposits.

High and variable contents of Rn in groundwater above the Phoenix deposits are similar to the results reported from the Millennium property by Devine et al. (2013). If Rn is ascending from deep sources, the values of Rn should be greater at deeper levels. High values of Rn at shallower depths in several drill holes suggest proximal sources of Rn at shallow levels. Furthermore, the short half-life, 3.8 days, of ^{222}Rn makes it impossible to migrate from deeply-seated U deposits to the surface. Although ^{226}Ra, Rn's immediate parent, has a reasonably long half-life of 1600 years, it would be more difficult for Ra to be vertically diffused in groundwaters from the deposits to the surface.

There are several possible local sources of U or Ra in drill holes: upper sandstones, soil and U brought to the surface by drilling (contamination by human activity). If mineralized cores brought U and Ra to the surface, Rn contents should be high in water samples collected from drill holes that intersected the mineralization. There is no significant difference in Rn contents between water from holes intersected and not-intersected the mineralization. To evaluate a possible contribution of soil to Rn in water, Rn contents in soil pore fluids were measured in the area close to drill holes, but high values were not confirmed. Although sporadic high values were recorded in highly disturbed soil adjacent to drill holes, the values were not reproduced. Another possible source of Rn is preferential enrichment of Rn or Ra by organic matter in water or soil because Rn has a strong affinity with organic material (Leaney and Herczeg, 2006). It is also known that plant roots incorporate Ra (Gunn and Mistry, 1970). Radium incorporated in plants would release Rn in shallow depths.

The fourth possibility is elevated U and Ra concentrations in sandstones at shallow depths. Power et al. (2012) documented high contents of metals including U, in the uppermost sandstones in the area directly above the Phoenix uranium deposits (Fig. 4A). Principal component analysis of sandstones by Chen et al., (2014, 2015) also shows high metal contents including U in the MFd (Fig. 9). The distribution of high metal contents form "chimney" like shape from the deposits to the uppermost sandstones (Dann et al., 2014). Uranium contents in the MFd are mostly below 1 ppm, but values greater than 1 ppm are not uncommon (Dann et al., 2014). Furthermore, many humus and B-horizon soil contain U greater than 1 ppm. The amount is sufficient to explain Rn contents in most samples. Therefore, we conclude that it is highly likely that U and probably Ra in sandstones at shallow levels and soil are the sources of Rn observed in groundwater.

The fifth possibility is U in granitic boulders and erratics in glacial sediments. This cannot be discounted, but we do not consider this as the most likely source of Rn and He. It is too fortuitous for high U-granitic boulders to be present in the areas directly above U deposits.

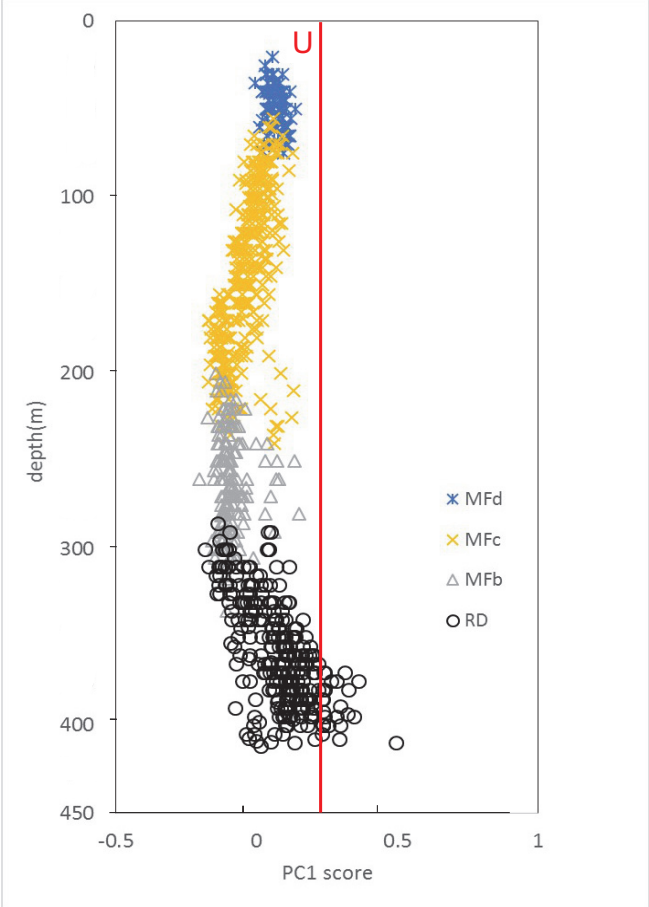

Figure 9. Vertical scores of Principal Component 1 of sandstones above the Phoenix deposits. Elements in component 1 are rare earth elements, Y, U, B, Na, Mg, K, Li and Pb (after Chen et al., 2014). The score of PC1 for U is shown with a red line. Note that sandstones of RD and MFd plot close to the vertical line of U.

Implications for Exploration

1. Sampling over the Phoenix and Millennium deposits has demonstrated that geochemical anomalies are detectable in surface media, even from deeply-seated deposits situated 400 m and 750 m below the surface, respectively. The surficial geochemical anomalies are influenced by many factors, such as groundwater flow, abundance of faults, and glacial sediments. Anomalies may not be apparent in a single medium in individual site. Different media, such as soil and gases need to be examined in concert.
2. The distributions of geochemical anomalies in soil suggest that faults are implicated in metal transfers to the surface media, perhaps through water movement. Multi-year surveys of soil show repeatable soil geochemical anomalies.
3. The chemical composition and alteration of sandstones at shallow levels may provide a clue for the presence of deeply-seated U deposits. The information is very useful in exploration, especially in the interior of the basins where drilling of thick sandstone covers would be expensive.
4. Helium dissolved in water far below the water table level yielded promising results in the detection of buried U deposits in the Millennium property. Since He moves with water, a careful selection of sites is essential, particularly with respect to porous till and sand. While elevated Rn concentrations were detected at both properties, the short half-life and relatively slow transport mechanisms from the deeply-buried ore likely prevents it from reaching surface media. Therefore, Rn observed in groundwater in drill holes likely originated from a proximal source such as U or Ra in the upper sandstones and/or soil.

Acknowledgments

We thank Denison Mines Corporation and the Exploration and Mining departments at Cameco Corporation for their logistic support. The project was funded by a grant

from Natural Resources of Canada through the Targeted Geoscience Initiative Four program. The manuscript benefited from helpful reviews by Donald Wright, Janet Campbell and Paul Gammon.

References

Alexandre, P., Kyser, T.K., Jiricka, D., and Witt, G., 2012. Formation and Evolution of the Centennial Unconformity-Related Uranium Deposit in the South-Central Athabasca Basin, Canada; Economic Geology, v. 107, p. 385–400.

Bonham-Carter, G., and Hall, G., 2010. Multi-media techniques for direct detection of covered unconformity uranium deposits in the Athabasca Basin, Phase III, Final report of results of soil geochemistry using selective leaches; Canadian Mining Industry Research Organization (CAMIRO) Exploration Division, 280 p. <https://www.appliedgeochemists.org/index.php/publications/other-publications/2-uncategorised/116-camiro-project-08e01>

Bosman, S.A. and Card, C.D., 2012. Data File Report 31, Geochemical analyses of Athabasca Group drillholes in Saskatchewan (NTS 64L, 74F to 74K, and 74N to 74P)-Supplementary to Data File Reports 24, 29, and 30; Saskatchewan Ministry of Energy and Resources.

Cameco Corporation, 2013. The strength to dig deeper, 2013 Annual Report; Cameco Corporation, http://www.cameco.com/invest/ financial-information/annual-reports/2013

Cameron, E.M., 1983. Uranium Exploration in Athabasca Basin, Saskatchewan, Canada; Geological Survey of Canada Paper 82-11, 310 p.

Cameron, E.M., Hamilton, S.M., Leybourne, M.I., Hall, G.E.M., and McClenaghan, M.B., 2004. Finding deeply buried deposits using geochemistry; Geochemistry: Exploration, Environment, Analysis, v. 4, p.7–32.

Campbell, J. E. 2007. Quaternary geology of the eastern Athabasca Basin, Saskatchewan; in EXTECH IV: Geology and Uranium Exploration TECHnology of the Proterozoic Athabasca Basin, Saskatchewan and Alberta, (ed.) C.W. Jefferson and G. Delaney; Geological Survey of Canada Bulletin v. 588, p. 211–228

Card, C. D, Bosman, S. A., Simmon, W. L., Zmetana, D. J. and Delaney, G. D., 2011. Data File Report 29, Geochemical Analyses of Athabasca Group Outcrops in Saskatchewan (NTS 64L, 74F to 74K, & 74N to 74P); Saskatchewan Ministry of Energy and Resources.

Chen, S., Hattori, K. and Grunsky, E.C., 2014. Principal component analysis of sandstones overlying the Phoenix uranium deposits, Athabasca Basin; Geological Survey of Canada, Open File 7578. doi:10.4095/29492

Chen, S., Hattori, K., Grunsky, E.C., and Liu, Y., 2015. Geomathematical study of sandstones overlying the Phoenix uranium deposits and the REE-rich Maw Zone, Athabasca Basin, Saskatchewan; *in* Targeted Geoscience Initiative 4: unconformity-related uranium systems, (ed.) E.G. Potter and D.M. Wright; Geological Survey of Canada, Open File 7791, p. 21-31. doi:10.4095/295776

Clark, L.A.C., 1987. Near surface lithogeochemical halos as an aid to discovery of deeply buried unconformity-type deposits, Athabasca Basin, Canada; Journal of Geochemical Exploration, v. 28, p. 71–84.

Cloutier, J., Kyer, T.K., Olivo, G.R., and Brisbin, D., 2011. Geochemical, isotopic, and geochronlologic constraints on the formation of the Eagle Point basement-hosted uranium deposit, Athabasca Basin, Saskatchewan, Canada and recent remobilization of primary uraninite in secondary structures; Mineralium Deposita, V. 46, p. 35–56.

Cloutier, J., Kyer, T.K., Olivo, G.R., Alexandre, R., and Halaburda, J., 2009. The Millennium uranium deposit, Athabasca Basin, Saskatchewan, Canada: An atypical basement-hosted unconformity-related uranium deposit; Economic Geology, v.104, p. 815–840

Coker, W.B., and Dunn, C.E., 1981. Lake water and sediment geochemistry; NEA-IAEA Athabasca Basin-Wollaston lake test area, Saskatchewan; Geological Survey of Canada, Open File 779, 100 p. doi:10.4095/129693

Dann, J., Hattori, K., Potter, E.G., and Sorba, C., 2014. Discrimination of elemental assemblages in the alteration halo of the Phoenix deposit, Saskatchewan, Through Applied GIS; Geological Survey of Canada, Open File 7463, doi: 10.4095/293122.

Devine, M., Hattori, K., and Kotzer, T., 2013. Radon concentrations of groundwater in the Millennium property, Athabasca Basin; Saskatchewan Geological Survey Open House.

Dimitrov, D.D., Bhatti, J.S., and Grant. R.F. 2014. The transition zones (ecotone) between boreal forests and peatlands: Modelling water table along a transition zone between upland blackspruce forest and poor forested fen in central Saskatchewan; Ecological Modelling, v. 274, p. 57–70.

Dudek, N., and Hattori, K., in press. Radon distribution and concentrations above buried uranium ore: Denison Mine's Phoenix deposits, Saskatchewan; Geological Survey of Canada, Scienific Presentation, 1 poster.

Dunn, C., 2010. Biogeochemical Surveys at Cigar West, and McClean South: Athabasca Basin, Saskatchewan; Unpublished CAMIRO Final Report, 39p.

Dyck, W., 1969. Development of uranium exploration methods using radon; Geological Survey of Canada, Paper 69-46, 26 p.

Gamelin, C., Sorba, C., and Kerr, W., 2010. The discovery of the Phoenix deposit: A new high-grade, Athabasca Basin unconformity-type uranium deposit, Saskatchewan, Canada; in Saskatchewan Geological Survey Open House 2010, Abstracts, 17, p. 10.

Gunn, K.B. and Mistry, K.B., 1970. The effect of chelating agents on the adsorption of radium by plants; Plant and Soil, v. 33, p. 7-16.

Hamilton, S.M., Hattori, K.H., Clark, I.D., 2005. Investigation into the source of forest-ring-related natural gas in northern Ontario; Ontario Geological Survey Open File Report 6172, p.19-1–19-4.

Hinchey, J.G., and Hattori, K., 2007. Lead isotope study of the late Archean Lac des Iles palladium deposit, Canada: Enrichment of platinum group elements by ponded sulfide melt; Mineralium Deposita, v. 42, p.601–611.

Jefferson, C.W., Thomas, D.J., Gandhi, S.S., Ramaekers, P., Delaney, G., Brisbin, D., Cutts, C., Portella, P., and Olso, R.A., 2007. Unconformity-associated uranium deposits of the Athabasca Basin, Saskatchewan and Alberta; in EXTECH IV: Geology and Uranium Exploration TECHnology of the Proterozoic Athabasca Basin, Saskatchewan and Alberta, (ed.) C.W. Jefferson and G. Delaney; Geological Survey of Canada, Bulletin 588, p.23–67.

Jiricka, D., 2010. The Centennial deposit—an atypical unconformity-related uranium deposit—an update; International Association on the Genesis of Ore Deposits (IAGOD), 13th Quadrennial IAGOD Symposium, Adelaide, Australia, 6–9 April 2010, Proceedings.

Kerr, W.C., 2010. The discovery of the Phoenix deposit: a new high-grade Athabasca Basin unconformity-type uranium deposit, Saskatchewan, Canada; in The Challenge of Finding New Mineral Resources: Global Metallogeny, Innovative Exploration, and New Discoveries, Volume II: Zinc-Lead, Nickel-Copper-PGE, and Uranium, (ed.) R.J. Goldfarb, E.E. Marsh and T. Monecke; Society of Economic Geologists, p. 703–725.

Krahenbil, A., Hattori, K., Power, M., and Kotzer, T., 2014. Surficial geochemistry associated with the deeply buried Millennium and Phoenix uranium deposits, Athabasca Basin, Northern Saskatchewan; Geological Survey of Canada, Open File 7611, doi:10.4095/293928

Leaney, F.W. and Herczeg, A.L., 2006. A rapid field extraction method for determination of radon-222 in natural waters by liquid scintillation counting; Limnology and Oceanography; Methods v. 4, p. 254–259.

Maurice, Y.T., Dyck, W., and Strand, J.G., 1985. Secondary dispersion around the uranium-nickel deposit at Key Lake, northern Saskatchewan; in Geology of Uranium Deposits, (ed.) T.I.I. Sibbald and W. Petruk; Canadian Institute of Mining and Metallurgy, v. 32, p. 38–47.

Power, M.J., Hattori, K., Sorba, C. and Potter, E.G., 2012. Geochemical anomalies in the soil and uppermost sandstones overlying the Phoenix uranium deposit, Athabasca Basin, Saskatchewan, Canada; Geological Survey of Canada, Open File 7257, 36 p., doi:10.4095/291981

Power, M.J., Hattori, K., Sorba, C., Kotzer, T., Potter, E.G., 2013a. Surface media expressions of buried uranium: the Phoenix and Millennium deposits, Athabasca Basin, Saskatchewan, Canada; 12th Biennial meeting of Society for Geology Applied to Mineral Deposits, Uppsala, Sweden. v. 1, p. 426–429.

Power, M., Hattori, K., Pinti, D., Potter, E.G., 2013b. Anomalous abundances of He and mobile metals in surface media over the deeply buried Millennium U deposit, Athabasca Basin, Canada; in 2013 Goldschmidt Conference, Mineralogical Magazine, v. 77, p.1993. doi:10.1180/minmag.2013.077.5.16

Power, M., Hattori, K., Krahenbil, A., Sorba, C., Kotzer, T. and Potter, E.G., 2014. Geochemical surface expression of the Phoenix and Millennium uranium deposits, Athabasca Basin: Improving exploration vectors; PDAC-CMIC-SEG Canada Student Minerals Colloquium, http://cmic-footprints.ca/pdac-smc/2014

Reid, K.D., Ansdell, K., Jiricka, D., Witt, G., and Card, C., 2014. Regional setting, geology, and paragenesis of the Centennial unconformity-related uranium deposit, Athabasca Basin, Saskatchewan, Canada; Economic Geology, v. 109, p. 539–566

Roscoe, W.E., 2014. Technical report on a mineral resource estimate update for the Phoenix uranium deposit, Wheeler River project, Eastern Athabasca Basin, northern Saskatchewan, Canada; NI 43-101 Technical Report prepared for Denison Mines Corp., 134 p.

Sanford, W. E., Shropshire, R.G., and Solomon, D. K., 1996. Dissolved gas tracers in groundwater: Simplified injection, sampling, and analysis; Water Resources Research, v. 32, p. 635–1642.

Schreiner, B.T. 1984. Quaternary geology of the Precambrian Shield, Saskatchewan; Saskatchewan Energy and Mines Report, 221, 1 map, scale 1:1 000 000.

Smith, R.S., Wood, G.R., Powell, B., 2010. Detection of alteration at the Millennium uranium deposit in the Athabasca Basin: a comparison of data from two airborne electromagnetic systems with ground resistivity data; Geophysical Prospecting, v. 58, p.1147–1158.

Sopuck, A.J., de Carla, A., Wray, E.M., and Cooper, B., 1983. The application of lithogeochemistry in the search for unconformity-type uranium deposits, northern Saskatachewan, Canada; Journal of Geochemical Exploration, v. 19, p. 77-99.

Thomas, D.J., Matthews, R.B., and Sopuck, V.J., 1998. Athabasca basin unconformity-type uranium deposits: A synopsis of the empirical model and review of exploration and production trends; Canadian Institute of Mining, Metallurgy and Petroleum meeting, Montreal 1998, Proceedings, CD-ROM.

Todt, W., Cliff, R.A., Houser, A. and Hofmann, A.W., 1995. Evaluation of a ^{202}Pb -^{205}Pb double spike for high precision analyses; in Earth Processes: Reading the Isotopic Code, (ed.) A. Basu and S. Hart; American Geophysical Union Geophysical Monograph v. 95, p. 429–437.

Wasyliuk, K., 2006. Geochemical methods in the Athabasca Basin: Past, Present and Future; in, Uranium: Athabasca Deposits and Analogues; Canadian Institute of Mining, Metallurgy and Petroleum Field Conference, Saskatoon, CD-ROM.

Wood, G., O'Dowd, C., Cosma, C., and Enescu, N., 2012. An interpretation of surface and borehole seismic surveys for mine planning at the Millennium uranium deposit, northern Saskatchewan, Canada; Geophysics, v. 77, p.WC20–WC212.

Yaws, C.L., 2009. Diffusion Coefficients in Water – Inorganic Compounds; in Transport of Chemicals and Hydrocarbons, (ed.) C.L. Yaws; Elsevier Inc., p. 594–596.

Yeo, G.M. and Delaney, G., 2007. The Wollaston Supergroup, stratigraphy and metallogeny of a Paleoproterozoic Wilson cycle in the Trans-Hudson Orogen, Saskatchewan; in EXTECH IV: Geology and Uranium Exploration TECHnology of the Proterozoic Athabasca Basin, Saskatchewan and Alberta, (ed.) C.W. Jefferson and G. Delaney; Geological Survey of Canada, Bulletin 588, p. 89–117.

Ground-truthing of the 'Eastern Athabasca Basin' Regional Airborne Gamma-ray Survey: Context for Exploration of Deeply Buried Unconformity-related Uranium Deposits in the Athabasca Basin of Northern Saskatchewan

Richard Fortin,[1] Janet E. Campbell[1], Brad J.A. Harvey[1], Martin W. McCurdy[1], Laurel E. Sinclair[1], Michelle, A. Hanson[2], Eric G. Potter[1] and Charles W. Jefferson[1]

1. Geological Survey of Canada, 601 Booth Street, Ottawa, Ontario, K1A 0E8

2. Saskatchewan Geological Survey, 2101 Scarth Street, Regina, Saskatchewan, S4P 2H9

Abstract

With uranium exploration shifting to greater depths and more indirect targets, new tools and better use of existing data are needed to maximize exploration efficiency. Recent and historical research has demonstrated that although deeply-buried beneath Athabasca Group sandstones, unconformity-related uranium deposits still may be targeted by understanding subtle surficial geochemical anomalies.

Airborne gamma-ray spectrometric surveys can be used for effective surficial geochemical mapping of K, U and Th over large areas and have been conducted by the Geological Survey of Canada across much of the Canadian Shield over the past 50 years, notably in partnership with Saskatchewan over the Athabasca Basin. To apply the results of these surveys to uranium exploration, the effects of deposit-related geochemical anomalies on airborne gamma-ray measurements must be predicted. And, just as importantly, the background in terms of K, U and Th above which these anomalies have to be detected, has to be quantified and its genetic linkages understood.

The "Eastern Athabasca Basin" airborne gamma-ray survey was conducted in partnership with the Saskatchewan Geological Survey in 2009. This regional survey was ground-truthed along the corridor between Key Lake and the McArthur River mine site in 2013. High-resolution helicopter-borne gamma-ray acquisition, ground gamma-ray spectrometry, surficial material mapping, sampling and laboratory analyses were performed. Results indicate that the relationships between subsurface processes, glacial dispersal and airborne gamma-ray measurements are very intricate and responsive to detailed local surficial geological processes that have modified elemental dispersion from bedrock sources. In many cases, surficial sediments and landforms can be discriminated based on their K, U and Th geochemistry, relating in turn, to their provenance. Quantitative analysis of the airborne data, integrated with surficial geological knowledge, can differentiate between the complex patchwork of background domain levels and deposit-related surficial geochemical anomalies.

Introduction

From 2004 to 2010, through various provincial and federal programs, the Geological Survey of Canada (GSC), in partnership with the Saskatchewan Geological Survey (SGS), conducted airborne gamma-ray spectrometry and magnetic surveys in northern Saskatchewan and completed coverage of the entire Saskatchewan portion of the Athabasca Basin (Buckle et al., 2011). Gamma-ray spectrometry data acquisition followed up-to-date specifications as recommended by the International Atomic Energy Agency (IAEA, 1991, 2003). Usage of self-stabilizing digital spectrometers, state-of-the-art data processing, and continuous coverage with 125m survey altitude and 400m line-spacing contributed to the high quality of this unique data set.

Recent and historical research has demonstrated that although buried beneath Athabasca Group sandstones, unconformity-related uranium deposits may be targeted by understanding subtle surficial geochemical anomalies that reflect a variety of processes from regional diagenetic-mineralogical alteration patterns, through hydrothermal alteration halos more directly associated with deposits, to specific sites where mobile metals including decay products may be brought to the uppermost sandstones and surficial media along structural pathways (Sopuck et al., 1983, Clark, 1987, Earle and Sopuck, 1989, Thomas et al., 2000; Bonham-Carter and Hall, 2010, Power et al., 2012; Dann et al., 2014; Hattori et al., 2015). In regard to the interpretation of airborne gamma-ray spectrometry maps, expressions of these anomalies in surficial media have to be quantified in terms of K, U and Th concentrations. The background above which these anomalies have to be detected has also to be defined and quantified, and its genetic linkages to bedrock and Quaternary geology have to be understood.

The regional Eastern Athabasca Basin airborne magnetic and gamma-ray spectrometric survey was conducted in 2009 (Buckle et al, 2010), and includes coverage of the producing Key Lake - McArthur River corridor (Fig. 1). Distinct patterns in radioelement concentrations are recognized on the airborne maps, and to define the nature of this background, field validation activities were carried out in 2013. The relationships of these radiometric features to surficial geology are examined and the implication for targeting surface anomalies related to uranium deposit is discussed.

Exploration Context

Airborne gamma-ray spectrometry (AGRS) surveys can be used for effective surficial geochemical mapping of potassium (K), uranium (U) and thorium (Th) over large areas, and have been conducted by the Geological Survey of Canada across much of the Canadian Shield over the past 50 years. Concentrations in uranium and thorium are usually reported as equivalent uranium (eU) and equivalent thorium (eTh) to emphasize that these measurements are based on the assumptions that these radioelements are in radioactive equi-

Fortin, R., Campbell, J.E., Harvey, B.J.A., McCurdy, M.W., Sinclair, L.E., Hanson, M.A., Potter, E.G., and Jefferson, C.W., 2015. Ground-truthing of the 'Eastern Athabasca Basin' Regional Airborne Gamma-ray Survey: Context for Exploration of Deeply Buried Unconformity-related Uranium Deposits in the Athabasca Basin of Northern Saskatchewan, *in* Targeted Geoscience Initiative 4: unconformity-related uranium systems, (ed.) E.G. Potter and D.M. Wright; Geological Survey of Canada, Open File 7791, p. 43–51. doi:10.4095/295776

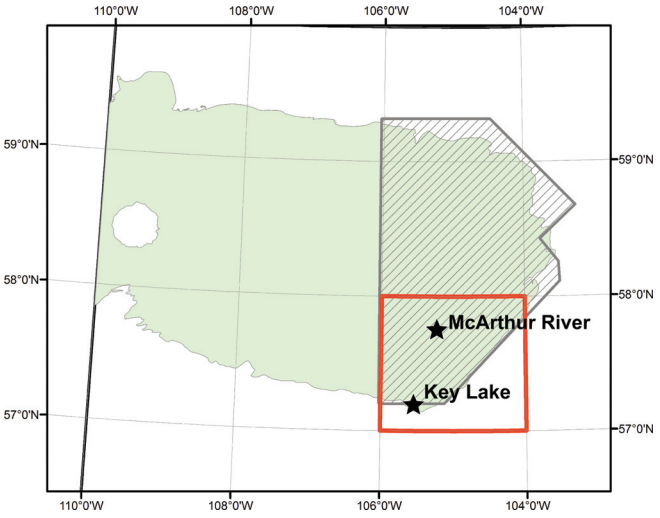

Figure 1. Location of the Athabasca Basin in Northern Saskatchewan (green), and of the Eastern Athabasca Basin airborne survey (hatched). Limits of NTS sheet 74H are outlined in red (see Fig. 3).

Table 1. Average radioelement concentrations in the Athabasca Basin in the area covered by NTS sheet 74H, calculated from the Eastern Athabasca airborne survey results.

	Potassium (%)	Equivalent Uranium (ppm)	Equivalent Thorium (ppm)
NTS sheet 74H – Basin limit	0.46	0.55	4.2
crustal averages	2.4	3	12
Sandstone	1.2	1.9	5.7

For comparison, average concentrations in the earth's crust (Dickson and Scott, 1997) and in sandstone (Galbraith and Saunders, 1983) are also presented. The very low radioactivity background observed in the surficial materials of the eastern Athabasca Basin appears favorable to the detection of weak anomalies.

librium (IAEA, 2003). In contrast to many of the other geophysical techniques that provide structural information about the subsurface, AGRS provides compositional information about surficial geological materials. As such, the interpretation approaches of exploration geochemistry are appropriate to AGRS data analysis. Applications of AGRS have been reviewed in various reports (e.g. Shives et al., 2000a; IAEA, 2003; Ford et al., 2007; Campbell et al., 2007).

Geophysical gamma-ray spectrometry is a surface technique; only about the first 30 cm of the surface is sampled by either airborne or ground-based measurements. It has however, a relatively large footprint, with a diameter of 2 to 3 m, for typical ground spectrometry instrument and about four times the flying height, for airborne spectrometry. The elements of the unconformity-related uranium deposit exploration model that are relevant to gamma-ray spectrometry surveying are therefore those which result in a surface expression.

An anomalous regional clay alteration pattern in the sandstone of the Athabasca Basin has been outlined by Earle and Sopuck (1989) and surrounds the Key Lake - Cigar Lake corridor where major deposits are located. Surface expressions of these alteration minerals have been observed in boulders (Earle et al., 1990, Shives et al., 2000b) and locally-derived till (Simpson and Sopuck, 1983). Illite anomalies, and resulting enrichment in potassium, could therefore provide a surface target for AGRS. Uranium anomalies in till and soils located above the alteration chimney of deposits have also been observed (Simpson and Sopuck, 1983; Matthews et al., 1997; Bonham-Carter and Hall, 2010; Power et al., 2012; Hattori et al., 2015) with concentration levels within the range of sensitivity of airborne and ground gamma-ray spectrometry. In many cases, these surficial anomalies have undergone secondary glacial dispersal and are displaced down-ice from their source, effectively enlarging the very subtle traces they are leaving at the surface.

Discriminating these weak potassium or uranium anomalies from the heterogeneous surficial background remains a challenge. For example, a 5 ppm uranium anomaly in the first 3 cm of soil, similar to results from Power et al. (2012), would appear diluted by a factor of 10 in the 30-cm deep sampling volume of a ground gamma-ray spectrometry measurement and would then result in values in the order of 0.5 ppm eU. This value is within the same range as the average background uranium concentrations measured in the surficial materials of the Athabasca Basin (Table 1), and exemplify that it is essential to characterize the radioelement background in terms of the Quaternary geological framework in order to discriminate anomalies of interest.

Geological and Quaternary Setting

The conglomeratic sandstone bodies that constitute the Athabasca Basin are thoroughly oxidized terrestrial redbed sequences with a complex alteration history (Ramaekers et al., 2007; Jefferson et al., 2007). In the area of interest, the underlying basement rocks are the supracrustal metasediments of the Wollaston Group that rest on Archean granitic gneiss domes (Card et al., 2007). Variations in surface concentrations of the natural radio-elements result from this geological context but also from the physical processes shaping the surface environment.

The present day landscape of the eastern Athabasca Basin area is primarily a product of the advance and retreat of the ice sheet during the Late Wisconsinan. The main ice flow direction during the deglaciation was to the south-west and produced the large drumlins seen in the eastern part of the basin. A more localised late stage re-advance or margin re-adjustment shifted the ice flow towards the south. This late flow is recorded primarily by flutings, small scale drumlinoids and minor east-trending moraine ridges which discontinuously overprint the large-scale drumlins (Campbell, 2007). The tills related to these two ice flows differ in composition and provenance. In this region, the material which comprises the regional large-scale landforms is generally a silty sandy basement-rich till while the overlying deposits

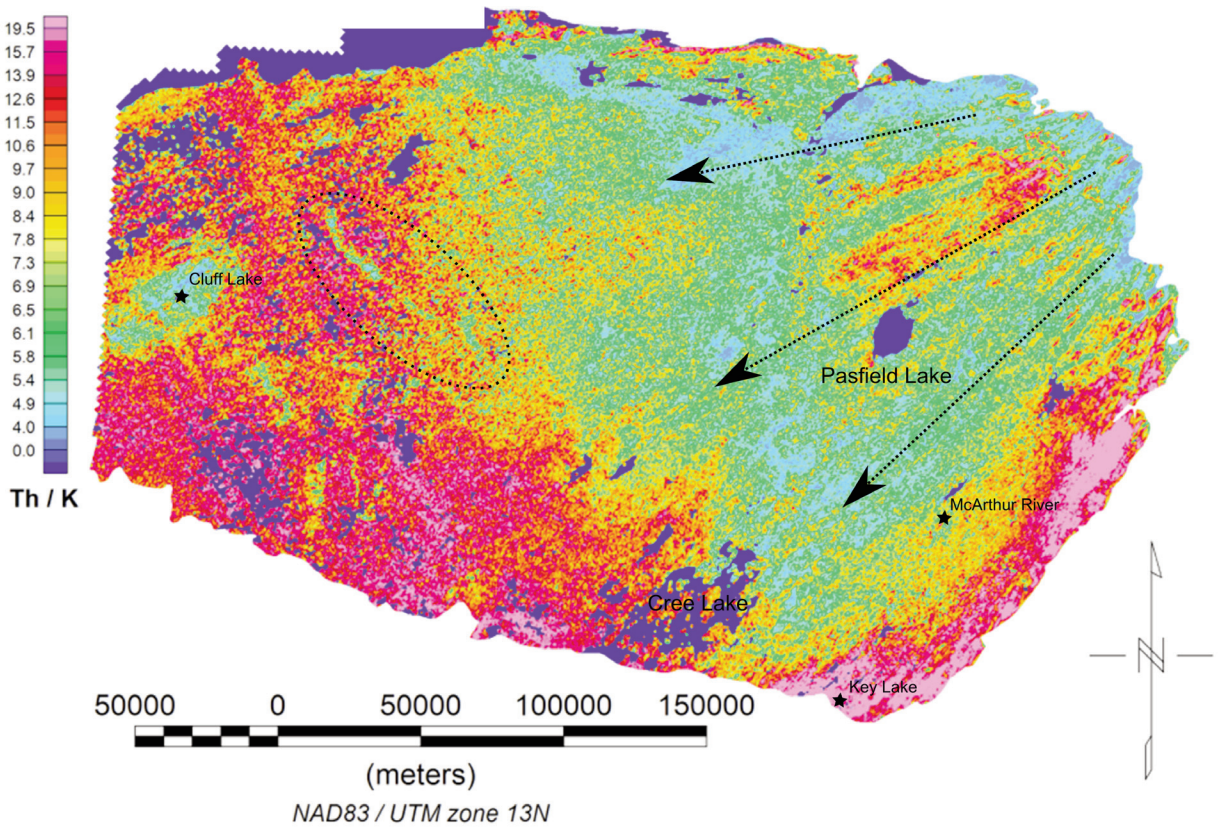

Figure 2. Compilation of thorium concentration over potassium concentration (RTK) obtained from airborne gamma-ray surveys conducted by the Geological Survey of Canada and Saskatchewan Geological Survey over the entire Saskatchewan portion of the Athabasca Basin. Southwest- to west-trending features (arrows), reflect regional ice flow during the Late Wisconsinan early deglaciation. An east-west transition from low RTK to high RTK values may represent the extent of the regional glacial dispersal of basement-derived material over the basin. Low RTK values with north-westerly trends, (dashed circles), are suggestive of end moraines of the retreating ice margin. Deep-blue color represents nulled values, due to waterbodies.

are a sandier, predominantly sandstone derived till.

In the eastern Athabasca Basin, this landform-sediment relationship and resulting compositional differences in surface tills are reflected in the map of the ratio of thorium to potassium concentrations (RTK), which exhibit numerous south to southwest trending features (Fig. 2) and comparatively elevated concentrations of potassium. These features are overprinted by distinctive areas of elevated concentration of thorium, especially on the south-eastern margin of the Basin and in southwest trending features, to the north. These features appear to be part of a regional scale pattern that fans out over the Athabasca Basin from the north-east in direction of the ice flow (Fig. 2). The potassium dominated and low RTK signature reaching past the middle of the basin toward the west may represent the extent of the regional glacial dispersal of basement-derived material over the basin. Northwesterly linear features just to the east of the Carswell structure and Cluff Lake are moreover suggestive of end-moraines that may relate to this dispersal. In contrast, the thorium-dominated and high RTK areas, bordering the south-eastern margin of the Basin and also observed locally in the northern-eastern part, appear as a surface trace of the thorium-rich Manitou Falls Formation Bird and Collins Members (Mwenifumbo and Bernius, 2007) and are therefore indicative of more locally derived material in the surface till.

The potassium dominated signature is indicative of a higher proportion of extra-basinal igneous or metamorphic materials in the surface media, while the thorium dominated signature relates to the potassium-poor and thorium-rich sandstones of the Athabasca group, with RTK values quantitatively discriminating between these basement-derived and sandstone-rich surface materials. As till is the most common glacial deposit in the eastern Athabasca Basin region, this first-level heuristic classification of surface materials based on RTK contrast appears to correlate with the Till 2 and Till 3 Quaternary stratigraphic units defined by Campbell (2007). Till 2 contains a significant component of more dis-

tally derived, crystalline shield detritus, and is the most extensive till deposit in the region. Till 3 has a higher component of locally derived sandstone material and discontinuously overlies till 2. Till 3 is associated with the late stage readvance of the ice sheet during the late Wisconsinan deglaciation.

Field Validation

Field validation activities were conducted in July and October 2013 in the region covered by NTS sheet 74H within seven areas located in the corridor between Key Lake and McArthur River (Fig. 3). These locations were selected to cover the radiometric domains identified in a preliminary data parsing exercise (Fortin et al., 2014). Each area also intersected either a known geological element potentially capable of producing a contrasting gamma-ray output, or a distinctive feature in term of its radioelement concentrations, as recognized from the regional Eastern Athabasca airborne survey.

High-resolution airborne gamma-ray spectrometry surveys were conducted over all seven areas with a Bell 206B helicopter. The survey system consisted of two 40 cm by 10 cm by 10 cm thallium-doped sodium iodide gamma-ray detectors, a geodetic GPS receiver, an inertial measurements unit and a laser altimeter, and was carried in an externally skid-mounted cargo expansion. The survey parameters for the two areas selected for discussion below are presented in Table 2. Maps of radioelements (K, eU and eTh) concentrations were produced.

Ground gamma-ray spectrometry measurements were collected at targeted stations in each of the seven areas. Typically, a series of 120-seconds measurements were taken using a hand held spectrometers equipped with either a 103 cm^3 bismuth germanate detector or a 347 cm^3 thallium-doped sodium iodide detector. The measurements were collected within 2 meters of the station's location and averaged. Sediments within the first 30 to 50 cm from the surface were documented and samples were collected from primarily the Ae or B soil horizon. The samples were prepared as bulk and less than 2mm size fraction subsamples for measurement of K, eU and eTh concentrations in the GSC gamma-ray spectrometry laboratory in Ottawa. Geochemistry of the less than 2 mm size fraction, matrix texture and pebble lithology were also determined for further composition characterisation of the sediments, although these results will not be discussed here.

Results

A preliminary analysis and interpretation of the high resolution airborne gamma-ray spectrometry surveys is presented below for field study areas A5 and A4 (Fig. 3).

A5 Area

This area was selected for ground validation activities because it contains a variety of glacial landforms ranging from large drumlins typical of this region, to streamlined, smaller drumlinoid ridges, smaller-scale flutings and flat plains, all within the 5 km^2 area covered. Potassium concentrations show southwestward trends (Fig. 4a), with ridges of elevated concentrations (0.5–0.8 % K) intercalated between "valleys" exhibiting comparatively lower concentrations (0.2–0.4 % K).

These low-potassium valleys are observed to be coincident with topographic highs that are expressed by small streamlined drumlinoid ridges, whereas in the southern corner of the survey area more prominent potassium features are observed in relation to larger scale landforms. This is confirmed by ground spectrometry measurements and laboratory analysis of the samples obtained from the 6 targeted ground-truthing stations, where RTK values offer a better contrast between the measurement stations (Fig. 4d).

Basement-derived Till 2 was observed on the large drumlin in the south corner of the survey area, where higher potassium content, and lower RTK values, is measured by both airborne and ground-based spectrometry. This is representative of the main ice-flow of the late stages of the late Wisconsinan glaciation. In contrast, sandstone-rich Till 3 was identified in the three smaller drumlinoid ridges to the north, where lower potassium concentrations, and higher RTK values, are obtained. The axis of the drumlinoid ridges have a slightly more southward orientation in comparison to the larger drumlin, suggestive of a remoulding of theses landforms, consequent from the re-advance and shift in flow direction of the ice margin towards the south. Finally, glaciofluvial deposits observed between the smaller drumlinoid ridges yield higher potassium content measurements, indicative of their more diverse provenance.

A4 area

This area, located along the P2 fault was selected to compare measurements with the study of Shives et al. (2000b) in which sandstone boulders were surveyed to identify potassium enrichment due to illite-rich clay alteration.

For the series of northeast-southwest trending drumlins sampled by stations 1 to 4 and extending from the south corner to the north border of the survey area, the low potassium concentrations obtained from the airborne measurements (0.15–0.30 % K) and comparatively higher RTK values obtained from ground spectrometry agrees with the observations of sandstone-rich till at the measurement stations (Fig. 5). However, the results from the gamma-ray spectrometry laboratory analysis don't agree as well with the airborne measurements and the till observations. It is suggested that the location of the targeted measurement stations, at the margins of the landforms, were not optimal. The samples collection was conducted in location of discontinuous Till 3 coverage and the larger footprint of the gamma-ray spectrometry measurements may have provided more representative measurements than the laboratory analysis, on much smaller samples, by effectively averaging local heterogeneity in till coverage.

Sandstone-rich till coverage would also be expected on the series of drumlins toward the southwest corner of the survey block, but airborne measurements shows a large region of higher concentrations in potassium, reaching values in the range of 0.50 % K, covering all these narrow landforms. By highlighting troughs between the drumlins, it can be seen, however that this seemingly uniform area in potassium concentration present in fact a series of southwest trending

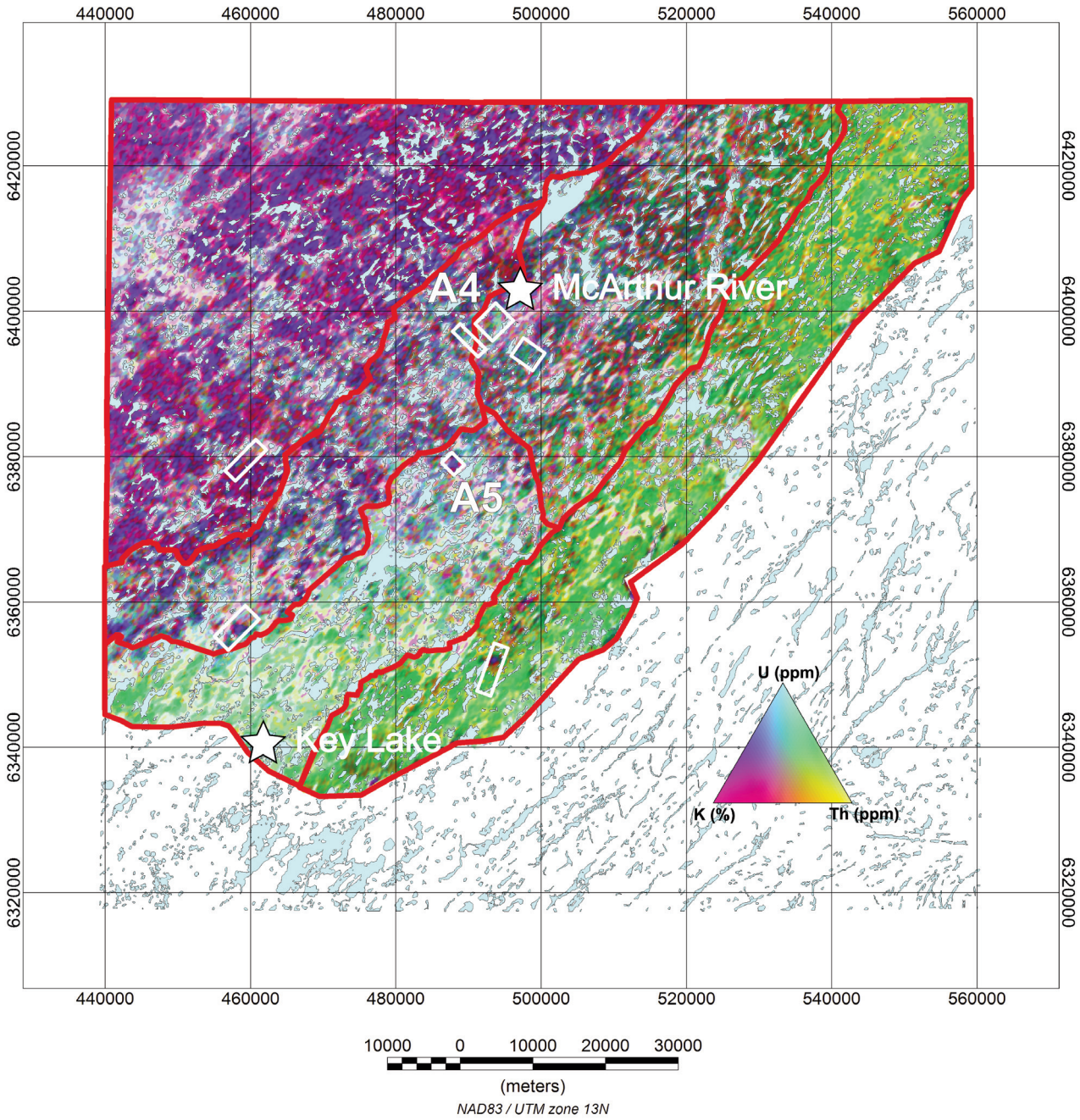

Figure 3. NTS 74H area map presenting the location of the field validation areas (white outline). Areas A4 and A5 that are discussed in the text are highlighted. Background map is the composite ternary image of natural radioelements computed from the Eastern Athabasca Basin airborne Survey data. Red outlines correspond to radiometric domains defined and reported by Fortin et al. (2013).

Table 2. Flight parameters of the airborne survey areas A4 and A5.

Survey Area	*line length* (m)	*line azimuth* (deg)	*line spacing* (m)	*lateral extent* (m)	*flight lines*	*total line-km* (km)	*nominal survey speed* (m/s)	*flight altitude* (m)
A4	3500	135	100	4000	41	143.5	30	40
A5	2400	135	25	2000	81	194.4	25	25

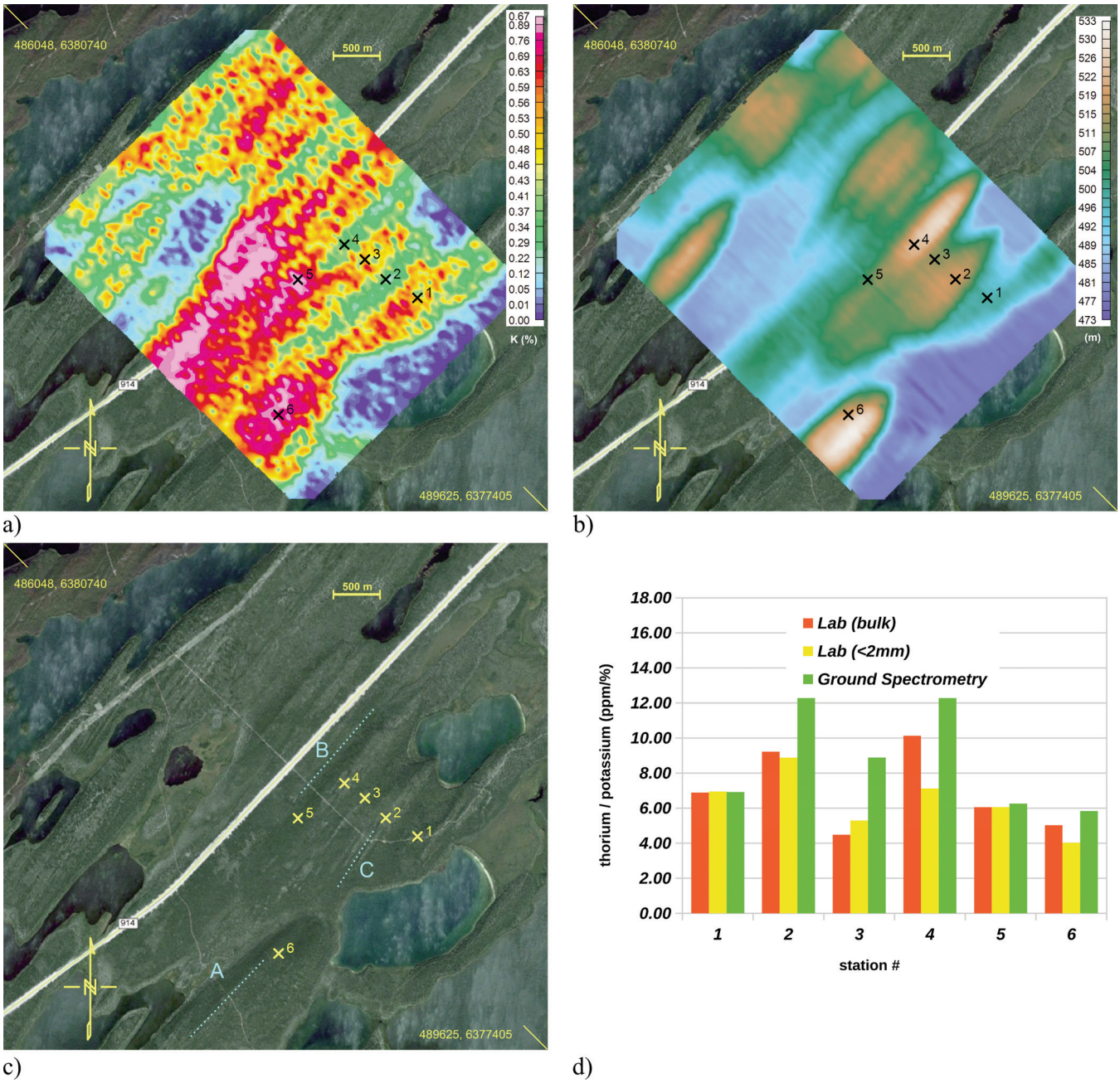

Figure 4. Field validation results from the A5 area. Crosses labelled 1 to 6 indicates locations of ground truthing measurement stations. Coordinates are in the UTM 13N, NAD 83 system. A) Map of K concentrations (%) obtained from the 2013 high resolution airborne survey. B) Digital terrain model (height above the GRS80 Ellipsoid) created with the laser altimetry data obtained from the 2013 high resolution survey. C) Interpreted satellite imagery (Google Earth) of Area A5. 'A' line indicates trend of large drumlin from main ice flow. Lines 'B' and 'C' indicate trends of remoulded drumlinoids and flutings, respectively, resulting from the ice readvance during the late stages of the Late Wisconsinan. D) Results of field measurements of K and Th concentrations (as RTK ratios) by ground and laboratory gamma-ray spectrometry for each of the ground stations.

ridges in potassium concentration (Fig. 5). A sandy diamicton with an elevated basement component, identified at station 6, as well as glaciofluvial sands filling the topographically low areas exhibit locally high signal in potassium concentrations that nearly mask the comparatively lower signature of the sandstone-rich till on top of the drumlins in the footprint of the airborne gamma-ray detector. A discontinuous low potassium signal can be observed along these topographical ridges on the airborne measurement map (Fig. 5a).

Conclusion and Implications for Exploration

Airborne gamma-ray spectrometry data is available for the entire Saskatchewan portion of the Athabasca Basin and its analysis should be part of exploration programs in this region. AGRS maps can be segmented into radiometric domains (Campbell et al., 2007; Fortin et al., 2014) to enhance their readability and to provide local baselines against which gamma-ray spectrometry measurements can be identified as anomalous. A further approach consists in

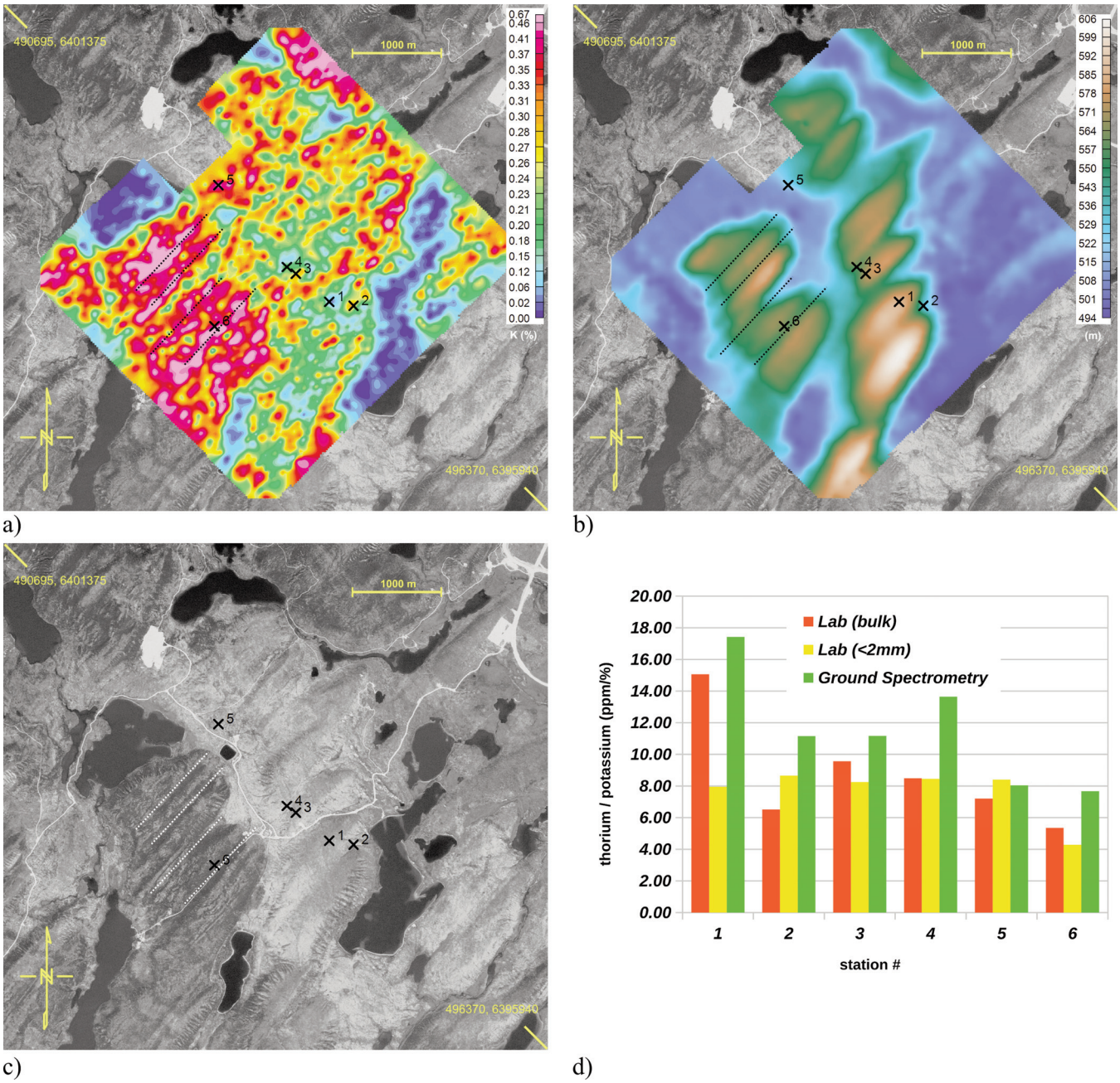

Figure 5. Field validation results from the A4 area. Crosses labelled 1 to 6 indicates locations of ground truthing measurement stations. Coordinates are in the UTM 13N, NAD 83 system. A) Map of the potassium concentration (in percent) obtained from the 2013 high resolution airborne survey. B) Digital terrain model (height above WGS84 Ellipsoid) created with the laser altimetry data obtained from the 2013 high resolution survey. Troughs between streamlined landforms in the western portion of the survey area have been highlighted and are reproduced on the other maps. C) Satellite imagery (SPOT) of area A4. D) Results of field measurements of K and Th concentrations (as RTK ratios) by ground and laboratory gamma-ray spectrometry for each of the ground stations.

integrating gamma-ray data with lineament analysis from aeromagnetic surveys and regional geochemical data to highlight hydrothermally altered structural features (Wright, 2014).

In this regard, characterizing the radioelement background to deposit-related surficial radiometric anomalies is an essential step and requires an understanding of the regional Quaternary geology. In the eastern Athabasca Basin, surficial sediments and landforms can be discriminated based on their K, U and Th geochemistry, linking to their provenance, but glaciofluvial sediments are pervasive in the areas studied and often mask signal of interests. Due to their higher concentrations in radioelements, the gamma-ray response of these sediments could cover anomalous signal from targets of exploration interest. From an exploration perspective, areas of sandstone-rich till, which exhibit a weak gamma-ray

background signature in K and eU, appear much more favorable to the detection of weak anomalies from deposits alteration halos. When combined with surficial geology, sandstone and surficial geochemistry, and bedrock structural framework, airborne gamma-ray spectrometry surveys can help delineate and prioritize areas of interest thus resulting in more successful and cost effective uranium exploration programs in the Athabasca Basin.

Acknowledgments

This report is a contribution to the Targeted Geoscience Initiative 4 (TGI-4), uranium ore systems project. This project would not have been possible without logistical support from Cameco Corporation. This manuscript benefitted from a constructive review by Victoria Tschirhart and the editorial handling of Donald Wright.

References

Bonham-Carter, G., and Hall, G., 2010. Multi-media techniques for direct detection of covered unconformity uranium deposits in the Athabasca Basin, Phase III, Final report of results of soil geochemistry using selective leaches; Canadian Mining Industry Research Organization (CAMIRO) Exploration Division, 280 p. URL<https://www.applied-geochemists.org/index.php/publications/other-publications/2-uncategorised/116-camiro-project-08e01>

Buckle, J.L., Carson, J.M., Miles, W.F., Ford, K.L., Fortin, R., Delaney, G., 2011. Geophysical series, geophysical compilation northern Saskatchewan; Geological Survey of Canada, Open File 7039, 10 map sheets.

Buckle, J.L., Coyle, M., Kiss, F., Carson, J.M., Delaney, G., and Hefford, S.W., 2010. Geophysical Series, airborne geophysical survey of the Eastern Athabasca Basin, Saskatchewan, NTS 74 H and part of 64 E, Geikie River, Compulsion Bay; Geological Survey of Canada, Open File 6347, 10 map sheets.

Campbell, J.E., 2007. Quaternary geology of the eastern Athabasca Basin, Saskatchewan; in EXTECH IV: Geology and Uranium EXploration TECHnology of the Proterozoic Athabasca Basin, Saskatchewan and Alberta, (ed.) C.W. Jefferson and G. Delaney; Geological Survey of Canada Bulletin 588, p. 211–228.

Campbell, J.E., Klassen, R.A., and Shives, R.B.K., 2007. Integrated field investigations of airborne radiometric data and drift composition, Nuclear Energy Agency–International Atomic Energy Agency Athabasca test area, Saskatchewan; in EXTECH IV: Geology and Uranium EXploration TECHnology of the Proterozoic Athabasca Basin, Saskatchewan and Alberta, (ed.) C.W. Jefferson and G. Delaney; Geological Survey of Canada Bulletin 588, p. 533–554.

Card, C.D., Pana, D., Portella, P., Thomas, D.J., and Annesley, I.R., 2007, Basement rocks to the Athabasca Basin, Saskatchewan and Alberta; in EXTECH IV: Geology and Uranium EXploration TECHnology of the Proterozoic Athabasca Basin, Saskatchewan and Alberta, (ed.) C.W. Jefferson and G. Delaney; Geological Survey of Canada Bulletin 588, p. 69–88.

Clark, L.A.C., 1987. Near surface lithogeochemical halos as an aid to discovery of deeply buried unconformity-type deposits, Athabasca Basin, Canada; Journal of Geochemical Exploration, v. 28, p. 71–84.

Dann, J., Hattori, K., Potter, E.G., and Sorba, C., 2014. Discrimination of elemental assemblages in the alteration halo of the Phoenix deposit, Saskatchewan, through applied GIS; Geological Survey of Canada, Open File 7463. doi:10.4095/293122

Dickson, B.L., and Scott, K.M., 1997. Interpretation of aerial gamma ray surveys; AGSO Journal of Australian Geology and Geophysics, v. 17, p. 187–200.

Earle, S., McGill, B, and Murphy, J., 1990. Glacial boulder lithogeochemistry: an effective new exploration technique in the Athabasca Basin, Saskatchewan; in Modern Exploration Techniques, (ed.) L.S. Beck and C.T. Harper; Saskatchewan Geological Society, Special Publication 10, p. 94–114.

Earle, S. and Sopuck, V., 1989. Regional lithogeochemistry of the eastern part of the Athabasca Basin uranium province, Saskatchewan; in Uranium resources and geology of North America, (ed.) E. Muller-Kahle; International Atomic Energy Agency, TECDOC-500, p. 263–269.

Ford, K., Keating, P. and Thomas, M.D., 2007. Overview of geophysical signatures associated with Canadian ore deposits; in Mineral Deposits of Canada: A Synthesis of Major Deposit- Types, District Metallogeny, the Evolution of Geological Provinces, and Exploration Methods, (ed.) W. Goodfellow; Geological Association of Canada, Mineral Deposits Division, Special Publication No. 5, p. 939–970.

Fortin, R., Harvey, B.J.A., Campbell, J.E., Potter, E.G., Sinclair, L.E., and Jefferson, C.W., 2014. Preliminary interpretations of high-resolution airborne radiometric data, Athabasca Basin region; Geological Survey of Canada, Open File 7609.

Galbraith, J. H., D. F. Saunders, 1983. Rock classification by characteristics of aerial gamma–ray measurements; Journal of Geochemical Exploration, v. 18, p. 49–73.

Hattori, K., Power, M.J., Krahenbil, A., Dudek, N., Sorba, C., Kotzer, T.G., and Potter, E.G., 2015. Surficial geochemical surveys over concealed uranium ore of the Phoenix and Millennium deposits in the Athabasca Basin, Saskatchewan; *in* Targeted Geoscience Initiative 4: unconformity-related uranium systems, (ed.) E.G. Potter and D.M. Wright; Geological Survey of Canada, Open File 7791, p. 32-42. doi:10.4095/295776

International Atomic Energy Agency, 1991. Airborne Gamma Ray Spectrometer Surveying; International Atomic Energy Agency, Technical Reports Series No. 323.

International Atomic Energy Agency, 2003. Guidelines for radioelement mapping using gamma ray spectrometry data; International Atomic Energy Agency, Technical Reports Series No. 1363.

Jefferson, C.W., Thomas, D.J., Gandhi, S.S., Ramaekers, P., Delaney, G., Brisbin, D., Cutts, C., Quirt, D., Portella, P., and Olson, R.A., 2007. Unconformity-associated uranium deposits of the Athabasca Basin, Saskatchewan and Alberta; in Mineral Deposits of Canada: A Synthesis of Major Deposit- Types, District Metallogeny, the Evolution of Geological Provinces, and Exploration Methods, (ed.) W. Goodfellow; Geological Association of Canada, Mineral Deposits Division, Special Publication No. 5, p. 273–305.

Matthews, R., Koch, R., and Leppin, M., 1997. Advances in integrated exploration for unconformity uranium deposits in western Canada, in Proceedings of Exploration 97: Fourth Decennial International Conference on Mineral Exploration, (ed.) A.G. Gubins; p. 993–1002.

Mwenifumbo, C.J., and Bernius, G.R., 2007. Crandallite-group minerals: host of thorium enrichment in the eastern Athabasca Basin, Saskatchewan; in EXTECH IV: Geology and Uranium EXploration TECHnology of the Proterozoic Athabasca Basin, Saskatchewan and Alberta, (ed.) C.W. Jefferson and G. Delaney; Geological Survey of Canada Bulletin 588, p. 521–532.

Power, M.J., Hattori, K., Sorba, C., and Potter, E.G., 2012. Geochemical anomalies in soils and uppermost siliciclastic units overlying the Phoenix uranium deposit, Athabasca Basin, Saskatchewan; Geological Survey of Canada, Open File 7257. doi:10.4095/291981

Ramaekers, P., Jefferson, C.W., Yeo, G.M., Collier, B., Long, D.G.F., Drever, G., McHardy, S., Jiricka, D., Cutts, C., Wheatley, K., Catuneanu, O., Bernier, S., Kupsch, B., and Post, R., 2007. Revised geological map and stratigraphy of the Athabasca Group, Saskatchewan and Alberta; in EXTECH IV: Geology and Uranium EXploration TECHnology of the Proterozoic Athabasca Basin, Saskatchewan and Alberta, (ed.) C.W. Jefferson and G. Delaney; Geological Survey of Canada Bulletin 588, p. 155–192.

Shives, R.B.K., Charbonneau, B.W., and Ford, K.L., 2000a. The detection of potassic alteration by gamma-ray spectrometry: Recognition of alteration related to mineralization; Geophysics, v. 65, p. 2001–2011

Shives, R.B.K., Wasyliuk, K., and Zaluski, G., 2000b. Detection of K enrichment, illite chimneys using ground gamma ray spectrometry, McArthur River area, northern Saskatchewan; in Summary of Investigations 2000, Volume 2; Saskatchewan Geological Survey, Miscellaneous Report 2000-4.2, p. 160–169.

Simpson, M.A., and Sopuck, V.J., 1983. Till geochemistry near the Midwest uranium deposit; in Uranium Exploration in Athabasca Basin, Saskatchewan, Canada, (ed.) E.M. Cameron; Geological Survey of

Canada, Paper 82-11, p. 207–214.

Sopuck, A.J., de Carla, A., Wray, E.M., and Cooper, B., 1983. The application of lithogeochemistry in the search for unconformity-type uranium deposits, northern Saskatchewan, Canada; Journal of Geochemical Exploration, v. 19, p. 77–99.

Thomas, D.J., Matthews, R.B., and Sopuck, V., 2000. Athabasca Basin (Canada) unconformity - type uranium deposits: Exploration model, current mine developments and exploration directions; in Geology and Ore Deposits 2000: The Great Basin and Beyond; Geological Society of Nevada Symposium, Proceedings, v. 1, p. 103–126.

Wright, D.M., 2014. Why think about unique uranium? emphasizing uranium mineralization patterns using geochemistry and radiometrics, Athabasca Basin, Saskatchewan; Saskatchewan Geological Survey, Open House 2014, Abstract Volume, p. 7.

Fe and Mg Signatures of the Bong Uranium Deposit, Thelon Basin, Nunavut

Eric G. Potter[1], Ryan Sharpe[2], Isabelle Girard[1], Mostafa Fayek[2], Paul Gammon[1], David Quirt[3], and John Robbins[3]

1. *Geological Survey of Canada, 601 Booth Street, Ottawa, Ontario, K1A 0E8, epotter@NRCan-RNCan.gc.ca*
2. *Department Geological Sciences, University of Manitoba, 125 Dysart Road, Winnipeg, Manitoba, R3T 2N2*
3. *AREVA Resources Canada Ltd., 817 – 45th Street West, Saskatoon, Saskatchewan, S7L 5X2*

Abstract

The Bong deposit is one of several uranium occurrences located ca. 5 km southeast of the faulted margin of the Proterozoic Thelon sub-basin, within altered metasedimentary rocks of the Woodburn Lake group. The deposit exhibits features in common with unconformity-related deposits of the Athabasca Basin, in particular a spatial association with the regional unconformity, alteration and ore mineralogy and structural context. Primary uranium enrichment is associated with a broad hydrothermal alteration halo characterized by an inner illite-rich zone and an outer chlorite-rich zone. Whole rock and clay-sized fraction $\delta^{57}Fe_{IRMM-014}$ and $\delta^{26}Mg_{DSM-3}$ values of the least-altered host rocks cluster near 0 ‰, within range of average values of crustal materials. Zones characterized by intense illite alteration have high $\delta^{57}Fe$ and $\delta^{26}Mg$ values, with average whole-rock values of $\delta^{57}Fe = 0.87 \pm 0.23$‰ and $\delta^{26}Mg = 0.61 \pm 0.29$‰, and clay-size fraction values of $\delta^{57}Fe = 0.77 \pm 0.29$‰ and $\delta^{26}Mg = 0.82 \pm 0.09$‰. These isotopic values correlate with reductions in Fe^{2+} concentrations (average of 0.47 mol. % versus average of 2.30 mol. % Fe^{2+} in least-altered hosts). The high $\delta^{57}Fe$ values support leaching of $Fe^{2+}_{(aq)}$ with low $\delta^{57}Fe$ compositions from the system, causing precipitation of iron-bearing minerals with $\delta^{57}Fe$ values higher than the host rocks. The $\delta^{57}Fe$ values may have been locally influenced by the formation of hematite and Fe-oxyhydroxide minerals in secondary miniature roll-front mineralization due to redox reactions. The high $\delta^{26}Mg$ values coincide with formation of illite, which preferentially incorporated heavier magnesium isotopes during the intense hydrothermal alteration observed in both the ore zone and an upper hematitic horizon. Despite the significant shifts in isotopic compositions, the net iron depletion in the ore zone via selective leaching of Fe^{2+} without Fe^{3+} enrichment implies that redox reactions were not the dominant mechanism of primary uranium mineralization at the Bong deposit. Mineralogical and geochemical data support primary uranium precipitation through reduction and neutralization of an oxidized, acidic fluid. As Fe^{2+} was leached from the system in solution, enrichment of Fe-oxides and low whole-rock $\delta^{57}Fe$ values may be a distal signature of these systems.

Introduction

Significant concentrations of hydrothermal Fe- and Mg-bearing minerals (e.g. Fe-oxides/hydroxides and chlorite) are often associated with Proterozoic unconformity-related U systems, with their presence typically cited as a product of U precipitation mechanisms. For example, both basement- and sandstone-hosted unconformity-related U deposits in the Athabasca Basin commonly exhibit an Mg-rich chlorite alteration halo and association with hematite (c.f. Hoeve and Sibbald, 1978; Quirt and Wasyliuk, 1997; Jefferson et al., 2007). One proposed mechanism for formation of Mg-rich chlorite (sudoite) associated with the deposits is by interaction between metamorphic biotite, amphibole and Fe-bearing chlorite present in the basement rocks with oxidizing, acidic fluids (e.g. Wallis et al., 1985; Alexandre et al., 2005). The Fe^{2+} oxidized during the mineral transformations releases electrons that reduce U^{6+} in the oxidized fluids to immobile U^{4+} (uraninite), while the liberated Fe^{3+} and elements in the fluids form Fe-oxide minerals and sudoite.

The average isotopic composition of iron ($\delta^{56}Fe_{IRMMS-014}$ value) in the crust is 0.00 ± 0.08 ‰, which extends to most siliclastic sedimentary rocks plus alteration and weathering products (Heimann et al., 2008; Johnson et al., 2008; Craddock and Dauphas, 2010). However, large Fe fractionation can occur during redox reactions, changes in bonding states or leaching of Fe^{2+} species under acidic conditions (Johnson et al., 2008). While ubiquitous Fe-oxyhydroxide minerals associated with basin-related U systems may reflect modern processes such as Fe-cycling during incursion of oxidized waters, the structure, morphology and isotopic composition can be applied in combination to determine the conditions of formation (Diderikson et al., 2010).

Similar to Fe isotopes, the upper continental crust and mantle derived minerals have Mg isotopic compositions ($\delta^{26}Mg_{DSM-3}$ values) between - 0.1 and - 0.3 ‰, with a mineralogical control on the fractionation of Mg between carbonates, clays and waters during low-temperatures processes such as weathering (Young and Galy, 2004; Pogge von Strandmann et al., 2008; Handler et al., 2009; Bourdon et al., 2010; Li et al., 2010; Wimpenny et al., 2014).

The hypothesis explored in this study is that by using mineralogical (primary minerals and alteration assemblages), textural (crystal size), Fe-speciation (Fe^{2+}, Fe^{3+} molecular concentrations), whole-rock geochemistry and isotopic data (Mg and Fe isotopes) in concert, there is potential to define isotopic compositions that reflect redox reactions and changes in Fe and Mg bonding states characteristic of fertile hydrothermal U systems.

Bong Deposit

The Bong deposit is one of several U occurrences (Kiggavik deposit area) located ca. 5 km SE of the faulted margin of the Proterozoic Thelon sub-basin, within altered rocks informally termed the Woodburn Lake group (WLG; Fig. 1). Regionally, the WLG consists of highly deformed Neoarchean metasedimentary, metavolcanic and volcaniclastic strata, ca. 2.6 Ga mylonitized rhyolite (quartz eye rhylolite) and hybrid Lone Gull granite intrusions (1.83 –

Potter, E.G., Sharpe, R., Girard, I., Fayek, M., Gammon, P., Quirt, D., and Robbins, J., 2015. Fe and Mg Signatures of the Bong Uranium Deposit, Thelon Basin, Nunavut, *in* Targeted Geoscience Initiative 4: unconformity-related uranium systems, (ed.) E.G. Potter and D.M. Wright; Geological Survey of Canada, Open File 7791, p. 52–60. doi:10.4095/295776

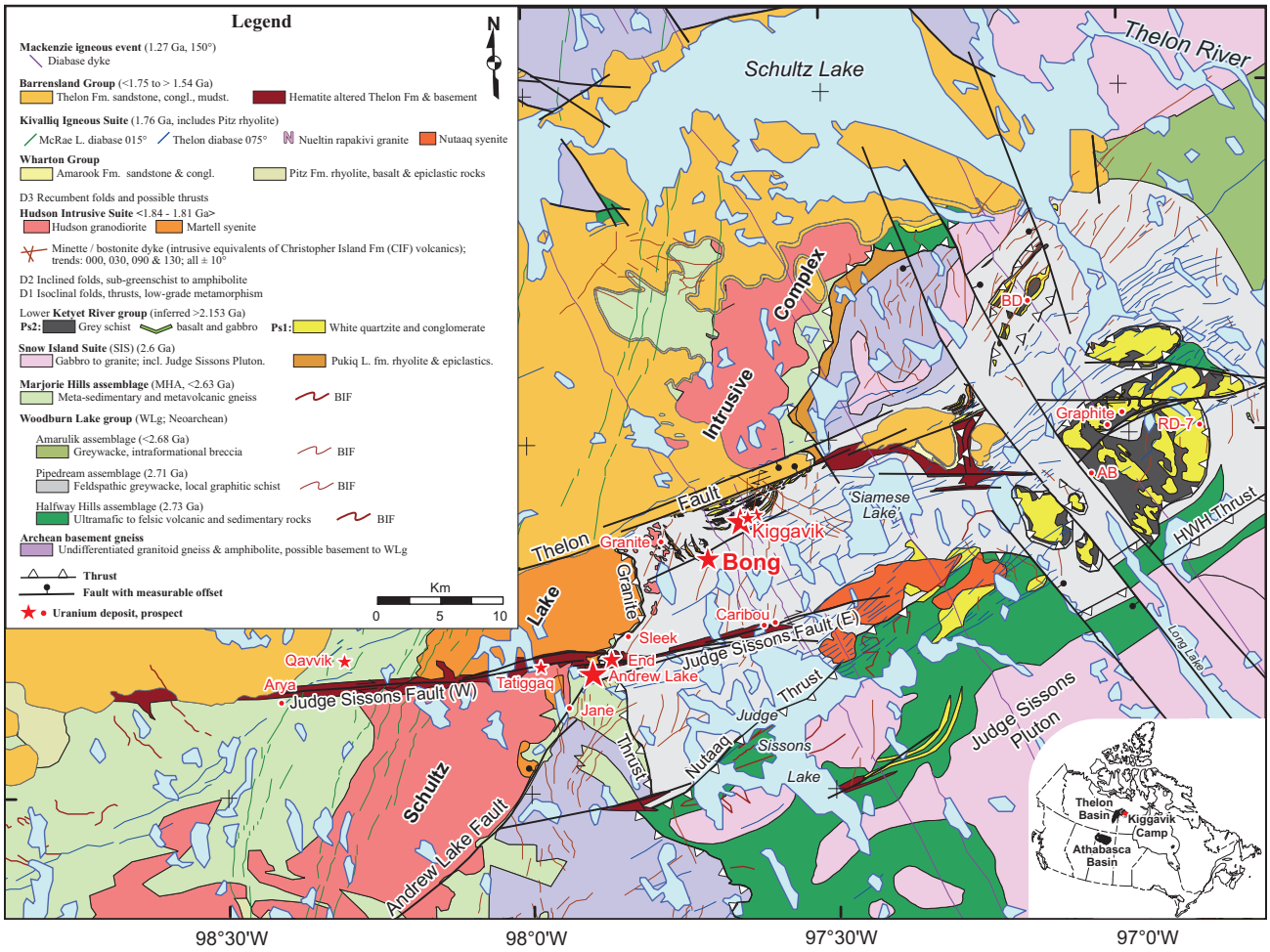

FIGURE 1. Regional geology of the Southeast Thelon Basin - Kiggavik deposit area, after Jefferson et al., (in prep.)

1.75 Ga; Scott et al. 2011) that are intruded by lamprophyre and syenitic dykes (Sharpe, 2013). At the deposit-scale, the host rocks are dominated by metagreywacke rocks interbedded with pelitic layers of the ca. 2711 Ma Pipedream assemblage, structurally intercalated with quartzite slices of early Paleoproterozoic Ketyet River group (Zaleski et al., 2000; Pehrsson et al., 2010; Sharpe, 2013; Scott et al., submitted; Fig. 2). All the deposits and showings in the Kiggavik area are located along approximately E-W trending faults that exhibit intense hydrothermal alteration (Fig.1). At the Bong deposit, the host metasedimentary rocks are fine- to medium-grained with subhorizontal foliation (Fig. 3). The primary minerals are quartz (60–70 modal %) and feldspar (15–25 modal %) with minor amounts of muscovite and biotite (ca. 5 modal %). The dominant feldspar is K-feldspar with minor plagioclase. Locally, there are layers that contain euhedral garnet porphyroblasts along with tabular biotite formed during peak metamorphism. Retrograde metamorphism resulted in pseudomorphic alteration of biotite to chlorite and sericitic alteration of feldspars along grain boundaries and fractures (Sharpe, 2013).

Uranium enrichment is associated with a broad alteration halo characterized by illite and lesser chlorite with minor pyrite, rutile and apatite, the details of which are outlined in Sharpe (2013) and Rielger et al. (2014). Syn-ore illite alteration is centered on fault zones, replaces muscovite, biotite, metamorphic chlorite, garnet and K-feldspar and is associated with corrosion of quartz grains (Figs. 2 and 3). Syn-ore chlorite occurs as laths surrounded by an illite-rich matrix. As outlined by Sharpe (2013), U is proposed to have precipitated in two generations at the Bong deposit: Stage 1 veins associated with illite plus chlorite alteration and organic matter; and stage 2 miniature roll-fronts. These are cut by post-ore carbonate (calcite and dolomite) and drusy quartz veins 1–5 mm and up to 2 cm wide, respectively. The twenty-four samples examined under this study were selected from exploration drill core (Bong-042) characterized by clay alteration from depths of 236–315m, U enrichment plus clay alteration from 315–442m and red, hematitic horizons from 0–9m and 26–43m (Fig. 2). A hematite-bearing fault zone was intersected from 220–240m. Assay highlights from the hole include: 1.0m of 0.966% U starting at 351.5m, 19.5m of 0.688% U starting at 391.5m and 8.5m of 1.101% U starting at 425m (Blain and Morrison, 2008).

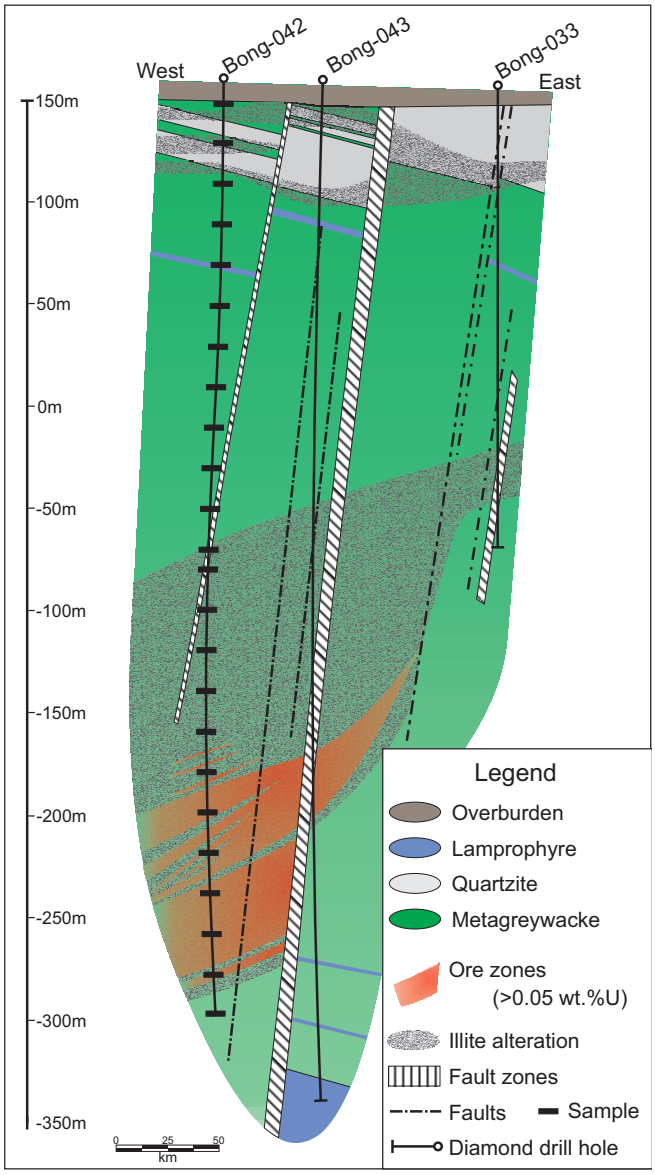

Figure 2. East-west cross-section of the Bong deposit, illustrating sampling locations from DDH Bong-042 (black boxes) examined in this study. Modified from Blain and Morrison (2008).

Methods

Samples for geochemical analysis were collected at 20 m intervals from a diamond drill hole that intersected alteration and mineralization at depth (Fig. 2). Representative samples (n=93) of the host rocks, alteration facies and ore mineralogy were also collected for petrography, the details of which are outlined in Sharpe (2013). The geochemical samples were pulverized until 95% passed through a 105µm sieve. Aliquots of the powdered material were then prepared for: 1) whole-rock geochemistry; 2) ferrous iron analysis; and 3) isotopic analysis.

The whole-rock geochemistry aliquot was mixed with a flux of lithium metaborate and lithium tetraborate and fused in an induction furnace. The molten melt was dissolved in a 5% nitric acid solution containing an internal standard. The

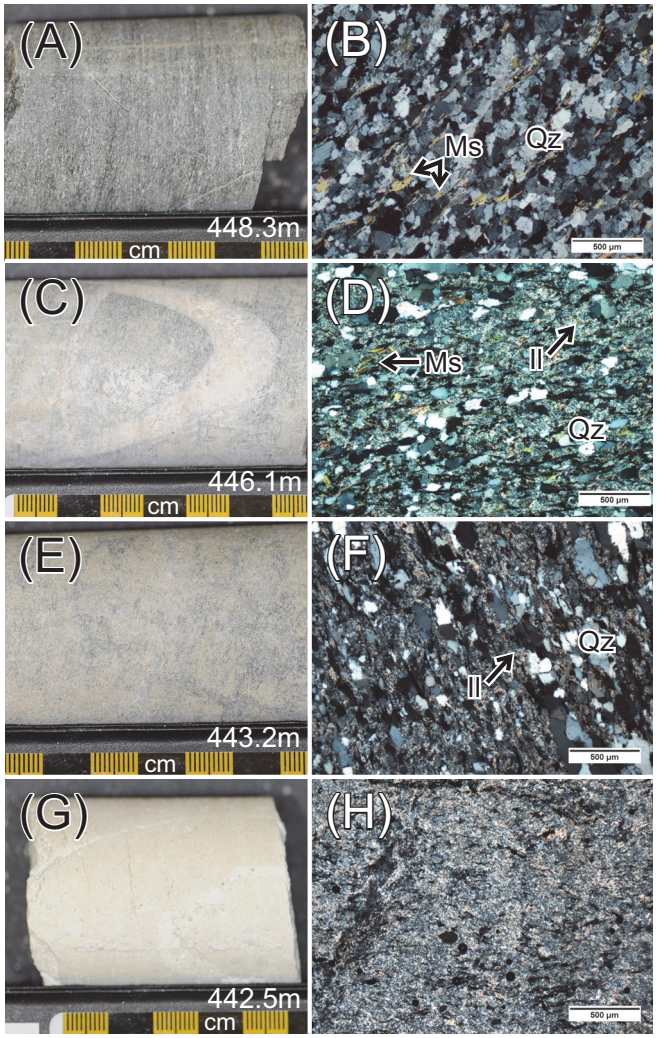

Figure 3. Representative photographs and corresponding photomicrographs (cross-polarized light) of drill core samples from Bong-042 illustrating the progression from least-altered (A and B) to highly illite-altered (G and H) metasedimentary host rocks at the Bong deposit. Il = illite, Ms = muscovite, Qz = quartz (from Sharpe, 2013).

samples were analyzed for major oxides and selected trace elements on a combination simultaneous/sequential Thermo Jarrell-Ash ENVIRO II ICP or a Varian Vista 735 ICP (Act-Labs ICP-MS Package 4B).

Ferrous iron contents were determined on whole-rock sample split by a titration method modified from Wilson (1955; ActLabs Package 4F). During titration, FeO was determined using a cold acid digestion of ammonium metavanadate and hydrofluoric acid in an open system. Ferrous ammonium sulphate was added after digestion and potassium dichromate was the titrating agent. When titrating, the endpoint was determined by colour. The contribution of ferrous iron, as FeO, was then subtracted from the total iron value determined by ICP-MS and the balance computed as ferric iron. The detection limit for FeO by titration is 0.01 wt. % (Act Labs, 2012).

Prior to Fe and Mg isotopic analysis, clay-sized fractions were made by centrifuge separation under distilled water.

Lab controls performed using a Particle Size Analyzer on clay-sized material indicated that approximately 95% of the recovered material is <0.004 mm, and that 85–90% is < 0.002 mm (Girard et al., 2004). Both whole-rock and clay-sized fractions were then subjected to a near-total four acid decomposition (HNO_3, HF, HCl and $HClO_4$). The mineralogy of whole-rock and clay-size separates was determined by X-ray powder diffraction analysis (XRD) at the Geological Survey of Canada. Suspensions (in water) of the samples were pipetted onto glass slides and air-dried overnight to produce oriented mounts. X-ray patterns of the air-dried samples were recorded on a Bruker D8 Advance Powder Diffractometer equipped with a Lynx-Eye Detector, Co Kα radiation set at 40 kV and 40 mA. Initial identification of minerals was made using EVA (Bruker AXS Inc.) software with comparison to reference mineral patterns using Powder Diffraction Files (PDF) of the International Centre for Diffraction Data (ICDD) and other available databases. Quantitative analysis is carried out using TOPAS (Bruker AXS Inc.), a PC-based program that performs Rietveld refinement (RR) of XRD spectra.

For isotopic analyses, the chromatographic separation of Mg was done by cation exchange resin (using a protocol adapted from Wombacher et al., 2008) while Fe was separated and purified by anion exchange (adapted from Chapman et al., 2005). In both cases, an aliquot of the elemental fraction obtained was analysed by ICP emission spectrometry to verify the purity of the fractions to avoid complicating matrix effects during the determination of the isotopic compositions and to ensure the >98% recovery necessary to avoid any potential fractionation during the chromatographic element separation. Procedural blanks were also analysed to ensure they were below the accepted limit of 1:1000 blank to analyte ratio. If this ratio was exceeded the digestion and chromatography was redone for that batch of samples.

Magnesium and Fe isotope ratios on samples, blanks and reference materials were determined using a Nu Plasma double-focusing multi-collector ICP-MS. A desolvating nebulization system (CETAC Aridus II) was used for sample introduction, with a 'micro-mist' nebulizer operated at 100 µL/min flow rate for Mg and 50 uL/min for Fe. The use of the Aridus II reduced the $^{12}C^{14}N$ interference on ^{26}Mg to insignificant levels while the ^{12}C dimer interference on ^{24}Mg could also be kept to insignificant levels by cleaning the sampler cone daily. Background signals coming from $^{40}Ar^{14}N$, $^{40}Ar^{16}O$ and $^{40}Ar^{16}O^{1}H$ on ^{54}Fe, ^{56}Fe and ^{57}Fe respectively were reduced to <0.03% ArN:^{54}Fe, <0.05 ArO:^{56}Fe and <0.005% ArOH:^{57}Fe by using lower flow rates and very careful optimization of the Aridus II gas flows. A 10^10 ohms amplifier (instead of the typical 10^11 ohm amplifier) was used for the detection of ^{56}Fe which changed the upper limit of the detector from 10 V to 100 V. This modification permitted the use of higher concentrations of Fe during multi-collector analyses which augmented the background to signal ratio. The use of a desolvator coupled to a lower nebulizer flow rate and higher background to signal ratio yielded the precision required to perform isotopic analysis on Fe. For both Mg and Fe isotope analyses, correction for background was done by measuring an on-peak zero and monitored on a regular basis to ensure the correction was valid throughout individual runs. Instrumental drift was corrected by using a standard sample bracketing technique (SBB protocol). Magnesium isotopes were calibrated to the DMS3 standard while Fe isotopes to the IRMM014 standard. Concentrations of standards and samples were matched to generate detector signals with no more than 10% difference. Typical concentrations for Mg analyses were ca. 75 ppb, whereas Fe was ran at ca. 500 ppb to ensure signal strengths significantly elevated above background. Average two standard deviation errors indicated by long-term repeat analyses of the isotopic standards are ±0.06 ‰ for $\delta^{57}Fe$, ±0.05 for $\delta^{56}Fe$ and ±0.07 ‰ for $\delta^{26}Mg$.

Results

Mineralogical controls

Illite from the ore-bearing alteration zones at the Bong deposit comprises more than 70 modal % of the rock. In these zones, illite contains on average 2.87 and 2.35 wt. % FeO and MgO, respectively, (Sharpe, 2013; Figs. 3G, H). In the illite zone, hematite can locally constitute 10 modal % of the rocks and is the dominant host of Fe. The illite zones contain trace to minor amounts of sudoite (chlorite) intergrown with illite, based on XRD of clay-size fractions in this study and previous work (Sharpe, 2013; Riegler et al., 2014). Just above the illite-bearing ore zone, the clay alteration assemblage is characterized by increased concentrations of sudoite (c.f. Riegler et al., 2014) and carbonate (calcite and dolomite) veins that are the dominant Mg-bearing phases.

Fe and Mg isotopic signatures

Isotopic results are reported as $\delta^{57}Fe$, $\delta^{56}Fe$ and $\delta^{26}Mg$, in per mil (‰) relative to Isotopic Reference Material (IRMM-014; Taylor et al., 1992) and Dead Sea Magnesium (DSM-3; Galy et al., 2003):

$$\delta^{56,\,57}Fe = \left(\frac{^{56,\,57}Fe/^{54}Fe_{Sample}}{^{56,\,57}Fe/^{54}Fe_{IRMM\text{-}014}} - 1\right)*10^3$$

$$\delta^{26}Mg = \left(\frac{^{26}Mg/^{24}Mg_{Sample}}{^{26}Mg/^{24}Mg_{DSM\text{-}3}} - 1\right)*10^3$$

The whole rock isotopic data reveal two zones with significantly higher Fe and Mg isotopic values: 9–29m and 319–439m (Fig. 4, Appendices I and II). Predictably, carbonate-bearing (calcite and dolomite) samples have much lower $\delta^{57}Fe$ and $\delta^{26}Mg$ values (259–299m and 339m). For both zones, average whole-rock values are: $\delta^{57}Fe$ = 0.87 ±0.23‰ and $\delta^{26}Mg$ = 0.61 ±0.29‰; Fig. 4). Averages of the less-altered (in terms of mineralogy and chemistry) whole-rock data are: $\delta^{57}Fe$ = 0.20 ±0.09‰ and $\delta^{26}Mg$ = -0.19 ±0.25‰. In the two zones with high values, average clay-sized fraction values are: $\delta^{57}Fe$ = 0.77 ±0.29‰ and $\delta^{26}Mg$ = 0.82 ±0.09‰; Fig. 4). The average less-altered, clay-sized fraction results are: $\delta^{57}Fe$ = 0.35 ±0.27‰ and $\delta^{26}Mg$ = 0.06 ±0.21‰. Plotting of $\delta^{57}Fe$ versus $\delta^{56}Fe$ and $\delta^{25}Mg$ versus $\delta^{26}Mg$ values for both whole-rock and clay fractions yielded linear trends consistent with mass dependent isotopic fraction, with slopes of 1.4831 and 0.5228, respectively.

The clay-sized fraction produced more variable Fe isotopic results, including an additional zone of high $\delta^{57}Fe$ values associated with the hematite-bearing fault sampled at

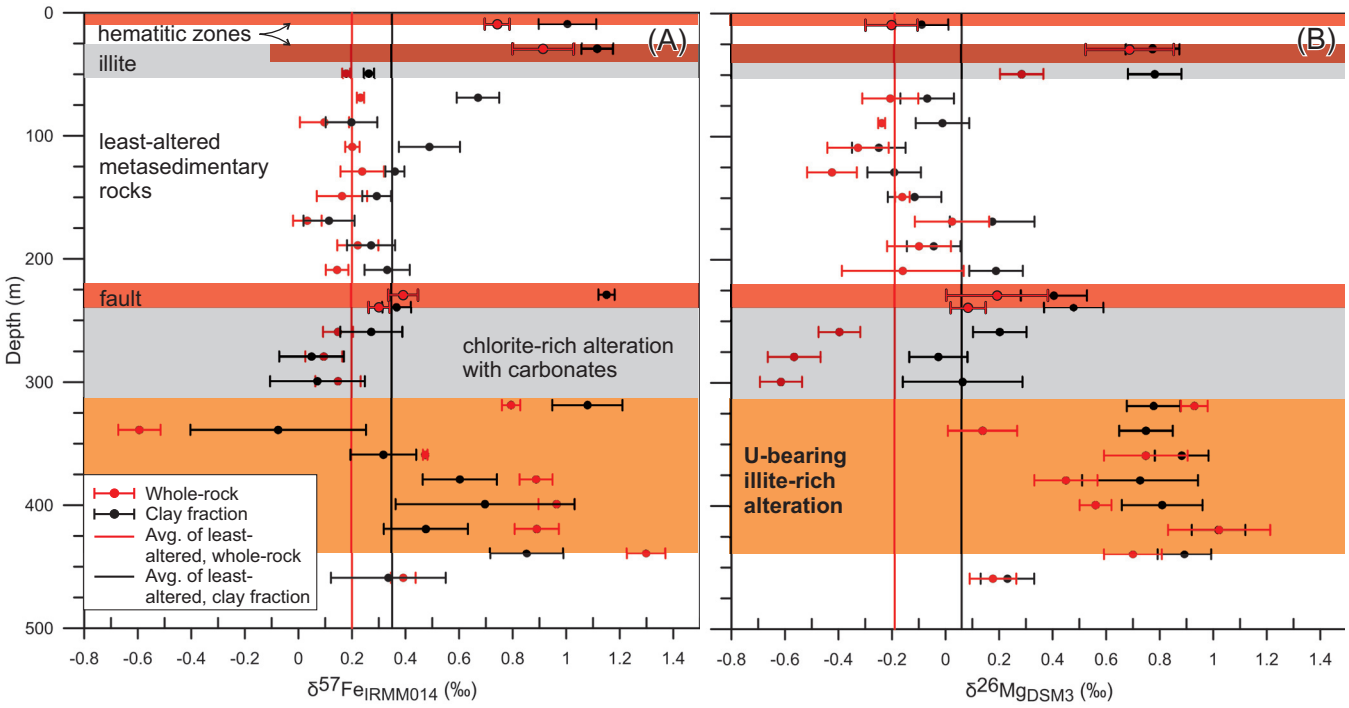

Figure 4. Depth profiles of (A) $\delta^{57}Fe$ isotope results for whole-rock (red data points and lines) and clay-size fractions (black points and lines) and (B) $\delta^{26}Mg$ results for both whole-rock (red points and lines) and clay-size fractions (black points and lines).

229m. Conversely, the Mg isotopic data from the clay-sized fractions has less spread in the data, with least altered rocks yielding $\delta^{26}Mg$ values near 0 ‰ (Fig. 4B).

Fe oxidation states

A plot of total Fe versus depth (Fig. 5A) indicates significant changes in the total Fe contents and oxidation states, with a reduction in total Fe (wt. %) in the upper red, hematitic and U-bearing zones at depths of 9m, 29, and 315–442m (Fig. 2). Figure 5B illustrates that this reduction in total Fe reflects significant reductions in Fe^{2+} concentrations (0.47 vs. 2.30 mol. Fe^{2+}) while Fe^{3+} contents remain relatively constant.

Discussion

Interpretation of isotopic data

Whole rock and clay-sized fraction $\delta^{57}Fe$ and $\delta^{26}Mg$ values of the least altered rocks in the study cluster near 0 ‰, within range of average values of crustal materials (c.f. Young and Galy, 2004; Johnson et al., 2008; Craddock and Dauphas, 2010). High $\delta^{26}Mg$ and $\delta^{57}Fe$ values in both whole-rock and clay-sized fractions are clearly associated the intense hydrothermal alteration at the Bong deposit that resulted in the breakdown of the pre-existing mineral assemblages (changes in bonding states for Fe and Mg) and significant leaching of Fe^{2+}. However, when examined in detail, only the U-bearing, illite-altered samples and red, hematitic horizons have high $\delta^{26}Mg$ and $\delta^{57}Fe$ values — the clay-altered zone above the U-bearing illite alteration (236–315m) has lower values, reflecting either the presence carbonate minerals enriched in lighter Mg relative to their formational fluids or the presence of sudoite as noted by

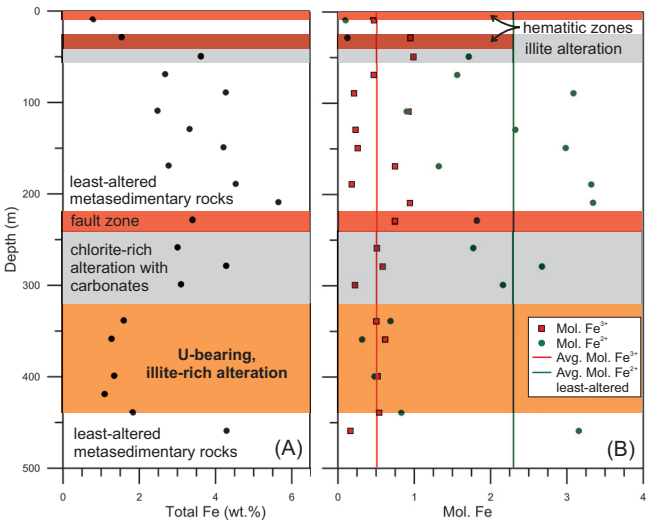

Figure 5. Depth profile of (A) total iron (FeO + Fe_2O_3) and (B) molecular proportions of Fe^{2+} and Fe^{3+}, after Sharpe (2013).

Riegler et al. (2014). Similar to carbonate minerals, chlorite has been shown to preferentially incorporate isotopically light Mg relative to the host rocks and fluids (Ryu et al., 2011). Leaching of Fe as Fe^{2+} species can produce net positive shifts in the whole-rock data as the relatively stable Fe^{3+}-bearing minerals preferentially incorporate the heavier Fe isotopes (Johnson et al., 2008), while clay minerals formed during such processes (i.e. illite) preferential incorporate isotopically heavier Mg (Tipper et al., 2006, 2012; Opfergelt et al., 2012; Wimpenny et al., 2014). The positive shift in $\delta^{57}Fe$ values in the ore zone may have been locally enhanced by

the formation of hematite and Fe-oxyhydroxide minerals in secondary miniature roll-front mineralization due to redox reactions. The high $\delta^{57}Fe$ values observed in the clay-sized fraction from the hematite-bearing fault may record very low temperature processes such as modern Fe-silicate weathering by oxidized meteoric fluids along faults (c.f. Diderikson et al., 2010), but further studies are required to verify the Fe mineralogical controls on the isotopic composition of the clay-sized fraction.

Linking isotopic data to processes

The upper hematitic horizon at the Bong deposit was originally thought to represent a paleoweathering horizon, much like the possibly coeval lateritic profile observed along the unconformity at the base of the Athabasca Group (MacDonald, 1980; Gall, 1994). Weathering under oxic conditions generates insoluble Fe^{3+} secondary silicate and oxide minerals and can produce large increases in Fe^{3+}/Fe^{2+} ratios. However, the stability of Fe^{3+}-bearing minerals typically results in little whole-rock Fe isotope fractionation because loss of mobile Fe can be insignificant (Beard et al. 2003; Kiczka et al., 2011). Therefore, the similarity in isotopic values and lack of enrichment in relatively stable Fe^{3+}-bearing minerals in the clay-altered and hematitic zones suggests that the red, hematitic horizons near the present surface are unlikely to have formed through intense paleoweathering processes. Gall (1994) characterized the Thelon paleosol as having lost TiO_2, total Fe, Fe^{2+} and K_2O, and enrichment in Fe^{3+}. In comparison to the least-altered units, the hematitic horizons at the Bong deposit are characterized by losses in total Fe (via leaching of Fe^{2+}) and MgO, no gains in Fe^{3+} and gains in K_2O. The increase in K_2O contents reflects the presence of illite, a feature ascribed to K-metasomatism by Matthews & Scharrer (1968), Erikson and Soegaard (1985) and Gall (1994) but herein proposed as a product of hydrothermal alteration. Furthermore, the uppermost hematitic zone has $\delta^{26}Mg$ values of -0.20‰ (whole rock) and -0.09 ‰ (clay fraction) plus contains K-feldspar; features similar to the less-altered host rocks and inconsistent with a lateritic paleoweathering origin for the hematitic zones.

As noted by Sharpe (2013), the proposed fluid chemistry during the primary U event (pH<4.5 at 200°C; Fig. 6) would have to be suitable for leaching of $Fe^{2+}_{(aq)}$ with low $\delta^{57}Fe$ compositions from the system, causing precipitation of alteration minerals with $\delta^{57}Fe$ values higher than the host rocks. As depicted in Figure 6, the destruction of the host rock mineral assemblages (feldspars, muscovite, biotite, metamorphic chlorite) and leaching of Fe^{2+} are consistent with the incursion of a warm (~225°C), oxidized, U-bearing, acidic fluid that was neutralized and reduced through interactions with the basement rocks, resulting in the formation of illite, uraninite, chlorite and pyrite. These processes are consistent with the shifts in mineralogy, geochemistry, and Fe and Mg isotopic data.

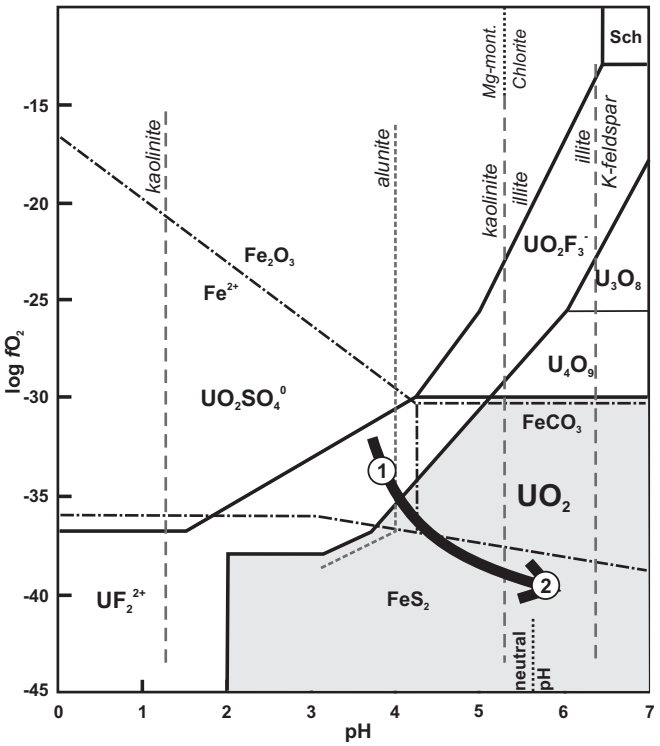

Figure 6. Log fO_2 - pH diagram illustrating the distribution and stability of U and Fe phases and K- and Mg-silicates in an aqueous system containing 10 ppm Fe, 100 ppm F, 1000 ppm S, 1000 ppm K, 100 ppm Mg and 1m NaCl at P_{CO3} of 10 atm and 200°C. Sch = schoepite. Shaded region denotes UO_2 field, and arrow approximate fluid pathway for primary U deposition: (1) Fe^{2+} leaching, and (2) formation of illite, reduction and neutralization of fluids resulting in uraninite and pyrite precipitation. Modified from Romberger (1984)

Implications for Exploration

The isotopic data clearly reflect fertile hydrothermal alteration in both the U-bearing zone and upper hematitic horizon. The net Fe depletion in the ore zone via selective leaching of Fe^{2+} without Fe^{3+} enrichment implies that redox reactions were not the dominant mechanism of primary U precipitation. As Fe^{2+} was leached from the system in solution, enrichment of Fe-oxides may be a distal signature of these systems – a hypothesis supported by the presence of significant hematite alteration along key regional faults in the district (Fig. 1). The high $\delta^{26}Mg$ and $\delta^{57}Fe$ values, presence of illite, and leaching of Fe^{2+} supports the hypothesis that the upper hematitic zone likely formed under conditions similar to the primary U event and thus may be considered as a potential indication of nearby U mineralization. Given the structural control on alteration and mineralization, expression of these signatures in fault systems may provide a means of evaluating prospective drill targets. On the deposit-scale, these results indicate that Fe and Mg isotopic data highlight fertile clay alteration and when coupled with geochemical and mineralogical data, provide constraints on the genesis of these U systems. In terms of signatures relevant to exploration, U-bearing zones and prospective fault systems are best characterized by an outer chlorite halo and an inner, highly altered illite zone that results in Fe depletion coupled with high $\delta^{26}Mg$ and whole-rock $\delta^{57}Fe$ values and nominal increases in the isotopic values in the clay-sized $\delta^{57}Fe$ values (Fig. 7).

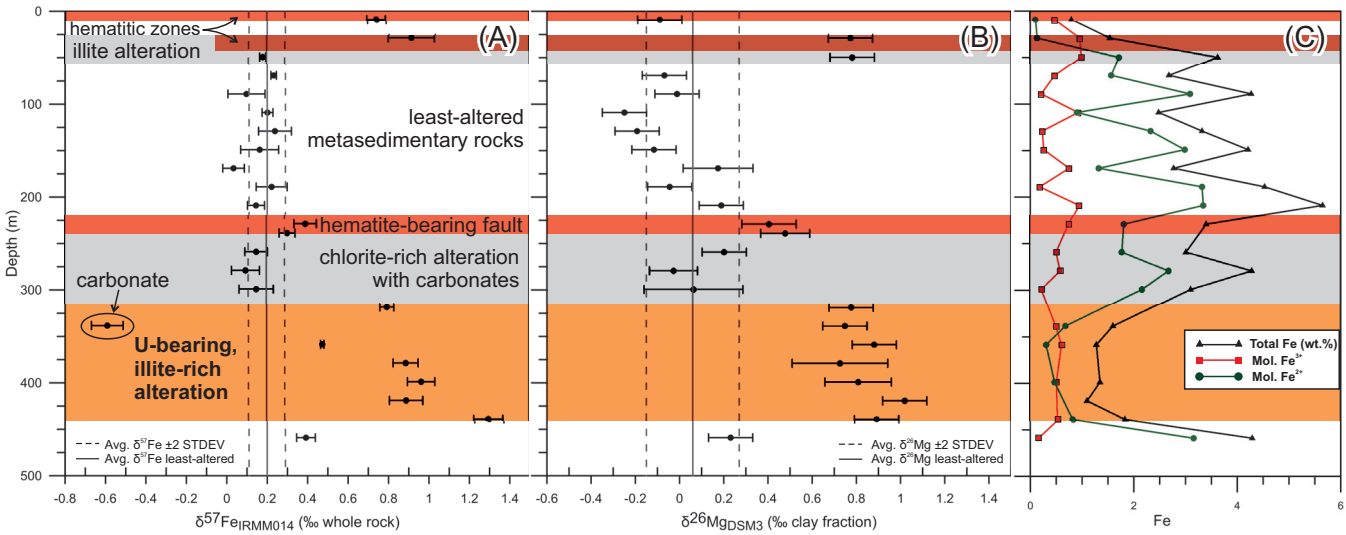

Figure 7. Alteration mineralogy at depth in relation to whole-rock δ^{57}Fe (A) and clay-size fraction δ^{26}Mg (B) signatures and changes in Fe oxidation states (C).

Future Work

Results are pending from sequential leach experiments, using 1M NH_4OAc, 1M NH_2OH, and four acid solutions to evaluate isotopic contributions from carbonate minerals, adsorbed species and fine-grained Fe-oxyhydroxides. Analyses are also underway on samples from the McArthur River deposit, with linkages to a detailed isotopic-mineralogical study by Acevedo and Kyser (this volume).

Acknowledgments

This research is a contribution to the Targeted Geoscience Initiative 4 (TGI-4), uranium ore systems project. This project would not have been possible without support from AREVA Resources Canada Ltd., who provided access to samples and permission to publish the results. Igor Bilot (GSC) is thanked for determining the mineralogy of separates by XRD. This research was aided by discussions with C.W. Jefferson, S. Pehrsson, S.E. Jackson and S. Madore at the Geological Survey of Canada. This manuscript benefitted from constructive reviews by Tom Kotzer and Kurt Kyser and the editorial handling of Donald Wright.

References

Act Labs, 2012. Canadian schedule of services and fees; Activation Laboratories Canada, 30p.

Alexandre, P., Kyser, K., Polito, P., and Thomas, D., 2005. Alteration mineralogy and stable isotope geochemistry of Paleoproterozoic basement-hosted unconformity-type uranium deposits in the Athabasca Basin, Canada; Economic Geology, v. 100, p. 1547–1563.

Beard B.L., Johnson C.M., Skulan J.L., Nealson K.H., Cox L. and Sun H., 2003. Application of Fe isotopes to tracing the geochemical and biological cycling of Fe; Chemical Geology, v. 195, p. 87–117.

Blain, M. and Morrison, D., 2008. Kiggavik Project, Annual Report, 2010, volume 1; AREVA Resources Canada Inc., Internal Report, 31 p.

Bourdon B., Tipper E. T., Fitoussi C. and Stracke A. 2010. Chondritic Mg isotope composition of the Earth; Geochimica et Cosmochimica Acta, v. 74, p. 5069–5083.

Chapman, J.B., Mason T.F.D., Weiss D. J., Coles B.J. and Wilkinson J.J., 2005. Chemical separation and isotopic variations of Cu and Zn from five geological reference materials; Geostandards and Geoanalytical Research, v. 30, p. 5–16.

Craddock, P. R. and Dauphas, N., 2011. Iron isotopic compositions of geological reference materials and chondrites; Geostandards and Geoanalytical Research, v. 35, p. 101–123.

Dideriksen, K., Christiansen, B. C., Frandsen, C., Balic-Zunic, T., Mørup, S. and Stipp, S. L. S., 2010. Paleo-redox boundaries in fractured granite; Geochimica et Cosmochimica Acta, v. 74, p. 2866–2880.

Eriksson, K.A. and Soegaard, K., 1985. The petrography and geochemistry of Archean and early Proterozoic sediments: implication of crustal compositional and surfaces processes; Geological Survey of Finland, Bulletin 331, p 8–32.

Gall, Q., 1994. Proterozoic paleoweathering and diagenesis, Thelon Basin, Northwest Territories, Canada; Ph.D. thesis, Carleton University, 369 p.

Galy, A., Yoffe, O., Janney, P.E., Williams, R.W., Cloquet, C., Alard, O., Halicz, L., Wadwha, M., Hutcheon, I.D., Ramon, E., and Carignan, J., 2003. Magnesium isotopes heterogeneity of the isotopic standard SRM980 and new reference materials for magnesium-isotope-ratio measurements; Journal of Analytical Atomic Spectrometry, v. 18, p. 1352-1356.

Girard, I., Klassen, R.A. and Laframboise, R.R., 2004. Sedimentary laboratory manual, Terrain Sciences Division; Geological Survey of Canada, Open File 4823, 137 p.

Handler M., Baker J., Schiller M., Bennett V. and Yaxley G., 2009. Magnesium stable isotope composition of Earth's upper mantle; Earth and Planetary Science Letters, v. 282, p. 306–313.

Heimann, A., Beard, B.L., Johnson, C.M., 2008. The role of volatile exsolution and sub-solidus fluid/rock interactions in producing high $^{56}Fe/^{54}Fe$ ratios in siliceous igneous rocks; Geochimica et Cosmochimica Acta 72, p. 4379–4396

Hoeve, J., and Sibbald, T. I., 1978. On the genesis of Rabbit Lake and other unconformity-type uranium deposits in northern Saskatchewan, Canada; Economic Geology, v. 73, p. 1450–1473.

Jefferson, C.W., Thomas, D.J., Gandhi, S.S., Ramaekers, P., Delaney, G., Brisbin, D., Cutts, C., Portella, P. and Olson, R.A., 2007. Unconformity-associated uranium deposits of the Athabasca basin, Saskatchewan and Alberta; in EXTECH IV: Geology and Uranium EXploration TECHnology of the Proterozoic Athabasca Basin, Saskatchewan and Alberta, (ed.) C.W. Jefferson and G. Delaney; Geological Survey of Canada Bulletin 588, p. 23–67.

Jefferson, C.W., Pehrsson, S., Peterson, T., Tschirhart, V., Anand, A., Wollenberg, P., Riegler, T., Bethune, K., Chorlton, L.B., McEwan, B., LeCheminant, A.N., Tschirhart, P., Scott, J.M.J., Davis, W., McNicoll, V., Riemer, W., White, J.C., Patterson, J., Morris, W.A., Keating, P. and Stieber, C., in prep. Bedrock geology of the western Marjorie-Tehek supracrustal belt and Aberdeen Sub-basin margin in parts of NTS 66A

and 66B, Nunavut — context of the Kiggavik uranium camp; Geological Survey of Canada, Open File 7241.

Johnson, C. M., Beard, B. L. and Roden, E. E., 2008. The iron isotope fingerprints of redox and biogeochemical cycling in modern and ancient Earth; Annual Review of Earth and Planetary Sciences, v. 36, p. 457–493.

Kiczka, W., Widerhold, J.G., Frommer, J., Voegelin, A., Kraemer, S.M., Bourdon, B. and Kretzschmar, R., 2011. Iron speciation and isotope fractionation during silicate weathering and soil formation in an alpine glacier forefield chronosequence; Geochimica et Cosmochimica, Acta 75, p. 5559–5573.

Li W.-Y., Teng F.-Z., Ke S., Rudnick R. L., Gao S., Wu F.-Y. and Chappell B. W., 2010. Heterogeneous magnesium isotopic composition of the upper continental crust; Geochimica et Cosmochimica Acta, v. 74, p. 6867–6884.

Matthews, P.E. and Scharrer, R.H., 1968. A graded unconformity at the base of the early Precambrian Pongola System; Transactions of the Royal Society of South Africa, v. 71, p. 257–271.

Macdonald, C., 1980. Mineralogy and geochemistry of a Precambrian regolith in the Athabasca Basin; M.Sc. Thesis, University of Saskatchewan, 151 p.

Opfergelt, S., Georg, R., Delvaux, B., Cabidoche, Y.M., Burton K. and Halliday, A., 2012. Mechanisms of magnesium isotope fractionation in volcanic soil weathering sequences, Guadeloupe; Earth and Planetary Science Letters, v. 341, p. 176–185.

Pehrsson, S., Jefferson, C.W., Peterson, T., Scott, J., Chorlton, L., and Hillary, B., 2010. Basement to the Thelon Basin, Nunavut - Revisited; Geoscience Canada 2010, May 10–14th.

Pogge von Strandmann P. A. E., Burton K. W., James R. H., van Calsteren P., Gislason S. R. and Sigfússon B., 2008. The influence of weathering processes on riverine magnesium isotopes in a basaltic terrain; Earth and Planetary Science Letters, v. 276, p. 187–197.

Quirt, D.H. and Wasyliuk, K., 1997. Kaolinite, dickite and other clay minerals in the Athabasca Group, Canada and the Kombolgie Formation, Australia; in Clays for Our Future — Proceedings of the 11th International Clay Conference, (ed.) A.R. Mermut and J.K. Torrance, Ottawa, June 15 – 21, Conference CD-ROM, p. A61

Riegler, T., Lescuyer, J-L., Wollenberg, P., Quirt, D. and Beaufort, D., 2014. Alteration related to uranium deposits in the Kiggavik-Andrew Lake structural trend, Nunavut Canada: new insights from petrography and clay mineralogy; The Canadian Mineralogist, v. 52, p. 27–45.

Romberger, S.B., 1984. Transport and deposition of uranium in hydrothermal systems at temperatures up to 300°C: geological implications; in Uranium geochemistry, mineralogy, geology, exploration and resources, (ed.) B. De Vivo; The Institution of Mining and Metallurgy, p. 12–18.

Ryu, J.S., Jacobson, A.D., Holmden, C., Lundstrom, C. and Zhang Z., 2011. The major ion, $\delta^{44/40}$Ca, $\delta^{44/42}$Ca, and $\delta^{26/24}$Mg geochemistry of granite weathering at pH=1 and T=25°C: power-law processes and the relative reactivity of minerals; Geochimica et Cosmochimica, Acta 75, p.6004–6026

Sharpe, R., 2013. The geochemistry and geochronology of the Bong uranium deposit, Thelon Basin, Nunavut Canada; M.Sc. thesis, University of Manitoba, Winnipeg, 213 p.

Scott, J., Peterson, T.D., Jefferson, C.W., and Cousens, B. 2010. Proterozoic (1.85-1.7 Ga) granitoid rocks and uranium in the Baker Lake – Thelon Basin region, Nunavut; GeoCanada 2010 Extended Abstracts, Calgary, p. 4.

Taylor, P.D.P., Maeck, R., and De Bièvre, P., 1992. Determination of the absolute isotopic composition and atomic weight of a reference sample of natural iron; International Journal of Mass Spectrometry and Ion Processes, v. 121, p. 111–125.

Tipper, E.T., Galy, A. and Bickle, M.J., 2006. Riverine evidence for a fractionated reservoir of Ca and Mg on the continents: Implications for the oceanic Ca cycle; Earth and Planetary Science Letters, v. 247, p. 267–279.

Tipper, E.T., Calmels, D., Gaillardet, J., Louvat, P., Capmas, F. and Dubacq, B., 2012. Positive correlation between Li and Mg isotope ratios in the river waters of the Mackenzie Basin challenges the interpretation of apparent isotopic fractionation during weathering; Earth and Planetary Science Letters, v. 333, p. 35–45.

Wallis, R. H., Saracoglu, N., Golightly, J. P. and Brummer, J. J., 1984. Geology of the McClean uranium deposits, northern Saskatchewan; in Geology of Uranium Deposits, (ed.) T.I.I. Sibbald, and W. Petruk; Canadian Institute of Mining, Metallurgy and Petroleum, Special Volume 32, p. 101–131.

Wilson A. D., 1955. Determination of ferrous iron in rocks and minerals; Bulletin of the Geological Survey of Great Britain, v. 9, p. 56–58.

Wimpenny, J., Colla, C. A., Yin, Q. Z., Rustad, J. R. and Casey, W. H., 2014. Investigating the behaviour of Mg isotopes during the formation of clay minerals; Geochimica et Cosmochimica Acta, v. 128, p. 178–194.

Wombacher, F., Eisenhauer, A., Heuserac, A. and Weyer, S., 2009. Separation of Mg, Ca and Fe from geological reference materials for stable isotope ratio analyses by MC-ICP-MS and double-spike TIMS; Journal of Analytical Atomic Spectrometry, v. 24, p. 627–636.

Young, E. D. and Galy, A., 2004. The isotope geochemistry and cosmochemistry of magnesium; Reviews in Mineralogy and Geochemistry, v. 55, p. 197–230.

Zaleski, E., Davis, W.J., and Wilkinson, L., 2000. Basement/cover relationships, unconformities and depositional cycles of the Woodburn Lake group, western Churchill Province Nunavut. Yellowknife Geoscience Forum, November 2000.

Appendix I. Whole-rock isotopic data from drill hole Bong-042

sample ID	Depth (m)	δ^{56}Fe IRMM014	±2σ	δ^{57}Fe IRMM014	±2σ	δ^{26}Mg DSM3	±2σ	δ^{25}Mg DSM3	±2σ
Whole-rock									
RS-11-081	9	0.48	0.07	0.74	0.05	-0.20	0.10	-0.11	0.13
RS-11-083	29	0.60	0.07	0.92	0.11	0.69	0.16	0.36	0.16
RS-11-085	49	0.12	0.02	0.18	0.01	0.28	0.08	0.17	0.05
RS-11-087	69	0.16	0.05	0.23	0.01	-0.21	0.10	-0.08	0.13
RS-11-089	89	0.06	0.05	0.10	0.09	-0.24	0.01	-0.14	0.02
RS-11-091	109	0.11	0.03	0.20	0.03	-0.33	0.11	-0.18	0.05
RS-11-093	129	0.16	0.07	0.24	0.08	-0.42	0.09	-0.19	0.04
RS-11-095	149	0.10	0.10	0.16	0.09	-0.16	0.03	-0.09	0.02
RS-11-097	169	0.03	0.05	0.03	0.05	0.02	0.14	0.00	0.04
RS-11-099	189	0.15	0.05	0.22	0.08	-0.10	0.12	-0.07	0.06
RS-11-101	209	0.11	0.04	0.14	0.04	-0.16	0.23	-0.09	0.05
RS-11-103	229	0.26	0.05	0.39	0.06	0.19	0.19	0.12	0.22
RS-11-113	239	0.21	0.05	0.30	0.04	0.09	0.07	0.04	0.05
RS-11-115	259	0.08	0.04	0.15	0.06	-0.40	0.08	-0.21	0.03
RS-11-117	279	0.04	0.05	0.10	0.07	-0.57	0.10	-0.31	0.06
RS-11-119	299	0.10	0.03	0.15	0.08	-0.61	0.08	-0.32	0.07
RS-11-121	319	0.54	0.07	0.80	0.03	0.93	0.05	0.47	0.03
RS-11-123	339	-0.41	0.06	-0.59	0.08	0.14	0.13	0.05	0.06
RS-11-125	359	0.33	0.02	0.48	0.01	0.75	0.16	0.39	0.05
RS-11-127	379	0.61	0.05	0.89	0.06	0.45	0.12	0.25	0.06
RS-11-129	399	0.64	0.04	0.97	0.07	0.56	0.06	0.29	0.06
RS-11-131	419	0.59	0.06	0.89	0.08	1.02	0.19	0.54	0.12
RS-11-133	439	0.85	0.05	1.30	0.07	0.70	0.11	0.34	0.06
RS-11-135	459	0.26	0.03	0.39	0.05	0.18	0.09	0.07	0.02

Appendix II. Clay-size fraction isotopic data from drill hole Bong-042.

sample ID	Depth (m)	δ^{56}Fe IRMM014	±2σ	δ^{57}Fe IRMM014	±2σ	δ^{26}Mg DSM3	±2σ	δ^{25}Mg DSM3	±2σ
Clay-size fraction									
RS-11-081C	9	0.68	0.07	1.00	0.11	-0.09	0.10	-0.03	0.10
RS-11-083C	29	0.76	0.05	1.12	0.06	0.77	0.10	0.41	0.10
RS-11-085C	49	0.17	0.02	0.27	0.02	0.78	0.10	0.40	0.10
RS-11-087C	69	0.44	0.11	0.67	0.08	-0.07	0.10	-0.03	0.10
RS-11-089C	89	0.13	0.07	0.20	0.10	-0.01	0.10	-0.02	0.10
RS-11-091C	109	0.33	0.08	0.49	0.11	-0.25	0.10	-0.13	0.10
RS-11-093C	129	0.24	0.01	0.36	0.04	-0.19	0.10	-0.10	0.10
RS-11-095C	149	0.20	0.03	0.29	0.05	-0.12	0.10	-0.08	0.10
RS-11-097C	169	0.09	0.09	0.11	0.10	0.17	0.16	0.11	0.11
RS-11-099C	189	0.18	0.08	0.27	0.09	-0.04	0.10	-0.02	0.10
RS-11-101C	209	0.22	0.09	0.33	0.08	0.19	0.10	0.08	0.10
RS-11-103C	229	0.78	0.00	1.15	0.03	0.41	0.12	0.20	0.10
RS-11-113C	239	0.26	0.04	0.37	0.05	0.48	0.11	0.26	0.05
RS-11-115C	259	0.19	0.09	0.27	0.12	0.20	0.10	0.10	0.10
RS-11-117C	279	0.03	0.07	0.05	0.12	-0.03	0.11	-0.02	0.10
RS-11-119C	299	0.02	0.13	0.07	0.18	0.06	0.22	0.02	0.11
RS-11-121C	319	0.71	0.12	1.08	0.13	0.78	0.10	0.40	0.10
RS-11-123C	339	-0.05	0.19	-0.07	0.33	0.75	0.10	0.38	0.10
RS-11-125C	359	0.21	0.10	0.32	0.12	0.88	0.10	0.46	0.10
RS-11-127C	379	0.40	0.08	0.60	0.14	0.73	0.22	0.40	0.11
RS-11-129C	399	0.45	0.20	0.70	0.33	0.81	0.15	0.41	0.10
RS-11-131C	419	0.31	0.12	0.48	0.16	1.02	0.10	0.53	0.10
RS-11-133C	439	0.58	0.04	0.85	0.14	0.89	0.10	0.47	0.10
RS-11-135C	459	0.21	0.13	0.34	0.21	0.23	0.10	0.11	0.10

Fe Isotopic Composition of Alteration Minerals From McArthur River Zone 4 Deposit, Athabasca Basin, Saskatchewan

Andrés Acevedo and T. Kurt Kyser
Department of Geologic Sciences and Geological Engineering, Queen's University, Kingston, Ontario K7L 3N6

Abstract

This study examines the Fe isotopic composition of alteration minerals from the McArthur River deposit Zone 4 and investigates the premise that Fe isotopic values can be used to indicate how and where uranium ore deposition occurred. Iron isotopic signatures can be used to discriminate areas where significant redox reactions have occurred and thus, may indicate areas fertile for uranium mineralization. Iron plays an important role as a reducing agent during the formation of U deposits, particularly Fe^{2+} as it is involved in reducing U as follows:

$$U^{6+}_{(aq)} + 2Fe^{2+}_{(aq)} + 2H_2O \leftrightarrow U^{4+}O_{2(uraninite)} + 2Fe^{3+}_{(chlorite\ or\ hematite)} + 4H^{+}_{(aq)}$$

Under equilibrium conditions, aqueous Fe^{3+} species or minerals that contain Fe^{3+} have higher $^{56}Fe/^{54}Fe$ ratios than those with Fe^{3+} and Fe^{2+} oxidation states.

The $\delta^{56}Fe_{IRMM-014}$ values in clay mineral separates from both sandstone and basement rocks near the McArthur River deposit have a range of nearly 1.5‰. The $\delta^{56}Fe$ values of clay separates, however, do not correlate with distance from the mineralization nor do they correlate with Fe^{3+}/Fe_{total}, other isotopic systems such as O or Pb, or any element other than Mg. Instead, $\delta^{56}Fe$ values are more complex than the single redox reaction above and can be divided into three distinct populations: (1) values ranging from 0 to 0.5‰ which represent background values for the McArthur River deposit, as reflected by early chlorite in basement rocks that occurs distal to faults and furthest from the system; (2) $\delta^{56}Fe$ values < 0‰ reflecting post-ore fluid events in samples that are located near lithologic boundaries or faults, which are susceptible to overprinting by the mineralizing system or later fluids; and (3) $\delta^{56}Fe$ values >0.5‰ resulting from the oxidation of Fe during reduction of U^{6+} as recorded in samples near the ore zone or in the sandstone directly above the extension of the P2 fault system. The $\delta^{56}Fe$ values indicate that samples above the silicified zone and up to 300m from the ore zone were affected by the primary dispersion of the mineralizing system and that Fe was a reductant of U in the mineralizing process. Based on these results, Fe isotopes reveal for the first time, processes associated with redox reactions in ore deposits. The redox population also provides an indication on the fertility of an alteration system, particularly along ore-hosting faults.

Introduction

Located in the eastern Athabasca Basin, the McArthur River deposit is the largest and highest grade unconformity-related U deposit in the world (Jefferson et al., 2007) with an average ore grade of 16.46 % U_3O_8 (14.31 % U) and combined proven and probable reserves of 385.5 million pounds U_3O_8 (Bronkhorst et al., 2012). Close to being a monometallic deposit, McArthur River also contains minor amounts of sulphide minerals (<3%) containing some Pb, Cu, Ni, Zn, Co, and As. Despite its size, the deposit has limited surficial geochemical expression and the spatial extent of hydrothermal host-rock alteration is relatively small, probably due to the extensive silicification above the deposit (McGill et al., 1993).

The Athabasca Basin currently hosts about 96% of its known U resources at the shallow (∽500 m) eastern margin, along a relatively narrow mineralized corridor (Jefferson et al., 2007). There is significant potential for deeper deposits within the basin, where conventional exploration techniques are not a viable option due to cost and technical problems, thus requiring new exploration tools. Exploration has expanded beyond the present limits of the Athabasca Basin as new basement-hosted mineralization has been discovered (e.g. Patterson Lake South discovery; Armitage, 2013). The diagnostic low-temperature alteration for these basement-hosted deposits is superimposed on metamorphic assemblages making it more challenging to find these targets, and demanding new and better exploration tools.

The stable isotopes of H, C, O and S have been applied since the 1980s to identify the origin and evolution of ore forming fluids in the Athabasca Basin (e.g. Wallis et al., 1983; Wilson and Kyser, 1987). Tracking fluids in this way is based on the premise that the fluids generate extensive primary dispersion alteration halos (Kotzer and Kyser, 1995; Kyser et al., 2000; Hiatt et al., 2007; Alexandre et al., 2009). Non-traditional stable isotope analysis of minerals is a more recent technique that has developed since our ability to measure small isotope fractionations has improved. Non-traditional isotopes that have been shown to record isotopic variations related to alteration and ore forming processes include light elements like Li and B, but also heavier metals such as Mg, Si, Ca, Cr, Cu, Fe, Zn, Se, Mo and U (Johnson et al., 2004). Elements that are redox sensitive and have multiple isotopes, such as Cr, Cu, Fe, Mo, Se, U and Zn, are most susceptible to fractionation because the bonding environments of their various oxidation states can differ significantly.

Stable isotopes of transition metals, such as Fe, record significant variations in low-temperature systems (Johnson and Beard, 2006) such as those associated with mineral weathering, soil formation and hydrothermal systems (Malinovsky et al., 2005; Wiederhold et al., 2007; Johnson et al., 2008). The most important controls on Fe isotope fractionations in low-temperature systems are oxidation state and

Acevedo, A. and Kyser, T.K., 2015. Fe Isotopic Composition of Alteration Minerals From McArthur River Zone 4 Deposit, Athabasca Basin, Saskatchewan, *in* Targeted Geoscience Initiative 4: unconformity-related uranium systems, (ed.) E.G. Potter and D.M. Wright; Geological Survey of Canada, Open File 7791, p. 61–73. doi:10.4095/295776

bonding environment. Johnson et al., (2008) found that under equilibrium conditions, aqueous Fe^{3+} species or minerals that only contain Fe^{3+} have higher $^{56}Fe/^{54}Fe$ ratios than those with both Fe^{3+} and Fe^{2+} oxidation states.

The purpose of this study was to measure the Fe isotopic composition of clay alteration minerals from the McArthur River deposit Zone 4 (Fig. 1) to assess whether Fe isotopes can be used to indicate how and where uranium ore deposition occurred and increase exploration effectiveness. Iron isotopic signatures are to be used to discriminate areas where significant redox reactions have occurred and as such may provide indications of areas fertile for uranium mineralization. Significant fractionation of Fe isotopes are expected because Fe^{2+} plays a role as a reducing agent (Ligar et al., 1999; Beyer et al., 2010; Alexandre and Kyser 2012) during the formation of U-deposits as follows (Stumm and Morgan, 1996):

$$U^{6+}_{(aq)} + 2Fe^{2+}_{(aq)} + 2H_2O \leftrightarrow U^{4+}O_{2(uraninite)} + 2Fe^{3+}_{(chlorite\ or\ hematite)} + 4H^{+}_{(aq)}$$

Mineral Paragenesis

Pre-ore alteration is recorded both above and below the unconformity. However, in the overlying Athabasca Group sandstones, early pre-ore quartz alteration created a 200 m thick silicified zone 100–200m above the unconformity that acted as a partial barrier to fluid flow. This silicified zone at Zone 4 limited the spatial extent of late pre- and syn-ore alteration associated with primary dispersion and prevented the mobilization of post-ore pathfinder elements into overlying strata during secondary dispersion (Ng, 2012).

The Manitou Falls Formation consists mainly of detrital quartz with minor muscovite and dravite. Early diagenetic kaolinite, dickite (K1) and a layer of diagenetic Mg-chlorite (C1) in the overlying Athabasca Group sandstones was partially replaced by a fibrous form of C1 chlorite followed by spherulitic-acicular T1 tourmaline (Fig. 2). The K1+C1+T1 assemblage was then variably replaced by illite (I1). Incomplete replacement of C1 by I1 formed an illite-chlorite mixed-layer (ICML) clay mineral. Furthermore, Mg- and Fe-rich chlorite (C2) was introduced in voids created by pre-ore alteration as illite (I1bsmt) and chlorite (C1bsmt, C2bsmt), which were contemporaneous with I1 alteration above the unconformity (Kotzer and Kyser, 1995). During the main ore stage, C3 chlorite was introduced replacing C2 locally in the ore zone and is differentiated by its association with sulphides and U minerals (Ng, 2012). Thus, pre-ore alteration in the Athabasca Group sandstones is characterized by K1, C1, T1 and then I1, which also formed ICML from reaction with C1. In the basement, pre-ore alteration is recorded by I1bsmt, C1bsmt and C2bsmt. Only C3 chlorite is paragentically associated with uraninite with any certainty, and only the timing of K1 and C1 clearly pre-date the alteration associated with the U mineralizing event (Fig. 2).

Fe Isotopic Relationships

The Fe isotopic composition of any phase depends on the initial isotopic composition of $Fe_{(aq)}$, which in turn depends on the Fe isotopic composition of the source and the process

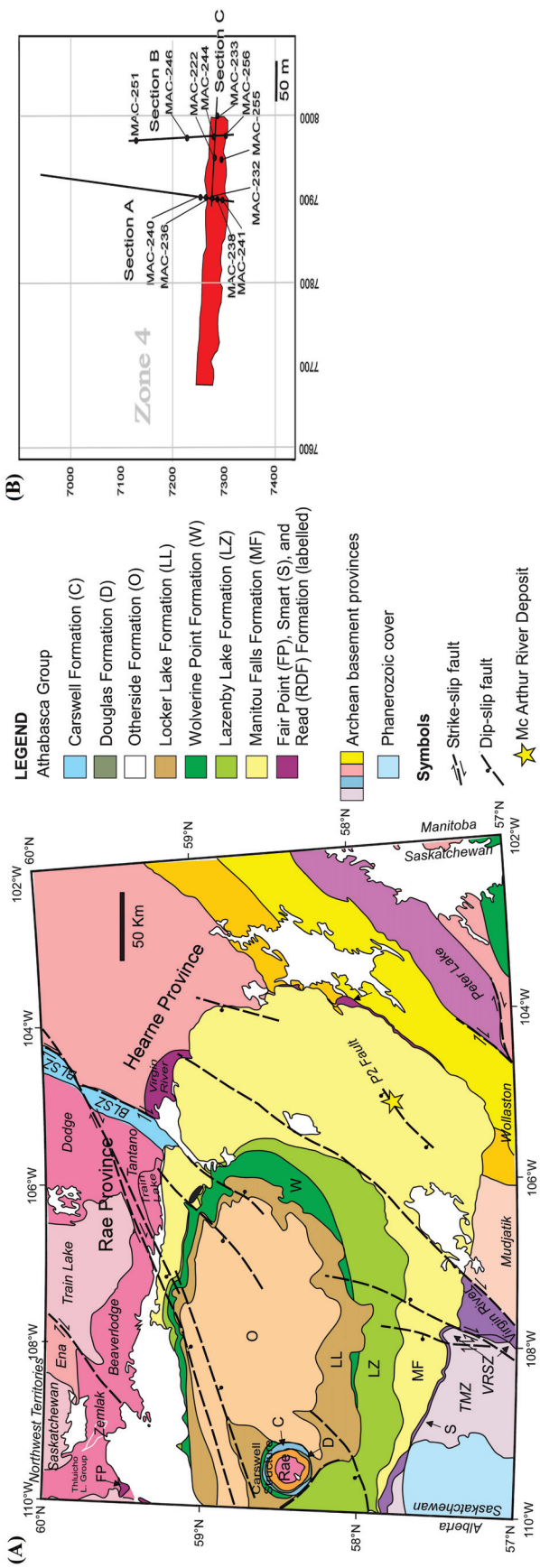

Figure 1. (A) Geology of the Athabasca Basin, northern Saskatchewan and location of the McArthur River Deposit (star). (B) Plan view of the Zone 4 deposit with 2 NE-SW oriented transects (Sections A and B) and one transect oriented NW-SE (Section C) and the drill holes sampled in this project as shown in Figure 4 (modified after Hoffman, 1988; Ramaekers et al., 2007; Ng et al., 2013).

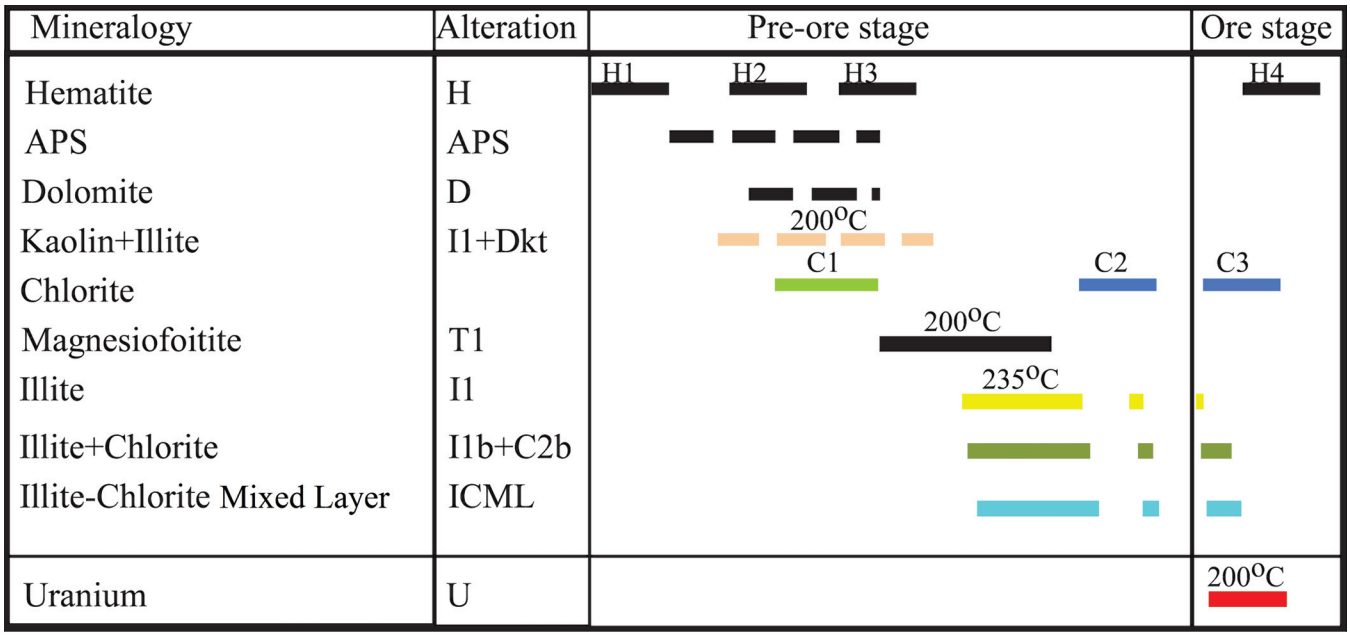

Figure 2. Simplified mineral paragenesis of Zone 4 of the McArthur River deposit, modified from Ng et al. (2013). APS = aluminum phosphate sulphate minerals.

by which the Fe is mobilized. In the Athabasca Basin, the $Fe^{2+}_{(aq)}$ is sourced from basement minerals under slightly acidic conditions with pH of about 4.5 at 200°C (Cuney et al., 2003). Therefore, the isotopic composition of Fe should be somewhat variable reflecting heterogeneity in the basement rocks (Fig. 3). In addition, solvation of the Fe in these minerals should result in low $^{56}Fe/^{54}Fe$ ratios in basement alteration minerals such as C1bsmt, coupled with higher $^{56}Fe/^{54}Fe$ ratios in the fluid, depending on the efficiency of the dissolution. Oxidation of the $Fe^{2+}_{(aq)}$ will result in chlorite or hematite (C2bsmt and C3) with the same isotopic composition as the $Fe^{2+}_{(aq)}$ if the oxidation efficiency is near 100%, or higher $^{56}Fe/^{54}Fe$ ratios in these minerals than in the initial $Fe^{2+}_{(aq)}$ if only a portion of the $Fe^{2+}_{(aq)}$ is oxidized (Fig. 3). The $Fe^{2+}_{(aq)}$ that then moves into the primary alteration halo away from the deposit and altering previously formed minerals will have similar or higher $^{56}Fe/^{54}Fe$ ratios than the initial $Fe^{2+}_{(aq)}$. Thus, proximal to the deposit $^{56}Fe/^{54}Fe$ ratios should be high in Fe^{2+}-rich minerals involved in the reduction of $U^{6+}_{(aq)}$, even higher in Fe^{3+}-rich alteration minerals and lower in the primary dispersion hydrothermal plume (Fig. 3).

Methods

Sample selection

Fifty-six samples of clay separates (< 2 µm fractions) from 13 diamond drill holes from the McArthur River Zone 4 deposit (Fig. 4) were selected for this project as representative of the alteration mineralogy. The separates were characterized using X-ray diffraction (XRD), Short-Wave Infrared Spectroscopy (SWIR) and Electron Probe Microanalysis (EPMA) by Ng (2012) to determine the compositions of the samples, their modal mineralogy and their mineral paragenesis (Figs. 2 and 4). Their characteristics by alteration facies are shown in Table 1. These samples were chosen not only to be representative of the alteration geology, but also selected due to the availability of ^{57}Fe Mössbauer spectroscopy data reported by Ng (2013). Mössbauer spectroscopy quantifies the oxidation state of Fe, with relative abundances of Fe^{3+} and Fe^{2+} expressed as the parameter $Fe^{3+}/\sum Fe$, where $\sum Fe$ equals the sum of Fe^{2+} and Fe^{3+}.

Sample preparation

To ensure that at least 10 µg Fe were available for isotopic measurements, 1–100 mg of sample was weighed into Savillex beakers. Samples were digested using a mixture of 1:4 HF and HNO_3 and placed on a hot plate at 180°C for 12 h. This process was repeated until no fluorides were observed in the Savillex beakers; the samples were then evaporated to dryness at 70°C and diluted in 10M HCl for separation of the Fe by ion chromatography.

Purification and separation of Fe was achieved using anion-exchange chromatography in a hydrochloric acid media (Strelow, 1980) using a prepFAST sample/standard dilution system with AG-MP-1M resin and a modified method from Maréchal et al., (1999). The resin was loaded into a column (1 ml), pre-cleaned with 10M HCl, 1M HCl and DI H_2O (18.2 MΩ), and conditioned for samples with 10M HCl. The purpose of ion chromatography is to minimize two phenomena related to sample impurities: (1) isobaric interferences that could cause apparent mass independent isotopic effects as a result of interferences on ^{54}Fe, ^{56}Fe, and ^{57}Fe (Anbar et al., 2000; Telus et al., 2012), and (2) matrix effects that change the properties of the plasma and result in mass dependent isotopic shifts. Recovery of Fe after passing through the ion exchange columns was 100±2%, thus resulting in no isotopic fractionation during ion-exchange chromatography due to incomplete recovery (Anbar et al., 2000).

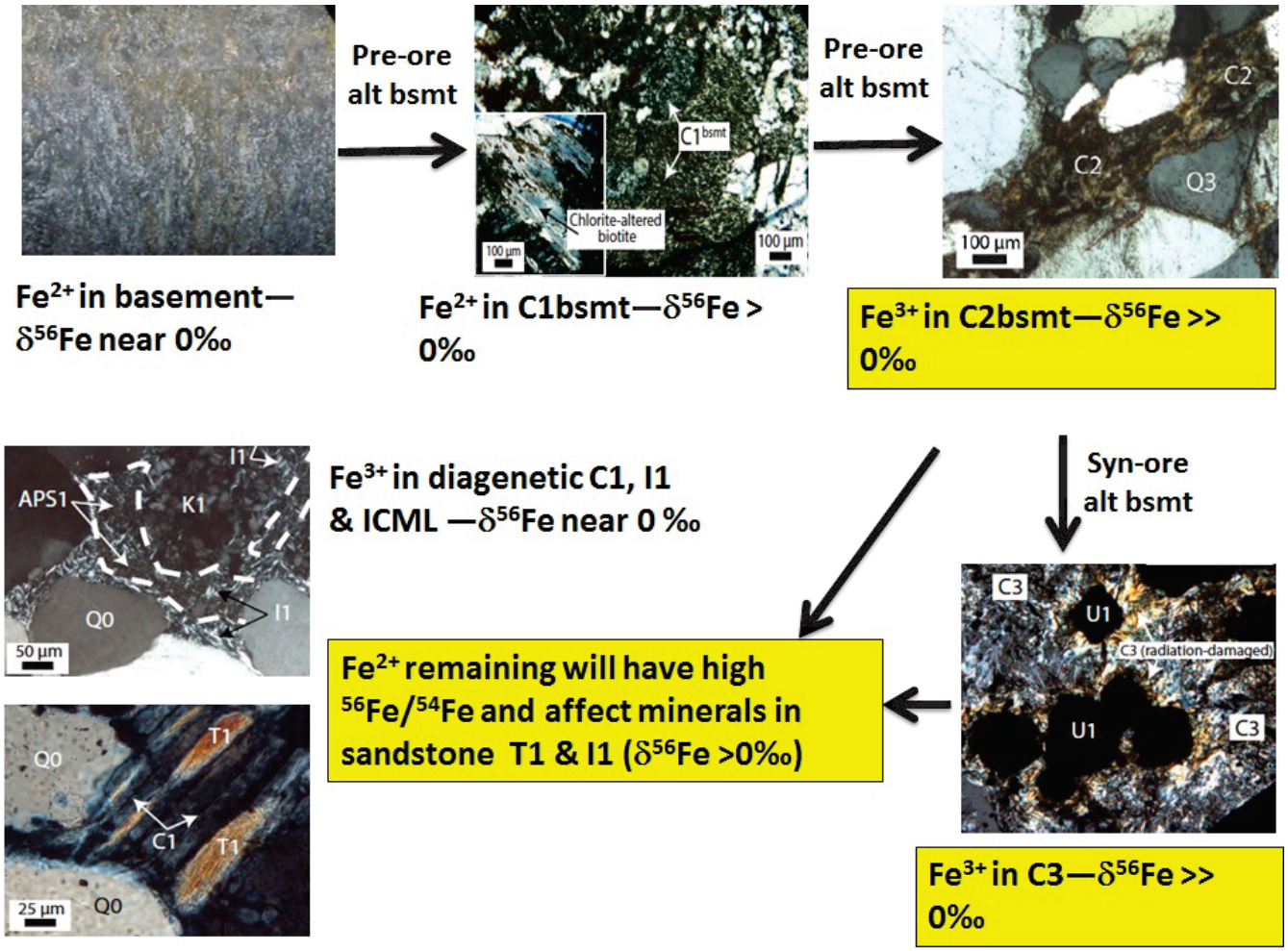

Figure 3. $^{56}Fe/^{54}Fe$ ratios and expected $\delta^{56}Fe$ values in the McArthur River alteration and mineralizing system. Minerals that record involvement in reducing the U^{6+} will have the highest $^{56}Fe/^{54}Fe$ ratios whereas those affected by hydrothermal alteration will have slightly higher values relative to Fe in the source.

The isotopic composition of Fe was analyzed by multi-collector inductively coupled plasma mass spectrometry (MC-ICP-MS) correcting for instrumental mass fractionation by standard bracketing with IRMM-014 reference material (Taylor et al., 1992). Fe measurements were carried out in medium mass resolution mode (R= 7000–8000) to resolve argon oxide (ArO) interferences (Malinovsky et al., 2003; Weyer and Schwieters, 2003; Schoenberg and von Blanckenburg, 2005). Iron isotope data are reported in the standard delta (‰) notation relative to the certified standard (IRMM-014):

$$\delta^{56}Fe = \{(^{56}Fe/^{54}Fe)_{sample}/(^{56}Fe/^{54}Fe)_{IRMM\text{-}014} - 1\} \times 10^3$$

For internal control on isotopic results, a synthetic standard similar in chemical composition to C2 Sudoite (Fe: 7.1 wt. %, Mg: 7.0 wt. %) was prepared using solutions with known isotopic compositions of Fe and Mg. This standard was prepared via separation with the AGMP-1M resin and analysed on the MC-ICP-MS (Thermo Finnigan, Neptune) with every 10 samples. Measured $\delta^{56}Fe$ and $\delta^{57}Fe$ values were monitored for QA/QC and followed a mass dependent relation ($\delta^{57}Fe = 1.5\pm0.2*\delta^{56}Fe$). The internal precision of each Fe isotope analysis was typically better than 0.09‰ (2σ). External precision was better than ±0.03‰ in $\delta^{56}Fe$ based on repeat analysis of samples and in-house standards.

Aliquots were taken from each sample and analyzed by high-resolution ICP-MS for trace elements and Pb isotope ratios, and ICP-OES for major elements to verify the results from the XRD and to refine the chemistry of the separates. Some samples showed anomalous values for LREE (Table 2). To verify that the host of the LREE was not a Fe-rich minor phase that could affect the isotopic composition of the Fe, a set of 12 samples were analyzed using a FEI-MLA Quanta 650 scanning electron microscope (SEM).

Results

Sample chemistry and mineralogy

Backscatter electron (BSE) images (Fig. 5) obtained by scanning electron microscopy (SEM) reveal the presence of both monazite and aluminum phosphate sulphate (APS) crystals associated with trioctahedral chlorite and sudoite in the clay separates, similar to what was noted by Gaboreau et al. (2007). These BSE images indicate that the LREEs are

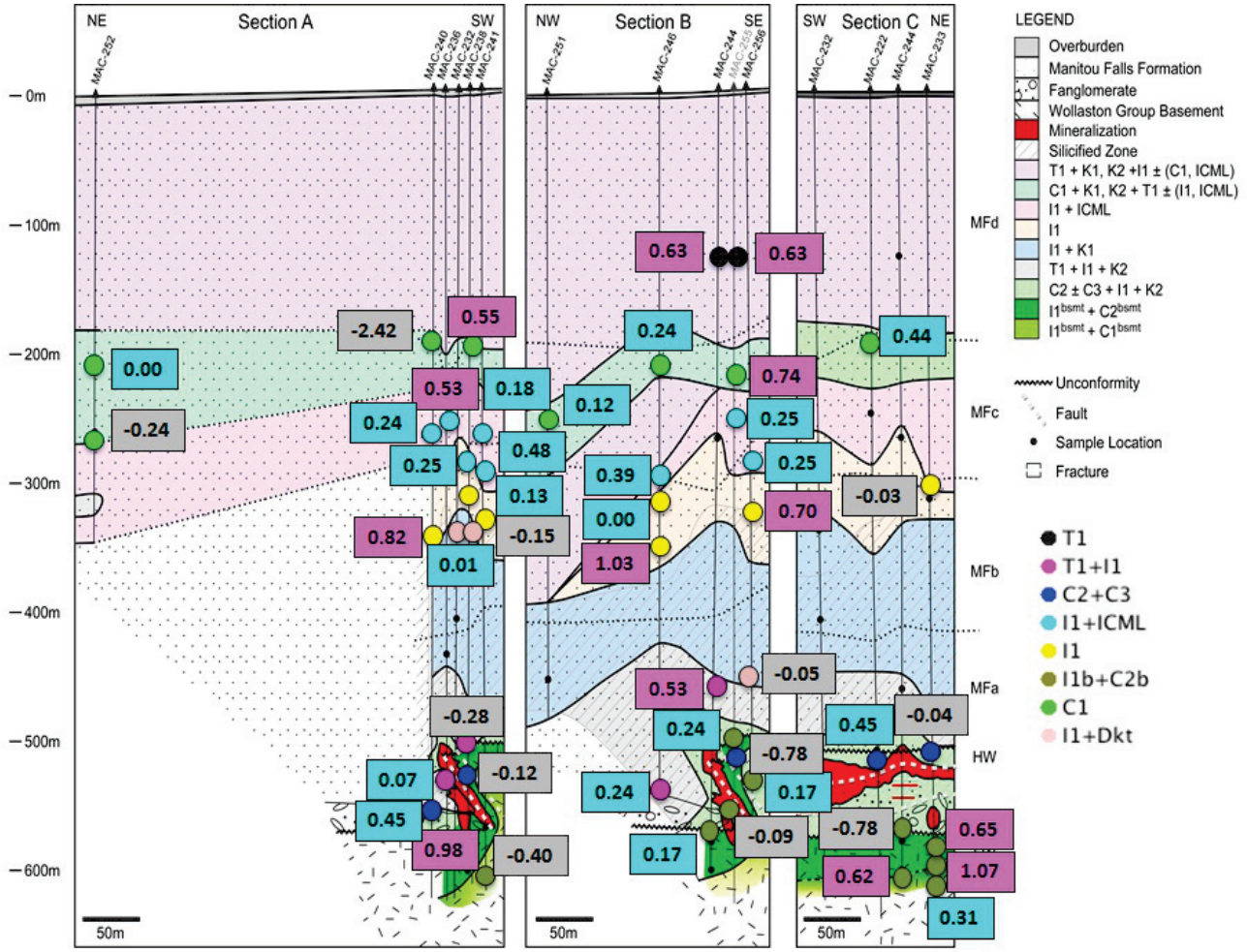

Figure 4. Spatial distribution of alteration minerals and sample locations (circles) within the Manitou Falls Formation and Wollaston Group basement at McArthur River Zone 4 along the cross sections through the deposit shown in Figure 1. Sample colors represent different mineral assemblages. Boxes represent the δ^{56}Fe values and their colors reflect distinct populations of values deduced from cumulative probabilities (Fig.7). Abbreviations: Dkt=dickite, Kln=kaolinite, ICML=illite-chlorite mixed layer clay. Modified from Ng et al., (2013).

contained in euhedral monazite crystals in the chlorite matrix and APS minerals present on the edges of larger illite crystals. The highest Fe contents are found in I1 and I1bsmt + C1bsmt samples, but these samples also contain some of the lowest concentrations of LREE, suggesting that APS minerals and monazite are not the main Fe-bearing minerals present in the samples. These observations are further supported by the lack of clear correlations between ΣLREE and Fe, indicating that the phosphates are not Fe-bearing (Fig.6).

In illite as well as di-trioctahedral and tri-trioctahedral chlorite, Fe^{2+} and Fe^{3+} can substitute in octahedral sites and Fe^{3+} into tetrahedral sites (Billault et al., 2002). Substitution of Fe^{3+} in the tetrahedral sites is rare in chlorite (Zazzi et al., 2006) but common in illite crystals (Murad and Wagner, 1994). Iron contents in samples containing illite correlate with K contents (Fig. 6), suggesting that the illite grains are Fe^{3+}-rich, and therefore should have relatively high δ^{56}Fe values.

Iron isotopes

The δ^{56}Fe values of clay mineral separates from both sandstone and basement rocks near the McArthur River deposit span a range of nearly 1.5‰ (Fig. 7). The δ^{56}Fe values in the clay separates do not correlate with depth or distance from the mineralization, nor do they correlate with Fe^{3+}/Fe_{total}, other isotopic systems such as O or Pb, or any element other than Mg (Fig. 7).

Most values range from 0 to 0.3‰, a few are less than 0‰ or greater than 0.5‰. The gap in data points between 350–450m depth reflects the silicified sandstone above the deposit (Fig. 7). Cumulative probability plots of the δ^{56}Fe values suggest there are three major populations of data, one with δ^{56}Fe values < 0, another from 0 to 0.5 and a third with values greater than 0.5‰ (Fig. 7).

Discussion

Pre-ore alteration

To understand the Fe cycle in this system using Fe isotopes as tracers, the initial δ^{56}Fe values in both the basement

Table 1. Alteration minerals of interest and their chemical characteristics. Except for C3, all alteration minerals mention in Table 1 belong to the late pre-ore alteration stage. Modified from Ng, 2012.

Alteration	Mineral	Characteristics
I1	Illite, occurs as interlocking fibrous laths replacing earlier mineral assemblages in the Athabasca Group sandstones.	Al_2O_3 32.94 wt.%, FeO 0.77 wt.%, MgO 0.48 wt.%, K_2O 8.83 wt.%, $Fe^{3+}/\sum Fe$ 1.00 and all Fe^{3+}
$I1_{bsmt}$	Illite in the altered basement, occurs in both the hanging wall and footwall basement rocks distal to the mineralization.	Al_2O_3 32.66 wt.%, FeO 1.09 wt.%, MgO 0.96 wt.%, K_2O 9.23 wt.%, $Fe^{3+}/\sum Fe$ not reported, all Fe^{3+}
ICML	Illite-chlorite mixed-layered clay mineral, formed by incomplete replacement of C1 by I1 and is spatially associated with I1.	60% illite and 40% sudoite, $Fe^{3+}/\sum Fe$ 1.00, all Fe^{3+}
C1	Sudoite, di-trioctahedral chlorite with an octahedral occupancy of 4.63 cations per formula unit ($O_{10}(OH)_8$)	Al_2O_3 31.78 wt. %, FeO 0.68 wt. %, MgO 10.36 wt. %, K_2O 1.16 wt. %, $Fe^{3+}/\sum Fe$ 0.93, mostly Fe^{2+}
$C1_{bsmt}$	Trioctahedral clinochlore in the altered basement, with octahedral occupancy of about 5.8 apfu.	Al_2O_3 20.63 wt. %, FeO 9.37 wt. %, MgO 25.77 wt. %, K_2O 0.18 wt. %, $Fe^{3+}/\sum Fe$ not reported, mostly Fe^{2+}
C2	Di-trioctahedral Mg-Fe-rich sudoite with one vacant octahedral site.	Al_2O_3 27.28 wt. %, FeO 9.12 wt. %, MgO 11.65 wt. %, K_2O 0.29 wt %, $Fe^{3+}/\sum Fe$ 0.45, mostly Fe^{3+}
$C2_{bsmt}$	Di-trioctahedral Mg-sudoite in the altered basement.	Al_2O_3 33.52 wt. %, FeO 1.47 wt. %, MgO 13.20 wt. %, K_2O 0.73 wt. %, $Fe^{3+}/\sum Fe$ not reported, all Fe^{2+}
C3	Fe-Mg-rich sudoite with ca. 1.2 octahedral vacancies per formula unit and radiation damage caused by nearby uraninite.	Al_2O_3 24.44 wt. %, FeO 15.36 wt. %, MgO 5.41 wt. %, K_2O 0.11 wt. %, $Fe^{3+}/\sum Fe$ not reported, mostly Fe^{3+}

and basin must be constrained. The isotopic composition of Fe in the rock record spans a total range of about 4‰, with most igneous and metamorphic rocks having $\delta^{56}Fe$ values near 0‰ (Craddock and Dauphas, 2011 and references therein). Based on available literature, the basement rocks in the McArthur River area, which are major reservoirs of Fe in the system, should have $\delta^{56}Fe$ values near 0‰. Metapelitic rocks in the basement at McArthur River should have slightly higher values based on similar rocks elsewhere (Beard et al., 2003), furthermore, these metapelitic rocks tend to have much lower Fe contents than mafic units. "Background" $\delta^{56}Fe$ values in the hydrothermal fluid from the basement should be reflected by chlorite in basement rocks that occurs distal to faults and furthest from the system. This is best reflected in a I1b+C2b sample with a $\delta^{56}Fe$ value of 0.31‰ which occurs furthest from the ore, similar to other basement samples distal to the mineralization (Figs. 4 and 8). Samples identified as I1b+C2b have a bimodal distribution, with one population having $\delta^{56}Fe$ values of 0–0.25‰, similar to the initial values for the Fe reservoir, and the other having values >0.5‰ (Fig. 8). Thus, based on compilations of Fe isotopic compositions in the literature in combination with the values of clay minerals from basement samples farthest from the ore (Fig. 8), the initial $\delta^{56}Fe$ values of the system at McArthur River would have been slightly above 0‰, as suggested in Fig. 3.

The Fe in the sandstone is hosted in diagenetic hematite that could be affected by the hydrothermal/mineralizing fluids. This Fe is most likely reflected in diagenetic I1+Dkt, diagenetic C1 chlorite and samples of early magnesio-foitite and illite (T1+I1). Although both I1+Dkt and T1+I1 have values of 0–0.5‰, those of C1 chlorite are variable and those of I1 and I1b+C2b are bimodal, with one group having values of 0–0.5‰, but the other being much higher. The higher values are reflective of the mineralizing process discussed below. Additional exceptions to the restricted range of 0–0.5‰ are samples that are located near lithologic boundaries or faults, which are susceptible to overprinting by the mineralizing system or later fluids, also discussed below. The "background" Fe has $\delta^{56}Fe$ values between 0 and 0.5‰, as shown in Figure 8, similar to the "background" values of the basement rocks (Figs. 3 and 8). Subtleties within this range relate to three major processes revealed in this study as reflected by the three populations of $\delta^{56}Fe$ values.

Fe isotope related to the mineralizing system

Oxidation of Fe during reduction of U^{6+} should result in $\delta^{56}Fe$ values that are higher than the initial Fe^{2+} in the source

Table 2. Average concentrations of major elements and LREE for each alteration layer (Fig. 2) in clay separates at the McArthur River Deposit Zone 4.

Alteration	T1 + Kln (K1, K2) + I1 ± (C1, ICML)		C1 + Kln (K1, K2) + T1 + (I1, ICML)		I1 + ICML		I1		I1 + Dkt (K1)		T1 + I1 + K2		C2 ± C3 + I1 + K2		I1bsmt + C2bsmt		I1bsmt + C1bsmt	
Layer	avg. (n=2)	±1σ	avg. (n=8)	±1σ	avg. (n=9)	±1σ	avg. (n=8)	±1σ	avg. (n=7)	±1σ	avg. (n=4)	±1σ	avg. (n=7)	±1σ	avg. (n=3)	±1σ	avg. (n=2)	±1σ
Major elements (wt. %)																		
Al	13.97	2.74	18.64	11.73	25.13	10.06	29.58	3.14	16.24	15.15	12.64	11.76	13.09	7.53	10.68	7.69	8.11	0.92
Ca	0.07	0.03	0.19	0.08	0.16	0.06	0.16	0.07	0.12	0.09	0.06	0.05	0.10	0.05	0.07	0.04	0.11	0.05
Fe	1.09	1.08	1.55	1.39	2.04	1.15	3.26	2.07	0.69	0.74	1.35	0.49	2.88	3.26	1.27	0.90	3.22	3.38
K	4.57	0.04	2.25	2.26	6.71	3.45	8.93	2.22	3.85	4.74	1.53	1.37	0.94	0.41	1.90	1.12	1.51	0.88
Mg	1.18	0.91	3.93	2.56	1.72	0.60	1.33	0.24	0.36	0.40	0.46	0.54	4.90	1.98	2.21	1.70	5.89	6.18
Na	0.09	0.05	0.43	0.39	0.05	0.03	0.12	0.07	0.03	0.04	0.07	0.09	0.11	0.08	0.03	0.02	0.04	0.02
P	0.08	0.04	0.19	0.12	0.17	0.09	0.14	0.05	0.10	0.07	0.04	0.03	0.07	0.04	0.01	0.01	0.01	0.00
Ti	0.84	0.84	0.59	0.68	0.11	0.03	0.19	0.05	0.69	0.62	0.94	0.63	0.52	0.48	0.16	0.09	0.25	0.16
LREE (ppm)																		
Ce	55.84	15.27	257.27	77.86	70.91	111.45	6.39	4.20	131.51	134.33	14.81	5.79	117.90	52.91	16.06	17.39	15.27	12.87
Eu	0.62	0.20	2.37	0.94	1.05	1.45	0.07	0.06	0.99	0.84	0.25	0.19	0.77	0.32	0.21	0.19	0.23	0.22
Gd	3.15	0.34	11.72	2.49	5.31	6.99	0.34	0.28	3.74	3.01	0.85	0.09	3.88	1.75	0.58	0.46	1.36	1.26
La	20.16	7.32	101.86	34.22	27.59	47.34	2.17	1.29	57.46	60.07	6.23	3.27	59.96	38.58	4.07	3.20	4.90	3.84
Nd	22.56	3.35	103.48	16.66	25.43	36.32	2.77	1.74	47.80	43.97	5.12	1.09	37.90	11.54	6.46	6.61	7.47	6.36
Pr	5.66	1.34	27.56	4.71	6.78	10.11	0.67	0.42	12.60	10.76	1.36	0.39	11.96	4.55	1.69	1.72	1.78	1.49
Sm	4.07	0.08	17.86	3.44	7.22	9.83	0.50	0.40	6.51	5.39	1.53	1.07	6.32	2.97	1.06	0.95	1.60	1.43

(Fig. 3). One of the sample populations has δ^{56}Fe values >0.5‰, higher than the values of 0–0.5‰ estimated for the initial Fe. Samples having high δ^{56}Fe values include T1, C2+C3, a subset of I1 and a subset of I1b+C2b (Fig. 9). Spatially, these samples are near the ore zone or in the sandstone directly above the extension of the P2 fault system that hosts the deposit, where primary dispersion during mineralization would occur (Fig. 9). If high values reflect primary dispersion of the mineralizing system, these results indicate that I1, C1 and I1+ICML were affected above the silicified zone and up to 300 m above the deposit. Similarly, T1 may reflect later hydrothermal alteration associated with this event.

Resetting by later fluids

Later fluids (i.e. groundwater, diagenetic fluids, or hydrothermal fluids) will move preferentially along lithologic boundaries, the unconformity and reactivated fault zones. These fluids would preferentially carry isotopically light Fe, as incomplete leaching from silicate releases isotopically light Fe into solution (Brantley et al., 2004). Samples with δ^{56}Fe values less than 0‰ are indeed located along boundaries, the unconformity and fault zones suggesting that these samples have interacted with later fluids (Fig. 10). However, because fluid flow and fault reactivation are both episodic and restricted to reactivated areas, not all samples near faults or the unconformity have low δ^{56}Fe values. The sample with the lowest δ^{56}Fe values also has the lowest δ^{2}H (Fig. 11) value because it has interacted with relatively recent fluids having low δ^{2}H (Ng et al., 2013). This would imply that other samples with higher δ^{56}Fe values have interacted with fluids during much older events, including those during the waning stages of the mineralizing process.

Summary

The most important controls on Fe isotope fractionations are oxidation state, bonding environment, and temperature. Significant fractionation of Fe isotopes in the McArthur River mineralizing system are expected because Fe^{2+} has been suggested as a reducing agent during the formation of U deposits (Ligar et al., 1999; Beyer et al., 2010; Alexandre and Kyser 2012). The δ^{56}Fe values in clay mineral separates from both sandstone and basement rocks near the McArthur River deposit have a range of nearly 1.5‰. However, δ^{56}Fe values in clay separates do not correlate with distance from the mineralization, Fe^{3+}/Fe_{total}, other isotopic systems such as H, O or Pb, or any ele-

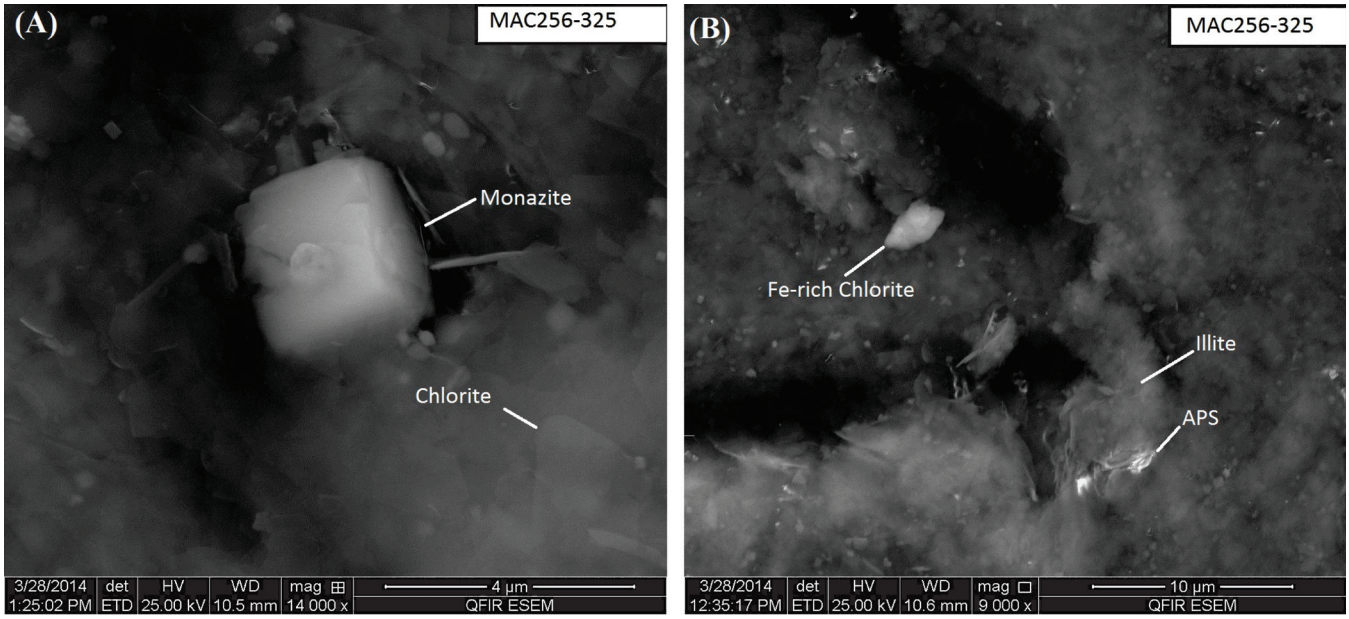

Figure 5. BSE-images of sample MAC 256-325 from the Manitou Falls Formation showing the presecence of both (A) monazite and (B) APS minerals in a chlorite and illite matrix.

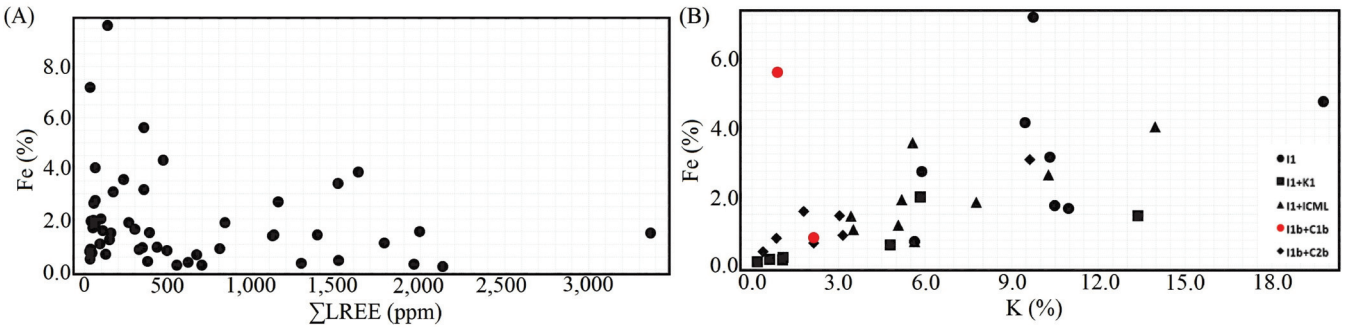

Figure 6. Plot of: (A) ∑LREE versus Fe (%) contents and (B) K against Fe contents from clay separates used in this study.

ment other than Mg (Fig. 11), the latter reflecting mixing between sudoite and other minerals. Such correlations would be expected if these clay minerals formed from homogeneous diagenetic, hydrothermal, or mineralizing systems and had no later overprinting.

Most δ^{56}Fe values are within the range from 0 to 0.5‰ that defines the initial isotopic composition of the source; few are less than 0‰ or greater than 0.5‰. Cumulative probability plots of δ^{56}Fe values indicate three major populations of data, one with δ^{56}Fe values < 0‰, another from 0 to 0.5‰ and a third with values > 0.5‰. Most clay types have values within all three populations, reflecting the complexity of the Fe system.

Oxidation of Fe during reduction of U^{6+} should result in alteration minerals with higher δ^{56}Fe values than the initial Fe^{2+} in the source of the reducing fluid. This process is reflected in the population of samples having δ^{56}Fe values >0.5‰. Spatially, these samples are near the ore zone in the basement or in the sandstone directly above the extension of the P2 fault system that hosts the deposit. Primary dispersion of Fe during mineralization would impart high δ^{56}Fe values on pre-existing minerals or form new minerals, such as I1, and such high values occur in some samples of I1, C1, I1+ICML and T1 above the silicified zone and distal to the deposit.

Low δ^{56}Fe values (< 0‰) reflect post-ore fluid events and are observed in clay separates located along lithologic boundaries, the unconformity between the Athabasca Group sandstones and the basement units, or fault zones especially near the fault zone that hosts the deposit. However, not all samples near faults or the unconformity have low δ^{56}Fe values because later fluid events are not universally extensive, as shown by the variably reset U-Pb ages in the ore (e.g., Alexandre et al., 2009) and the low $^{207}Pb/^{206}Pb$ ratios in the separates near the ore zone. Samples with low δ^{56}Fe values also have low δ^{2}H values because they have interacted with relatively recent fluids characterized by low δ^{2}H signatures.

In addition to Fe isotope analyses, aliquots of the dissolved samples were analyzed by high-resolution ICP-MS for trace elements, Pb isotope ratios and major elements via ICP-OES. Some samples showed anomalous concentrations of LREE. Energy dispersive spectroscopy and BSE-imaging

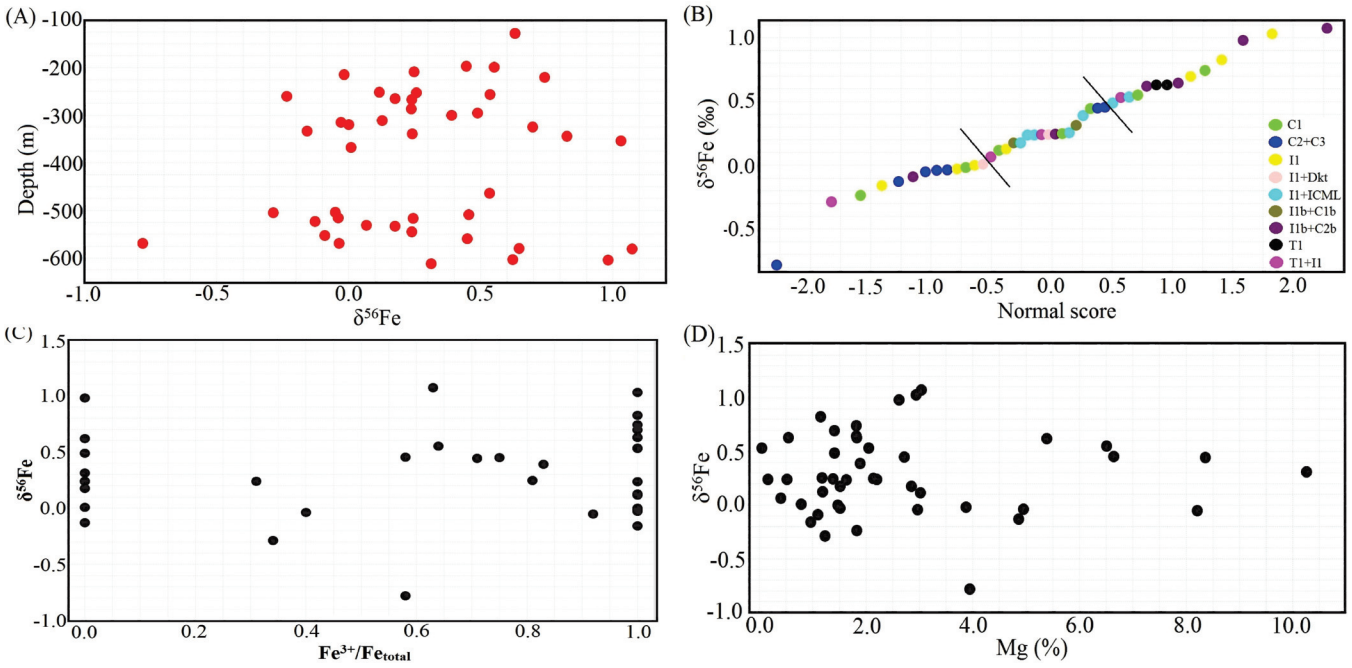

Figure 7. (A) δ^{56}Fe values versus depth of clay separates from McArthur River Deposit Zone 4. B) cumulative probability plots of Fe isotopic compositions for various generations of alteration minerals at McArthur River Zone 4. C) Plot of Fe^{3+}/Fe_{total} vs δ^{56}Fe. D) Mg concentration in samples vs δ^{56}Fe. The gap in data with depth (A) reflects the silicified sandstone above the deposit, which is almost devoid of clay minerals.

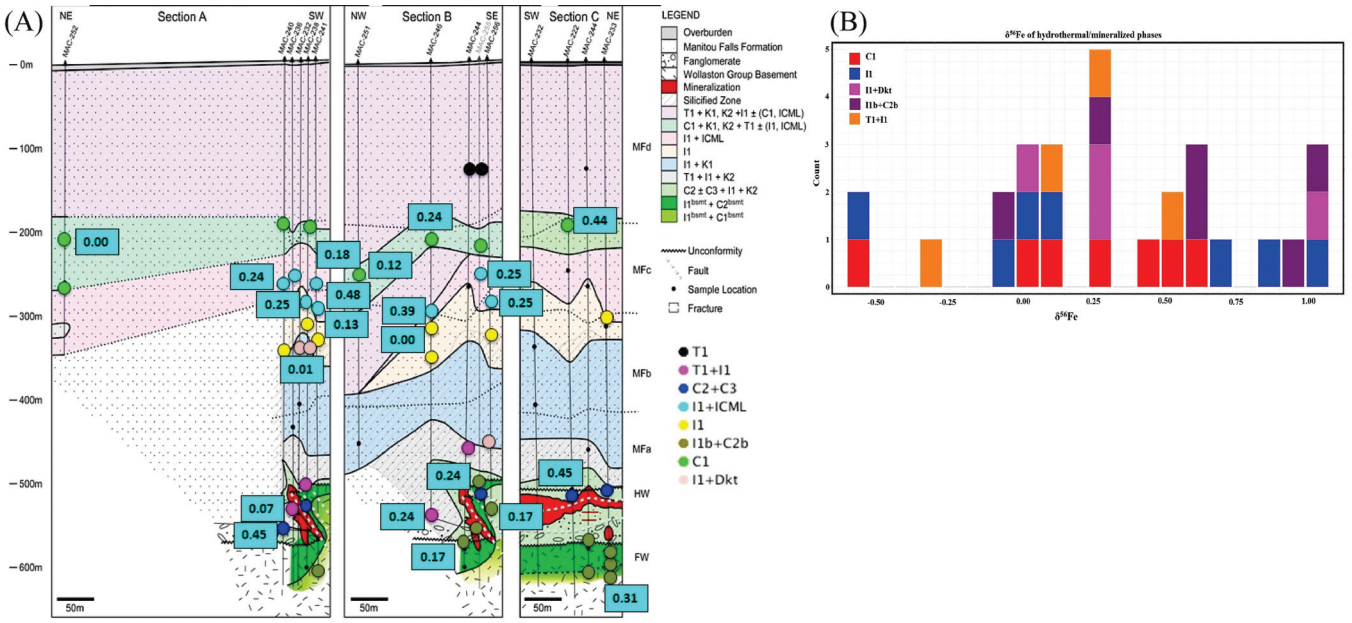

Figure 8. A) Spatial distribution of various sample types having δ^{56}Fe values of 0–0.5‰. Most samples reflect diagenetic minerals in the sandstones or are located in distal alteration in the basement. B) Histogram of δ^{56}Fe values for minerals that are related to diagenesis or early alteration of the basement. I1 and I1b+C2b have a bimodal distribution because the diagenetic minerals have been affected by ^{56}Fe-rich fluids from oxidation of the Fe in the fluid. The low value for one C1 sample, which is at a lithologic contact, reflects loss of ^{56}Fe during later fluid interaction (Fig. 3).

on the SEM reveals the presence of both monazite and APS crystals associated with trioctahedral chlorite and sudoite in the clay separates. The highest Fe contents are in samples with the lowest concentrations of LREE, suggesting that the APS minerals and the monazite do not contribute to the Fe isotopic compositions. There is minimal correlation between ∑LREE and Fe, indicating that the phosphates are not Fe-bearing.

This study demonstrates that Fe isotopes can reveal processes associated with redox reactions in ore deposits. These processes have not been revealed before, only surmised, but the data presented here support the role of Fe as a

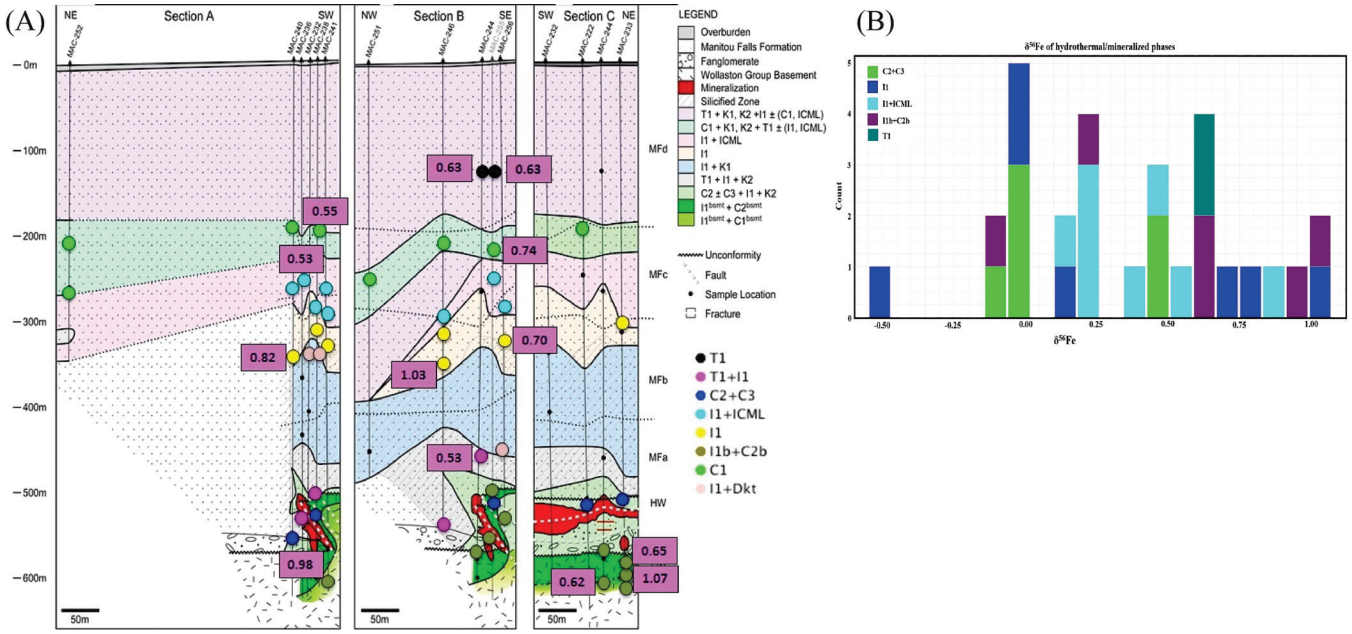

Figure 9. A) Spatial distribution of various sample types having δ^{56}Fe values >0.5‰. Most samples are related to the pre-ore or ore stages and proximal to the ore in the fault zone or the projection of the fault zone that hosts the ore. B) Histogram of δ^{56}Fe values for minerals related to hydrothermal alteration or the mineralizing system. I1 and I1b+C2b have a bimodal distribution that reflects enrichment or formation from ^{56}Fe-rich mineralizing fluids after oxidation of the Fe in the fluid. Lower values for one C2+C3 sample reflect loss of ^{56}Fe during resetting by later fluids (Fig. 3 and 10).

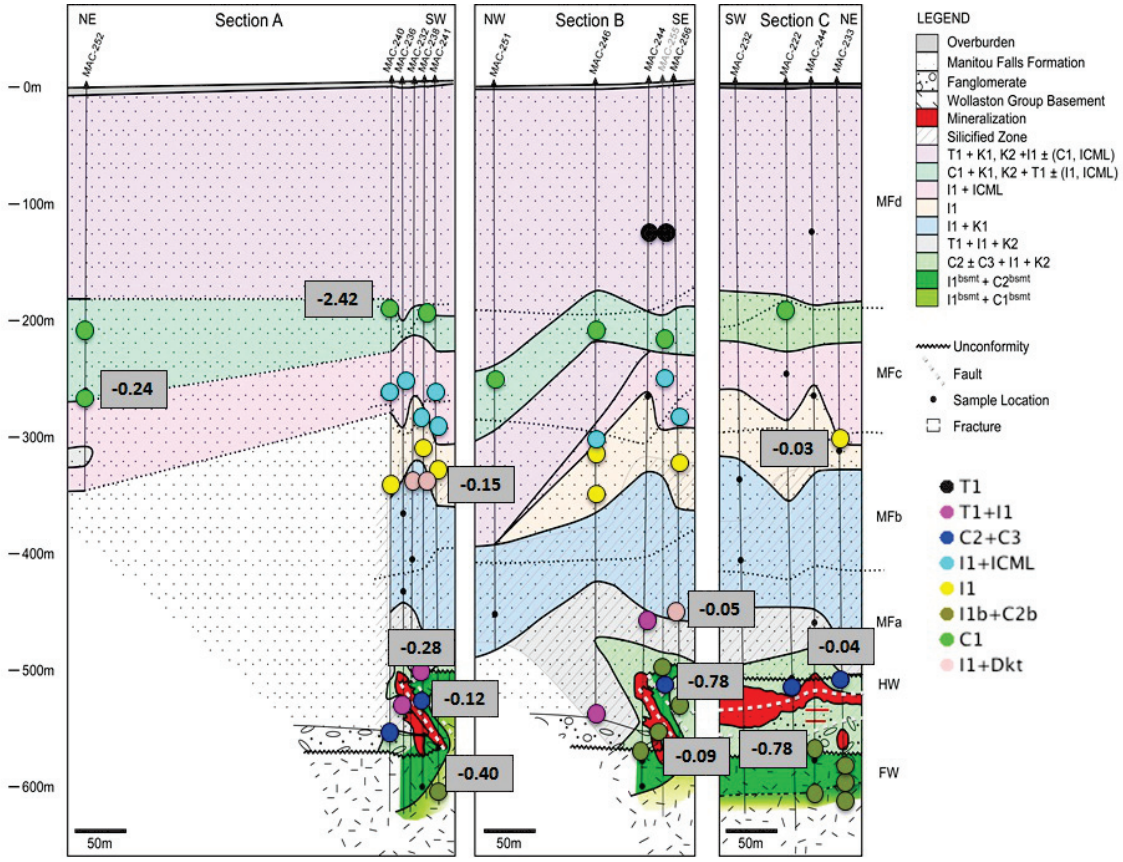

Figure 10. Spatial distribution of various sample types having δ^{56}Fe values <0‰. All samples are related to lithologic boundaries, the unconformity or selected fault zones. The low values reflect interaction with later fluids (Fig. 3).

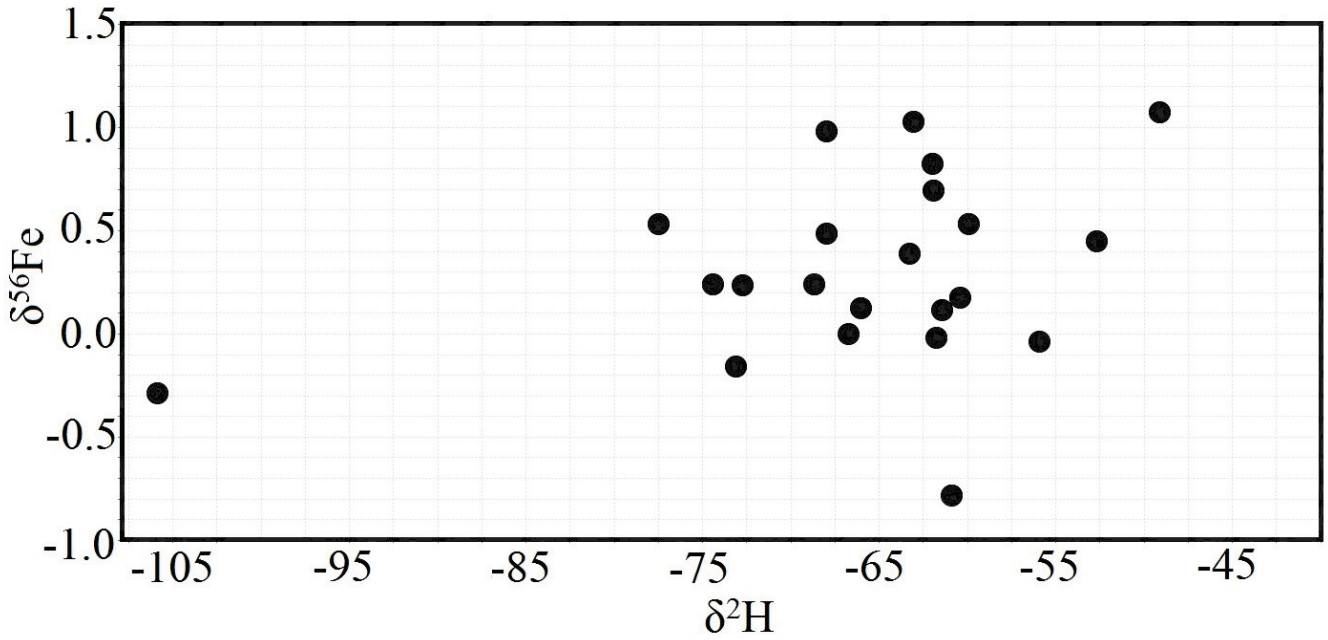

Figure 11. Plot of δ^2H vs $\delta^{56}Fe$ from samples used in this study. δ^2H data from Ng (2012).

reductant for U in deposits in the Athabasca Basin. The redox population also provides an indication on the fertility of an alteration system, particularly along ore-hosting faults targeted during exploration.

Acknowledgments

Funding for this research was provided by the Targeted Geoscience Initiative 4 (TGI-4) uranium ore systems project, through a grant to Kurt Kyser, with support for Queen's University. The report benefitted from constructive reviews by an anonymous reviewer and Eric Potter.

References

Armitage, A., 2013. Technical report on the Patterson Lake, Patterson lake South and Clearwater West Properties; N.I. 43-101 technical report prepared for Fission Uranium Corp. and Fission Energy Corp., 132 p.

Alexandre, P., Kyser, K., and Jiricka, D., 2009. Critical geochemical and mineralogical factors for the formation of unconformity-related uranium deposits: comparison between barren and mineralized systems in the Athabasca Basin, Canada; Economic Geology, v. 104, p. 413–435.

Alexandre, P., and Kyser, K., 2012. Reductants involved in the formation of the Athabasca Basin unconformity-related uranium deposits; Joint Annual Meeting of the Geological Association of Canada – Mineralogical Association of Canada, Abstracts, v. 35, p. 2.

Anbar, A., Roe, J., Barling, J., and Nealson, K., 2000. Nonbiological fractionation of iron isotopes; Science, v. 288, p. 126-128.

Beard, B. L., Johnson, C. M., Von Damm, K. L., and Poulson, R. L., 2003. Iron isotope constraints on Fe cycling and mass balance in oxygenated Earth oceans; Geology, v. 31, p. 629–632

Beyer, S. R., Kyser, K., Hiatt, E. E., and Fraser, I., 2010. Geological evolution and exploration geochemistry of the Boomerang Lake unconformity-type uranium prospect, Northwest Territories, Canada; Society of Economic Geologists Special Publication 15, p. 675–702.

Billault, V., Beaufort, D., Patrier, P., and Petit, S., 2002. Crystal chemistry of Fe-sudoites from uranium deposits in the Athabasca Basin (Saskatchewan, Canada); Clays and Clay Minerals, v. 50, p. 70–81.

Brantley, S., Liermann, L.J., Guynn, R.L., Anbar, A., Icopini, G.A., and Barling, J., 2004. Fe isotopic fractionation during mineral dissolution with and without bacteria; Geochimica et Cosmochimica Acta, v. 68, p. 3189–3204.

Bronkhorst, D., Mainville, A.G., Murdock, G.M., and Yesnik, L.D., 2012. McArthur River operation, Northern Saskatchewan, Canada; NI 43-101 Technical Report prepared for Cameco Corporation, November 2012, 206 p.

Craddock, P.R., and Dauphas, N., 2011. Iron isotopic compositions of geological reference materials and chondrites; Geostandards and Geoanalytical Research, v. 35, n. 1, p. 101–123.

Cuney, M., Brouand, M., Cathelineau, M., Derome, D., Freiberger, R., Hecht, L., Kister, P., Lobaev, V., Lorilleux, G., Peiffert, C., and Bastoul, A.M., 2003. What parameters control the high grade-large tonnage of the Proterozoic unconformity related uranium deposits?; in Uranium Geochemistry 2003, International Conference, Proceedings, (ed.) M. Cuney; Unité Mixte de Recherche CNRS 7566G2R, Université Henri Poincaré, Nancy, France, p. 123–126.

Gaboreau, S., Cuney, M., Quirt, D., Beaufort, D., Patrier, P., and Mathieu, R., 2007. Significance of aluminum phosphate-sulfate minerals associated with U unconformity-type deposits: The Athabasca Basin, Canada; American Mineralogist, v. 92, p. 267–280.

Hiatt, E.E., Kyser, T.K., Fayek, M., Polito, P., Holk, G.J., and Riciputi, L.R., 2007. Early quartz cements and evolution of paleohydraulic properties of basal sandstones in three Paleoproterozoic continental basins: Evidence from in situ $\delta^{18}O$ analysis of quartz cements; Chemical Geology, v. 238, p. 19–37.

Hoffman, P. F., 1988. United plates of America, the birth of a craton: Early Proterozoic assembly and growth of Laurentia; Annual Review of Earth and Planetary Sciences, v. 16, p. 543–603.

Jefferson, C. W., Thomas, D. J., Gandhi, S. S., Ramaekers, P., Delaney, G., Brisbin, D., Cutts, C., Quirt, D., Portella, P., and Olson, R. A., 2007. Unconformity-associated uranium deposits of the Athabasca Basin, Saskatchewan and Alberta; in EXTECH IV: Geology and uranium EXploration TECHnology of the Proterozoic Athabasca Basin, Saskatchewan and Alberta, (ed.) C.W. Jefferson and G. Delaney; Geological Survey of Canada, Bulletin 588, p. 23–67.

Johnson, C.M., and Beard, B.L., 2006. Fe isotopes: An emerging technique for understanding modern and ancient biogeochemical cycles; Geological Society of America, Today, v. 16, no. 11.

Johnson, C.M., Beard, B.L., and Albarede, F., 2004. Overview and general concepts; in Geochemistry of Non-Traditional Stable Isotopes, (ed.) C.M. Johnson, B. Beard and F. Albarède; Reviews in Mineralogy and

Geochemistry, v. 55, p. 1–24.

Johnson, C.M., Beard, B.L., and Roden, E.E., 2008. The iron isotope fingerprints of redox and biogeochemical cycling in modern and ancient Earth. Annual Review of Earth and Planetary Sciences, v. 36, p. 457–493.

Kotzer, T.G., and Kyser, T.K., 1995. Petrogenesis of the Proterozoic Athabasca Basin, northern Saskatchewan, Canada, and its relation to diagenesis, hydrothermal uranium mineralization and paleohydrogeology; Chemical Geology, v. 120, p. 45–89.

Kyser, K., Hiatt, E., Renac, C., Durocher, K., Holk, G., and Deckart, K., 2000. Diagenetic fluids in paleo- and meso-Proterzoic sedimentary basins and their implications for long protracted fluid histories; in Fluids and Basin Evolution (ed.) T.K. Kyser; Mineralogical Association of Canada, Short Course Notes, v. 28, p. 225–262.

Ligar, E., Charlet, L., and van Cappellan, P., 1999. Surface catalysis of uranium(VI) reduction by iron(II); Geochemica et Cosmochimica Acta, v. 63, p. 2939–2955.

Malinovsky D., Stenberg A., Rodushkin I.V., Andrén H., Ingri J., Öhlander B., and Baxter D.C., 2003. Performance of high resolution MC-ICP-MS for Fe isotope ratio measurements in sedimentary geological materials; Journal of Analytical Atomic Spectrometry, v. 18, p. 687–695.

Malinovsky, D., Rodushkin I.V., Shcherbakova, E.P., Ponter, C., Öhlander, B., and Ingri, J., 2005. Fractionation of Fe isotopes as a result of redox processes in a basin; Geochemistry International, v. 43, p. 797–803.

Maréchal, C. N., Télouk, P., and Albarède, F., 1999. Precise analysis of copper and zinc isotopic compositions by plasma-source mass spectrometry; Chemical Geology, v. 156, p. 251–273.

McGill, B.D., Marlatt, J.L., Matthews, R.B., Sopuk, V.J., Homeniuk, L.A., and Hubregtse, J.J., 1993. The P2 North uranium deposit, Saskatchewan, Canada; Exploration and Mining Geology, v. 2, p. 321–331.

Murad, E., and Wagner, U., 1994. The Mössbauer spectrum of illite; Clay Minerals, v. 29, p. 1–10.

Ng, R., 2012. Geochemical and mineralogical evolution of the McArthur River Zone 4 unconformity-related uranium ore body and application of iron oxidation state in clay alteration as indicator of uranium mineralization; M.Sc. thesis. Queen's University, Kingston, Canada, 207 p.

Ng, R., Alexandre, P., Kyser, K., Cloutier, J., Abdu, Y., and Hawthorne, F., 2013. Oxidation state of iron in alteration minerals associated with sandstone-hosted unconformity-related uranium deposits and apparently barren alteration systems in the Athabasca Basin, Canada: Implications for exploration; Journal of Geochemical Exploration, v. 130, p. 22–43.

Ramaekers, P., Jefferson, C.W., Yeo, G.M., Collier, B., Long, D.G.F., Drever, G., McHardy, S., Jiricka, D., Cutts, C., Wheatley, K., Catuneanu, O., Bernier, S., Kupsch, B., and Post, R.T., 2007. Revised geological map and stratigraphy of the Athabasca Group, Saskatchewan and Alberta; in EXTECH IV: Geology and uranium Exploration Technology of the Proterozoic Athabasca Basin, Saskatchewan and Alberta, (ed.) C.W. Jefferson and G. Delaney; Geological Survey of Canada, Bulletin 588, p. 155–191.

Schoenberg R., and von Blanckenburg F., 2005. An assessment of the accuracy of stable Fe isotope ratio measurements on samples with organic and inorganic matrices by high-resolution multicollector ICP-MS; International Journal of Mass Spectrometry, v. 242, p. 257–272.

Strelow F.W.E., 1980. Improved separation of iron from copper and other elements by anion-exchange chromatography on a 4% cross-linked resin with high concentrations of hydrochloric acid; Talanta, v. 27, p. 727–732.

Stumm, W., and Morgan, J.J., 1996. Aquatic chemistry: Chemical equilibria and rates in natural waters 3rd edition; Wiley-Interscience, New York, 1040 p.

Taylor, P.D.P., Maeck, R., and De Bièvre, P., 1992. Determination of the absolute isotopic composition and atomic weight of a reference sample of natural iron; International Journal of Mass Spectrometry and ion Processes, v. 121, p. 111–125.

Telus, M., Dauphas, N., Moynier, F., Tissot, F.L.H., Teng, F-Z., Nabelek, P.I., Craddock, P.R., and Groat, L.A., 2012. Iron, zinc, magnesium and uranium isotopic fractionation during continental crust differentiation: The tale from migmatites, granitoids, and pegmatites; Geochimica et Cosmochimica Acta, v. 97, p. 247–265.

Wallis, R., Saracoglu, N., Brummer, J., and Golightly, J., 1983. Geology of the McClean uranium deposits; in Uranium exploration in the Athabasca Basin, Saskatchewan, Canada, (ed.) E.M. Cameron; Geological Survey of Canada, Paper 82-1, p. 71–110.

Weyer S., and Schwieters J.B., 2003. High precision Fe isotope measurements with high mass resolution MC-ICP-MS; International Journal of Mass Spectrometry, v. 226, p. 355–368.

Wiederhold, J.G., Teutsch, N., Kraemer, S.M., Halliday, A.N., Kretzschmar, R., 2007. Iron isotope fractionation during pedogenesis in redoximorphic soils; Soil Science Society of America Journal, v. 71, p. 1840–1850.

Wilson, M., and Kyser, T.K., 1987. Stable isotope geochemistry of alteration associated with the Key Lake uranium deposit, Canada; Economic Geology, v. 82, p. 1540–1557.

Zazzi, A., Hirsch, T.K., Leonova, E., Kaikkonen, A., Grins, J., Annersten, H., and Edén, M., 2006. Structural investigations of natural and synthetic chlorite minerals by X-ray diffraction, Mössbauer spectroscopy, and solid-state nuclear magnetic resonance; Clays and Clay Minerals, v. 54, p. 252–265.

APPENDIX. Data generated or used in this study

Sample	δ^{56}Fe (‰)	δ^{57}Fe (‰)	Sample	δ^{56}Fe (‰)	δ^{57}Fe (‰)
MAC222-197	0.45±0.04	0.68±0.08	MAC241-333	-0.55±0.23	-0.80±0.36
MAC222-509	0.45±0.06	0.68±0.10	MAC241-569	-0.04±0.05	-0.06±0.09
MAC232-339	1.05±0.03	1.56±0.05	MAC244-128	0.63±0.06	0.91±0.10
MAC233-315	-0.03±0.08	-0.04±0.11	MAC244-464	0.53±0.05	0.77±0.09
MAC233-516	-0.04±0.07	-0.04±0.10	MAC244-581	1.07±0.05	1.60±0.11
MAC233-580	0.65±0.11	0.97±0.15	MAC244-603	0.62±0.07	0.93±0.11
MAC233-612	0.31±0.05	0.47±0.07	MAC246-209	0.25±0.11	0.37±0.21
MAC236-256	0.53±0.08	0.77±0.12	MAC246-300	0.39±0.05	0.57±0.07
MAC236-368	0.01±0.05	0.01±0.08	MAC246-320	0.00±0.04	0.02±0.07
MAC236-435	0.28±0.02	0.43±0.06	MAC246-354	1.03±0.09	1.54±0.15
MAC236-531	0.07±0.06	0.09±0.08	MAC246-545	0.24±0.04	0.37±0.07
MAC238-199	0.55±0.04	0.81±0.07	MAC251-252	0.12±0.08	0.18±0.14
MAC238-287	0.24±0.06	0.37±0.09	MAC252-215	-0.02±0.07	-0.05±0.13
MAC238-311	0.18±0.06	0.19±0.07	MAC252-260	-0.61±0.16	-0.91±0.23
MAC238-339	0.24±0.05	0.37±0.08	MAC255-128	0.63±0.06	0.91±0.10
MAC238-505	-0.29±0.06	-0.41±0.10	MAC255-220	0.63±0.07	0.94±0.12
MAC238-523	-0.13±0.04	-0.21±0.06	MAC255-253	0.26±0.06	0.35±0.11
MAC238-604	0.98±0.04	1.46±0.07	MAC255-504	-0.05±0.06	-0.09±0.10
MAC240-267	0.24±0.08	0.38±0.14	MAC255-517	0.24±0.03	0.38±0.06
MAC240-344	0.83±0.04	1.22±0.08	MAC255-553	-0.09±0.06	-0.14±0.11
MAC240-560	0.45±0.05	0.67±0.10	MAC256-287	0.85±0.03	1.30±0.06
MAC241-265	0.18±0.06	0.27±0.08	MAC256-325	0.70±0.07	1.05±0.10
MAC241-295	0.49±0.03	0.71±0.08	MAC256-533	0.17±0.16	0.27±0.25

Mineralogy of a Fertile Fluid Conduit Related to Unconformity-type Uranium Deposits in the Athabasca Basin, Saskatchewan

Erin E. Adlakha[1], Keiko Hattori[1], Gerard Zaluski[2], Tom G. Kotzer[2],
William J. Davis[3], and Eric G. Potter[3]

*1. Department of Earth Sciences, University of Ottawa, 25 Templeton Street, Ottawa, Ontario, K1N 6N5 (*correspondance: eadla028@uottawa.ca)*

2. Cameco Corporation, Exploration Office, 2121 - 11th Street West, Saskatoon, Saskatchewan, S7M 1J3

3. Geological Survey of Canada, 601 Booth Street, Ottawa, Ontario, K1A 0E8

Abstract

This report documents the occurrence and chemical variation of hydrothermal alteration minerals along the P2 fault, the structural host for the world-class McArthur River uranium deposit, in order to identify the mineralogical footprint of ore-forming fluids, define exploration criteria for fertile basement structures associated with this deposit type and infer the nature of the fluids. An assemblage of florencite (LREE-rich aluminum phosphate-sulphate; APS) and magnesio-foitite (alkali deficient Mg tourmaline) with sudoite and illite formed in the basement rocks along the P2 fault and is distinct relative to the alteration assemblages that formed in the basement rocks outside the fault. This assemblage occurs along the entire P2 fault, regardless of its proximity to the McArthur River uranium deposit and is interpreted to be the mineralogical footprint of ore-forming fluids. It may be useful when targeting fertile basement faults during exploration. Compositional zoning in APS minerals indicate that earlier fluids were SO_4^{2-}-rich and became P and LREE-rich through interactions with the basement rocks. The chemical composition of florencite and magnesio-foitite indicates that mineralizing fluids contained low Na and were enriched in REE, especially in the ore zone. High $\delta^{11}B$ values in magnesio-foitite are interpreted as being sourced from B dissolution by fluids from evaporitic rocks. The similar chemistry and occurrence of these minerals along the entire P2 fault, regardless of proximity to ore, indicate that the P2 fault was a conduit for mineralizing fluids and that the precipitation of uranium was selective to the location of the McArthur River deposit.

Introduction

The P2 fault is a reverse dip-slip structure situated in the southeastern Athabasca Basin, Saskatchewan, Canada. The fault is spatially associated with the McArthur River deposit, currently the world's largest high-grade uranium deposit (Fig. 1). The purpose of this TGI-4 supported project, which started in August 2012, was to examine alteration minerals in the basement rocks along the P2 fault in order to evaluate the role of this major structure in the uranium mineralization processes and define exploration criteria for fertile basement structures associated with this deposit type. Furthermore, the hydrothermal alteration of the basement rocks is not well studied compared to the Athabasca Group sandstones partly due to the more complex mineralogy and compositions of the basement rocks.

Early work of this study is described in Adlakha et al. (2014) and involved detailed sampling of representative rocks, mineral chemistry and the establishment of an alteration paragenesis in order to unravel the alteration history of the basement rocks. Currently, work is progressing on identification of the mineralogical signatures left by ore-bearing fluids. Here we describe alteration assemblages and their distribution along the P2 fault, and present the occurrence and chemical variation of aluminum phosphate-sulphate (APS) minerals and tourmaline[1] (magnesio-foitite) along the P2 fault. These minerals were studied as they are chemically complex and their chemistry reflects that of fluids (van Hinsberg et al., 2011). We also discuss APS minerals and magnesio-foitite as mineralogical footprints of ore-bearing fluids, the role of P2 fault during mineralization, and the nature and source of mineralizing fluids.

Geological context

The basement rocks below the eastern Athabasca Basin are part of the Wollaston domain and host the Zone 2 orebody of the McArthur River deposit. The Wollaston domain here consists of pelite, semipelite, arkose, calcsilicate and quartzite that were metamorphosed during the Trans-Hudson Orogeny (ca. 1.81.9 Ga; Lewry and Sibbald, 1980) under upper amphibolite facies conditions. Granitic pegmatite lenses intrude the metasediments and likely formed from local partial melting during peak metamorphism (Annesley et al., 2005). Substantial erosion during the exhumation of the basement rocks beginning at ca. 1.73 Ga (Kyser et al., 2000) resulted in weathering of the basement and the development of a weathering profile, a lower chlorite-dominated

[1] Hydrothermal tourmaline associated with uranium deposits of the Athabasca Basin is commonly referred to as "dravite"; however, it is noted here that the only true dravite in the study area is metamorphic in origin and found as relic grains in the basement or as detrital grains in the Athabasca Group. The hydrothermal tourmaline associated with uranium deposits is actually the species magnesio-foitite (alkali deficient dravite; e.g. Wasyliuk, 2002).

Adlakha, E.E., Hattori, K., Zaluski, G., Kotzer, T.G., Davis, W.J., and Potter, E.G., 2015. Mineralogy of a fertile fluid conduit related to unconformity-type uranium deposits in the Athabasca Basin, Saskatchewan, *in* Targeted Geoscience Initiative 4: unconformity-related uranium systems, (ed.) E.G. Potter and D.M. Wright; Geological Survey of Canada, Open File 7791, p. 74–82. doi:10.4095/295776

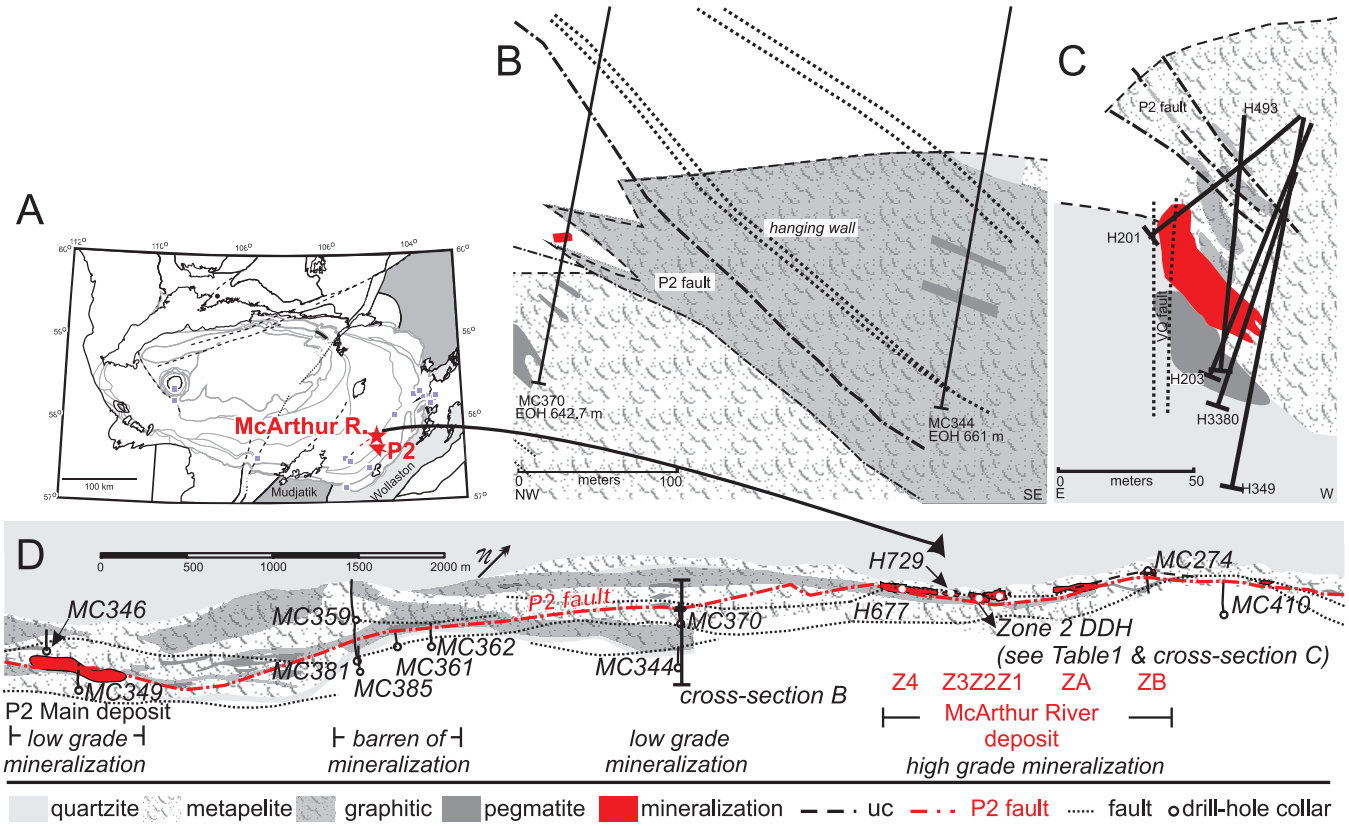

Figure 1: (A) A simplified map of the Athabasca Basin showing location of the P2 fault and McArthur River deposit (modified from Jefferson et al., 2007). (B) A schematic cross-section showing an example of a drill hole that intersected the P2 fault proximal to low-grade mineralization (DDH MC370) and a "background" drill hole that did not intersect the P2 fault (DDH MC344). (C) A cross-section of the Zone 2 basement hosted orebody showing sampled drill core which intersect the orebody and/or the alteration halo. (D) An interpreted geological strip map at the unconformity showing the P2 fault, the locations of sampled drill holes (italicized MC### or H###), ore bodies and the sites of the cross sections (B) and (C). Low-grade mineralization occurs along the middle and southeast (P2 Main deposit) portions of the P2 fault. The P2 fault is essentially barren in the southwestern part. Z1–4 = Zone numbers of orebody at the McArthur River deposit; uc = unconformity. Cross-sections (A) and (B) plan view map (D) and were modified from Cameco internal reports.

Green Zone and upper hematite and kaolinite dominated Red Zone (Macdonald et al., 1985), before deposition of the Athabasca Group conglomerate and sandstone sequences. The Athabasca Group comprises four major sequences, including the basal Read Formation, of dominantly fluvial to marine, quartz pebble conglomerate and quartz-dominated sandstone (99% quartz framework grains with minor K-feldspar + clay matrix), currently preserved at a maximum thickness of 1500 m in the centre of the basin (Ramaekers et al., 2007).

Above the McArthur River deposit, the thickness of the conglomerate-sandstone succession is approximately 500 m. Some conglomerate and sandstone units have been intensely silicified (Jefferson et al., 2007). During and after deposition of the Athabasca Group, diagenetic fluids extensively altered much of the stratigraphic section (except for the intensely silicified units), as well as the weathered basement rocks close to the unconformity. The alteration of the basement weathering profile at the unconformity formed what is known as the Bleached Zone and comprises illite with kaolinite (Macdonald, 1985). Subsequent hydrothermal activity further altered and brecciated the sandstone and basement rocks, particularly along intersecting faults that provided the fluid pathways during mineralization (McGill et al., 1993).

The P2 fault (045°/45–60°SE) developed in graphitic pelite in the metamorphosed basement rocks of the Wollaston domain below the basin and propagated as a number of splays into the overlying sandstone during fault re-activation (Figs. 1B, C). The P2 fault zone is a series of reverse faults with a strike length of approximately 13 km and has been traced seismically at least 2 km below the unconformity (McGill et al., 1993). In the basement, the several fault planes of the P2 fault are mostly constrained to graphite-bearing metapelite and trend parallel to the basement foliation (McGill et al., 1993). Reactivation of P2 faulting formed differences in the thickness of the basal conglomerate at the unconformity and broad fracture and breccia zones in the sandstones and the reverse movement of the P2 fault raised a wedge of basement rocks above the unconformity with the vertical displacement of up to 80 m (McGill et al., 1993; Figs. 1B, C).

While a few sub-economic (< 1 wt. % U_3O_8) uranium occurrences have been found along the P2 fault, the McArthur River deposit is the only high-grade deposit discovered to date. The McArthur River deposit comprises six main mineralized zones (Zones 1, 2, 3, 4, A, B). Current production at the McArthur River mine is from the Zone 2 ore lens which is almost entirely hosted in the basement rocks

Table 1: List of studied diamond drill holes (DDH). See Fig. 1 for the locations.

Area	DDH[a]	Samples[b]	Depth ranges[c]	Notes
least altered and alteration outside P2 fault	MC344	16	651.5 – 499.4 m	
	MC346	9	737.1 – 580.5 m	
	MC381*	4	660.5 – 603 m	
	MC385	8	686 - 652.2 m	
P2, unmineralized	MC359	7	626.1 – 491 m	
	MC361	26	652.9 – 493 m	
	MC362	15	643.9 – 520.2 m	
	MC381*			
P2, sub-ec (<1 wt% U3O8)	MC349	13	659 – 573 m	
	MC370	17	630.8 - 533.2 m	
	MC410	7	790.9 – 527.7 m	
P2, Z1	H729	20		
P2, Z2	H201	11		
	H203	7		
	H231	7		VQ fault
	H347	10		
	H493	7		
	MO227	5		
	H3380	5		2 ore samples
P2, Z3	H3559	2		
	H3576	1		
P2, Z4	H677	5		2 ore samples
P2, ZB	MC274	7	618.3 – 502.4 m; 93.1 m; 62.8 m	1 ore sample

Notes:
[a] exploration holes beginning with MC, underground collared drill holes are denoted H or MO;
[b] number of samples collected from respective DDH;
[c] depth ranges given for core lengths of exploration DDH collared at surface.

immediately below the unconformity (Fig. 1C). The Zone 2 orebody is bounded by the vertical quartzite (VQ) fault and ~140° trending cross faults in the basement rocks (Fig. 1D). The VQ fault is a steeply dipping structure located between the footwall quartzite and cordierite-bearing metapelite (Fig. 1C; McGill et al., 1993). The rocks adjacent to the P2 fault and below the Zone 2 orebody are highly brecciated and intensely altered. The five other ore bodies of the McArthur River deposit are hosted in the sandstones of the Read Formation immediately above the unconformity.

Sampling

This study commenced with examination and sampling of drill core from along 7 km of the P2 structure and within the McArthur River underground mine (Table 1; Fig,. 1B–D). A total of 209 drill core samples were collected that represent the least altered rocks outside the P2 fault (> 50 m from the fault plane and the unconformity), altered basement rocks outside the P2 fault (found within 50 m of the unconformity), P2 fault rocks in barren areas, P2 fault rocks below sub-economic mineralization, P2 fault rocks proximal to the Zone 2 orebody, VQ rocks proximal to Zone 2 orebody and P2 fault rocks associated with sandstone-hosted ore bodies, such as Zones 1, 3, 4 and B. Representative samples were chosen based on specific features, e.g. alteration style (green, red or bleached). Ore samples were collected from the Zone B, Zone 2, and Zone 4 ore bodies. Most samples are metapelite/pelitic gneiss and anatectic pegmatite from the basement, below the unconformity. Additionally, 18 samples of sandstone close to the unconformity were collected for comparison.

Methodology

Petrographic studies using plane-polarized and cross-polarized transmitted light microscopy on 151 polished thin sections were carried out for this study. Due to the fine-

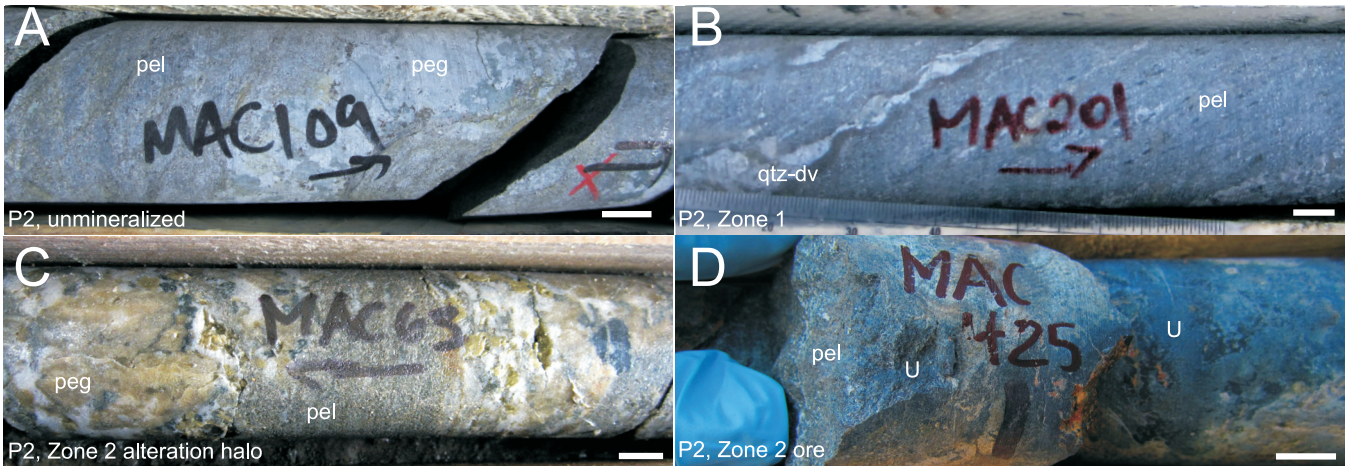

Figure 2: Drill core photographs of altered basement rocks from various areas of the P2 fault: (A) metapelite (pel) with pegmatite (peg) vein; (B) metapelite with quartz-dravite (qtz-dv) vein; (C) pegmatite and metapelite; (D) metapelite hosting uranium ore (U). Scale bars = 1 cm.

grained nature of alteration minerals, detailed textural analysis was carried out on carbon-coated polished thin sections using a JEOL 6610LV scanning electron microscope (SEM) at University of Ottawa. Energy-dispersive spectroscopy (EDS) was used to semi-quantitatively determine the compositions and identify minerals. Quantitative analysis of minerals for major and minor constituents was conducted at the University of Ottawa using a JEOL 8230 electron-probe microanalyzer (EMPA) with a wavelength-dispersive spectrometer (WDS).

Aluminum phosphate-sulphate minerals and tourmaline in polished thick sections were analyzed for trace elements by laser ablation inductively coupled plasma mass spectrometer (LA-ICPMS) at the Geological Survey of Canada, Ottawa. Ablation was performed using Photon-Machines Analyte193 excimer laser ($\lambda = 193$ µm) ablation system with Helex ablation cell and Agilent 7700x quadrupole ICP-MS. The reference National Institute of Standards and Technology (NIST610) was used as a calibration standard for APS mineral analysis and the concentration of Al (previously determined by EMPA) was used an internal standard to calculate trace element abundances. For magnesio-foitite, NIST GCD-1G was used as the calibration standard and the Mg (previously determined by EMPA) was used an internal standard.

The B isotopic composition of tourmaline was measured using a SHRIMP (sensitive high-resolution ion microprobe) II at the Geological Survey of Canada, Ottawa. Composition based instrumental mass fractionation was corrected using four tourmaline standards with known B isotope compositions. The results of the B isotopic analyses are reported in delta annotation (δ) as the variation in the $^{11}B/^{10}B$ ratios of sample compared to standard SRM NBS 951 as per mil (‰).

Results

Alteration mineralogy of P2 fault rocks

In general, rocks along the P2 fault (wall-rocks within 50 m of the fault plane) are moderately to highly altered. Samples with moderate alteration retain pseudomorphs of metamorphic minerals (Fig. 2), such as feldspar or cordierite. In intensely altered rocks, brecciation and veining destroy original mineral textures (Figs. 2C, D) with the exception of quartz and dravite (Mg-rich early tourmaline). Quartz and early dravite are associated. Strong degrees of alteration also produced an unconsolidated mixture of graphite and clay, especially immediately adjacent to ore. Rocks in the P2 fault are mostly green and graphitic (Figs. 2A, B) with patches of "bleached" alteration.

The alteration assemblage of competent rocks along the P2 fault comprises sudoite with varying amounts of illite, magnesio-foitite and APS minerals (Fig. 3). Sudoite forms needle-like crystals (< 2 µm in length) that are low-relief and colorless to very faint green in plane polarized light with anomalous blue birefringence (Figs. 3A-C, E–F). Illite occurs as colorless laths (usually < 2 µm in length, but can be up to 10 µm; Figs. 3A, B, D) that in thin section have high third order birefringence colours, typically light pink, blue and orange. Sudoite and illite are commonly found mixed in varying proportions. Magnesio-foitite is characterized as colourless, acicular aggregates (5 – 500 µm in length), overgrowths on dravite, in veinlets (up to 0.5 cm wide) or as disseminations in matrix of sudoite or illite. In ore samples, it is commonly coated with remobilized uraninite (Fig. 3D). Magnesio-foitite is distinguished from illite and chlorite by its second order birefringence (yellow, orange and purple; Fig. 3C), relatively high relief, and optically negative elongation. Small (typically <1 – 20 µm, rarely up to 40 µm), pseudo-cubic (rarely hexagonal) APS minerals are disseminated and/or clustered in fine-grained clay minerals (Fig. 3B). The textural relationships with surrounding clays suggest that they are in equilibrium. The APS minerals are commonly zoned, with darker cores and lighter rims in BSE-images (Fig. 3).

Hematite, kaolinite, clinochlore (Mg-rich chlorite) and chamosite (Fe-rich chlorite) are irregularly dispersed along the P2 fault. Hematite forms fine grained (< 2 µm) crystals and occurs with illite. Kaolinite forms aggregates or "books" of 2 µm thick stacked crystals.

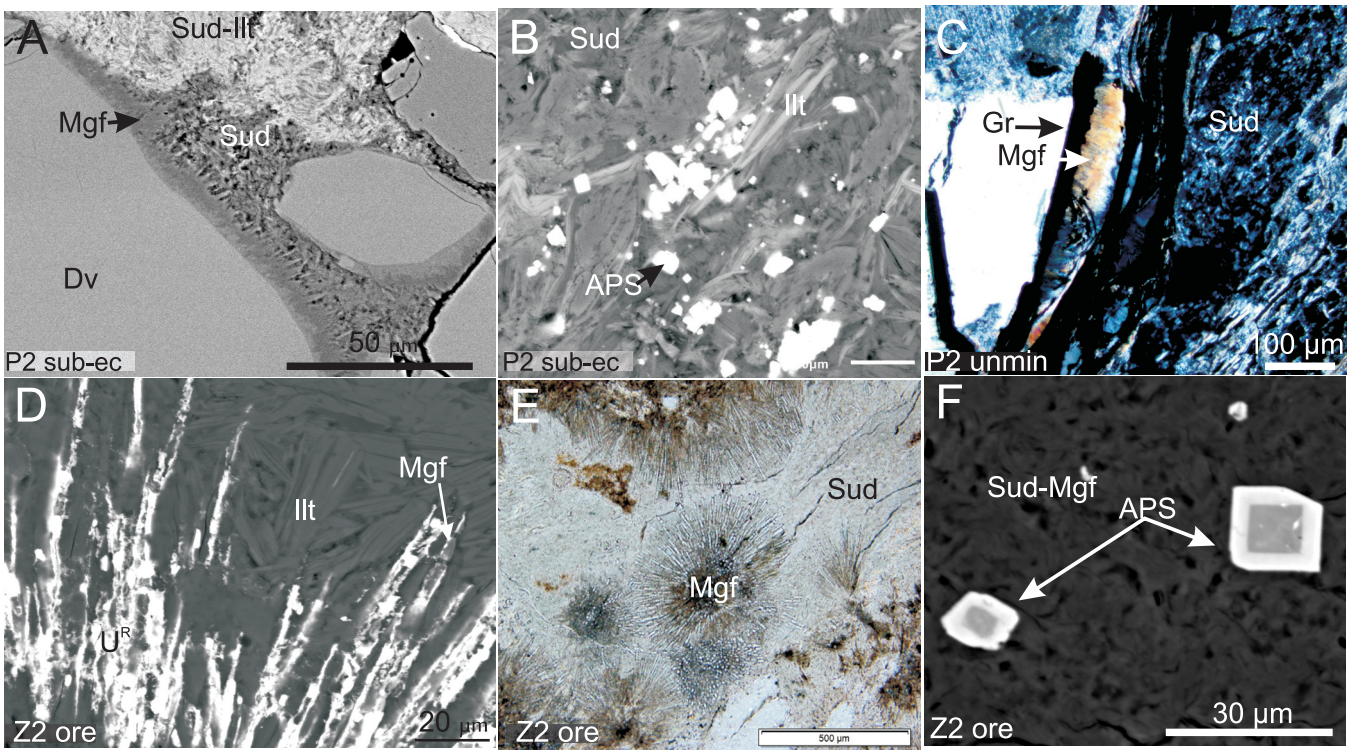

Figure 3: Photomicrographs (PPL = plane polarized light, XPL = cross-polarized light) and BSE images of alteration phases along the P2 fault: (A) relic dravite (Dv) overgrown by magnesio-foitite (Mgf) (BSE), (B) APS minerals surrounded by sudoite and illite (Ilt) (BSE), (C) magnesio-foitite with sudoite and relic graphite (Gr) (XPL), (D) magnesio-foitite occurring with illite and overprinted by remobilized uraninite (U^R) (BSE), (E) radial magnesio-foitite occurring with sudoite (PPL), and (F) zoned APS minerals surrounded by sudoite (Sud) and magnesio-foitite (BSE).

Quartz, dravite, graphite and pyrite are the only relic metamorphic minerals. Quartz grains are partially dissolved and are commonly replaced by sudoite or magnesio-foitite.

Distribution of alteration along the P2 fault

Samples from the unmineralized and sub-economic areas along the P2 fault (Table 1; Fig. 1D) are moderately to strongly altered. Unmineralized samples have a high proportion of illite to sudoite and low concentrations of magnesio-foitite. The APS minerals occur with illite. In sub- economic samples, illite and sudoite are of equal proportions (Fig. 3B). Magnesio-foitite is more common in sub-economic samples relative to barren samples and APS minerals occur with sudoite or kaolinite with magnesio-foitite.

Below the Zone 1 orebody, the P2 fault is strongly graphitic (> 5 modal % graphite) and contains abundant relic dravite. Sudoite and illite are the most abundant alteration minerals and magnesio-foitite forms overgrowths on relic dravite. The rocks below the Zone 3 orebody generally exhibit moderate degrees of alteration where the grains of cordierite are still discernable but replaced by sudoite-illite and biotite, which is then chloritized (Fe-Mg chlorite) or illitized. The APS minerals are mixed with sudoite and illite. Magnesio-foitite forms sporadic aggregates. Hematite is common and overprints biotite and illite laths.

Samples from the P2 fault in the Zone 2 alteration halo (Table 1; Fig. 1C) are strongly altered (Fig. 2C, D). Sudoite and magnesio-foitite are common alteration minerals and occur with pyrite and graphite. Sudoite is strongly associated with magnesio-foitite and can be intermixed with illite and APS minerals. Hematite occurs locally along fractures. Samples of Zone 2 ore contains magnesio-foitite, sudoite, sudoite-illite that is intermixed, and relatively coarse-grained illite (up to 10 µm long axis), APS minerals and minor sulphides (pyrite, galena etc.) and kaolinite. Primary uraninite (as per the characterization of Fayek and Kyser, 1995) occurs as masses while remobilized uraninite overprints sudoite, magnesio-foitite and illite (Fig. 3C).

Mineral chemistry – major elements

The chemical formula of tourmaline was calculated based on ideal formula $XY_3Z_6(T_6O_{18})(BO_3)_3V_3W$, which assumes 3 B atoms in the B-site, 18 O associated with the T-site and 3 OH in the V-site. For cation site assignment, the T-site was filled first with Si^{4+}, then Ti^{4+} and Al^{3+} to sum 6 cations. The Z-site was occupied by Al^{3+}, and the remaining Al^{3+} was assigned to the Y-site. The Y-site was filled by Fe^{2+} or Fe^{3+} and Mg^{2+}. All Ca^{2+}, K^+ and Na^+ are assigned to the X-site. The W-site accommodates F^-, OH^- and O^{2-}. The fraction of O^{2-} was calculated to compensate excess cation charges. Magnesio-foitite has an average composition of $(Na_{0.20}Ca_{0.02}K_{0.01})(Mg_{1.95}Fe^{3+}_{0.09}Al_{0.94})Al_6(Si_{6.02}O_{18})(BO_3)_3(OH_3)(F_{0.04}OH_{3.66}O_{0.30})$ and is alkali deficient where X-site vacancies range from 0.70 – 0.85 atoms per formula unit (apfu) (Fig. 6). X-site vacancies were calculated as 1 apfu subtract the sum of Na, Ca and K apfu.

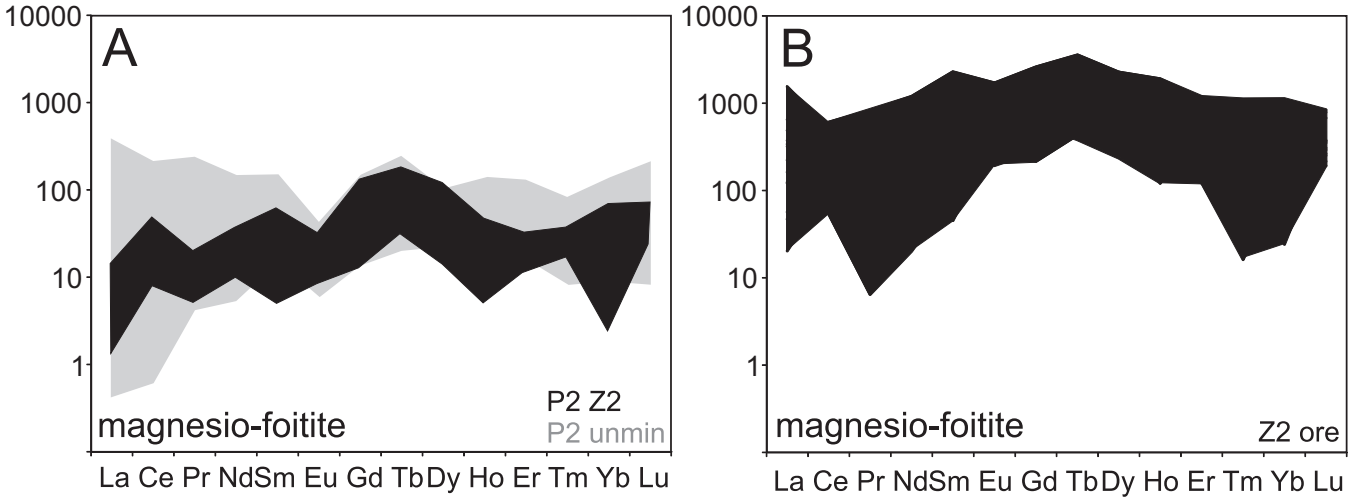

Figure 4: REE + Y plots (normalized to chondrite; McDonough and Sun (1995) of magnesio-foitite from the P2 fault: (A) in unmineralized areas of the basement (black) and sandstone (grey); and (B) near or in mineralization, including the alteration halo around Zone 2 orebody (grey) and in the Zone 2 and Zone B ore bodies (black).

The APS minerals show a range in composition (Adlakha and Hattori, in press; Fig. 5). The APS mineral formulae were calculated based on 6 cations as the ideal formula is expressed as $AB_3(XO_4)_2(OH)_6$, where A = mono-, di-, tri- or, more rarely, tetravalent cations (K^+, Na^+, Rb^+, Ca^{2+}, Sr^{2+}, REE^{3+}, Th^{4+} etc.); B = Al^{3+}, Fe^{3+}; and X = P^{5+}, S^{6+}, and As^{5+}. They contain high ΣLREE (0.35 – 0.58 apfu; LREE = La + Ce + Pr + Nd) relative to Sr (0.16 – 0.32 apfu) and Ca (0.18 – 0.28), and high PO_4^{3-} (1.70 - 1.97 apfu) relative to SO_4^{2-} (0.06 – 0.35 apfu) and AsO_4^{3-} (<0.01 apfu). Ce is high (0.15 – 0.27 apfu) relative to La (0.09 – 0.17), Pr (<0.01 – 0.03 apfu) and Nd (0.05 – 0. 12 apfu), showing [Ce]/[Ce]* of ~0.8 – 1.6. Compositional zoning in the APS minerals consists of cores enriched in Sr, Ca, and SO_4^{2-}, and rims high in LREE and P. Within the cores of APS minerals, Ca and P contents are inversely correlated with Sr and S contents.

Mineral chemistry – trace elements

Magnesio-foitite along the P2 fault has variable concentrations of REE. Magnesio-foitite from basement (DDH MC381 and MC361) and sandstone (DDH MC361) samples from unmineralized areas along the P2 fault contain low concentrations of ΣREE (avg. 0.7 ± 0.02 (1σ) and 0.4 ± 0.07 ppm, respectively; La – Lu). The data plot as a "bell-shaped" normalized REE pattern characterized by high HREE relative to LREE, with an average $[LREE]_N/[HREE]_N \approx 0.5$ and 0.4, respectively (Fig. 4A). Magnesio-foitite from the basement alteration halo near the Zone 2 ore body (DDH MO227) have low ΣREE contents (avg. 1.0 ± 0.3 ppm), plot as "bell-shaped" normalized REE patterns and contain high HREE relative to LREE, average $[LREE]_N/[HREE]_N \approx 0.6$ (Fig. 4B). Ore samples from Zones 2 and B ore bodies (DDH MC274 and H3380), magnesio-foitite contains relatively high concentration of ΣREE (avg. 15.0 ± 6.1 ppm), shows a "bell-shaped" normalized REE pattern with high HREE, $[LREE]_N/[HREE]_N$ value ≈ 0.7 (Fig. 4B).

Samples from the P2 fault located proximal to Zone 3 ore (DDH H729) have APS minerals containing appreciable U and Pb with a mean averages of 0.6 ppm) and 158 ppm, respectively. Similarly, APS from the Zone 2 alteration halo (DDH H201 and H493) have high U (avg. 5.7 ppm), and Pb (avg. 159 ppm) contents.

Boron isotope compositions

Magnesio-foitite from unmineralized and sub-economic mineralization areas of the P2 fault, and areas proximal to Zone 1 and Zone 2 ore bodies were analyzed. Magnesio-foitite has $\delta^{11}B$ values from +13.1 to +23.2 ‰, with a mean of +18.5 ± 1.9 ‰. Magnesio-foitite co-existing with uraninite has $\delta^{11}B$ values from +13.0 to +19.8 ‰. In low-grade areas along the P2 fault, magnesio-foitite has $\delta^{11}B$ values of +15.5 to +18.5 ‰ while in unmineralized samples range between +15.0 and +15.8 ‰.

Discussion

Mineralogical footprint of ore fluid and assessment of the P2 fault during mineralization

Sudoite, illite, magnesio-foitite and florencite are in textural equilibrium, which is consistent with contemporaneous crystallization (Fig. 3). Linked REE abundances of magnesio-foitite (Fig. 4) and florencite also imply co-precipitation, with high LREE contents in florencite (up to 0.58 apfu; Fig. 5) and lower the concentrations of LREE in magnesio-foitite reflecting precipitation of a common fluid. The occurrence of trace uranium in florencitic APS minerals and their proximity to ore suggest formation by a uranium-bearing fluid — indicating that magnesio-foitite and florencite are mineralogical footprints of ore-forming fluids.

The alteration assemblage of sudoite, illite, magnesio-foitite and APS minerals (florencite) is widely distributed in basement rocks along the P2 fault, being present in both mineralized and unmineralized areas of the fault (Fig. 3). This alteration assemblage along the P2 fault differs from that observed outside the fault, which is comprised predominately of illite and sudoite with no magnesio-foitite or florencite (Adlakha et al., 2014; Adlakha and Hattori, in press).

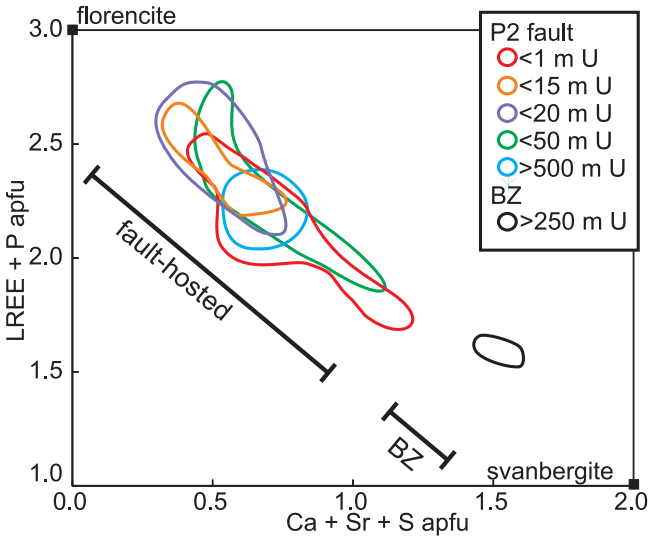

Figure 5: Cross-plot showing coupled substitution of Ca-Sr-S for LREE-P for APS minerals along the P2 fault (colored fields), and within the Bleached Zone (BZ) sample (black field). P2 fault samples are color coded with respect to distance in metre from the uranium mineralization (McArthur River deposit and low-grade): the red field represents samples < 1 m from U, the orange field represents samples < 15 m from U, the purple field represents samples < 20 m from U, the green field represents samples < 50 m from U and the blue field represents samples from unmineralized areas >500 m from U.

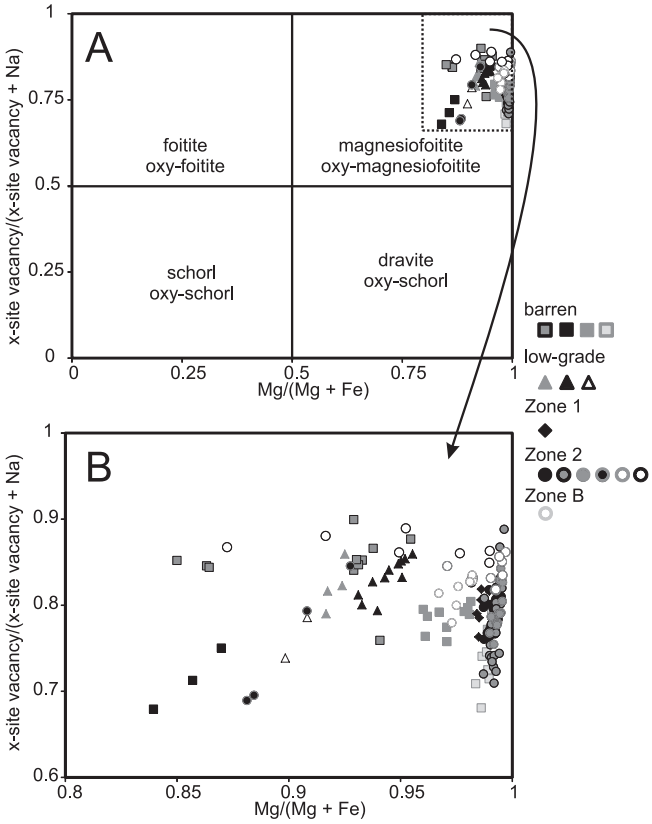

Figure 6: Cross–plots of magnesio-foitite data, Mg/(Mg + Fe) vs. x-site vacancy/(x-site vacancy + Na apfu), showing the alkali-deficiency of magnesio-foitite (after Henry et al., 2011). Cross-plot B shows a smaller range and therefore a larger amount of detail than cross-plot A. Data of magnesio-foitite from unmineralized areas are represented by squares, from low-grade areas by triangles, from Zone 1 by diamonds and from Zone 2 and B by circles. Magnesio-foitite from Zone 2 and B samples that contain uraninite are represented by open circles and show high x-site vacancies.

Therefore, magnesio-foitite and APS minerals may be useful in exploration programs when targeting fertile basement faults.

The widespread presence of this mineral assemblage along the P2 fault indicates that the P2 fault was a conduit for mineralizing fluids. Furthermore, it is evident that similar fluids travelled along the entire P2 fault, but ore was selectively precipitated (i.e. at the McArthur River deposit; Fig. 1).

Implication of APS mineral chemistry for nature of the fluid

The APS minerals along the P2 fault are florencitic in composition (ideal florencite is $CeAl_3(PO_4)_2(OH)_6$) with high LREE and P contents. These APS minerals are compositionally distinct relative to those of the Bleached Zone along the unconformity described by Adlakha and Hattori (in press; Fig. 5). The latter are closer to svanbergite-goyazite compositions ($SrAl_3(PO_4)(SO_4)(OH)_6$ - $SrAl_3(PO_4)_2(OH)_6$) (Fig. 5). Florencitic APS minerals along the P2 fault are also zoned with florencite rims and svanbergite-goyazite cores (Fig. 3F).

The composition of APS minerals along the entire P2 fault have a large range in concentrations of LREE and P (Fig. 5). For example, the (LREE+P)/(Ca+Sr+S) ratios of APS minerals close (<1 m) to ore range from 1.6–5.6, whereas APS minerals from unmineralized samples far from mineralization (>500 m) show moderate ratios of (LREE+P)/(Ca+Sr+S), from 2.8–4 (Fig. 5).

Gaboreau et al. (2005, 2007) found that APS minerals proximal to uranium deposits in the Athabasca and Kombolgie Basins contained high LREE+P relative to those in intermediate and distal areas. The data of this study shows that APS minerals less than 1 metre from low-grade mineralization have a larger range than that presented by Gaboreau et al. (2005, 2007) for APS minerals proximal to uranium deposits (Fig. 5). There is no significant difference in the APS mineral data from high-grade and unmineralized parts of the P2 fault (Fig. 5). The broad range in composition likely reflect the evolution of fluids that passed through the ore zone. The earlier fluids contained high Ca, Sr and SO_4^{2-}, and evolved to have high LREE and P contents (Adlakha and Hattori, in press).

Implication of magnesio-foitite chemistry for the nature and source of the fluid

Magnesio-foitite exhibits a large X-site vacancy (Fig. 6). The X-site vacancy likely reflects high H+/Na+ ratio of the fluid from which it crystallized. This indicates low pH or a fluid with low Na+ concentrations. A low pH fluid is consistent with the type locality of magnesio-foitite which formed by acidic fluid (Hawthorne et al., 1999) and recent fluid inclusion studies by Richard et al. (2012) on the genesis of the Athabasca deposits. A low pH fluid is inconsistent with thermodynamic modelling by Kister et al. (2005), who

reported that fluids responsible for the crystallization of magnesio-foitite, illite, and sudoite were slightly alkaline. A possible interpretation is that the tourmaline-crystallizing fluid contained low Na+ contents. This interpretation is consistent with previous studies that suggests mineralization associated alteration in the basement formed, in part, by Ca-rich, Na-poor brines (Derome et al., 2005; Richard et al., 2010). These brines have been found as quartz-hosted fluid inclusions in proximity to mineralization.

The REE chemistry of magnesio-foitite in unmineralized and mineralized areas of the P2 fault show similar LREE/HREE ratios and bell-shaped REE patterns (Fig. 4). One notable difference is that magnesio-foitite from mineralized samples contain much higher concentrations of REE than magnesio-foitite in barren areas (Fig. 4). This indicates that the mineralizing fluid contained higher REE, at least on a local scale.

The $\delta^{11}B$ values of magnesio-foitite along the P2 fault are high, ranging from +13 to +23 ‰. The $\delta^{11}B$ values of fluid are calculated using the fractionation factor between magnesio-foitite and fluid of Meyer et al. (2008) at ore forming temperatures (180 – 220°C; Kister et al., 2005), assuming that B is boric acid in the fluid. The $\delta^{11}B$ values for fluids range from +18 to +29 ‰.

High $\delta^{11}B$ values in the fluids indicate a contribution of evaporates or sea water because there is no other reservoir of B with such high $\delta^{11}B$ values. However, $\delta^{11}B$ values of Precambrian seawater are unknown which makes absolute interpretation on the source difficult. Based on B-isotope composition of tourmaline, microthermometry of high salinity fluid inclusions, and Cl and Br isotopes of fluid inclusions, many authors support the hypothesis of an evaporated sea water source fluid for tourmaline and uranium ore (Derome et al., 2005; Richard et al., 2010; Mercadier et al., 2012). As marine brines contain high Na^+/H^+ ratios, it is unlikely that an alkali deficient tourmaline would crystallize from a NaCl-rich fluid. It is possible that the evaporitic fluid evolved to the $CaCl_2$-rich brine through interactions with the basement, as suggested by the authors. A fluid with this composition could allow for precipitation of magnesio-foitite as suggested above. However, Na-rich phases such as albite which would have been produced through brine interaction with the basement (as suggested by Richard et al., 2010) are not preserved in the area (Adlakha et al., 2014). An alternative interpretation is that boron-bearing evaporitic rocks may have been dissolved by meteoric and diagenetic waters (Bray and Spooner, 1988; Kotzer and Kyser, 1995). Although evidence for evaporites in the Athabasca Basin is lacking, it is possible that they did exist at one time but were completely dissolved to form basinal brines or eroded. We support the latter hypothesis where fluids dissolved boron from carbonates and evaporites, as this interpretation is consistent with the Na+ deficient nature of tourmaline.

Summary

Sudoite, illite, magnesio-foitite and florencitic APS occur along the entire P2 fault. The relative amounts of these minerals differ depending upon the distance from ore: sudoite and magnesio-foitite are abundant close to the ore and illite is abundant in unmineralized areas. The presence of magnesio-foitite and florencite is restricted along the P2 fault. This study concludes that the assemblage of florencitic APS minerals and magnesio-foitite can be used as an exploration vector to identify fertile basement structures associated with uranium deposits.

An important conclusion in this study is that sudoite, illite, magnesio-foitite and florencite all crystallized from an uraniferous fluid. In particular, florencite contains appreciable uranium. These minerals were formed contemporaneously with uranium mineralization as they occur in equilibrium with each other and in high abundance proximal to uranium ore. The HREE enrichment of magnesio-foitite is coupled to the incorporation of LREE in APS minerals.

Low sodium contents in magnesio-foitite are consistent with fluids with low sodium concentrations. The high $\delta^{11}B$ values in magnesio-foitite are interpreted as being sourced from boron dissolution by fluids from evaporitic rocks. The REE chemistry of magnesio-foitite indicates that the fluid in the ore zone contained high concentration of REE but fluids in barren areas of the P2 fault contain lower REE. Compositional zoning in APS minerals are consistent with earlier SO_4^{2-}-rich fluid becoming to P- and LREE-rich through interactions with the basement rocks.

The alteration minerals of sudoite, illite, magnesio-foitite and florencite have similar chemistry along the entire 7 km strike length of the P2 fault studied, including areas barren of uranium mineralization. The uranium-bearing fluids likely passed along the entire P2 fault, but only precipitated uranium in localized areas where more reducing conditions prevailed.

Acknowledgments

This is a contribution to the Targeted Geoscience Initiative Four (TGI-4) Uranium ore systems project of Natural Resources Canada and was made possible through grant funding to KH and a Research Affiliate Program (RAP) bursary to EEA. EEA also received a graduate fellowship from the Society of Economic Geologists. Cameco Corporation graciously provided logistical support for the field studies and permission to publish the results. This report benefitted from constructive reviews by Colin Card, David Thomas and Donald Wright.

References

Adlakha, E.E., and Hattori, K., in press. Compositional variation and timing of aluminum phosphate-sulfate minerals in the basement rocks along the P2 fault and in association with the McArthur River uranium deposit, Athabasca Basin, Saskatchewan, Canada; American Mineralogist, in press.

Adlakha, E.E., Hattori, K., Zaluski, G., Kotzer, T. and Potter, E.G., 2014. Alteration within the basement rocks associated with the P2 fault and the McArthur River uranium deposit, Athabasca Basin; Geological Survey of Canada, Open File 7462; 35 p., doi:10.4095/293364.

Annesley, I.R., Madore, C., and Portella, P., 2005. Geology and thermotectonic evolution of the western margin of the Trans-Hudson Orogen: evidence from the eastern sub-Athabasca basement, Saskatchewan; Canadian Journal of Earth Sciences, v. 42, p. 573–597.

Bray, C. J., and Spooner, E.T.C. 1988. Unconformity-related uranium mineralization, McClean deposits, North Saskatchewan, Canada; The Canadian Mineralogist, v. 26, p. 246–268.

Derome, D., Cathelineau, M., Cuney, M., Fabre, C., Lhomme, T., and Banks, D.A., 2005. Mixing of sodic and calcic brines and uranium deposition at McArthur River, Saskatchewan, Canada: a Raman and laser-induced breakdown spectroscopic study of fluid inclusions; Economic Geology, v. 100, p. 1529–1545.

Fayek, M., and Kyser, T.K., 1997. Characterization of multiple fluid events and rare-earth-element mobility associated with formation of unconformity-type uranium deposits in the Athabasca Basin, Saskatchewan; The Canadian Mineralogist v. 35, p. 627–658.

Gaboreau, S., Cuney, M., Quirt, D., Beaufort, D., Patrier, P., and Mathieu, R., 2007. Significance of aluminum phosphate-sulfate minerals associated with U unconformity-type deposits: The Athabasca basin, Canada; American Mineralogist, v. 92, p. 267–280.

Gaboreau, S., Beaufort, D., Vieillard, P., Patrier, P., and Bruneton, P., 2005. Aluminum phosphate–sulfate minerals associated with Proterozoic unconformity-type uranium deposits in the East Alligator River Uranium Field, Northern Territories, Australia; The Canadian Mineralogist, v. 43, p. 813–827.

Hawthorne, F.C., Selway, J.B., Kato, A., Matsubara, S., Shimizu, M., Grice, J.D., and Vajdak, J., 1999. Magnesiofoitite (Mg2Al)Al6(Si6O18)(BO3)3(OH)4, a new alkali-deficient tourmaline; The Canadian Mineralogist, v. 37, p. 1439–1443.

Henry, D.J., Novak, M., Hawthorne, F.C., Ertl, A., Dutrow, B.L., Uher, P., and Pezzotta, F., 2011. Nomenclature of the tourmaline-supergroup minerals; Amercian Mineralogist, v. 96, p. 895–913.

Jefferson, C.W., Thomas, D.J., Gandhi, S.S., Ramaekers, P., Delaney, G., Brisbin, D., Cutts, C., Portella, P. and Olson, R.A., 2007. Unconformity-associated uranium deposits of the Athabasca basin, Saskatchewan and Alberta; in EXTECH IV: Geology and Uranium EXploration TECHnology of the Proterozoic Athabasca Basin, Saskatchewan and Alberta, (ed.) C.W. Jefferson and G. Delaney; Geological Survey of Canada Bulletin 588, p. 23–67.

Kister, P., Vieillard, P., Cuney, M., Quirt, D., and Laverret, E., 2005. Thermodynamic constraints on the mineralogical and fluid composition evolution in a clastic sedimentary basin the Athabasca Basin (Saskatchewan, Canada); European Journal of Mineralogy, v. 17, p. 325–342.

Kotzer, T.G., and Kyser, T.K., 1995. Petrogenesis of the Proterozoic Athabasca Basin, northern Saskatchewan, Canada, and its relation to diagenesis, hydrothermal uranium mineralization and paleohydrogeology; Chemical Geology, v. 120, p. 45–89.

Kyser, T.K., Hiatt, E., Renac, C., Durocher, K., Holk, G., and Deckart, K., 2000. Diagenetic fluids in Paleo- and Meso-Proterozoic sedimentary basins and their implications for long protracted fluid histories; in Fluids and Basin Evolution, (ed.) K. Kyser; Mineralogical Association of Canada Short Course Series, v. 28, p. 225–262

Lewry, J.F., and Sibbald, T., 1980. Thermotectonic evolution of the Churchill province in northern Saskatchewan; Tectonophysics, v. 68, p. 45–82

Macdonald, C., 1985. Mineralogy and geochemistry of the sub-Athabasca regolith near Wollaston Lake; in Geology of Uranium Deposits, (eds.) T.I.I. Sibbald, and W. Petruk; Canadian Institute of Mining and Metallurgy, Special v. 32, p. 155–158.

McDonough, W.F., and Sun, S.S., 1995. The composition of the Earth; Chemical geology, v. 120, p. 223-253.

McGill, B., Marlatt, J., Matthews, R., Sopuck, V., Homeniuk, L., and Hubregtse, J., 1993. The P2 North uranium deposit Saskatchewan, Canada; Exploration Mining Geology v. 2, p. 321–333.

Mercadier, J., Richard, A., and Cathelineau, M., 2012. Boron-and magnesium-rich marine brines at the origin of giant unconformity-related uranium deposits: $\delta^{11}B$ evidence from Mg-tourmalines; Geology, v. 40, p. 231–234.

Ramaekers, P., Jefferson, C.W., Yeo, G.M., Collier, B., Long, D.G.F., Drever, G., McHardy, S., Jiricka, D., Cutts, C., Wheatley, K., Catuneau, O., Bernier, S., Kupsch, B and Post, R.T., 2007. Revised geological map and stratigraphy of the Athabasca Group, Saskatchewan and Alberta; in EXTECH IV: Geology and Uranium EXploration TECHnology of the Proterozoic Athabasca Basin, Saskatchewan and Alberta, (ed.) C.W. Jefferson and G. Delaney; Geological Survey of Canada Bulletin 588, p. 155–192.

Richard, A., Pettke, T., Cathelineau, M., Boiron, M. C., Mercadier, J., Cuney, M., and Derome, D., 2010. Brine–rock interaction in the Athabasca basement (McArthur River U deposit, Canada): consequences for fluid chemistry and uranium uptake; Terra Nova, v. 22, p. 303–308.

Richard, A., Rozsypal, C., Mercadier, J., Banks, D.A., Cuney, M., Boiron, M.C., and Cathelineau, M., 2012. Giant uranium deposits formed from exceptionally uranium-rich acidic brines; Nature Geoscience, v. 5 p. 142–146.

Van Hinsberg, V.J., Henry, D.J., and Marchall, H.R., 2011. Tourmaline: an ideal indicator of its host environment; The Canadian Mineralogist, v. 49, p. 1–16.

Wasyliuk, K., 2002. Petrogenesis of the kaolinite-group minerals in the eastern Athabasca basin of northern Saskatchewan: applications to uranium mineralization; unpublished M.Sc. Thesis, University of Saskatchewan. 140 p.

Graphite-bearing and Graphite-depleted Basement Rocks in the Dufferin Lake Zone, South-central Athabasca Basin, Saskatchewan

Marjolaine Pascal, Kevin M. Ansdell, and Irvine R. Annesley
Department of Geological Sciences, University of Saskatchewan, 114 Science Place, Saskatoon, Saskatchewan, S7N 5E2
(kevin.ansdell@usask.ca)

Abstract

Unconformity-type uranium deposits from the Athabasca Basin are interpreted to be the result of mixing between oxidized basinal brines and basement-derived reduced fluids/gases, and/or reduced basement rocks. Graphite and/or its breakdown products may be responsible for uranium mineralization by acting as a reductant that could trigger deposition of uranium. Also, graphite is considered to be indicative of basement structures as it is often concentrated along structures which can be identified as electromagnetic conductors. Underlying the sedimentary rocks of the basin in the Dufferin Lake zone (south-central Athabasca Basin) are variably graphitic pelitic schists (VGPS), which are altered to chlorite and hematite (Red/Green Zone: RGZ), and locally bleached (BZ) near the unconformity. These "graphite-depleted zones" contain rocks which are similar in texture to the VGPS, and are assumed to have contained graphite prior to alteration. The major element composition of the VGPS and RGZ are similar, but the RGZ and BZ are characterized by lower concentrations of carbon and sulphur. The BZ also has higher concentrations of uranium and boron. Raman analyses indicate that well-ordered carbon species (graphite to semi-graphite) are present in the VGPS, with both types more common within shear zones. In contrast, only rare low-ordered carbon species (carbonaceous matter) were detected in the graphite-depleted samples within the RGZ. Secondary fluid inclusions (FI) examined in different quartz vein generations provide an indication of the fluids that have interacted with the basement rocks. Monophase vapor, dominated by CH_4 and N_2 as identified by Raman, are the most common type of fluid inclusion in the VGPS, whereas aqueous two-phase (L+V) and three-phase (L+V+Halite) FI occur in the RGZ. The latter are rich in NaCl and $CaCl_2$ and are similar to brines identified elsewhere in the basin.

Overall, several events are considered to be potentially responsible for graphite consumption. However, the most important processes likely occurred during retrograde metamorphism, and during fluid-rock interactions that ultimately created the RGZ and BZ. CH_4 can be generated by the breakdown of graphite during hydration reactions and/or cooling of C-O-H fluids, and N_2 could have been generated by the breakdown of ammonium (NH_4^+)-bearing feldspar and micas. Basinal brines that circulated through the RGZ could also have broken down graphite and sulphides, and released gases/fluids into the sedimentary rocks of the basin. However, the absolute timing of graphite consumption is not known, and so the direct link with uranium deposition remains unclear.

Introduction

The Athabasca Basin is located in northern Saskatchewan, Canada. It hosts the highest grade unconformity-type uranium deposits in the world, which are mainly located in the eastern part of the basin. Uranium mineralization and associated alteration are often concentrated where structures intersect the unconformity between the basin and the underlying basement rocks (Fig. 1).

Different geochemical and geophysical methods (summarized in Jefferson et al., 2007) are used to target uranium mineralization and one of the most important is determining the location of strong electromagnetic (EM) conductors. These EM conductors are often associated with graphite-rich basement rocks (Madore and Annesley, 1997; Thomas et al., 2000), because graphite is a highly conductive mineral. Graphitic conductors are often associated with shear zones/fault zones, which may provide the structural controls on fluid flow and ultimately focus precipitation of uranium minerals (Madore and Annesley, 1997; Thomas et al., 2000). In addition to acting as a conduit for fluids, graphite (s.s.) has been proposed to act as a reductant for uranium mineralization, by reacting with water to produce methane (CH_4) and carbon dioxide (CO_2) (Hoeve and Sibbald, 1978).

Geology of the Dufferin Lake Zone

The Dufferin Lake Zone is located in the south-central part of the Athabasca Basin, spatially associated with the southern-most part of the Snowbird Tectonic Zone, a 4.5 km wide zone of cataclasites and mylonites (Gilboy, 1985a) named the Virgin River shear zone (VRSZ) (Hoffman, 1990). This forms the boundary between the Mudjatik Domain to the east and the Taltson Domain to the west (Fig.1). The VRSZ was reactivated after the deposition of the Athabasca Group as a northwest-dipping reverse fault, named the Dufferin Lake fault, which offsets the unconformity by over 250 metres (Card et al., 2007; Powell et al., 2007). This fault probably had an important role in the development of uranium mineralization in the area, as it appears to have acted as a fluid conduit over an extended period of time (Thomas et al., 2000). The basement rocks in the Mudjatik Domain are composed mainly of felsic gneisses (Gilboy, 1985a) with lesser quartzites, pelitic and variably graphitic metasedimentary rocks, and deformed amphibolites, granitoids, and pegmatites that have been metamorphosed to upper greenschist to amphibolite grade. The basement rocks in the Taltson Domain consist mainly of orthogneisses (dominated by granodiorite compositions), that have been metamorphosed to granulite-facies in its northwest part and amphibolite-facies near the VRSZ (Card

Pascal, M., Ansdell, K.M., and Annesley, I.R., 2015. Graphite-bearing and Graphite-depleted Basement Rocks in the Dufferin Lake Zone, South-central Athabasca Basin, Saskatchewan, *in* Targeted Geoscience Initiative 4: unconformity-related uranium systems, (ed.) E.G. Potter and D.M. Wright; Geological Survey of Canada, Open File 7791, p. 83–92. doi:10.4095/295776

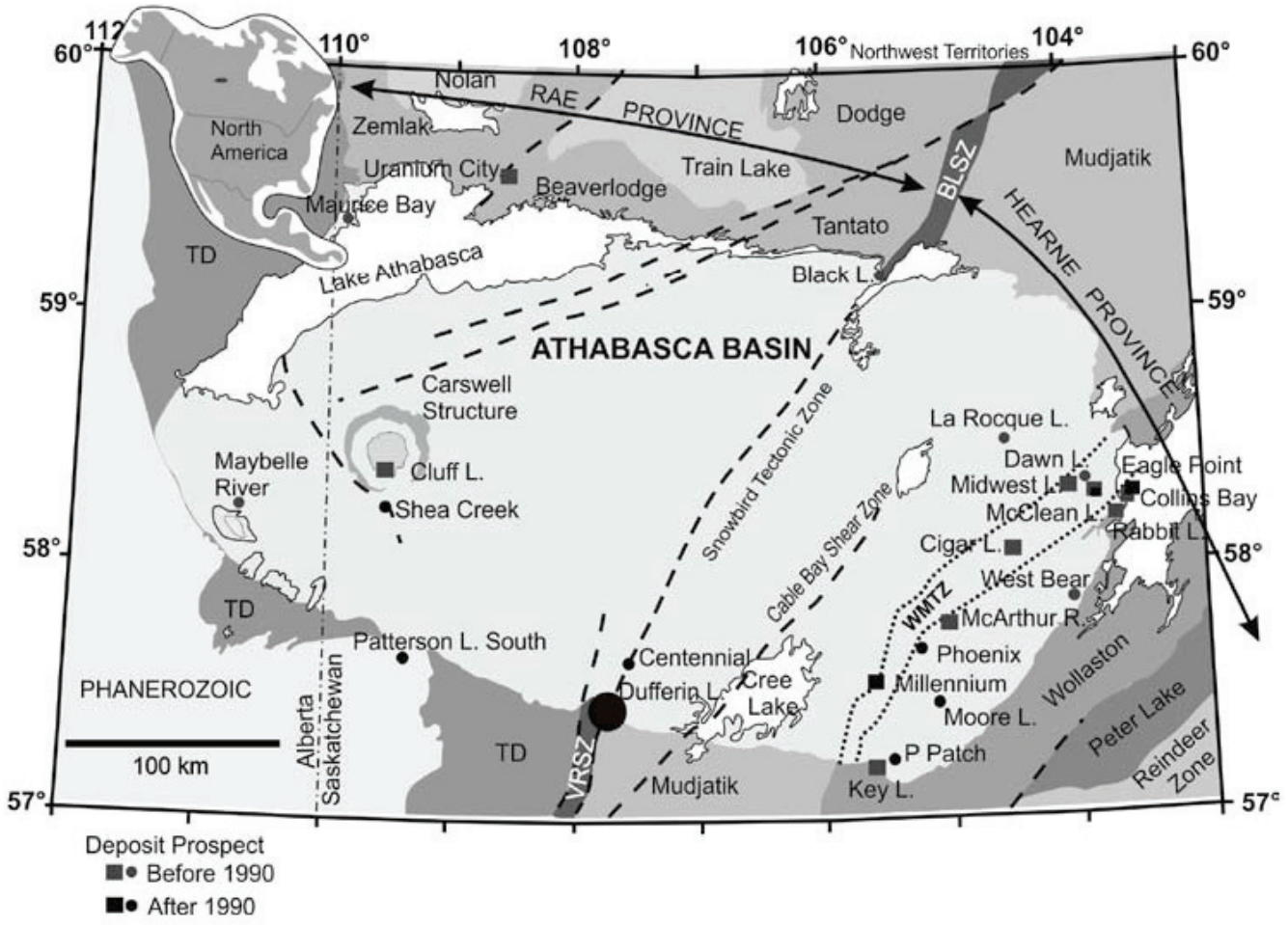

Figure 1. Simplified geological map of the Athabasca Basin and underlying tectonic domains (northern Saskatchewan and Alberta), showing the location of unconformity-associated uranium deposits and occurrences of the Athabasca Basin region of northwestern Canada (modified after Jefferson et al., 2007; Card, 2012). Heavy dashed lines are selected major reactivated fault zones. TD: Taltson Domain, WMTZ: Wollaston Mudjatik transition zone, VRSZ: Virgin River Shear Zone, BLSZ: Black Lake Shear Zone.

et al., 2008).

Graphitic-rich EM conductors are present in the study area, parallel to the Dufferin Lake fault (Jiricka et al., 2007). In the DLZ, uranium mineralization (Jiricka et al., 2007) is hosted in quartz-rich arenites of the Manitou Falls Formation (Fig. 2) just above (5 to 10 m) the unconformity and is associated with bleaching and clay alteration. The basement rocks directly underlying the DLZ are composed primarily of variably graphitic (locally sulphidic) pelitic schists (VGPS), with a strong sub-vertical foliation, and cut by numerous shear zones. The rocks in the red/green zone (RGZ) have the same metamorphic textures and structures, but contain no graphite, suggesting that the graphite had been removed by some process. The graphite depletion zone is composed of the RGZ and a bleached zone (Fig. 2). The lower part of the RGZ is more chloritic (green zone) and progressively becomes enriched in hematite to form the red zone in the upper part of the RGZ. This profile is interpreted to be the result of paleoweathering (Macdonald, 1980, 1985). However, this model has been modified to incorporate the circulation of basinal brines into the basement rocks (Cuney et al., 2003); overprinting the original paleoweathering profile.

Objectives

In this study, we examined the variably graphitic pelitic schists and their altered equivalents depleted in graphite and sulphides, in order to observe and document the consumption of these minerals and to characterize the carbon species present in the graphitic samples. The purpose of this project was to document the consumption of graphite in the basement rocks and to determine how and under what conditions it has been removed. An additional aim was to determine the possible relationship between graphite and/or its breakdown in the uranium mineralizing process and thus, determine if the location of graphitic conductors is important for the localization of a deposit. A summary of the results of this study are provided in this report, and more detailed discussion is available in Pascal (2014).

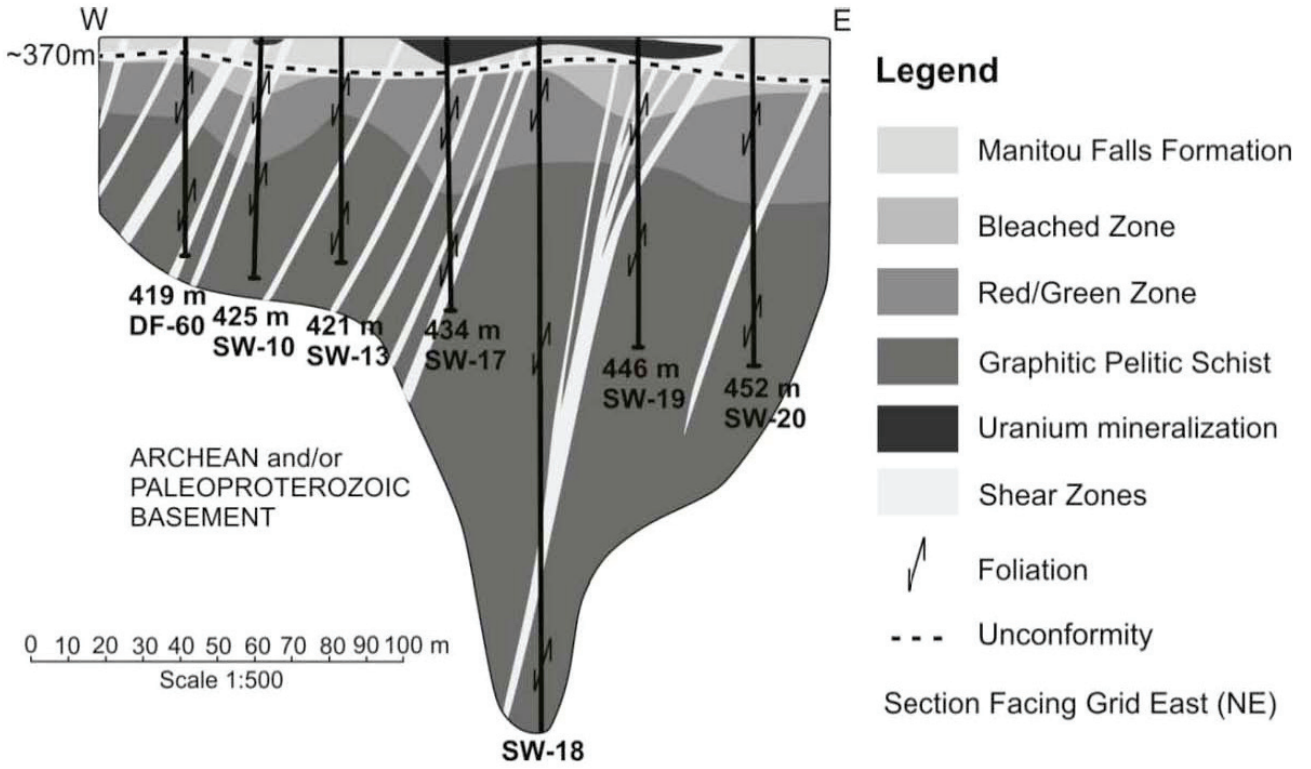

Figure 2. Geological cross section along grid line L250E, illustrating the presence of graphite-depleted (bleached zone and red/green zone) and graphite-rich (variably graphitic pelitic schist) zones.

Results

Petrography summary

The basement rocks are porphyroblastic to granoblastic, and variably mylonitic. The samples display a strong ductile deformation fabric comprising mainly quartz, chlorite and muscovite. The porphyroblasts, when present, are garnet, staurolite, and/or andalusite (Wallis, 1970; Gilboy, 1985b), which are always retrograded (i.e. altered and recrystallized), even within the deeper drilling intersections of the basement rocks. Pyrite occurs as disseminated grains or in late veins. The mylonitic fabric can be contorted and locally microfolded, and shows a C-S structure, rotated porphyroblasts, and quartz boudinage. Primary layering (S0) and early foliation (S1) are isoclinally folded.

In the variably graphitic pelitic schists, the carbon species are often associated with pyrite and spatially associated with quartz veins. Locally, alternating quartz-rich and graphite-rich bands are observed. The porphyroblasts (garnet, staurolite, and andalusite) are generally silicified. Some carbonates veins are present. Graphite to semi-graphite (Fig. 3a), and carbonaceous matter (CM) (Fig. 3b), can sometimes be identified using reflected light microscopy, as the reflectivity is correlated with the degree of crystallinity. Graphite, semi-graphite and CM are concentrated along the foliation, within shear zones and along younger brittle fault zones. The carbon species are very fine grained and consist of small irregular or elongate particles, that can be dispersed in the matrix or form irregular aggregates or elongated parallel to the bedding (Fig. 3).

The alteration assemblage in the RGZ consists mainly of a mixture of chlorite, and hematite (Fig. 4a), with no macroscopic graphite. However, some minor carbon species are dispersed as small grains within the chloritic fabric of the green-zone, i.e. the lower part of the RGZ (Fig. 4b). Several quartz generations overprint the original fabric (Pascal, 2014) and all the porphyroblasts are replaced by quartz or by a mixture of Mg-Fe chlorite or by hematite. It appears that carbon species are not present where both hematite and quartz have strongly overprinted the fabric. The extent of "red alteration" increases upwards through the RGZ into the hematite zone (red zone; Fig. 4c), which is composed mainly of pervasive hematite and clay minerals. In the bleached zone, overlying the red zone and just below the unconformity, the rock texture is destroyed and drill core recovery is very poor. All the original silicate minerals are replaced by kaolinite, and a mixture of Mg-Fe chlorite (Fig. 4d). This bleaching process overprinted both chlorite and hematite and thus postdates the formation of the RGZ and the red zone. This zone also contains ubiquitous hydrothermal dravite. Zircon, rutile, and goyasite occur locally. Graphite was not observed.

Raman analysis summary

Raman analysis provides conclusive evidence for different types (i.e. species) of graphite and carbonaceous matter in the basement rocks of the DLZ (Pascal, 2014).

Samples from the variably graphitic pelitic schists exhibit similar Raman spectra, characterized by the presence of

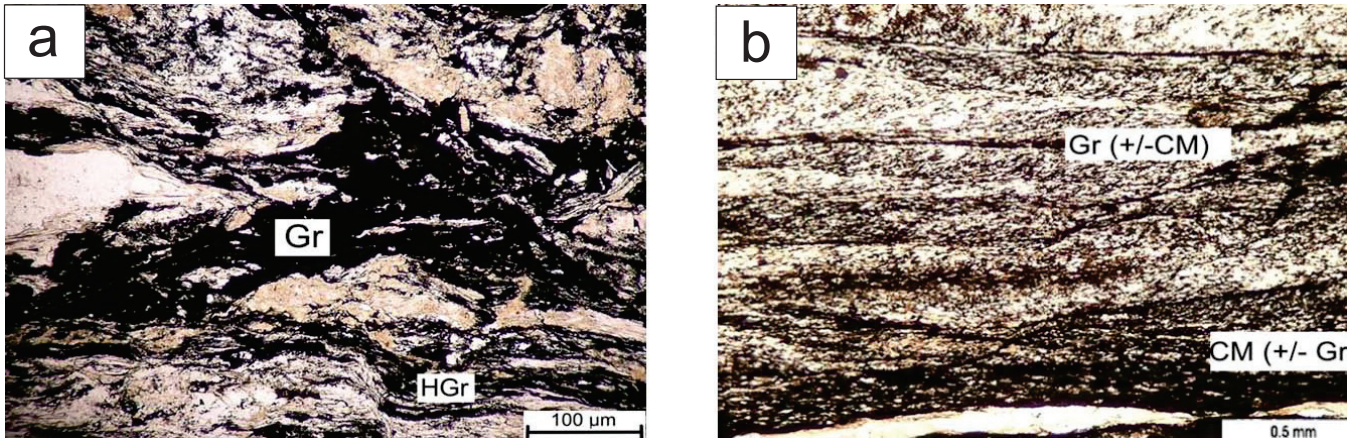

Figure 3. Photomicrograph of different types of carbon species in the graphitic pelitic schists (PPL Transmitted light). (A) High temperature retrograde graphite (Gr) and semi-graphite (HGr) within a high C content pelitic schists (DF60-384.2). (B) Graphite and carbonaceous matter (CM) in a medium C content pelitic schist (SW18-495.0).

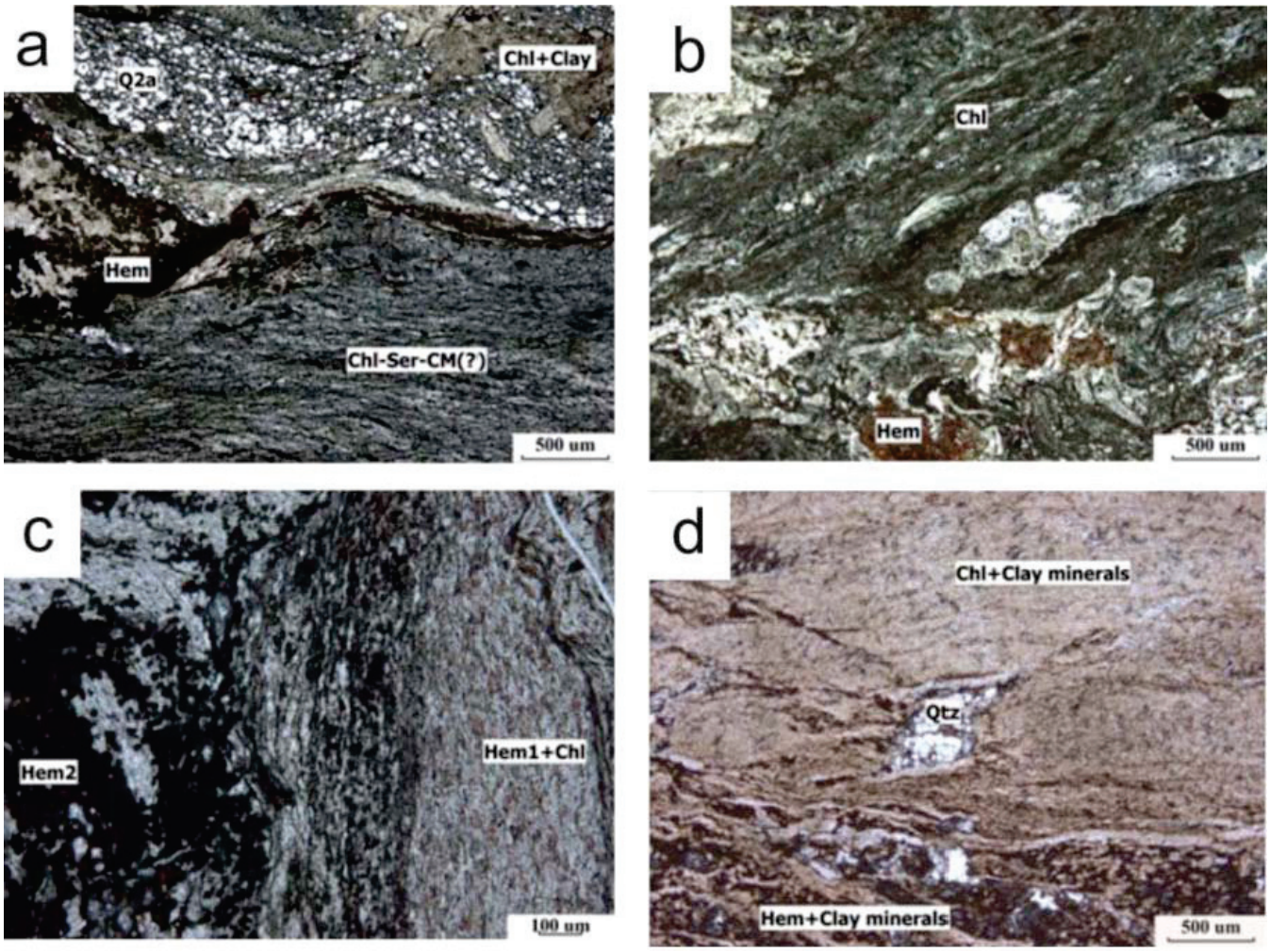

Figure 4. Photomicrographs of altered basement rocks (PPL Transmitted light). (A) Characteristic appearance of the RGZ with chlorite (Chl) and hematite (Hem) (SW20-380.6). (B) Green alteration (SW17-395). (C) Red alteration (SW20-381.6). (D) Bleached zone (SW18-369.9).

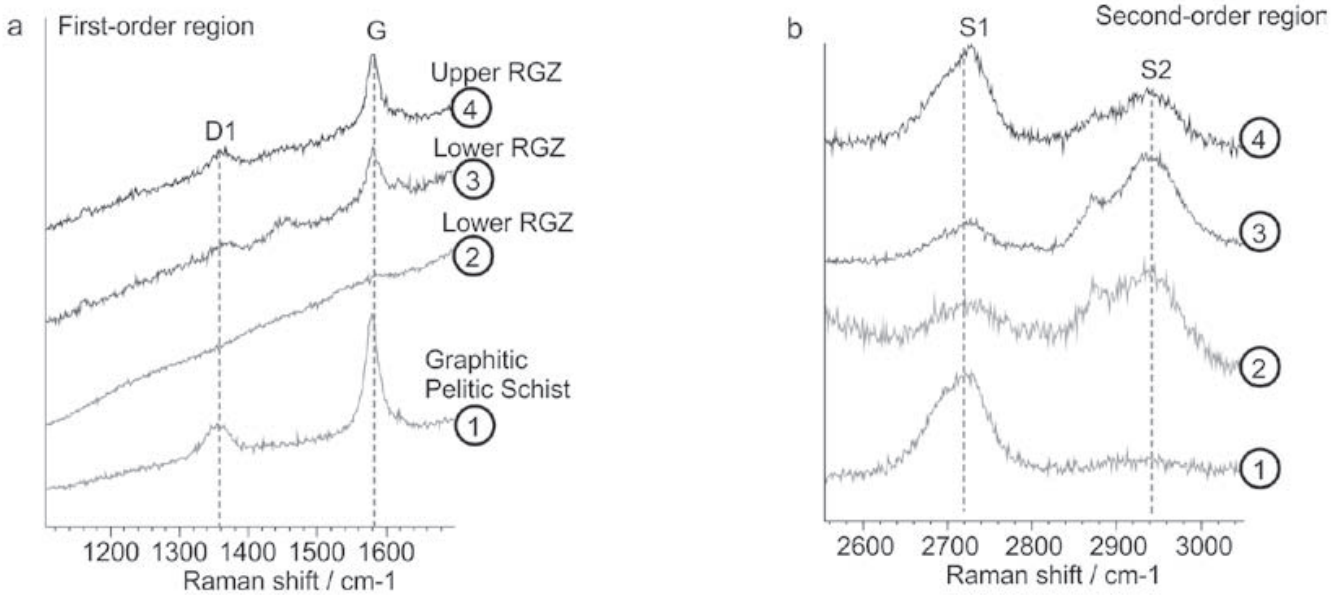

Figure 5. Raman spectra of carbon species in the different zones of the basement. (A) First-order region Raman spectra. (B) Second-order region Raman spectra. Spectrum 1 shows well-crystallised carbon species in the graphitic pelitic schists (SW17-415.1). Spectra 2 and 3 show low-ordered carbon species in the lower part of the RGZ (SW18-409.5, SW17-385.1, respectively). Spectra 4 show crystallised carbon species in the upper part of the RGZ (SW30-389.5).

the graphite (G) band and D1 bands in the first-order region (Fig. 5a), and in some samples the presence of an additional very weak band, D2. The second-order Raman spectra are characterized by S1 and S2 bands (Fig. 5b). Overall, the carbon species within the graphitic pelitic schists exhibit a relatively high structural organization that is typical of graphite to semi-graphite.

In the RGZ, Raman spectra are more variable. Spectra exhibiting G, D1 and D2 bands in the first-order region, and a strong Si band relative to the S2 band in the second-order region (Figs. 5a, b) are rare, and has only been identified in sample SW10-389.5 from the upper part of the RGZ (i.e. the red zone). However, this spectrum suggests that well-crystallized carbon species are present. In contrast, some spectra exhibit an indistinct G band and very wide D1 band with low intensity (Fig. 5a-spectrum 2), characteristic of amorphous carbon species. The second-order region for this sample has a S2 band which is stronger than the S1 band (Fig. 5b), which provides evidence for the presence of very weak structural organization, and is similar to spectra from bitumen (Jehlicka et al., 2003). A small peak can be present around 2880 cm^{-1}, associated with the S2 band, and suggests the presence of an organic compound. Overall, the samples from the RGZ have spectra with a stronger S2 band in the second-order region compared to those from the graphitic pelitic schists, indicating that the carbon-species are less well-ordered.

Geochemistry summary

The pelitic schists have a total carbon content that varies between 0.08 and 5.37 wt. %, which correlates with the amount of visually estimated graphite in each sample. Also, the samples exhibit a positive correlation between total carbon and total sulphur (Fig. 6a), with sulphur reflecting the pyrite content of the schists. In contrast, the samples from the RGZ, including the green zone to the red zone, and the bleached zone have low but variable carbon contents (mainly between 0.08 and 0.98 wt. %, but as high as 1.99 wt. %), whereas sulphue is completely depleted in all the altered rocks (Fig. 6a). Although the carbon content in the RGZ is sometimes similar to the lower carbon content in the variably graphitic pelitic schist, there are no samples from the RGZ that have high carbon content comparable to the variably graphitic pelitic schist. The lowest carbon content can be correlated with the loss of graphite upward into the bleached zone. The Fe^{2+}/Fe^{3+} ratio is approximately 1 in the upper part of the RGZ and less than 1 in the bleached zone, whereas the lower part of the RGZ and the graphitic pelitic schists are variably reduced (Fe^{2+}/Fe^{3+} >1).

Major element geochemistry of samples from the RGZ, including the green zone and the red zone, is quite similar to that of the graphitic pelitic schists. The major element composition of the green zone, in particular, is indistinguishable from the variably graphitic schists (Fig. 6). A lower SiO_2 content (down to 20 wt. %) and a higher MgO content (up to 16.9 wt. %) may be observed in the rocks from the RGZ and is related to the presence of pervasive chlorite alteration. In contrast, the samples from the bleached zone have higher Al_2O_3, K_2O, TiO_2, and Na_2O contents (Figs. 6b, c, d). The sodic enrichment may result from the possible growth of fine-grained hydrothermal dravite within the clay mineral assemblage. The pelitic schists from the bleached zone are weakly mineralized (U up to 187 ppm) (Fig. 6e) with the presence of small amounts of hydrothermal uraninite along fractures. Usually, there is a close relationship between carbon and uranium (Landais, 1996), but the bleached zone and the RGZ are enriched in uranium relative to the less altered graphitic pelitic schists (Fig. 6e). Also, the samples from the

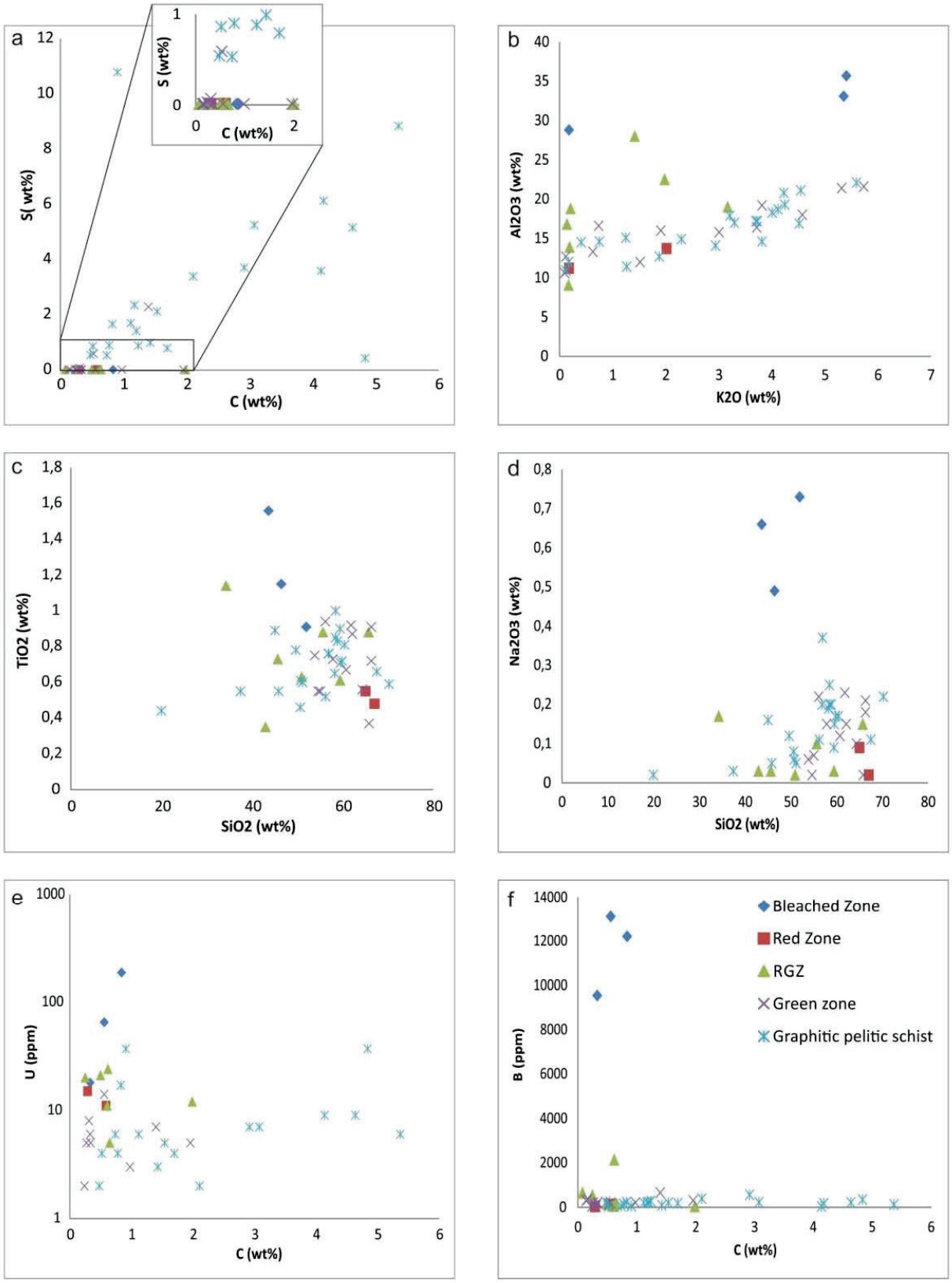

Figure 6. Major element composition of the graphitic and graphite depleted rocks of the different zones of the basement. The inset in (a) shows that C content is sometimes similar in the VGPS and the RGZ, but the sulphur content in the latter is always low.

bleached zone have very high boron contents (from 30 ppm to 13.100 ppm) (Fig. 6f) due to their high dravite content.

Samples from the less altered basement rocks, the RGZ, and the bleached zone have very similar chondrite normalized REE patterns. They show higher LREE content, with $(La/Yb)_N$ varying from 1.2 to 36.9, and a negative Eu anomaly. Furthermore, the HREE (total Tb to Yb)/LREE (total La to Gd) ratio is less than 1 (0.04 to 0.41). These observations are typical of the basement alteration halo associated with unconformity-type mineralization (Fayek and Kyser, 1997; Mercadier et al., 2011). Also, these chondrite-normalized REE patterns, and the presence of a well-pronounced Eu anomaly, are similar to the chondrite-normalized REE distributions found in average post-Archean shales (Condie, 1993) and to the graphitic pelitic gneisses of the basal Wollaston Group below the eastern Athabasca Basin (Madore and Annesley, 1997).

Mass-balance calculations also confirm the loss of carbon and sulphur in the RGZ, including the green zone, and the bleached zone relative to the variably graphitic pelitic schist, and a large gain of boron in the bleached zone, compared to an insignificant variation in the RGZ and the green zone (Fig. 6). The bleached zone is the zone which shows the most significant variations when compared to the other zones. The bleached zone overprints the RGZ and is therefore a younger alteration event. This alteration resulted in an enrichment of Na_2O, B, Cu and U, and a loss of Fe_2O_3, SiO_2 and CaO, compared to the RGZ.

Fluid inclusion summary

Fluid inclusion investigations were undertaken to document the characteristics of fluids that interacted with the variably graphitic pelitic schists and their equivalent graphite-depleted rocks (Pascal, 2014; Pascal et al., 2015). Several quartz generations have been identified in the basement samples (Pascal, 2014). Early quartz veins (Q1 and Q2) formed before the deposition of the Athabasca Basin, and two later quartz vein sets (Q3 and Q4) that could be related to post-Athabasca deformation and fluid flow, and therefore could potentially be related to uranium mineralization.

In the graphitic pelitic schists, monophase vapor (V) secondary fluid inclusions have been observed. They all homogenize into the vapor phase at very low temperatures (mainly between -135 and -125°C and -90 and -70°C). Raman analysis of these fluid inclusion types showed the presence of two different types of fluid; methane (CH_4)-dominant and nitrogen (N_2)-dominant fluids, with the latter having the lowest temperature of homogenization. Isochores have been determined and the range of pressure-temperature estimated for these vapour inclusions is 4.5 to 80 MPa for a temperature range of 200 to 500°C under hydrostatic regime (Pascal, 2014).

In the RGZ, aqueous two-phase (Liquid (L) + V) and three-phase (L + V + Halite) secondary fluid inclusions are the dominant type of fluid inclusions observed. The temperature of melting ice for the two-phase fluid inclusions varies between -35.5°C and -16.4°C with a dominant population between -26°C and -23°C. These temperatures indicate that salts other than NaCl are present in the fluid and are similar to those observed by Derome et al. (2005) and Mercadier et al. (2010). These temperatures yield a range of salinity between 27.4 and 19.8 wt. % equivalent NaCl-$CaCl_2$. The temperature of melting of halite in the three-phase fluid inclusions range from 190 to 240°C, which convert to a salinity varying between 31 and 34 wt. % equivalent NaCl.

Comparison of the Characteristics of Graphite-Bearing and Graphite-Depleted Rocks

The graphitic pelitic schists and the graphite-depleted rocks are texturally very similar which suggests that the rocks were similar mineralogically before alteration occurred but some process or combination of processes removed graphite. Our analyses show that the graphite-depletion reflects fluid-rock interactions, in particular within the bleached zone, leading to gain and loss in some elements. Carbon and sulphur have been completely removed, compared to the variably graphitic pelitic schists. Several events through time could be responsible for the breakdown of graphite, carbonaceous matter and sulphides. The resulting products of the breakdown may have included carbon and sulphur as gas and/or fluid (i.e. rich in CH_4) which migrated upward to and above the unconformity. If the timing was appropriate these products could have played a role in uranium precipitation, as suggested by Hoeve and Sibbald (1978). However, this depletion of graphite could have started during retrograde metamorphism, continued through paleoweathering, and been completed during fluid-rock interaction with basin brines.

The presence of CH_4-rich fluids and N_2-rich fluids in coexisting fluid inclusions within quartz from the graphitic pelitic schists support interaction of these fluids with the graphitic rocks. Methane can be generated by the breakdown of graphite to CH_4 (Cabrera et al., 1982) during hydration reactions and/or cooling of C-O-H fluids (Huizenga, 2011; Annesley and Wheatley, 2011; Card and Annesley, 2012), and N_2 could have been generated by the breakdown of ammonium (NH_4^+)-bearing feldspar and micas (Bebout et al., 1999; Hurai et al., 2000; Sadofsky and Bebout, 2000). In the upper part of the basement, within the RGZ, where graphite is absent, brines rich in NaCl and $CaCl_2$ have been identified that are similar to those observed elsewhere in the Athabasca Basin (Derome et al., 2005; Mercadier et al., 2010). These fluids have been interpreted to be the regional basinal fluid and the evolved fluid resulting from fluid/rock interactions between the NaCl-rich brines and Ca-rich rocks of the basement, and the latter are considered to be related to uranium mineralization (Derome et al., 2005; Derome et al., 2007; Mercadier et al., 2010; Richard et al., 2010). As these fluids have circulated in the RGZ, where graphite has been lost, these fluids could also be responsible for the consumption of graphite. In this case, the fluids may have reacted with graphite and leading to its breakdown to CH_4 which could have acted as a reductant driving deposition of uranium. A summary of these observations is presented in figure 7.

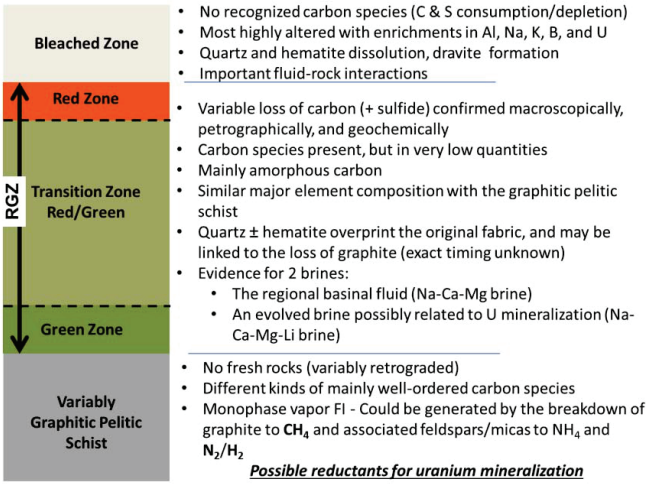

Figure 7. Summary of the characteristics of graphitic-bearing and graphite-depleted rocks.

Implications for graphite consumption and uranium exploration.

The aim of this study was to confirm and document the depletion of graphite in the basement rocks underlying the Dufferin Lake Zone in the south-central part of the Athabasca Basin, and to determine the mechanism(s) which could be responsible for this depletion. An attempt is made to relate the changes to the basement rocks along their PT-t path (Fig. 8), with the characteristics of carbon species and composition of fluid inclusions (Pascal, 2014; Pascal et al., 2015).
In summary we documented the following through PT-t space:

1. During prograde metamorphism:
   i. The original rocks, interpreted to be black shales, rich in carbonaceous (organic) matter, were metamorphosed to graphitic pelitic schists.
   ii. NH_4^+ may have been liberated from the carbonaceous matter and stored in K-micas. Carbonaceous matter became more ordered and crystalline (semi-graphite to graphite) as metamorphic grade increased (Beyssac et al., 2002).
   iii. Early quartz veins (Q1) formed during the peak metamorphism.
2. During retrograde metamorphism:
   i. Fluids interacted with the graphitic basement rocks, leading to the breakdown of graphite to CH_4 and the liberation of NH^{4+} from the phyllosilicate minerals (Bottrell et al., 1988). This may have led to the formation of N_2 following: $2NH^{4+} \rightarrow N_2 + 8H^+$. Overall, the C-O-H fluid that formed during retrograde metamorphism and the uplift of the basement rocks may have been the one responsible for incipient, but not total, graphite consumption (Huizenga, 2011) (stage 1 – Fig. 8). In this case, these fluids would have had no role in uranium mineralization.
   ii. Pre-Athabasca quartz (Q2) veins formed.

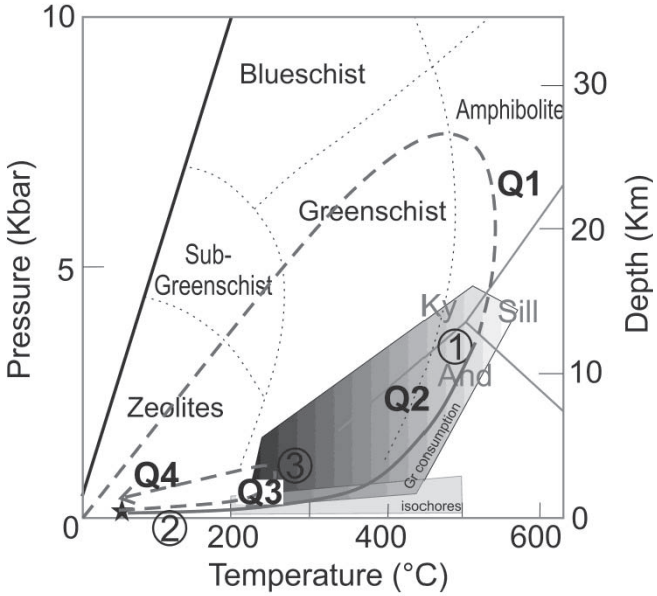

Figure 8. Pressure-temperature diagram illustrating the path followed by the basement rocks (long-dashed and solid line), the approximate timing of quartz generations (Q1, Q2, Q3 and Q4), fluid inclusions isochores calculated for CH_4 –rich and N_2-rich fluid inclusions (clear grey field), and the possible periods during which graphite was depleted (shaded grey field, modified after Ault and Selverstone, 2008) (1, 2, 3).

3. Pre-Athabasca paleoweathering (stage 2 – Fig. 8): alteration of the upper part of the basement leading to the formation of the RGZ (Macdonald, 1980, 1985). Graphite and sulphides in the basement rocks may have broken down during paleoweathering leading to the release of carbon and sulphur species into the environment at this time.
4. Post-Athabasca Basin:
   i. Athabasca Basin is deposited and post-Athabasca (Q3 and Q4) veins are formed.
   ii. Post-Athabasca circulation of oxidized basinal brines with associated hydrothermal alteration (stage 3 – Fig. 8) occurred in the basement. These fluids altered the upper part of the basement (RGZ) and produced the bleached zone which overprints the regolith profile. These brines could also have reacted with graphite and sulphides in the variably graphitic schists resulting in the migration of carbon and sulphur as fluid and/or gas to the unconformity and into the sandstone, utilizing the original graphite-sulphide-rich fault structures.

Thus, several events are considered to be responsible for graphite consumption. However, graphite depletion is interpreted to be more prevalent with decreasing pressure along retrograde PT-t paths (Ault and Selverstone, 2008), and particularly near the lower temperature part of retrograde metamorphism. Therefore, the late retrograde and diagenetic hydrothermal alterations are interpreted to be the major processes that have played the most important role in the depletion/consumption of graphite. This is supported by the fact that the most altered zone, the bleached zone, has no

graphite, but contains evidence of significant fluid-rock interactions, including the one(s) that are most likely related to uranium mineralization. The interaction of fluids with early graphite led to its consumption and to the formation of CH_4 (as observed in the fluid inclusion study; Pascal, 2014; Pascal et al., 2015). If the timing of graphite consumption was appropriate, the upward migration of gases (and associated fluids) could have interacted with uranium-bearing oxidized basinal fluids above the unconformity and acted as a reductant for deposition of uranium. Previous studies have identified hydrocarbon buttons in the sandstone adjacent to mineralization, which suggests the migration of carbon species at the appropriate time (Hoeve and Sibbald, 1978; Landais, 1996). Recent numerical modelling by Chi et al. (2014) has shown that hydrocarbons generated in the Douglas Formation could have migrated to the unconformity and played a role in uranium mineralization. The authors further propose that (although not proven yet) the solid bitumen crosscutting uraninite could reflect hydrocarbons remaining as fluids after mineralization, flowing into fractures in the ores and forming bitumen. However, Leventhal et al. (1987), Wilson et al. (2007), and Ramaekers and Catuneanu (2013) proposed that CH_4 may be related to post-ore alteration of hydrocarbons derived from the overlying Douglas Formation or Western Canada sedimentary basin rocks.

This study has provided relative age constraints on the possible processes leading to the consumption of graphite in this part of the basin, although the absolute age of these processes especially with respect to the timing of uranium mineralization is still not known.

Acknowledgments

This work forms part of a Master of Science thesis project by the senior author. The authors acknowledge the financial support of Cameco Corporation, Natural Science and Engineering Research Council of Canada through a Discovery Grant to Ansdell, and the Department of Natural Resources of Canada Targeted Geoscience Initiative Phase 4 (TGI4) Grants program. Thanks to Aaron Brown and Gary Witt (Cameco) for organizing field logistics, Kyle Reid for field support, Blaine Novakovski for preparation of thin sections, Tom Bonli for microprobe analyses, Jason Maley for his help and discussion about the Raman and the results, and Marie-Christine Boiron for training in fluid inclusion analysis and interpretation. Dan Jiricka and Tom Kotzer provided suggestions throughout the project. Gerard Zaluski is thanked for a highly constructive review of the initial draft of the manuscript and Eric Potter for the editorial handling.

References

Annesley, I.R., and Wheatley, K., 2011. Insights into understanding the carbon-uranium (± sulfur and boron) geochemical system along a retrograde P-T-t path from 600°C to 250°C: New constraints with implications for U/C-type uranium deposits; Joint annual meeting of the Geological Association of Canada – Mineralogical Association of Canada, Abstracts, v. 34, p. 4–5.

Ault, K.A., and Selverstone, J., 2008. Microtextural constraints on the interplay between fluid–rock reactions and deformation; Contributions to Mineralogy and Petrology, v. 156, p. 501–515.

Bebout, G.E., Cooper, D.C., Bradley, A.D., and Sadofsky, S.J., 1999. Nitrogen-isotope record of fluid-rock interactions in the Skiddaw aureole and granite, English Lake District; American Mineralogist, v. 84, p. 1495–1505.

Beyssac, O., Goffé, B., Chopin, C., and Rouzaud, J.N., 2002. Raman spectra of carbonaceous material in metasediments: a new geothermometer; *Journal of Metamorphic Geology, v.* 20, p. 859–87.

Bottrell, S.H., Carr, L.P., and Dubessy, J., 1988. A nitrogen-rich metamorphic fluid and coexisting minerals in slates from North Wales; *Mineralogical Magazine, v.* 52, p. 451-457

Cabrera A.L., Heinemann, H., and Somorjai, G.A., 1982. Methane production from the catalyzed reaction of graphite and water vapor at low temperatures (500-600 K); Journal of Catalysis, v. 75, p. 7–22, doi: 10.1016/0021-9517(82)90117-8

Card, C.D., 2012. A proposed domainal reclassification for Saskatchewan's Hearne and Rae provinces; in Saskatchewan Summary of Investigations 2012; Saskatchewan Geological Survey, Miscellaneous Report 2012-4(2), p. 9.

Card, C.D., and Annesley, I.R., 2012. The origin(s) of graphite-rich rocks in the Wollaston-Mudjatik Transition Zone: syngenetic versus epigenetic?; Saskatchewan Geological Survey, Open House 2012, Abstract volume, p 6.

Card, C.D., Pana, D., Portella, P., Thomas, D.J., and Annesley, I.R. , 2007. Basement rocks to the Athabasca Basin, Saskatchewan and Alberta; in EXTECH IV: Geology and Uranium EXploration TECHnology of the Proterozoic Athabasca Basin, Saskatchewan and Alberta, (ed.), C.W. Jefferson and G. Delane; Geological Survey of Canada, Bulletin 588, p. 69–87.

Card, C.D., McEwan, B., and Bosman, S.A., 2008. The Cree Lake South Project 2008: Regional Implications of Bedrock mapping along the Virgin River Transect; in Summary of Investigations 2008, Saskatchewan Geological Survey, Miscellaneous Report 4(2), 23 p.

Chi, G., Li, Z., and Bethune, K.M., 2014. Numerical modeling of hydrocarbon generation in the Douglas Formation of the Athabasca Basin (Canada) and implications for unconformity-related uranium mineralization; Journal of Geochemical Exploration, v. 144, p. 37–48

Condie, K.C., 1993. Chemical composition and evolution of the upper continental crust: Contrasting results from surface samples and shales; Chemical Geology, v. 104, p. 1–37.

Cuney, M., Brouand, M., Cathelineau, M., Derome, D., Freiberger, R., Hecht, L., Kister, P., Lobaev, V., Lorilleux, G., Peiffert, C., and Bastoul, A.M., 2003. What parameters control the high grade-large tonnage of the Proterozoic unconformity related uranium deposit?; in Uranium Geochemistry 2003, International Conference, Proceedings, (ed.) M. Cuney; Unité Mixte de Recherche CNRS 7566G2R, Université Henri Poincaré, Nancy, France, p. 123–126.

Derome, D., Cathelineau, M., Cuney, M., Fabre, C., and Lhomme, T., 2005. Evidences of brine mixings in the McArthur River unconformity-type uranium deposit (Saskatchewan, Canada). Implications on genetic models; Economic Geology v. 100, p. 1529–1545.

Derome, D., Cathelineau, M., Fabre, C., Boiron, M.-C, Banks, D., Lhomme, T., and Cuney, M., 2007. Reconstitution of paleo-fluid composition by Raman, LIBS and crush-leach techniques: application to mid-proterozoic evaporitic brines (Kombolgie formation basin, northern territories, Australia); Chemical Geology, v. 237, p. 240–254.

Fayek, M., and Kyser, T.K., 1997. Characterization of multiple fluid-flow events and rare-earth-element mobility associated with formation of unconformity-type uranium deposits in the Athabasca Basin, Saskatchewan; The Canadian Mineralogist, v. 35, p. 627–658.

Gilboy, C.F., 1985a. Basement geology, part of the Cree Lake (south) area; Saskatchewan Energy and Mines, Report 203, 1-47.

Gilboy, C.F., 1985b. Compilation bedrock Geology, Cree Lake, NTS Area 74G; Saskatchewan Energy and Mines, Report 237.

Hoeve, J., and Sibbald, T., 1978. On the Genesis of Rabbit Lake and Other Unconformity-type Uranium Deposits in Northern Saskatchewan, Canada; Economic Geology, v. 73, p. 1450–1473.

Hoffman, P.F., 1990. Subdivision of the Churchill Province and extent of the Trans-Hudson orogeny; in The Early Proterozoic Trans-Hudson Orogen of North America, (eds.) J.F. Lewry and M.R. Stauffer; Geological Association of Canada, Special Paper 37, p. 15–39.

Huizenga, J.M., 2011. hermodynamic modelling of a cooling C–O–H fluid–graphite system: implications for hydrothermal graphite precipi-

tation; Mineralium Deposita, v. 46, p. 23–33.

Hurai, V., Janak, M., Ludhova, L., Horn, E.E., Thomas, R., and Majzlan, J., 2000. Nitrogen-bearing fluids, brines and carbonate liquids in Variscan migmatites of the Tatra Mountains, Western Carpathians; heritage of high-pressure metamorphism; European Journal of Mineralogy, v. 12, p. 1283–1300.

Jefferson, C.W., Thomas, D.J., Gandhi, S.S., Ramaekers, P., Delaney, G., Brisbin, D., Cutts, C., Portella, P., and Olson, R.A., 2007. Unconformity associated uranium deposits of the Athabasca Basin, Saskatchewan and Alberta; in EXTECH IV: Geology and Uranium EXploration TECHnology of the Proterozoic Athabasca Basin, Saskatchewan and Alberta, (ed.) C.W. Jefferson and G. Delaney; Geological Survey of Canada, Bulletin 588, p. 23–67.

Jehlicka, J., Urban, O., and Pokorny, J., 2003. Raman spectroscopy of carbon and solid bitumens in sedimentary and metamorphic rocks; Spectrochimica Acta Part A, v. 59, p. 2341–2352.

Jiricka, D.E., Witt, G., and Fiolleau, K., 2007. Southwest Athabasca Project; 2006 annual exploration report, Internal Cameco Corporation report, p. 1–77.

Landais, P., 1996. Organic geochemistry of sedimentary uranium ore deposits; Ore Geology Reviews v. 11, p. 33–51.

Leventhal, J.S., Grauch, R.I., Threlkeld, C.N., and Lichte, F.E., 1987. Unusual organic matter associated with uranium from the Claude deposit, Cluff Lake, Canada; Economic Geology, v. 82, p. 1169–1176.

Macdonald, C., 1980. Mineralogy and geochemistry of a Precambrian regolith in the Athabasca Basin; unpublished M.Sc. thesis: University of Saskatchewan, 151 p.

Macdonald, C., 1985. Mineralogy and geochemistry of the sub-Athabasca regolith near Wollaston Lake; in Geology of Uranium Deposits, Proceedings of the CIM-SEG Uranium Symposium, (ed.) T.I.I. Sibbald and W. Petruk; The Canadian Institute of Mining, Metallurgy and Petroleum, v. 32, p. 155–158.

Madore, C., and Annesley, I.R., 1997. Graphitic pelitic gneisses of the paleoproterozoic Wollaston Group, Hearne Province, Saskatchewan; in Mineral deposits, Research and Exploration- Where do they meet? (ed.) H. Papunen and H. Balkema, p. 79–82.

Mercadier, J., Cuney, M., Cathelineau, M., and Lacorde, M., 2011. U redox fronts and kaolinisation in basement-hosted unconformity-related U ores of the Athabasca Basin (Canada): late U remobilization by meteoric fluids; Mineralium Deposita, v. 46, p. 105–135.

Mercadier, J., Richard, A., Boiron, M.-C., Cathelineau, M., and Cuney, M., 2010. Migration of brines in the basement rocks of the Athabasca Basin through microfracture networks (P-Patch U deposit, Canada); Lithos, v. 115, p. 121–136.

Pascal, M., 2014. Graphite-bearing and graphite-depleted basement rocks in the Dufferin Lake Zone, south-central Athabasca Basin, Saskatchewan; unpublished M.Sc. thesis, University of Saskatchewan, Saskatoon, Canada, 193 p (http://hdl.handle.net/10388/ETD-2014-07-1628).

Pascal, M., Boiron, M.-C., Ansdell, K., Annesley, I.R., Kotzer, T., Jiricka, D., and Cuney, M., 2015. Fluids preserved in variably altered graphitic pelitic schists in the Dufferin Lake zone, south-central Athabasca Basin, Canada: Implications for graphite loss and uranium deposition; Mineralium Deposita (in revision after review).

Powell, B., Wood, G., and Bzdel, L., 2007. Advances in Geophysical Exploration for Uranium Deposits in the Athabasca Basin; in Proceedings of Exploration 07: Fifth Decennial International Conference on Mineral Exploration, (ed.) B. Milkereit; p. 771–790.

Ramaekers, P. and Catuneanu, O., 2013. Rifting and the generation and modification of Athabasca Basin uranium deposits; Saskatchewan Geological Survey Open House 2013. http://economy.gov.sk.ca/Technical%20Session%201%20Uranium%20Geoscience

Richard, A., Pettke, T., Cathelineau, M., Boiron, M.-C., Mercadier, J., Cuney, M., and Derome, D., 2010. Brine–rock interaction in the Athabasca basement (McArthur River U deposit, Canada): consequences for fluid chemistry and uranium uptake; Terra Nova, v. 22, p. 303–308.

Sadofsky, S.J., and Bebout, G.E., 2000. Ammonium partitioning and nitrogen-isotope fractionation among coexisting micas during high-temperature fluid-rock interactions; examples from the New England Appalachians; Geochimica et Cosmochimica Acta, v. 64, p. 2835–2849

Thomas, D., Matthews, R.B., and Sopuck, V., 2000. Athabasca Basin (Canada) unconformity-type uranium deposits: exploration model, current mine developments and exploration directions; in Geology and Ore Deposits 2000: The Great Basin and Beyond, (ed.) J.K. Cluer, J.G. Price, E.M. Struhsacker, R.F. Hardyman and C.L. Morris; Geological Society of Nevada, Symposium Proceedings, v. 1, p. 103–126.

Wallis, R.H., 1970. The geology of the Dufferin Lake Area (West Half) Saskatchewan; Department of Mineral Resources, Geological Sciences Branch, Precambrian Geology Division (Regina), Geological Report 132.

Wilson, N.S.F., Stasiuk, L.D., and Fowler, M.G., 2007. Origin of organic matter in the Proterozoic Athabasca Basin of Saskatchewan and Alberta, and significance to unconformity uranium deposits; in EXTECH IV: Geology and Uranium Exploration TECHnology of the Proterozoic Athabasca Basin, Saskatchewan and Alberta, (ed.) C.W. Jefferson and G. Delaney; Geological Survey of Canada, Bulletin 588, p. 325–339.

Fluid Composition, Thermal Conditions, Fluid-structural Relationships and Graphite Alteration of the Phoenix Uranium Deposit, Athabasca Basin, Saskatchewan

Kewen Wang[1], Guoxiang Chi[1], Kathryn M. Bethune[1], and Colin D. Card[2]

1. *Geology Department, University of Regina, 3737 Wascana Parkway, Regina, Saskatchewan, S4S 0A2*
2. *Saskatchewan Geological Survey, Regina, 2101 Scarth Street, Regina, Saskatchewan, S4P 2H9*

Abstract

The Phoenix deposit is a high-grade unconformity-related uranium deposit located in the southeastern Athabasca Basin. Previous studies have revealed similar features to other well-known unconformity-related uranium deposits in the region, but the composition and thermal conditions of the mineralization fluids, the hydrodynamic relationship between structures and fluid pressure, and the nature of graphite degradation near mineralization zones remain unclear. Field (drill core) investigations, petrographic studies of altered and mineralized host rocks, and microthermometric and microstructural studies of fluid inclusions indicate that different structural regimes and fluid systems were developed in the pre-Athabasca stage versus the syn- to post-Athabasca, uranium mineralization stage. The pre-Athabasca stage was characterized by ductile deformation and circulation of metamorphic fluids in a relatively high *P–T* environment, whereas the syn- to post-Athabasca mineralization stage was characterized by brittle deformation and circulation of basinal brines in a relatively low *P–T* environment (with fluid inclusion homogenization temperatures of 80 to 135 °C), in which the fluid may have experienced boiling, as indicated by the coexistence of vapour-only and biphase aqueous inclusions. Preliminary fluid inclusion plane (FIP) orientation studies reveal the dominance of subvertical microfractures in cross-cutting quartz veins in the basement, possibly indicating an extensional regime during certain periods of time in the syn- to post-Athabasca mineralization stage. Preliminary petrographic and Raman spectroscopic studies of graphite suggest that the crystal structure of the graphite tends to be more disordered toward the mineralized zones, which may potentially be used as an indicator of mineralization.

Introduction

The Phoenix uranium deposit is located 35 km southwest of the world-class McArthur River uranium deposit in the southeastern Athabasca Basin (Fig. 1). It consists of a series of high-grade unconformity-related uranium zones associated with a NE-trending, moderately SE-dipping reverse fault, the WS shear zone. Previous geological and geochemical studies have revealed features similar to other unconformity-related uranium deposits in the region (e.g. Gamelin et al., 2010; Kerr, 2010; Power et al., 2012; Dann et al., 2014), but the composition, temperature and pressure of the fluids associated with mineralization have not yet been investigated by fluid inclusion techniques. In addition, like other well-studied unconformity-related uranium deposits, the structural controls on mineralization, particularly the hydrodynamic relationship between structures (and related stresses) and fluid pressure, are not well understood. Furthermore, the prevalence of graphite in metapelite in basement rocks at the Phoenix deposit provides an opportunity to explore potential roles of graphite in the formation of unconformity-related uranium deposits, given the known spatial association between graphite and many deposits (Hoeve and Sibbald, 1978) and the observation that graphite becomes increasingly degraded toward the ore zones in some deposits (Wang et al., 1989). The main objectives of this study are to determine the fluid composition, thermal conditions, fluid-structural relationships, and the role of graphite in the formation of the Phoenix deposit, through a combination of field (drill core) investigations, petrographic studies of altered and mineralized host rocks, microthermometric and microstructural studies of fluid inclusions, and petrographic and Raman spectroscopic studies of graphite.

Sampling and core description

In the summers of 2013 and 2014, a total of 120 samples were collected from 15 drill holes in the Wheeler River property, mostly from the Phoenix deposit (Fig. 2). Most of the drill cores examined are located on or near a NW-SE cross-section (Figs. 2 and 3), which is perpendicular to the regional structural trend in the area (Fig. 2). The drill cores were examined for lithological characteristics, with emphasis on fracture/vein fillings and associated alteration (Fig. 4). Ten oriented samples were collected for microstructural study.

Drill core samples from the basement are dominated by lower granulite facies metapelite to meta-psammopelite (Fig. 4A), containing graphite, garnet and/or cordierite. The metapelites are invaded by decimeter- to meter-thick foliation-parallel bodies of massive quartz (Fig. 4B) and spatially associated granitic pegmatite (Fig. 4C), which predate mineralization. In the graphitic metapelite unit, the amount of graphite appears to decrease toward the uranium orebody (Fig. 4D). Graphite is also locally concentrated in fractures cutting granitic pegmatite and associated quartz (Fig. 4E).

Samples from drill cores of the Athabasca Group overlying the unconformity are characterized by fragile, desilicified sandstone with interstitial clay alteration (Fig. 4F), with less developed intervals of relatively hard, silicified sandstone (Fig. 4G). Drusy quartz filled fractures and dissolution vugs are abundant in the Athabasca sandstone (Fig. 4H), and are locally developed in the basement as well (Fig. 4I). The abundance of drusy quartz near the mineralized zones is considered to be related to local silica oversaturation due to mineralization-related desilicification within the ore zones, and therefore it is considered to be syn- to post-mineralization.

Wang, K., Chi, G., Bethune, K.M., and Card, C.D., 2015. Fluid Composition, Thermal Conditions, Fluid-structural Relationships and Graphite Alteration of the Phoenix Uranium Deposit, Athabasca Basin, Saskatchewan, *in* Targeted Geoscience Initiative 4: unconformity-related uranium systems, (ed.) E.G. Potter and D.M. Wright; Geological Survey of Canada, Open File 7791, p. 93–102. doi:10.4095/295776

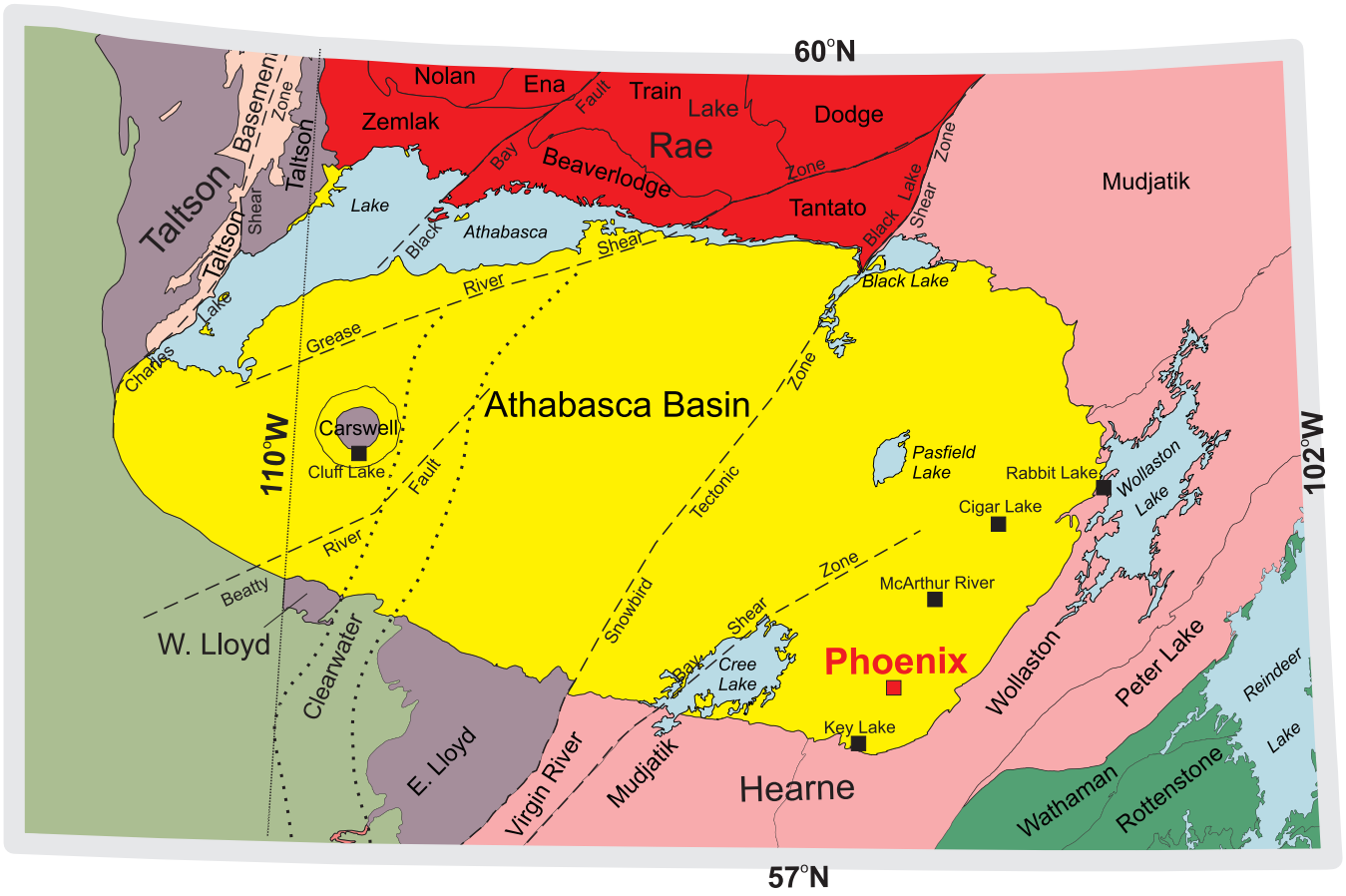

Figure 1. A regional geological map showing the location of the Phoenix uranium deposit in the southeastern part of the Athabasca Basin (modified from Card et al., 2007).

Analytical Methods

A hundred and one polished thin sections and seventy-six doubly polished thin sections were prepared for petrographic and fluid inclusion studies, respectively. The methods of fluid inclusion petrography, microthermometry, fluid inclusion plane (FIP) orientation measurement, and Raman spectroscopic study of graphite are described below.

Fluid inclusion petrography and microthermometry

Microthermometry was performed mainly on fluid inclusions distributed in growth zones of drusy quartz. The fluid inclusion assemblage (FIA) method (Goldstein and Reynolds, 1994) was used to evaluate the validity of microthermometric data. For spatially close fluid inclusions that cannot be strictly defined as FIAs, large variations in vapour percentage or homogenization temperature are still considered to indicate heterogeneous trapping or post-trapping modification (Chi and Lu, 2008). Microthermometry was carried out with a Linkam THMSG 600 heating/freezing stage in the Geofluids Laboratory at the University of Regina. The stage was calibrated with synthetic fluid inclusions of H_2O (ice-melting temperature = 0 °C; critical temperature = 374.1 °C) and H_2O-CO_2 (CO_2-melting temperature = -56.6 °C). The precision of the measured ice-melting temperature is ±0.2°C, and that for the homogenization temperature is ±2°C.

Fluid inclusion plane measurement

The orientations of FIPs (strike, dip direction, and dip angle) are measured from horizontally and vertically cut doubly polished sections with a conventional petrographic microscope, as described in Liu et al. (2011). The strike of the FIP is estimated by rotating the microscope stage to measure the angle between the strike of the FIP and the marked orientation on the section. The dip angle of the FIP was determined by changing the focus on different depths of the FIP as described below. First, the stage is rotated so that the FIP is oriented N-S, and focus is made on the upper part of the FIP. After recording the readings of the FIP on the horizontal crosshair (H_1) and the focusing screw (V_1), the focus is then changed to the lower part of the FIP, and new readings of both parameters (H_2, V_2) are recorded. The horizontal displacement of the focus of the FIP (ΔH) is equal to (H_2-H_1) multiplied by the length per unit for the objective used (e.g., for the x50 objective the length per unit is 2 mm). The vertical displacement of the focus of the FIP (ΔV) is equal to (V_2-V_1) multiplied by the depth per unit reading, which can be obtained by using a slide of known thickness. The dip angle (α) can then be calculated from the equation $\alpha = \tan^{-1}(\Delta V/\Delta H)$.

Raman spectrometry

Raman analysis was carried out with a Renishaw

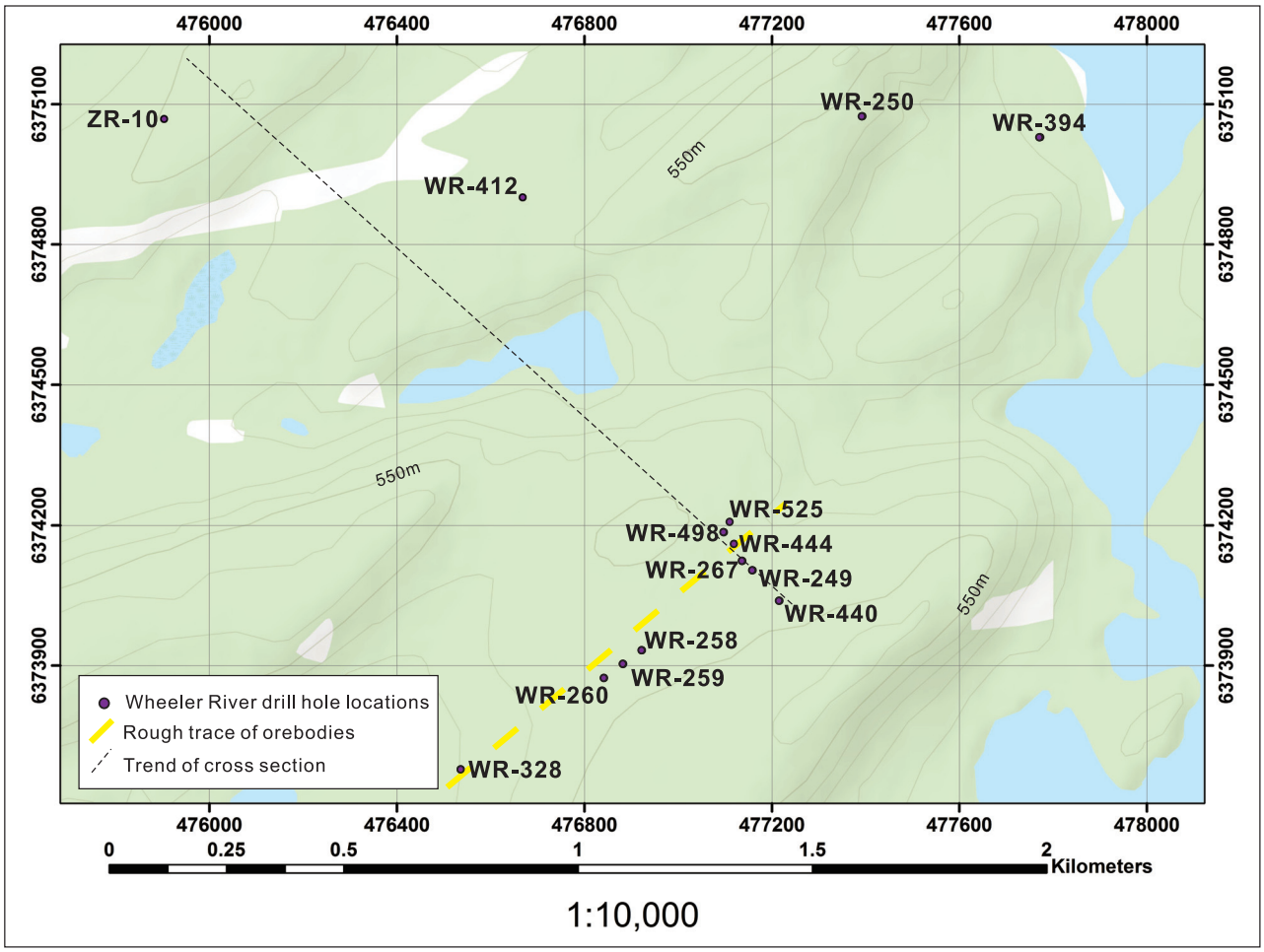

Figure 2. A map showing the locations of diamond drill holes studied from the Wheeler River area.

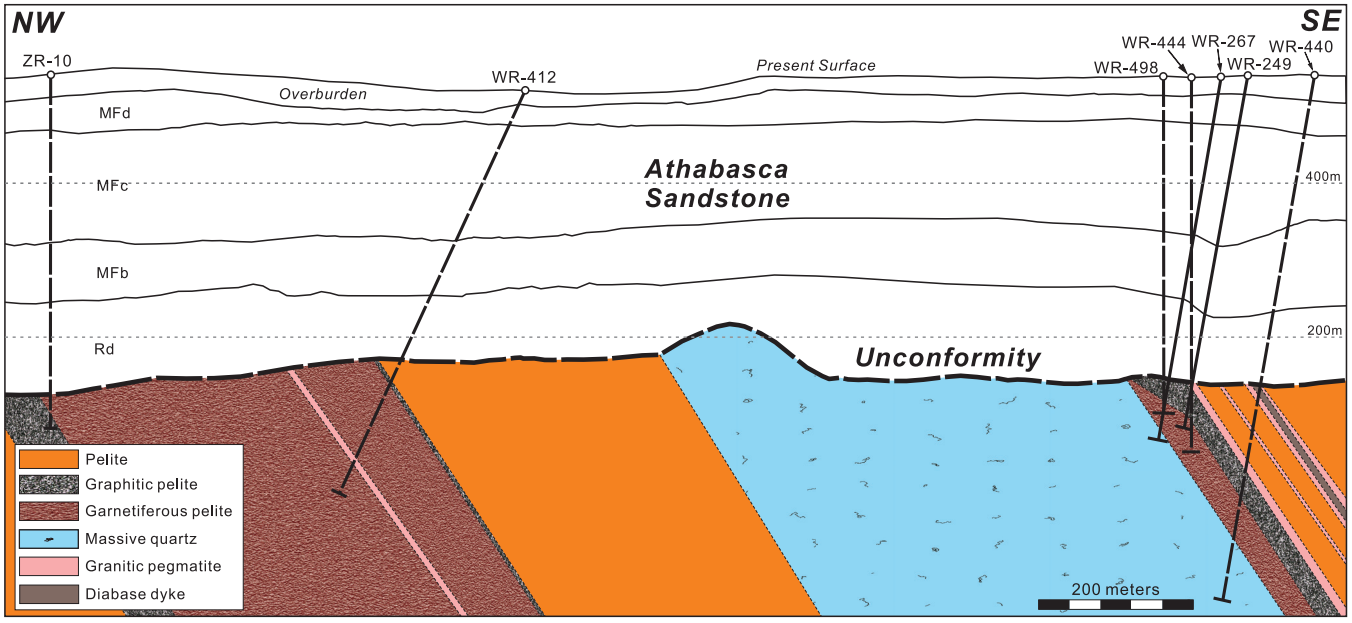

Figure 3. A schematic NW-SE cross section of the Phoenix deposit and neighboring area. Note only drill holes examined are shown (modified from Arseneau and Revering, 2010); the mineralization and the fault zones are not shown due to the limitation of the horizontal scale. Sandstone units: Rd = Read Formation, MF = Manitou Falls Formations: MFb = Bird Member, MFc = Collins Member, MFd = Dunlop Member.

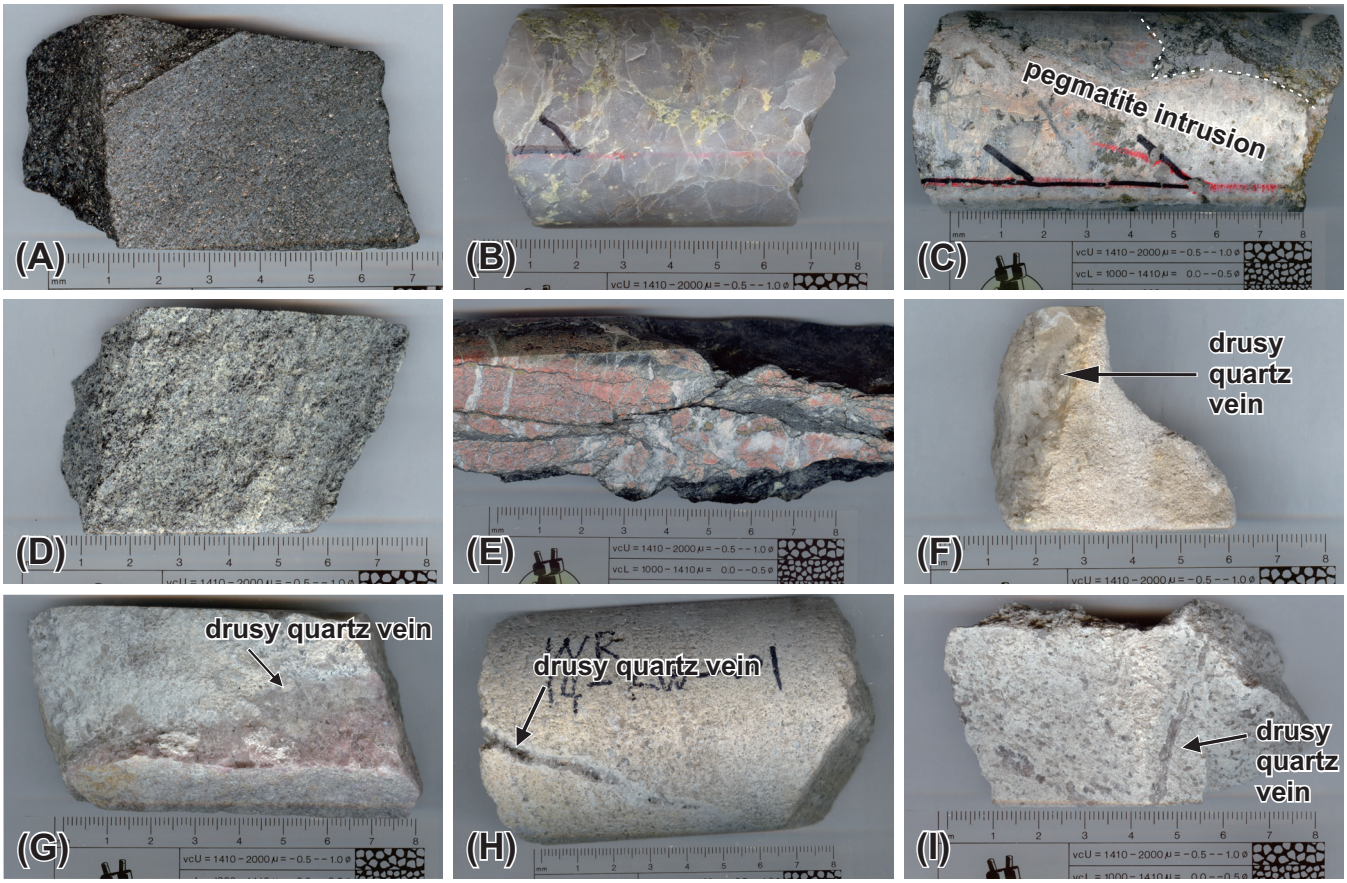

Figure 4. Photographs of drill core samples showing representative lithological units from the basement and the Athabasca Basin. A) Garnetiferous pelite with interstitial graphite (WR-440, 618.8m). B) Oriented sample of massive quartz (WR-440, 674m). C) Pegmatite intrusion cut by a calcite vein with minor quartz (WR-440, 479.6m). D) Weakly mineralized graphitic pelite (WR-328, 394.2m). E) Granitic pegmatite cut by black graphite-filled fractures (WR-440, 603m). F) Drusy quartz cutting intensely clay-altered sandstone (14-KW-046, WR-267). G) Drusy quartz cutting silicified sandstone (WR-328, 348.9m). H) Drusy quartz vein cutting weakly clay-altered sandstone (WR-525, 355.3m). I) Drusy quartz cutting strongly clay-altered granite (WR-560, 736m).

RM2000 laser Raman spectroscope at the Geofluids Laboratory of the University of Regina. The excitation laser wavelength is 514 nm, the grating is 1800, and the objective is x50 on the long working distance setting. For graphite analysis, as advised by Beyssac et al. (2003), the laser was focused on graphite below a contacting transparent mineral on the thin section surface, to avoid the polish defect typically developed on the surface of carbonaceous materials (Fig. 5). For each sample, six data points were analyzed, each with a 30-second acquisition time, in order to check the within-sample structural heterogeneity (Beyssac et al., 2002, 2003; Sadezky et al., 2005; Lahfid et al., 2010). We focused on the 1000–2000 cm^{-1} region, which includes all the first-order bands, and on 2000–3500 cm^{-1} for the second-order region (Beyssac et al., 2002, 2003; Sadezky et al., 2005; Lahfid et al., 2010).

Results

Petrographic and microthermometric study of fluid inclusions

Several types of aqueous fluid inclusions were identified in the drusy quartz from the sandstones above the unconformity, including: 1) biphase inclusions dominated by liquid with vapour percentage mainly from 5 to 13 % (Fig. 6A); 2) inclusions having a halite crystal at room temperature (Fig. 6B); 3) biphase inclusions with intermediate to very large vapour percentages (Fig. 6C); and 4) vapour-only inclusions (Fig. 6D). These inclusions occur randomly, as isolated inclusions or inclusion clusters, or along growth zones in the quartz (Fig. 6E). Based on the of FIA concept, fluid inclusions showing variable vapour percentages within a spatially close group (Fig. 6C.) are interpreted to have been heterogeneously entrapped, and only the inclusion with the lowest vapour percentage (hence homogenization temperature) is adopted (Goldstein and Reynolds, 1994; Chi and Lu, 2008). Therefore, most fluid inclusions examined are liquid-dominated biphase inclusions with a relatively consistent vapour percentage, with derived homogenization temperatures (T_h) mainly from 80 to 135 °C (L+V→L) (Fig. 7), ice-melting temperatures ranging from -23.6 to -33.6 °C, and corresponding salinities from 23.6 to 26.8 eq. wt. % NaCl, as calculated with the program of Chi and Ni (2007).

These T_h and salinity values (Fig. 7) are generally within the ranges reported for other unconformity-related uranium deposits and quartz overgrowths in the Athabasca Basin (e.g. Pagel et al., 1980; Kotzer and Kyser, 1995; Derome et al.,

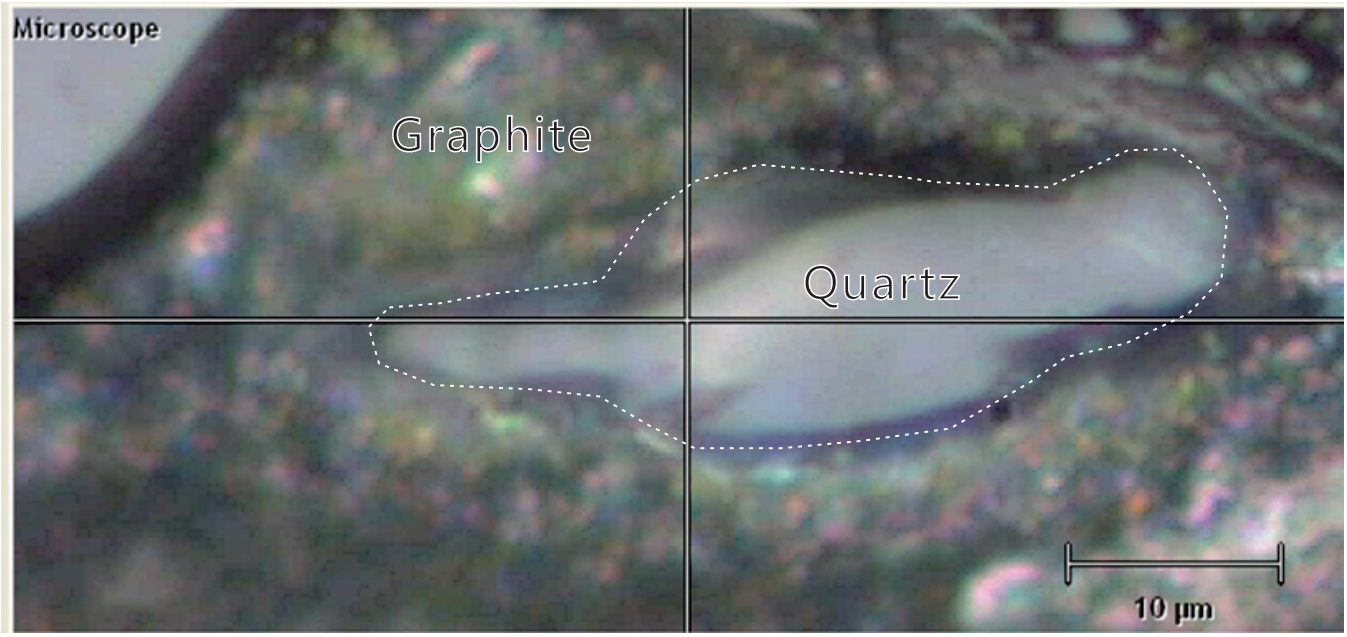

Figure 5. Photomicrograph showing a grain of quartz covering a graphite flake (14-KW-051).

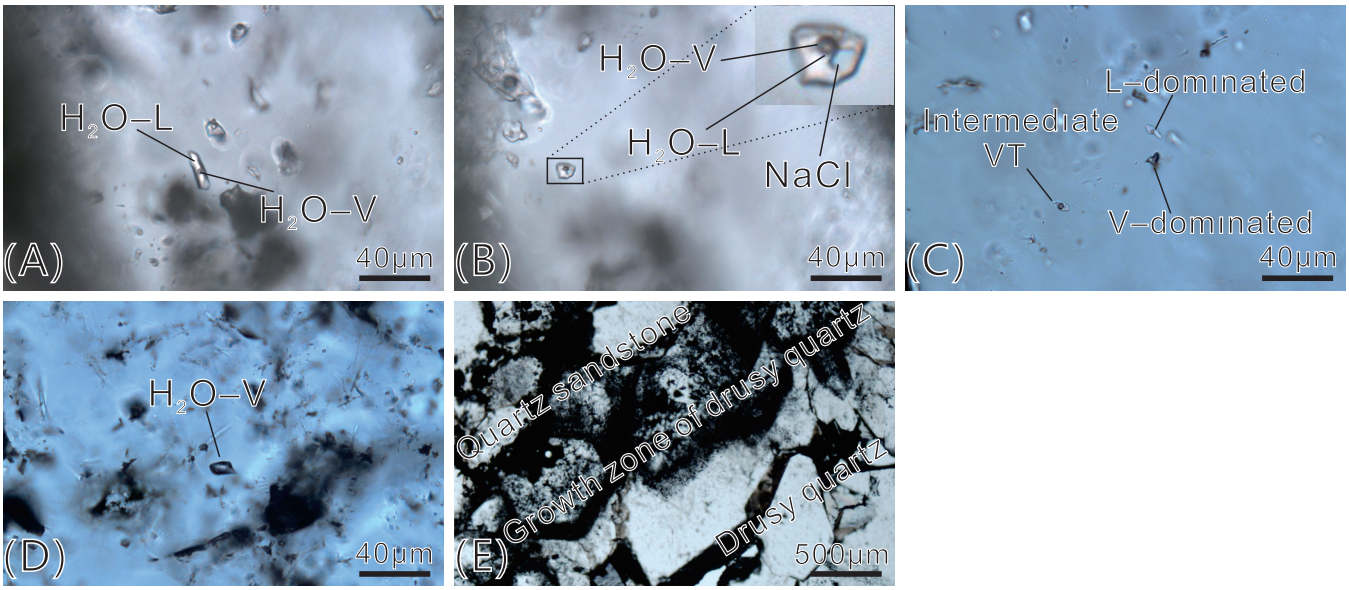

Figure 6. Microphotographs illustrating the types and occurrences of fluid inclusions in drusy quartz from the Manitou Falls Formation. A) Biphase aqueous fluid inclusions with relatively constant V/T ratios in a growth zone (WR-250, 341.8m). B) An isolated aqueous fluid inclusion with a halite cube (WR-250, 341.8m). C) A trail of fluid inclusions with variable V/T ratios (WR-328, 369.8m). D) A vapour-only inclusion (WR-328, 369.8m).

2005; Scott et al., 2011), although the T_h values are limited to the lower end of the spectrum. The abundance of vapour-only aqueous inclusions and their coexistence with biphase aqueous inclusions suggest boiling during the formation of the drusy quartz. This, together with the relatively low homogenization temperatures, indicates that the drusy quartz may have been formed during the waning stages of the uranium mineralization process, at lower pressures and temperatures than the main phase of mineralization.

Both aqueous and CO_2-dominated inclusions were found in the basement rocks. CO_2-dominated inclusions are well developed in densely distributed, parallel microfractures in the massive and pegmatoid quartz in the basement (Fig. 8A). These inclusions generally consist of three phases (vapour CO_2, liquid CO_2 and liquid water; Fig. 8B) or two phases (vapour CO_2 and liquid CO_2, without visible aqueous phase; Fig. 8C) at room temperature. Some biphase aqueous fluid inclusions with approximately 10 % of vapour also occur along the same microfractures as the CO_2-dominated fluid inclusions (Figs. 8B and C).

The CO_2-dominated inclusions in the basement were likely entrapped before the formation of the Athabasca Basin

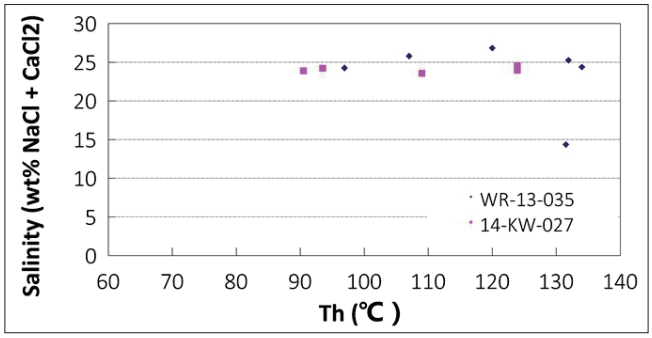

Figure 7. Homogenization temperature (T_h) versus salinity diagram for the studied aqueous inclusions (in WR-250, 341.8m and WR-328, 369.8m).

and uranium mineralization, probably in the retrograde metamorphic stage of Trans-Hudson orogenesis. Some of the microfractures formed at this stage may have been re-opened during the formation of the Athabasca Basin, facilitating circulation of basinal brines into the basement. Mercadier et al. (2010) provided evidence of such re-activation of pre-existing fractures in basement rocks, with infiltration of basinal brines, proximal to the P-Patch deposit along the southern margin of the basin.

Microstructural study of fluid inclusion planes

The orientations of (FIP) were measured for an oriented sample of a dolomite-quartz vein cutting graphitic metapelite in the basement (Fig. 9A, WR-440, 604.1m). Two main sets of subvertical FIPs were observed in the euhedral quartz from the vein in a horizontally-cut oriented thin section (Fig. 9B): one striking 190–210° and the other striking 90–110° (Fig. 9C). One set is long and is perpendicular or sub-perpendicular to the foliation of the host rock, whereas the other set is relatively short and is parallel or sub-parallel to the foliation. Mutual crosscutting relationships are not evident in this thin section, therefore the relative timing of the two sets remains uncertain. Vertically-cut oriented thin sections from the same drill core also show that subvertical FIPs are dominant (Fig. 10), indicating that the data obtained from the horizontally-cut thin section are not biased. The fluid inclusions entrapped in the FIPs in the horizontally-cut thin section were generally too small to conduct microthermometric measurements.

The FIPs are interpreted as simple Mode I extension fractures, therefore the pole to an FIP corresponds to the minimum principal stress (σ3) direction of the stress field (Lespinasse and Pecher, 1986; Lespinasse, 1999). Accord-

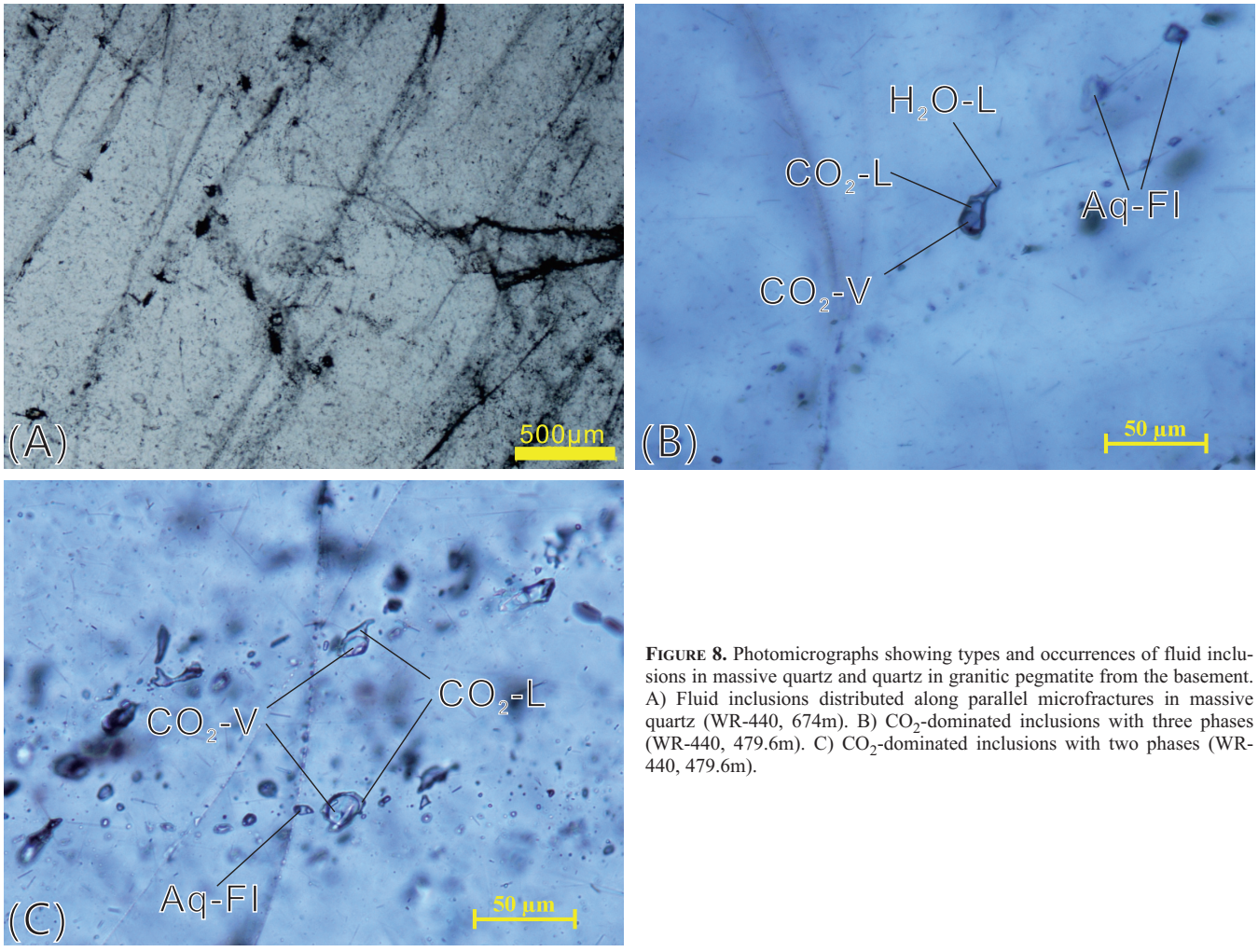

Figure 8. Photomicrographs showing types and occurrences of fluid inclusions in massive quartz and quartz in granitic pegmatite from the basement. A) Fluid inclusions distributed along parallel microfractures in massive quartz (WR-440, 674m). B) CO_2-dominated inclusions with three phases (WR-440, 479.6m). C) CO_2-dominated inclusions with two phases (WR-440, 479.6m).

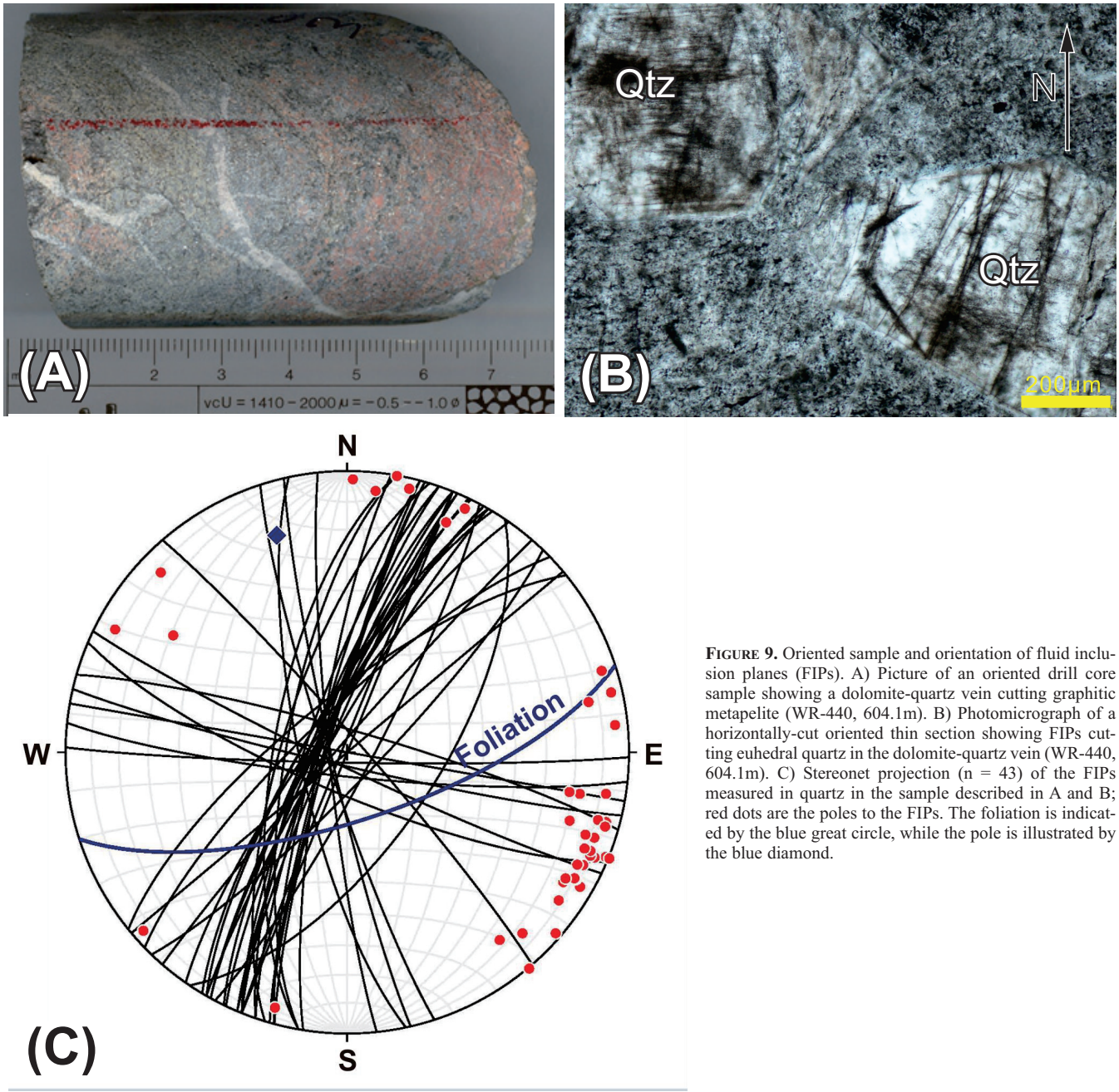

Figure 9. Oriented sample and orientation of fluid inclusion planes (FIPs). A) Picture of an oriented drill core sample showing a dolomite-quartz vein cutting graphitic metapelite (WR-440, 604.1m). B) Photomicrograph of a horizontally-cut oriented thin section showing FIPs cutting euhedral quartz in the dolomite-quartz vein (WR-440, 604.1m). C) Stereonet projection (n = 43) of the FIPs measured in quartz in the sample described in A and B; red dots are the poles to the FIPs. The foliation is indicated by the blue great circle, while the pole is illustrated by the blue diamond.

ingly, the two main directions of FIPs discussed above are considered to be related to two different stress fields, one stage with the σ3 direction trending WNW- ESE and another stage with σ3 direction trending NNW- SSE. It remains to be determined whether the maximum principal stress (σ1) and intermediate principal stress (σ2) also switched between horizontal and vertical directions. If σ1 was vertical, both σ2 and σ3 must have been horizontal, and the FIPs formed in the vertical plane. However, subvertical FIPs could still have formed if σ1 was horizontal but in that case one cannot discriminate if σ2 or σ3 was the vertical stress. In short, the dominance of subvertical FIPs may indicate an extensional stress field (σ1 vertical), but the possibility of a compressional stress field (σ1 horizontal) cannot be ruled out.

Petrographic and Raman spectroscopic study of graphite

A suite of samples of graphitic metapelite were collected from the alteration zones hosting the uranium mineralization near the unconformity down to the relatively unaltered basement in drill core of WR-267. Three samples have been selected with increasing distance from the lower boundary of the major uranium concentration: 14-KW-048 (5 m), 14-KW-051 (15 m), 14-KW-053 (25 m). The graphite in the samples was examined with a petrographic microscope and a Raman spectrometer.

Petrographic observations of graphite indicate that the graphite closer to the uranium mineralization has more jagged grain boundaries than that further from the uranium mineralization (Fig. 11).

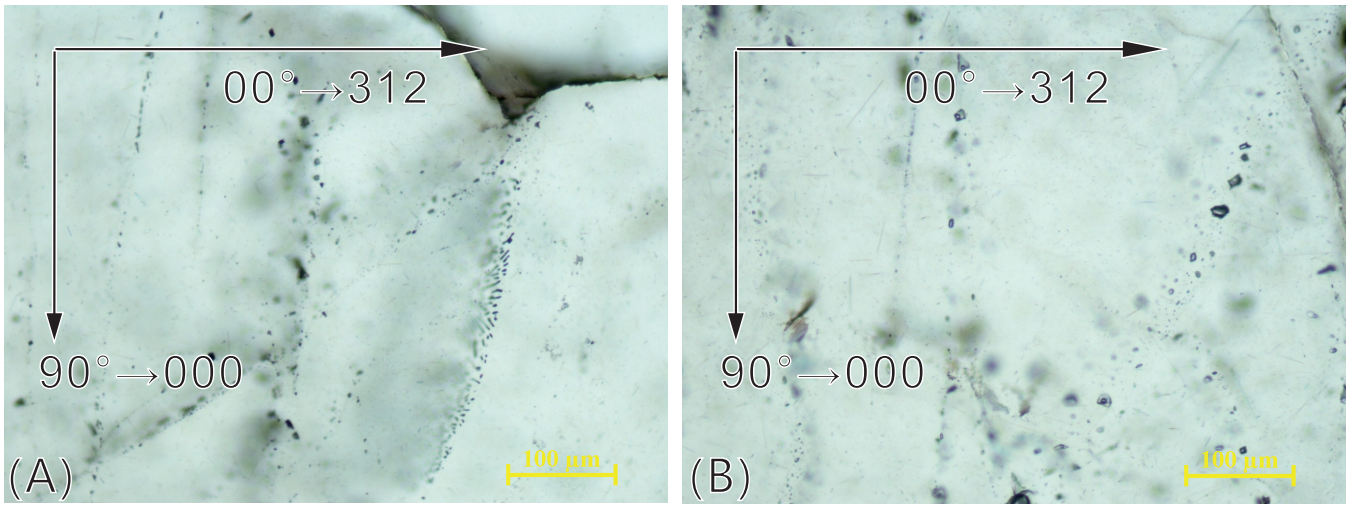

Figure 10. Photomicrographs of vertically-cut oriented thin sections showing the dominance of subvertical FIPs in pegmatoid quartz from a pegmatite vein (WR-440, 479.6m). Note the FIPs comprise CO_2-dominated fluid inclusions, biphase aqueous inclusions and monophase aqueous inclusions.

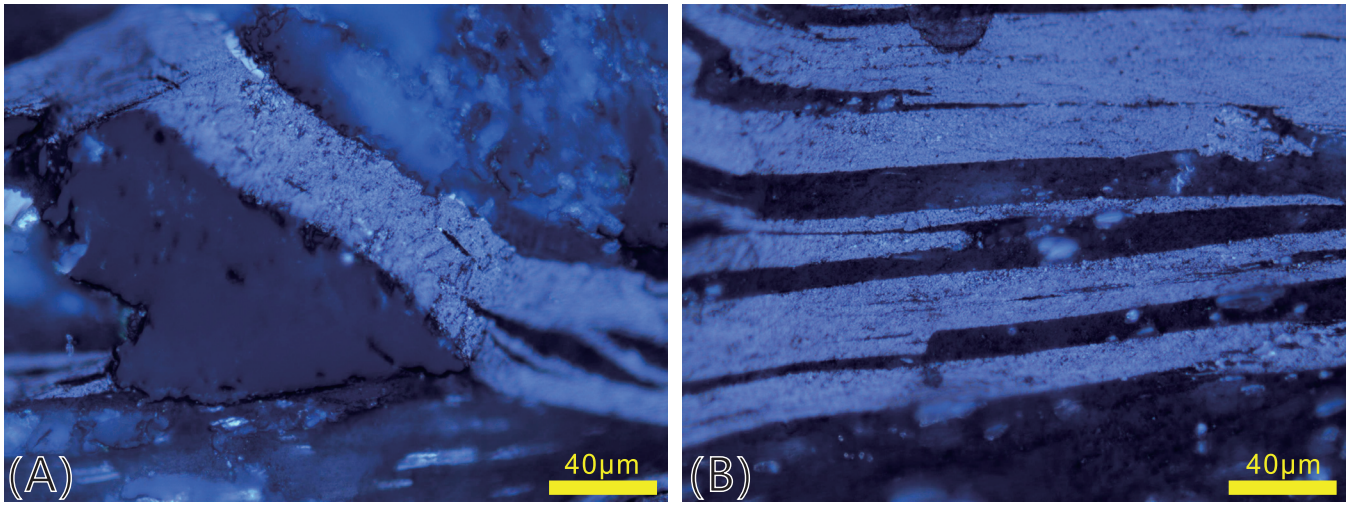

Figure 11. Photomicrographs showing graphite in reflected light: A) in metapelite 5m from orebody (WR-267, 414.1m); and B) in metapelite 25m from orebody (WR-267, 433m).

The Raman spectra of the three samples located at different distances from the mineralized zone, as described above, are shown in Figure 12. All of the spectra show a prominent G band (~1583 cm^{-1}) in the first-order region (Fig. 12A), indicative of well-crystallized graphite (Beyssac et al., 2002, 2003; Sadezky et al., 2005; Lahfid et al., 2010). However, graphite in sample 14-KW-048 (red), which is closest to the mineralization zone, appears to have more obvious D1 and D2 bands (~1367 cm^{-1} and 1609 cm^{-1}), which are related to defects in graphite (Beyssac et al., 2002). In contrast, the spectrum of the sample furthest from the mineralization zone, 14-KW-053 (blue; Fig. 12A), shows almost no additional bands to the G band. The spectra in the second-order region are similar among the three samples (Fig. 12B), although 14-KW-048 appears to have a higher contribution of S2 bands than other samples.

Although some studies suggested that graphitization is an irreversible process (Beyssac et al., 2002), a gradual loss of the structural ordering of graphite toward some uranium deposits in the Athabasca Basin has been demonstrated by Wang et al. (1989) and Pascal et al. (2015). In this study, the higher D1 and S2 intensities of the sample closest to the mineralization zone than those away from it, as described above, also suggest that the graphite near the mineralization is relatively disordered.

Summary and implications for exploration

Collectively, the field and petrographic observations, coupled with preliminary fluid inclusion analysis, support previous studies (e.g. Jefferson et al., 2007 and references therein) that noted different structural regimes and fluid systems were developed in the pre-Athabasca stage versus the syn- to post-Athabasca, uranium mineralization stages. The pre-Athabasca stage was characterized by ductile deformation as demonstrated by the development of foliation, followed by pegmatization, massive silicification, and circula-

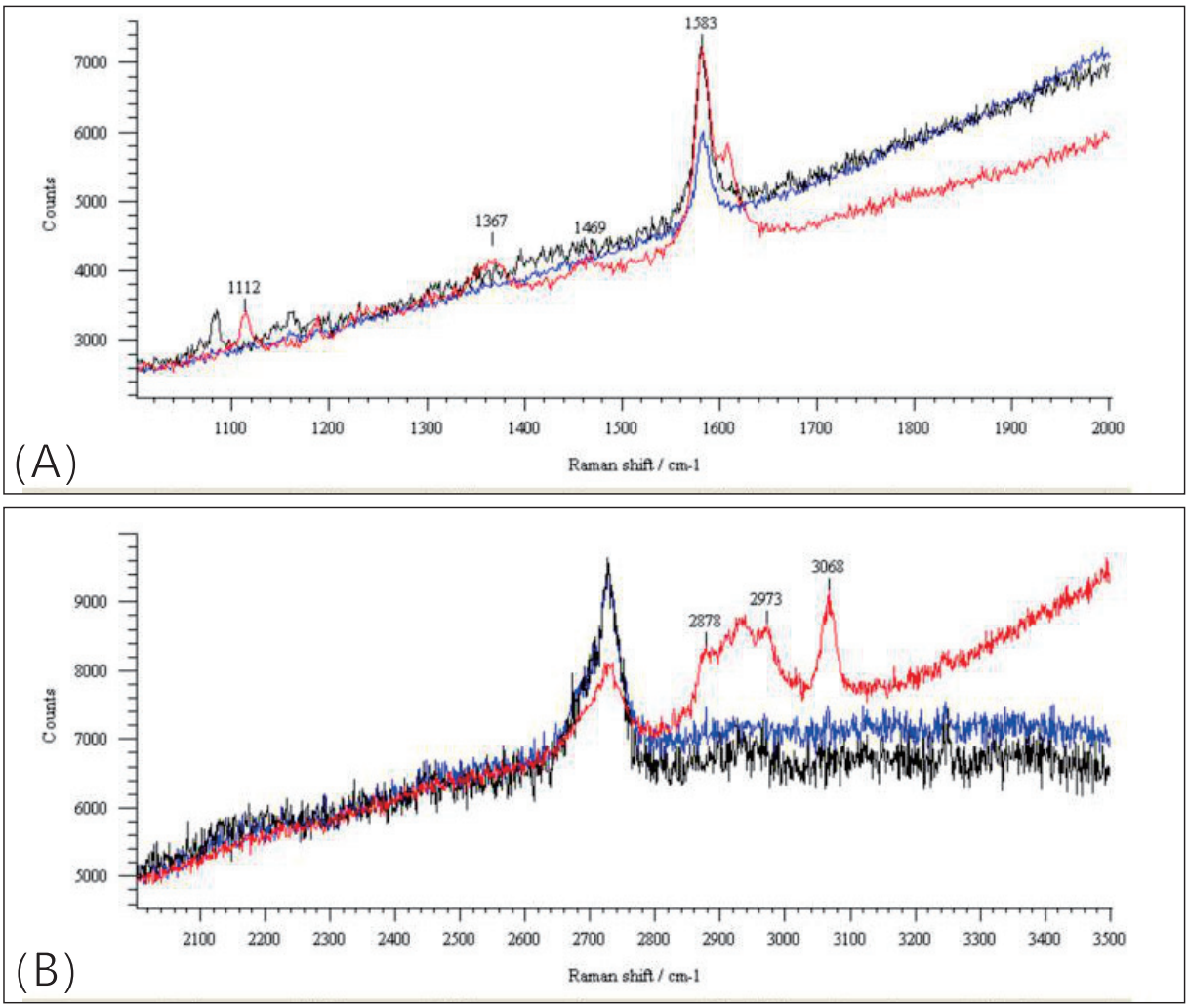

Figure 12. Representative Raman spectra of graphite of three samples with different distances from the ore zone. A) In the first-order region; Red: 14-KW-048, 5m from ore zone; Black: 14-KW-051, 15m from the ore zone; and Blue: 14-KW-053, 25m from the ore zone. B) In the second order region; Red: 14-KW-048, 5m from ore zone; Black: 14-KW-051, 15m from ore zone; and Blue: 14-KW-053, 25m from the ore zone.

tion of metamorphic fluids in a relatively high *P–T* environment, as indicated by the abundance of CO_2-bearing fluid inclusions. In contrast, the syn- to post-Athabasca stages were characterized by brittle deformation, as reflected by the development of fractures filled by drusy quartz in the basal Athabasca Group and the uppermost part of the basement, and by circulation of basinal brines in a relatively low *P–T* environment, as recorded by the aqueous fluid inclusions in the drusy quartz. Furthermore, the fluid may have experienced boiling at this stage, as indicated by the coexistence of vapour-only and biphase aqueous inclusions, again pointing to a relatively low *P* environment. Fluid boiling has been recognized in many other Proterozoic uranium deposits in northern Canada (Chi et al., 2014), and its significance for uranium mineralization is the subject of several on-going studies, including this one. It remains to be investigated whether the low fluid pressure that appears to have instigated boiling was caused by faulting, i.e. through the fault-valve or seismic pumping mechanisms (Sibson et al., 1988; Sibson, 1994), or was related to a shallow, epithermal environment. These structural-fluid relationships and associated geochemical signatures are potentially important for uranium exploration.

Preliminary FIP orientation studies indicate that subvertical microfractures are developed in the basement rocks, likely after the ductile deformation stage. These microfractures, dominantly subvertical, suggest that the local stress field in the Phoenix deposit may have been extensional at certain periods of time in the post-Athabasca, brittle deformation stage, although the subvertical FIPs may also have formed in a compressional regime.

The close spatial relationship between uranium mineralization and graphitic units in the basement in the Phoenix deposit, as also observed in many other unconformity-related uranium deposits, suggests that graphite played a role in uranium mineralization. However, its exact role remains unclear — was it directly involved in reducing U^{6+} in the fluids, or was it the precursor to hydrocarbons that acted as the reductants for uraninite precipitation? More work on fluid inclusion composition, especially the volatile components, is

being conducted to address this question. Preliminary Raman spectroscopic studies of graphite samples from different localities suggest that the graphite becomes increasingly disordered toward the ore zone. This trend, if confirmed by further studies (ongoing), could be used as an indicator of mineralization.

Acknowledgments

Funding for this research was provided by the Targeted Geoscience Initiative 4 (TGI-4) uranium ore systems project, through a grant to K.M. Bethune and G. Chi, and in part by a NSERC-Discovery grant (to G. Chi). Logistical support from Denison Mines Corp., and assistance from Clark Gamelin, Yongxing Liu, Zenghua Li and Morteza Rabiei during the field work are gratefully acknowledged. The paper has benefited from the review by Antonin Richard and detailed review and editing of Eric Potter.

References

Arseneau, G., and Revering, C., 2010. Technical report on the Phoenix deposit (Zones A & B) - Wheeler River project, eastern Athabasca Basin, Northern Saskatchewan, Canada; NI 43-101 technical report prepared for Denison Mines Corp., by SRK Consulting, 95 p.

Beyssac, O., Goffé, B., Chopin, C., and Rouzaud, J.-N., 2002. Raman spectra of carbonaceous material in metasediments: a new geothermometer; Metamorphic Geology, v. 20, p. 859–871.

Beyssac, O., Goffé, B., Petitet, J.P., Froigneux, E., and Rouzaud, J.-N., 2003. On the characterization of disordered and heterogeneous carbonaceous materials using Raman spectroscopy; Spectrochimica Acta Part A, v. 59, p. 2267–2276.

Card, C., Pana, D., Portella, P, Thomas, D.J., and Annesley, I.R., 2007. Basement rocks of the Athabasca Basin, Saskatchewan and Alberta; in EXTECH IV: Geology and Uranium EXploration TECHnology of the Proterozoic Athabasca Basin, Saskatchewan and Alberta, (ed.) C.W. Jefferson and G. Delaney; Geological Survey of Canada, Bulletin 588, p. 69–87.

Chi, G., and Ni, P., 2007. Equations for calculation of NaCl/(NaCl+$CaCl_2$) ratios and salinities from hydrohalite-melting and ice-melting temperatures in the H_2O-NaCl-$CaCl_2$ system; Acta Petrologica Sinica, v. 23, p. 33–37.

Chi, G., Liang, R., Ashton, K., Haid, T., Quirt, D., Fayek, M. 2014. Evidence of fluid immiscibility from uranium deposits in northern Saskatchewan and Nunavut and potential relationship with uranium precipitation; 2014 GAC-MAC Annual Conference, Program with Abstracts, v. 37, p. 57.

Chi, G. and Lu, H. 2008. Validation and representation of fluid inclusion microthermometric data using the fluid inclusion assemblage (FIA) concept; Acta Petrologica Sinica, v. 24, p. 1945–1953.

Dann, J., Hattori, K., Potter, E.G., and Sorba, C., 2013. Discrimination of elemental assemblages in the alteration halo of the Phoenix deposit, Saskatchewan, through applied GIS; Geological Survey of Canada, Open File 7463. doi:10.4095/293122

Derome, D., Cathelineau, M., Cuney, M., Fabre, C., Lhomme, T., and Banks, D. A., 2005. Mixing of sodic and calcic brines and uranium deposition at McArthur River, Saskatchewan, Canada: A Raman and laser-induced breakdown spectroscopic study of fluid inclusions; Economic Geology, v. 100, p. 1529–1545.

Gamelin, C., Sorba, C., and Kerr, W., 2010. The discovery of the Phoenix Deposit: A new high-grade Athabasca Basin unconformity-type uranium deposit, Saskatchewan, Canada; Saskatchewan Geological Survey Open House, 2010 Abstract Volume, p. 17.

Goldstein, R.H. and Reynolds, T.J. 1994. Systematics of fluid inclusions in diagenetic minerals; SEPM Short Course, v. 31, 199 p.

Hoeve, J., and Sibbald, T.I., 1978. On the genesis of Rabbit Lake and other unconformity-type uranium deposits in northern Saskatchewan, Canada; Economic Geology, v. 73, p. 1450–1473.

Jefferson, C.W., Thomas, D.J., Gandhi, S.S., Ramaekers, P., Delaney, G., Brisbin, D., Cutts, C., Portella, P. and Olson, R.A., 2007. Unconformity-associated uranium deposits of the Athabasca basin, Saskatchewan and Alberta; in EXTECH IV: Geology and Uranium EXploration TECHnology of the Proterozoic Athabasca Basin, Saskatchewan and Alberta, (ed.) C.W. Jefferson and G. Delaney; Geological Survey of Canada, Bulletin 588, p. 23–67.

Kerr, W.C., 2010. The discovery of the Phoenix deposit: a new high-grade Athabasca Basin unconformity-type uranium deposit, Saskatchewan, Canada; in The Challenge of Finding New Mineral Resources: Global Metallogeny, Innovative Exploration, and New Discoveries, Volume II: Zinc-Lead, Nickel-Copper-PGE, and Uranium, (ed.) R.J. Goldfarb, E.E. Marsh and T. Monecke; Society of Economic Geologists, p. 703–725.

Kotzer, T., Kyser, T., 1995. Petrogenesis of the Proterozoic Athabasca Basin, northern Saskatchewan, Canada, and its relation to diagenesis, hydrothermal uranium mineralization and paleohydrogeology; Chemical Geology, v. 120, p.45–89.

Lahfid, A., Beyssac, O., Deville, E., Negro, F., Choppin, C., and Goffé, B., 2010. Evolution of the Raman spectrum of carbonaceous material in low-grade metasediments of Glarus Alps (Switzerland); Terra Nova, v. 22, p. 354–360.

Lespinasse, M., Pecher, A., 1986. Microfracturing and regional stress field: a study of preferred orientations of fluid inclusion planes in a granite from the Massif Central, France; Journal of Structural Geology, v. 8, p. 169–180.

Lespinasse, M., 1999. Are fluid inclusion planes useful in structural geology?; Journal of Structural Geology, v. 21, p.1237–1243.

Liu, Y., Chi, G., Bethune, K.M., and Dube, B., 2011. Fluid dynamics and fluid-structural relationships in the Red Lake mine trend, Red Lake greenstone belt, Ontario, Canada; Geofluids, v. 11, p. 260–279.

Mercadier, J., Richard, A., Boiron, M.C., Cathelineau, M., Cuney, M., 2010. Migration of brines in the basement rocks of the Athabasca Basin through microfracture networks (P-Patch U deposit, Canada); Lithos, v. 115, p. 121–136.

Pagel, M., Poty, B., Sheppard, S.M.F., 1980. Contribution to some Saskatchewan uranium deposits mainly from fluid inclusion and isotopic data; in International Uranium Symposium on the Pine Creek Geosyncline, International Atomic Energy Agency, Vienna, p. 639–654.

Pascal, M., Ansdell, K.M., and Annesley, I.R., 2015. Graphite-bearing and graphite-depleted basement rocks in the Dufferin Lake zone, south-central Athabasca Basin, Saskatchewan; *in* Targeted Geoscience Initiative 4: unconformity-related uranium systems, (ed.) E.G. Potter and D.M. Wright; Geological Survey of Canada, Open File 7791, p. 83-92. doi:10.4095/295776

Power, M.J., Hattori, K., Sorba, C., and Potter, E.G., 2012. Geochemical anomalies in the soil and uppermost siliciclastic units overlying the Phoenix uranium deposit, Athabasca Basin, Saskatchewan; Geological Survey of Canada, Open File 7257, 36 p. doi:10.4095/291981

Sadezky, A., Muckenhuber, H., Grothe, H., Niessner, R., and Pöschl, U., 2005. Raman microspectroscopy of soot and related carbonaceous materials: spectral analysis and structural information; Carbon, v. 43, p. 1731–1742.

Scott, R., Chi, G., and Bosman, S., 2011. A petrographic and fluid inclusion study of the Athabasca Group sandstones from the Rumpel Lake drill core, Athabasca Basin, Northern Saskatchewan; in Summary of Investigations 2011, volume 2, Saskatchewan Geological Survey, Miscellaneous Report 2011-4.2, Paper A5, 10 p.

Sibson, R.H., 1994. Crustal stress, faulting and fluid flow; Geological Society Special Publications, v. 78, p. 69–84.

Sibson, R.H, Robert, F., and Poulsen, K.H., 1988. High angle reverse faults, fluid pressure cycling, and mesothermal gold-quartz deposits; Geology, v. 16, p. 551–555.

Wang, A., Dhamelincourt, P., Dubessy, J., Guerard, D., Landais, P., and Lelaurain, M., 1989. Characterization of graphite alteration in an uranium deposit by micro-Raman spectroscopy, X-Ray diffraction, transmission electron microscopy and scanning electron microscopy; Carbon, v. 27, p. 209–218.

Geometric and Hydrodynamic Modelling and Fluid-structural Relationships in the Southeastern Athabasca Basin and Significance for Uranium Mineralization

Zenghua Li[1], Guoxiang Chi[1], Kathryn M. Bethune[1], Sean A. Bosman[2] and Colin D. Card[2]

1. Department of Geology, University of Regina, Regina, Saskatchewan, S4S 0A2

2. Saskatchewan Geological Survey, Saskatchewan Ministry of the Economy, Regina, Saskatchewan, S4P 2H9

Abstract

Unconformity-type uranium deposits in the Athabasca Basin are spatially associated with reactivated basement faults intersecting the unconformity surface. However, questions such as what special factors focused fluid flow along and within fault zones, and why some faults are more fertile than others, are still unclear. This study aims to tackle these questions through examination of the southeastern Athabasca Basin. First, a basement structural map was compiled based on basement geophysical signatures, which shows three dominant sets of faults trending NE, NW, and NNW. A 3D model of the sub-Athabasca unconformity was constructed with GoCAD® using publicly available geological and drill-hole data, revealing a number of dominantly NE-trending ridges and valleys. These unconformity topographic features are interpreted to be the products of the combined action of three main factors: 1) pre-Athabasca group ductile faulting and alteration; 2) differential weathering and erosion; and 3) post-Athabasca reactivation of pre-existing, graphite-rich ductile shear zones. The basin-scale numerical modelling of hydrodynamics indicates that fluid pressures in the Athabasca Basin were close to hydrostatic throughout its sedimentary history, and that thermal convection cells may have been well developed in the lower part of the basin, particularly below the Wolverine Point Formation aquitard. The modeling results also show that individual convection cells are less than 2 km, implying that individual mineralization centres, if controlled by thermal convection, may be spaced at just a few kilometers. Local-scale numerical modelling of fluid flow indicates that the location and spacing of basement faults influence thermally-driven fluid convection. In a model with an isolated fault, the fault coincides with an upwelling plume. In the case of two faults, the faults may coincide with upwelling flow or alternatively be centrally located below convection cells, depending on fault spacing. In the latter case, fluid may flow into and out of individual fault zones. Modelling of fluid-flow in response to mechanical compression suggests that fluid migrates up the fault during compression, and that the models with the most shallowly dipping fault and those with offset on the fault have slightly greater flow rates than the other models. The various relationships between fluid-flow and faults can explain why some faults are more favourable for fluid flow than others, which may be potentially used to evaluate whether a given structure has the potential to host mineralization.

Introduction

Unconformity-type uranium deposits are the largest known high-grade deposits of uranium in the world. A common feature is their close spatial association with reactivated basement faults intersecting the unconformity surface (Jefferson et al., 2007). However, significant gaps remain in our understanding of these deposits. One important question concerns what special factors focused fluid flow at specific sites within the basin, especially along fault zones and within wider structural zones, and why some faults are more prospective than others. While recent studies advocate that fluid flow was either downward into basement fault zones ("ingress" deposits), or upward and outward from such zones ("egress" deposits), and that these systems were potentially linked (Jefferson et al., 2007), the dynamics involved remain poorly understood. It has been proposed that the fluid flow related to uranium mineralization in the Athabasca Basin was driven by thermally induced fluid convection (Raffensperger and Garven, 1995), but little is known about the sizes of the convection cells and how these may affect the localization of mineralization. There is also the question of whether ingress flow and egress flow were associated with alternating compressional and extensional stress fields, accompanied by fluid pressure fluctuation (Cui et al., 2012). Finding answers to these questions is of economic significance, because it will help to discriminate between fault-fluid-alteration/lithology combinations fertile for uranium mineralization and those that are less prospective.

This study focused on the southeastern Athabasca Basin, which hosts all of Canada's current producing unconformity-related uranium mines, to tackle these questions. First, a basement structural map was compiled in GoCAD® based on geophysical data (Card et al., 2010). This was subsequently combined with a 3D model of the unconformity surface constructed using drill-hole data (data from Geological Atlas of Saskatchewan) to illustrate the relationships between basement structures, the unconformity surface topography and uranium mineralization. The basin-scale hydrodynamic background was then analyzed based on fluid pressure modeling, which was used as the initial conditions for numerical modelling of heat and deformation related fluid flow. Simulations of thermal convection, with consideration of the influence of basement faults and their spacing on convection cells, and fluid flow in response to compressional stresses, taking into account different orientations of the faults, were carried out using FLAC3D® software. FLAC3D® is a finite difference code capable of simulating the interaction of fluid flow, tectonic deformation, and heat transport based on various material constitutive models (Itasca, 2012). Finally, the significance of the modelling results for localization of uranium deposits was examined. Some of the study results have been published (Li et al., 2013, 2014a and b; Chi et al., 2014), and more modelling is

Li, Z., Chi, G., Bethune, K.M., Bosman, S.A., and Card, C.D., 2015. Geometric and Hydrodynamic Modelling and Fluid-structural Relationships in the Southeastern Athabasca Basin and Significance for Uranium Mineralization, *in* Targeted Geoscience Initiative 4: unconformity-related uranium systems, (ed.) E.G. Potter and D.M. Wright; Geological Survey of Canada, Open File 7791, p. 103–114. doi:10.4095/295776

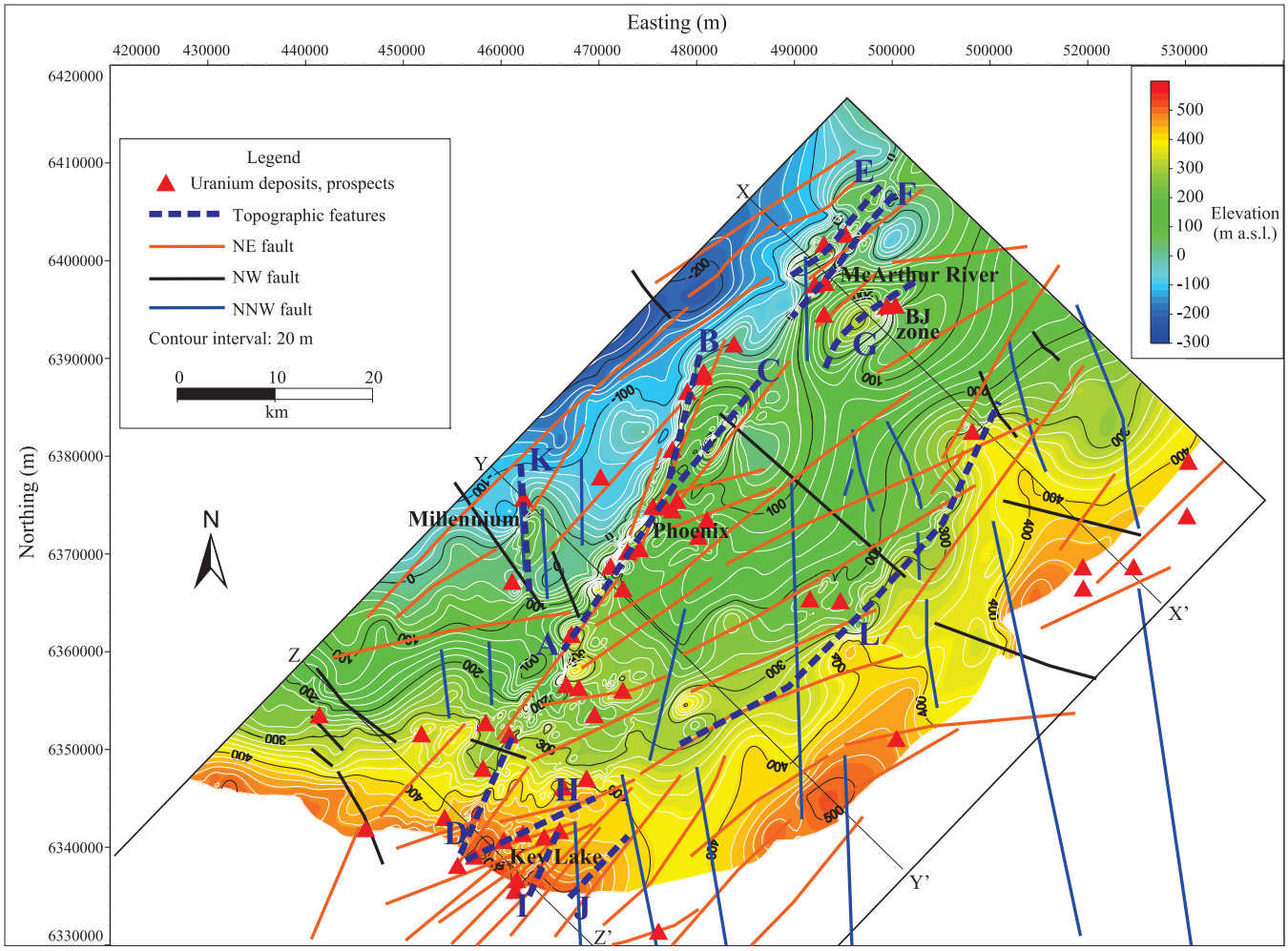

Figure 1. Contour maps showing the elevations of the sub-Athabasca unconformity in the study area. Faults, interpreted on the basis of aeromagnetic data (Card et al., 2010) are also superimposed on the contoured unconformity surface.

underway to further test the influence of fault dip angles, kinematics, spacing and networking on fluid flow, as well as the interaction between thermally-driven and deformation-driven flow.

Modelling results

Three-dimensional modelling of the unconformity surface of the southeastern Athabasca Basin

A 3D model of the southeastern Athabasca Basin was constructed to evaluate the spatial configuration of basement structures and the unconformity, as well as clay alteration patterns in relation to lithology and structures. The main purpose of this model was to determine where, when and how uranium-bearing fluids may have travelled (Li et al., 2013), which can then be used to guide subsequent fluid-flow modelling under different deformational and thermal conditions (Li et al., 2014b), as discussed in more detail in the sections below.

The 3D model highlights an approximately NE-trending zone of elevated topography of the unconformity surface associated with the Phoenix-McArthur River deposit trend, as well as a number of other prominent topographic features (Figs. 1 and 2). Several prominent ridges of metaquartzite proximal to faults along this trend (Earle and Sopuck, 1989), including those at the McArthur and Phoenix deposits (Marlatt et al., 1992; Kerr, 2010), were recognized. These topographic features can be explained through the combined action of three main factors: 1) pre-Athabasca group ductile faulting and alteration; 2) differential weathering and erosion; and 3) post-Athabasca fault reactivation, localized in pre-existing, graphite-rich ductile shear zones (e.g. Györfi et al., 2007; Jefferson et al., 2007; Ramaekers et al., 2007; Tourigny et al., 2007; Yeo et al., 2007).

Faults were identified using the basement geophysical signature, in combination with evidence of unconformity offset. Three dominant sets of faults, inferred to be sub-vertical, were identified on this basis: NE, NW, and NNW, in chronological order from oldest to youngest (Fig. 1). Nearly all the uranium deposits and prospects are associated with the NE-trending structures and adjacent unconformity topographic highs (Fig. 1). Regional clay anomalies documented in previous studies (Earle and Sopuck, 1989) are also broadly aligned with this dominant trend (Li et al., 2013).

It is inferred that pre-Athabasca faulting likely con-

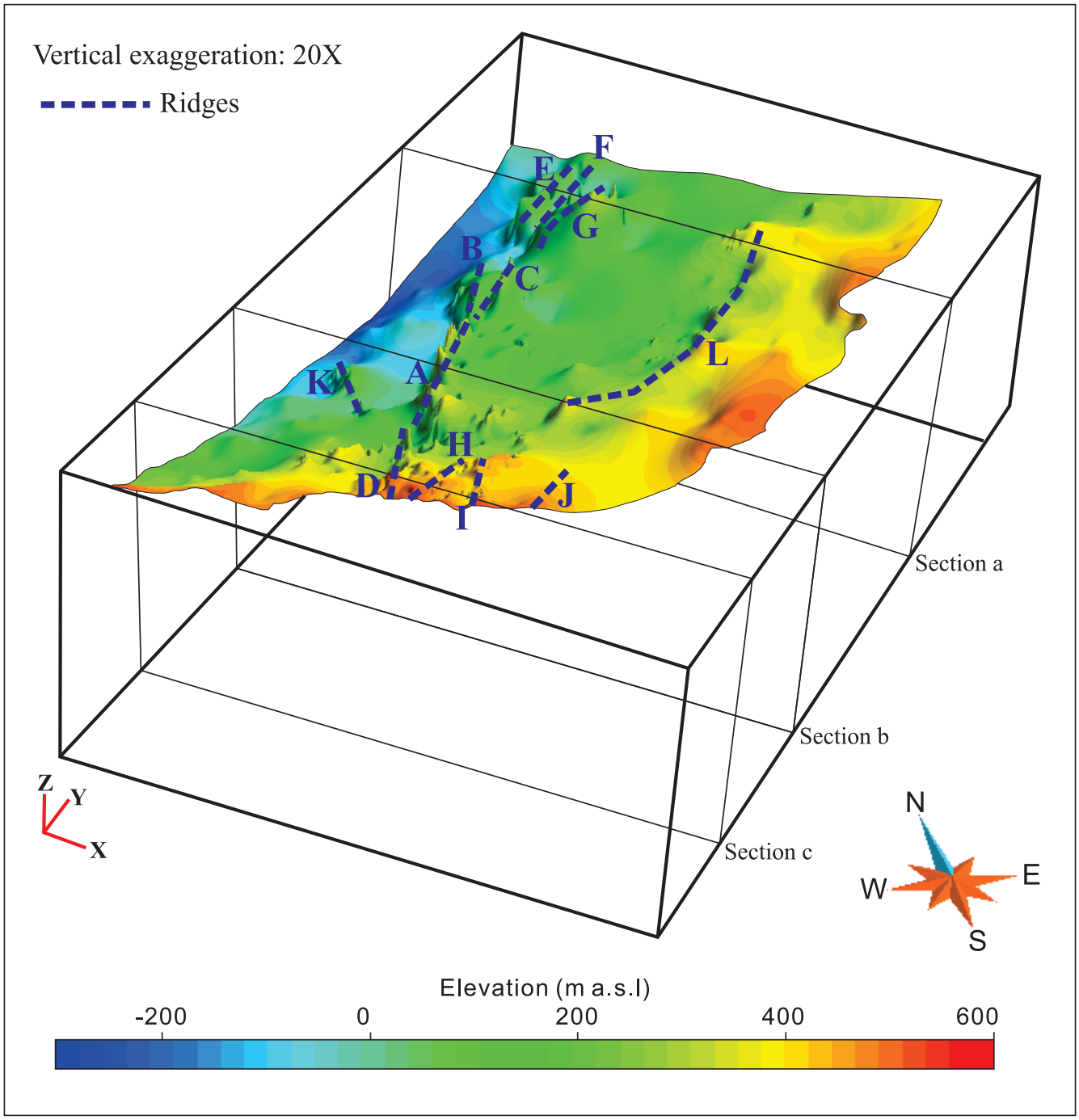

Figure 2. 3D view of the sub-Athabasca unconformity in the study area. Prominent basement ridges are highlighted.

tributed in a substantial way to shaping the paleo-topography of the unconformity surface, which in turn controlled early sedimentation in the basin. Some of the faults were reactivated during and after deposition of the Athabasca Group, further modifying the topography of the unconformity surface. Both the primary unconformity topography and post-Athabasca faulting may have played a role in fluid flow, controlling alteration patterns and uranium mineralization (e.g. Earle and Sopuck, 1989; Harvey and Bethune, 2007; Jefferson et al., 2007; Long, 2007).

Hydrodynamic background of the Athabasca Basin

In order to decipher the mechanisms of fluid flow responsible for uranium mineralization, it is important to understand the background hydrodynamic conditions and temperatures of the basin. These parameters also provide constraints on the initial and boundary conditions required for numerical modelling of fluid flow.

Recent numerical studies by Chi et al. (2013) confirmed that no significant fluid overpressure due to disequilibrium sediment compaction was developed in the basin during sed-

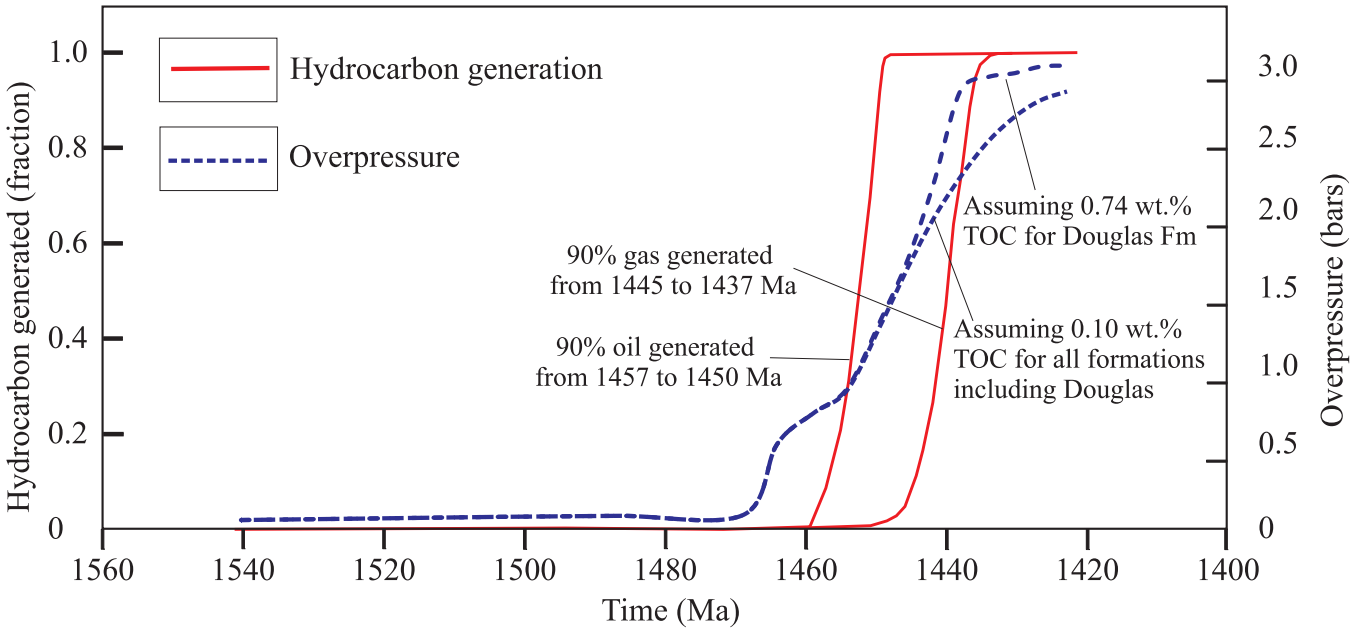

Figure 3. Numerical modeling results showing the time intervals of oil and gas generation in the Douglas Formation in the basin centre, and the evolution of fluid overpressure in the Douglas Formation in the basin centre, as compared to a model with 0.1 wt. % TOC (modified from Chi et al., 2014).

imentation. In other words, the fluid pressure within the basin was near the hydrostatic regime throughout its depositional history, i.e., from ca. 1740 to 1541 Ma (Rainbird et al., 2007). Fluid flow related to sediment compaction was very slow and the temperature profile was undisturbed, implying that if compaction-driven flow was responsible for mineralization, the sites of mineralization would not record thermal anomalies (Chi et al., 2013).

A complementary study was undertaken by Chi et al. (2014) to evaluate how hydrocarbon generation processes in the Douglas Formation, which contains total organic carbon (TOC) of up to 3.56 wt. % (Stasiuk et al., 2001), may have affected fluid overpressure development in the basin (Fig. 3). The authors reported that if each lithology is assigned a moderate permeability (the 'base model'), oil and gas generation processes contribute little to the development of fluid overpressure, and fluid pressure in the basin was close to hydrostatic regardless of whether or not hydrocarbon generation in the Douglas Formation is included in the modelling. However, if the permeability of each lithology is assigned a value one order of magnitude lower than in the base model, significant fluid overpressures are developed in the eroded strata in the upper part of the model. In the base model, oil generated in the Douglas Formation may migrate downward, driven by an overpressure zone situated above the Douglas Formation, but gas migrates upward. In the low-permeability model, however, the overpressures developed above the Douglas Formation are so high that both oil and gas generated in the Douglas Formation will migrate downward. The numerical modelling therefore indicates that, under certain conditions, it would be hydrodynamically possible for oil and gas generated in the ca. 1541 Ma Douglas Formation to migrate to the base of the basin and reach the sites of the unconformity-related uranium deposits, which formed at ca. 1600 – 1500 Ma and 1460 – 1350 Ma, with significant remobilization events at ca. 1176 Ma, 900 Ma, and 300 Ma (Hoeve and Quirt, 1984; Cumming and Krstic, 1992; McGill et al., 1993; Kyser et al., 2000; Fayek et al., 2002; Alexandre et al., 2003; 2009; Creaser and Stasiuk, 2007).

The inference that fluid pressures in the Athabasca Basin were close to hydrostatic values throughout its history has important implications for further fluid flow models. Fluid flow driven by topographic relief and fluid convection driven by density variation are relatively easy to develop when the initial fluid-pressure system is near hydrostatic; strong fluid overpressure in the basin tends to suppress such fluid flow (Chi et al., 2013). This suggests that fluid flow driven by topographic relief (e.g. Alexandre and Kyser, 2012) or convection related to fluid density variation due to thermal gradients (e.g. Raffensperger and Garven, 1995) are both theoretically plausible.

Fluid convection due to geothermal gradients

In order to accurately address the question of how fluid behaved at a local scale and in relation to faulting, a basin-scale modeling of fluid convection is required. Such work has been done for the Athabasca Basin by Raffensperberg and Garven (1995), but the actual sizes of the individual convection cells and their relationship with the thicknesses of the strata remain unclear due to scaling factors. Therefore, we carried out a modeling of basin-scale thermal convection with a more realistic physical model, using FLAC3D® (Itasca, 2012).

The physical model is similar to that used by Chi et al. (2013), where the basin is divided into sedimentary formations and members, each with a different permeability (Fig. 4). Hydrostatic pressure and a thermal field with a gradient of 35°C/km were the initial conditions assigned to the sys-

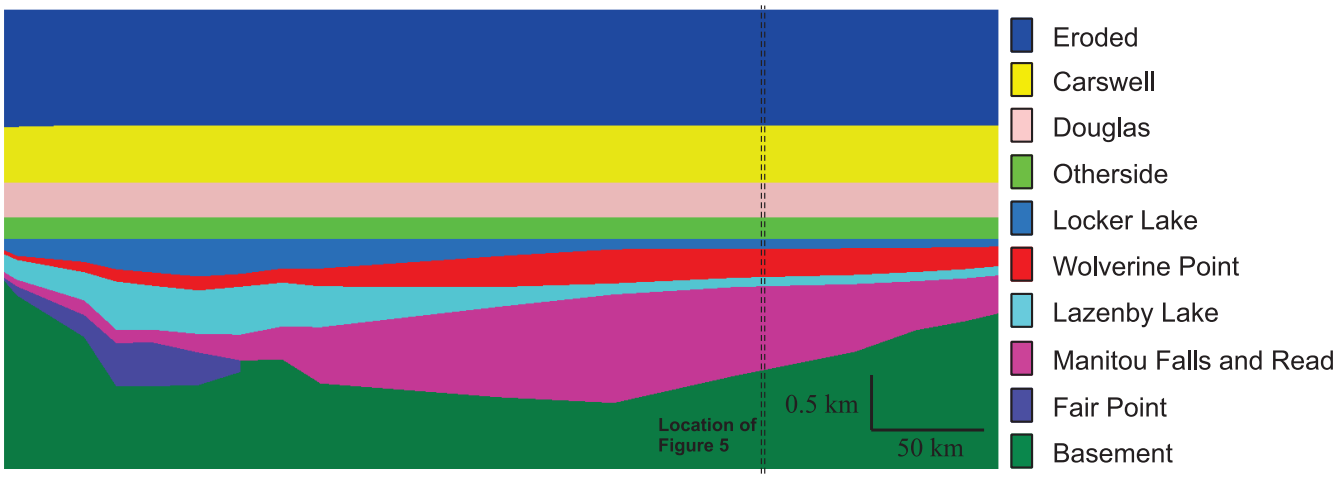

FIGURE 4. Sectional view of the geometric basin model developed for numerical modelling. Dashed lines show the location of Figure 5. Note vertical exaggeration.

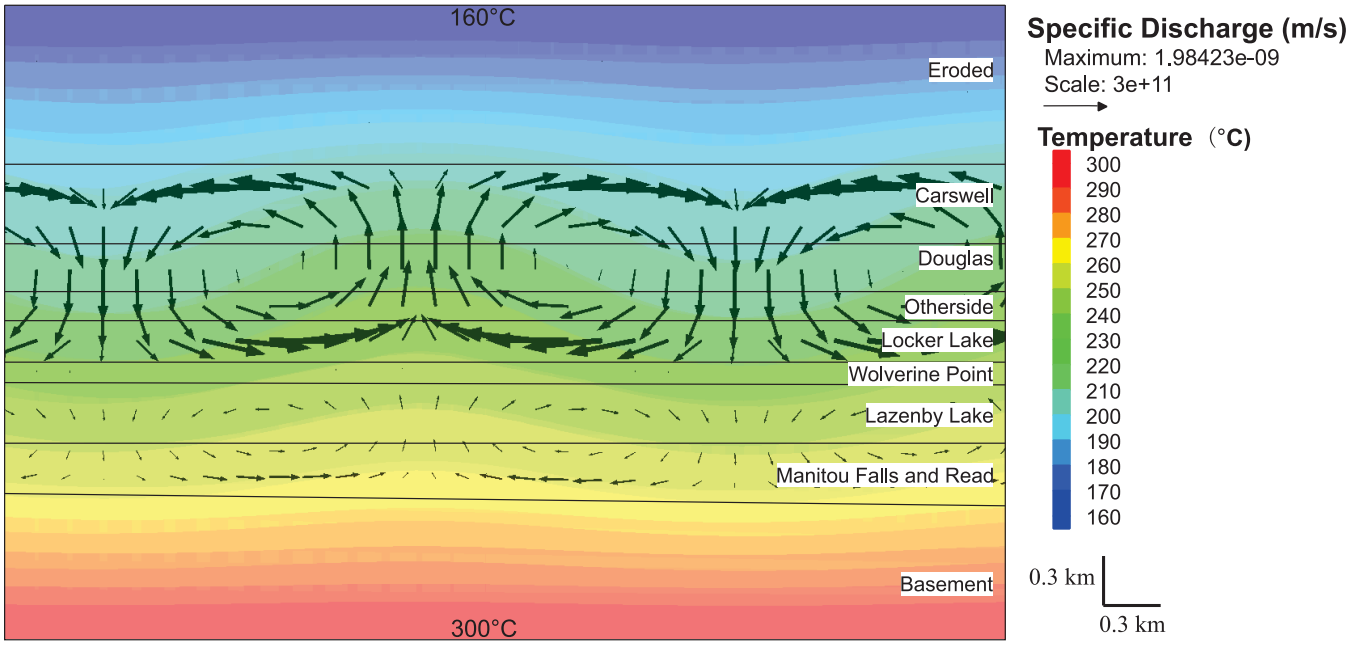

FIGURE 5. Numerical modelling results showing area of the basin outlined by the dash lines in Figure 4. Temperatures are indicated by colour-coded isotherms. Fluid-flow patterns are shown by streamlines, with arrows indicating fluid-flow directions and the size of the arrows reflecting flow rate.

tem. The upper boundary was open to fluid flow and the side and bottom boundaries were assumed to be impermeable to fluid flow. For heat transport, the temperature of the top and bottom boundaries was fixed based on a geothermal gradient of 35°C/km and surface temperature 20 °C. The two side boundaries were insulated to heat transport.

The numerical experiments suggest that when low permeability is assigned to the mudstone-rich Wolverine Point Formation aquitard (Jefferson et al., 2007; Ramaekers et al., 2007), thermal convection cells were developed in the lower part of the basin, particularly below the Wolverine Point Formation, as well as in the upper part of the basin (if high permeability is assumed for the strata now eroded) at geothermal gradients of 25 to 35 °C/km (Fig. 5). The results also show that the largest convection cells formed above the Wolverine Point Formation (Fig. 5). Changes to the assumed geothermal gradient do not modify the fluid flow patterns at the basin scale.

It is notable that the sizes of the convection cells are controlled by the thickness of the sandstone units when all other parameters are held constant; that is, larger thicknesses give rise to larger convection cells. A sensitivity study shows that convection cell size is also controlled by the permeability of the sandstone layers (i.e. higher permeability produces smaller cell sizes).

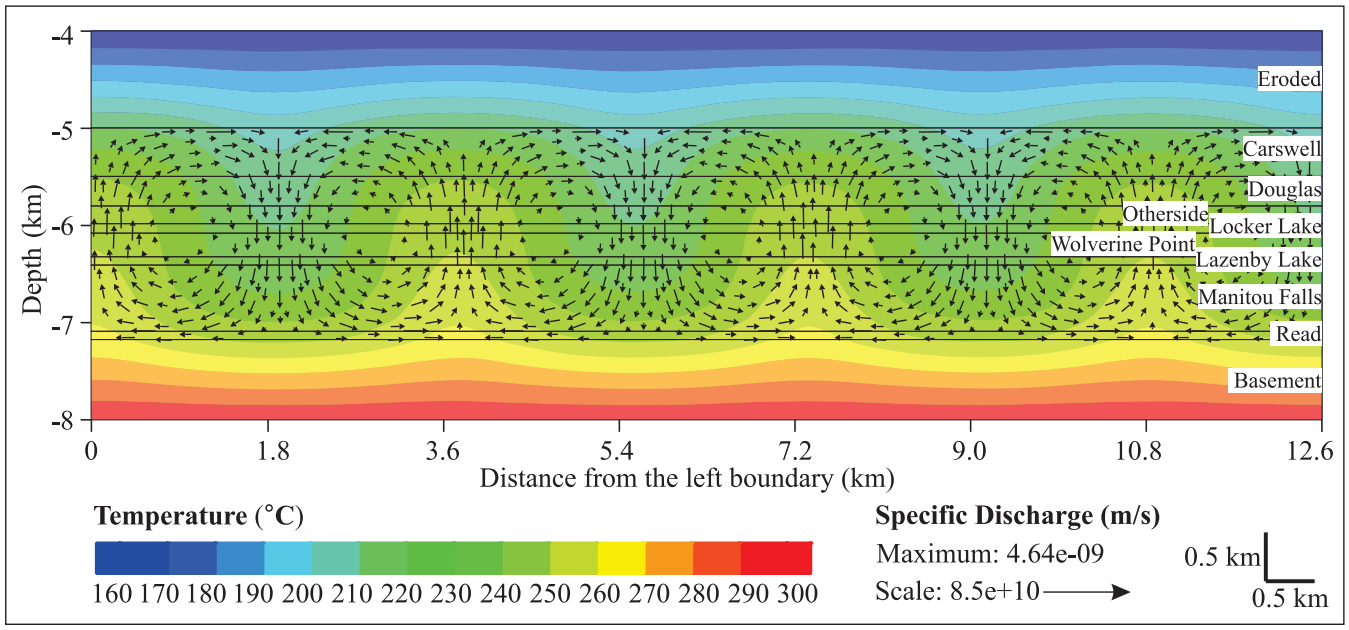

FIGURE 6. Numerical modelling results showing fluid-flow patterns without any faults.

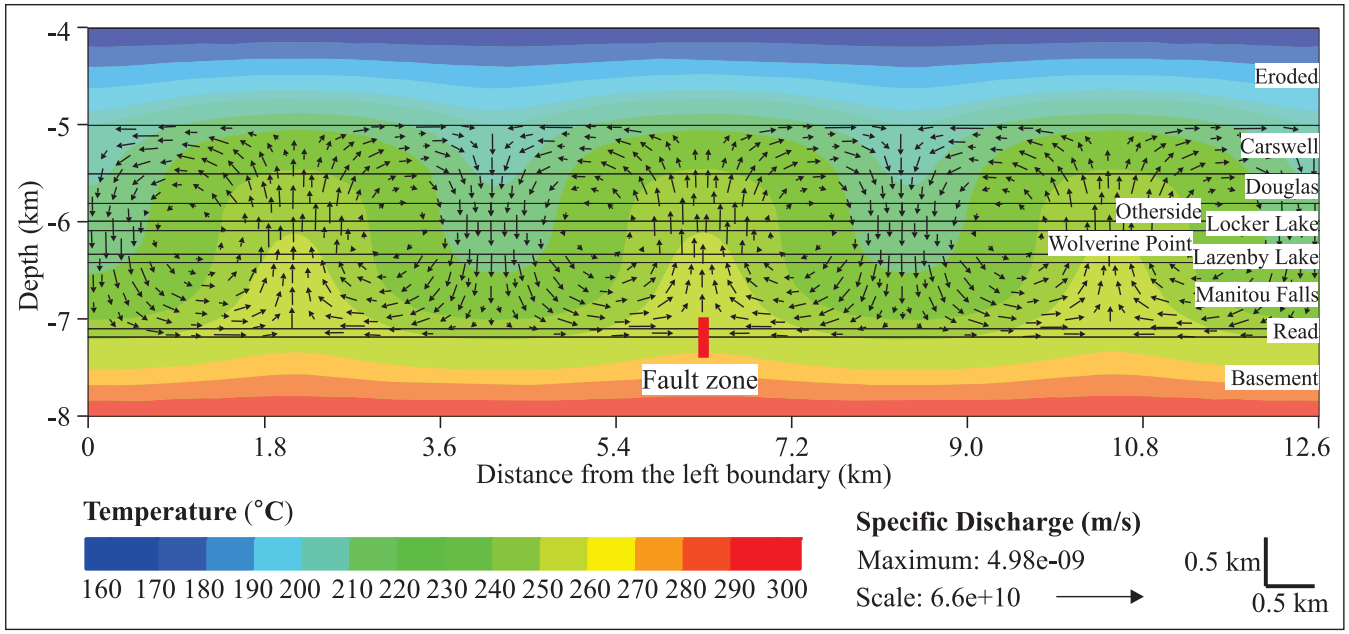

FIGURE 7. Numerical modelling results showing fluid-flow patterns associated with one fault in the centre.

Effects of basement faults on fluid convection cells

To better understand the effects of basement faults on fluid convection due to geothermal gradient, two scenarios were tested. The first scenario incorporated one vertical fault, whereas the second incorporated two vertical faults spaced at 1.8 km and 3.6 km, respectively. The model fault zone was 100 m wide by 400 m high and straddled the unconformity. At this stage of study, only the space and position of the fault zones are considered in the models; faults with different dip angles will be incorporated in the next step. The boundary and initial conditions are the same as those employed in basin-scale model.

For the models with one fault, the fault controls the initial position of the convection cells, i.e. it coincides with the upwelling plume of two adjacent cells (Figs. 6–8). When the fault is moved from the centre to the left for half the size of a convection cell, the upwelling plume shifts from the centre to left accordingly (Figs. 7 and 8).

Like the one-fault model, the faults in the two-fault model also control the initial position of the convection cells, each fault coinciding with an upwelling plume in the beginning. Depending on the spacing of the two faults, however, the final results are different after the models reach steady state. When the spacing of the two faults is equal to the size

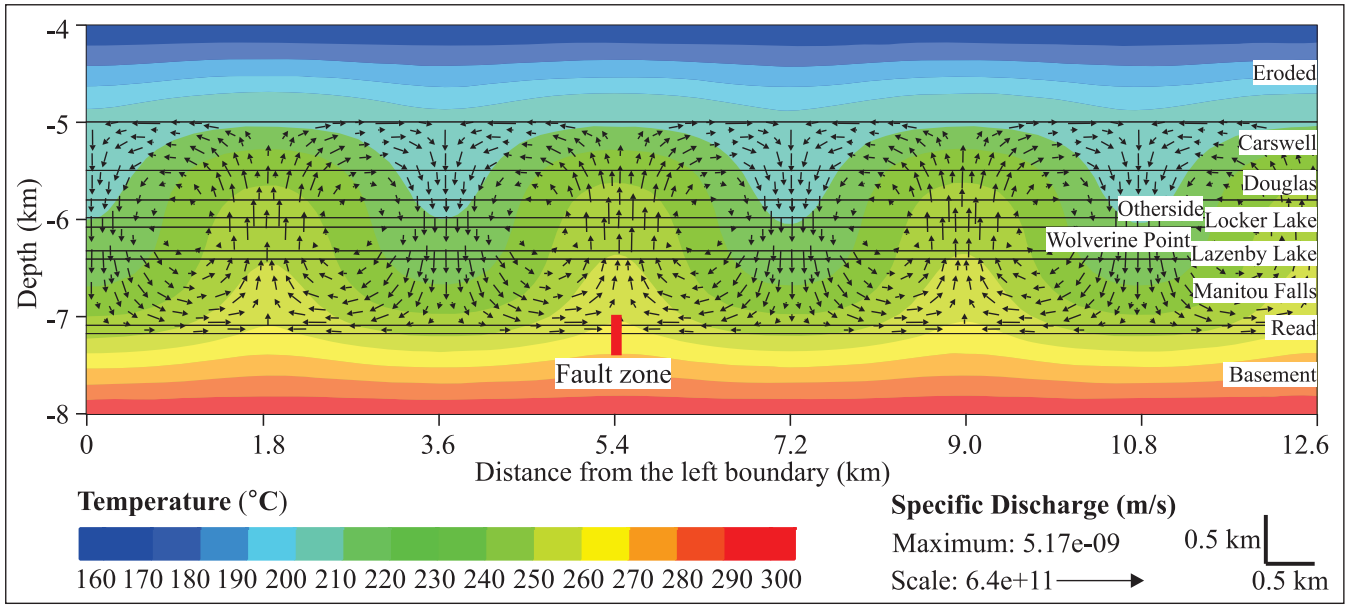

Figure 8. Numerical modelling results showing fluid-flow patterns associated with one fault situated to the left relative to the model shown in Figure 7.

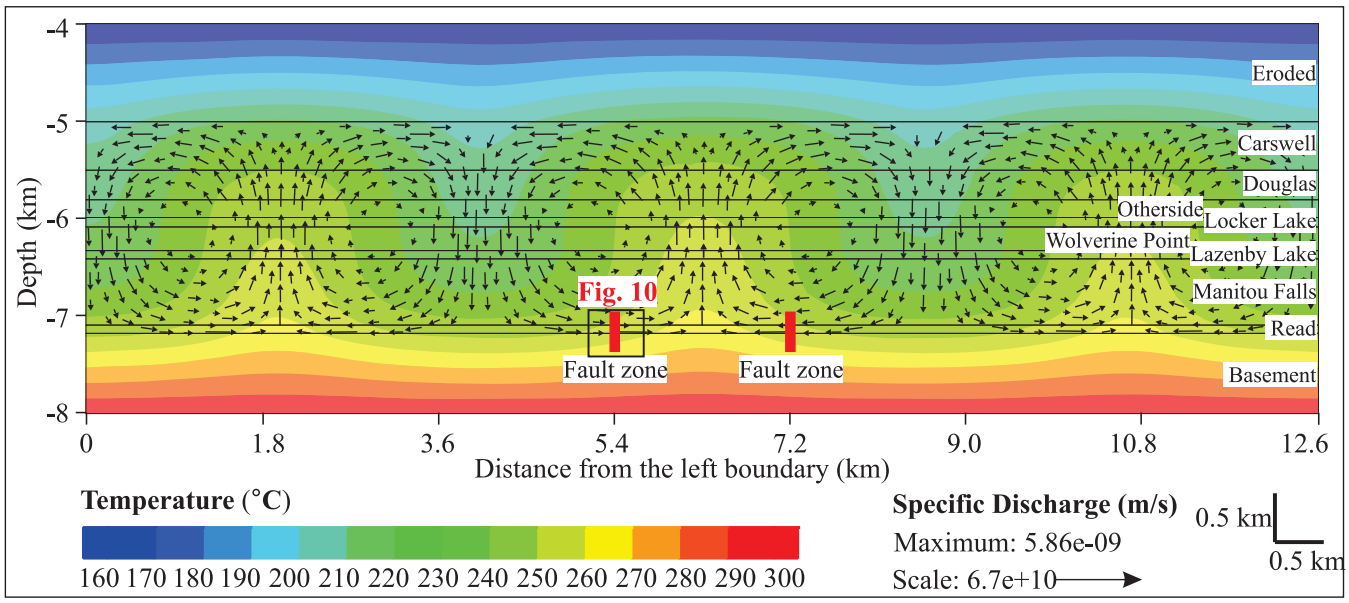

Figure 9. Numerical modelling results showing fluid-flow patterns associated with two faults, with spacing one size of the convection cell in the non-fault model.

of the convection cells in the one-fault model (i.e. 1.8 km), the unstable and weak cells developed at the early stage are destroyed by neighbouring cells after the model reaches a stable state. As a result, the size of the convection cells corresponding to the fault zones is increased; furthermore, neither of the faults coincides with an upwelling or downwelling stream (Fig. 9). Unlike the models with one fault, fluid can penetrate into basement along the fault zone through thermal convection, flowing down one side and up on the other side, depending on the flow direction and where the fault zone is located (Fig. 10). However, when the spacing of the faults is twice as large as the size of the convection cell in the one-fault model (i.e. 3.6 km), the total number and size of the cells remain the same as in the one-fault model, and no fluid penetrates into the basement along fault zone (Fig. 11).

Relationship between fluid-flow and mechanical compression

Preliminary numerical modelling of fluid flow in response to mechanical compression using the 3D model of the Athabasca Basin described above as a guide has been conducted with FLAC3D®. Four scenarios incorporating reverse faults with different dip angles have been tested (Li

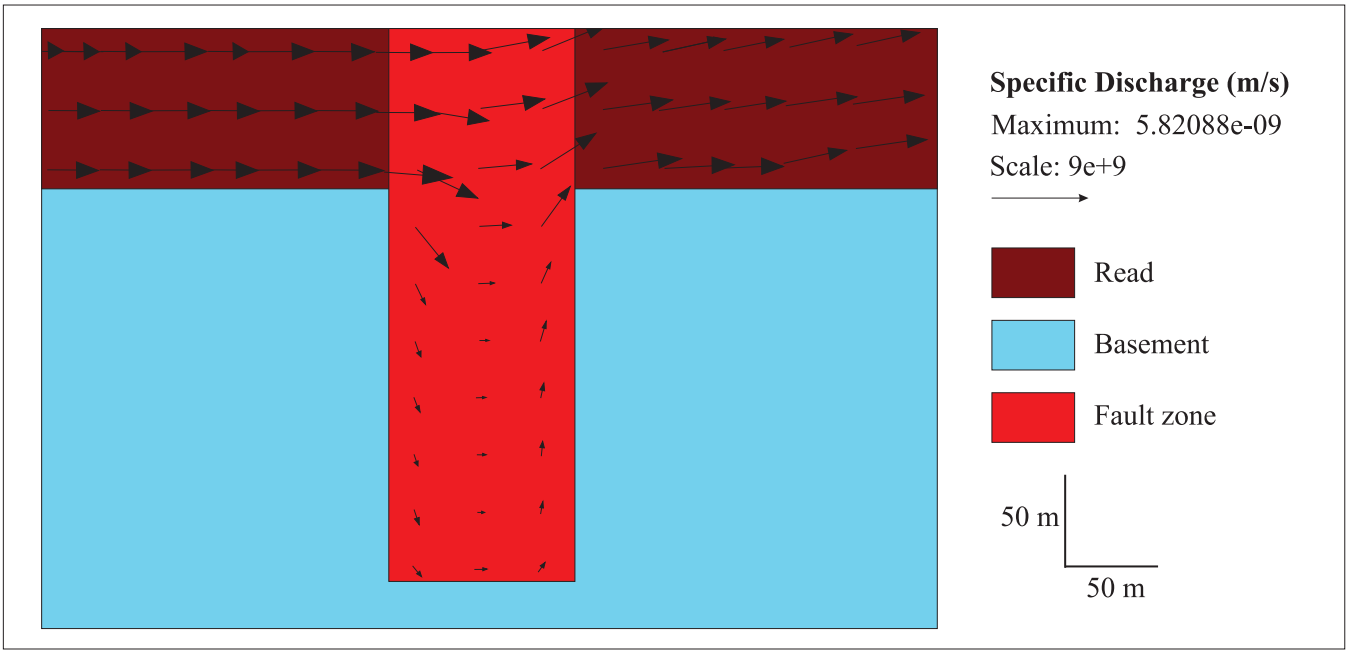

FIGURE 10. Expanded view of the left fault in figure 9, illustrating fluid penetration into the basement rocks along the fault zone.

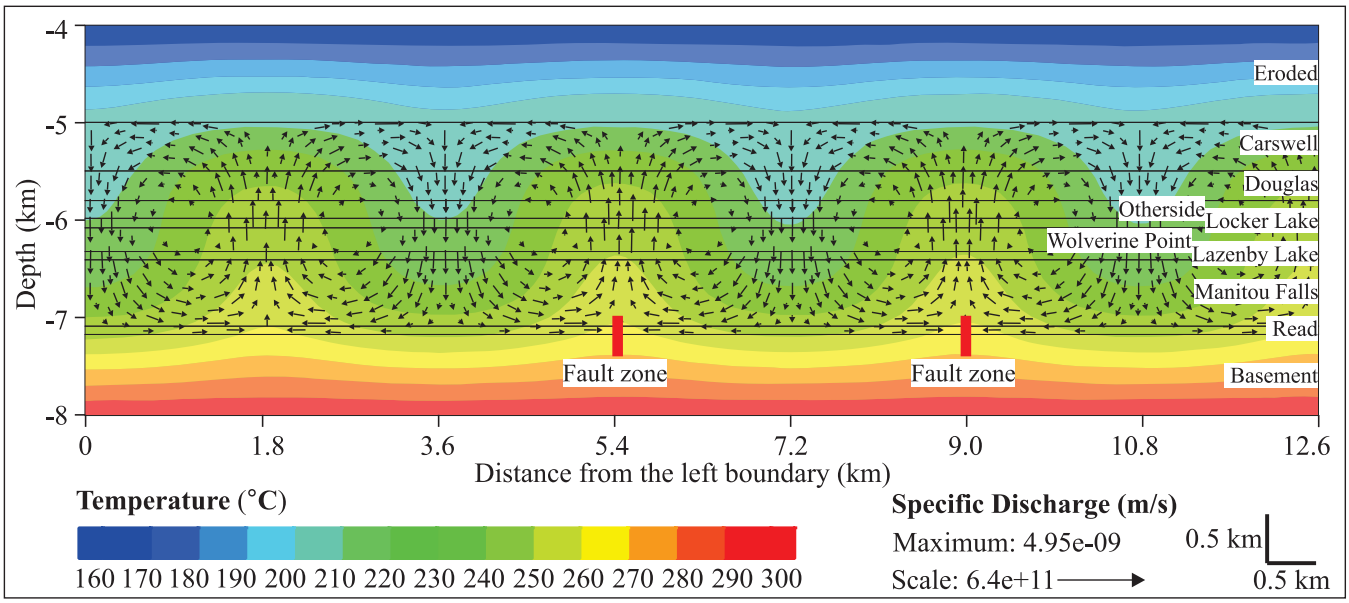

FIGURE 11. Numerical modelling results showing fluid-flow patterns associated with two faults, with spacing at double the size of the convection cell in the non-fault model.

et al., 2014b).

An initial model is shown in Figure 12. This model portrays a relatively simple geological situation based on aggregate thickness of stratotypes (Ramaekers et al., 2007) and estimates of eroded units, where basement rocks are overlain by 2 km of more permeable sandstone representing the basal Athabasca Group, which are in turn overlain by 4 km of eroded strata. A 300 m wide northwest-dipping fault (with a dip angle of 45°) transects the unconformity but does not offset it; the fault is inferred to extend one km above and below the unconformity (Figs. 12 and 13b). The other two scenarios have the same model parameters, except for dip angles of 30° and 60°, respectively (Figs. 13a and 13c), whereas the last scenario tests the effect of offset of the unconformity on fluid flow during compression (Fig. 13d). All the models are subjected to NW-SE horizontal shortening to simulate the tectonic compression. The top of the model was free to deform in both the vertical and horizontal directions to reflect the fact that topography changes during tectonic deformation. The base was fixed vertically, but was free to move horizontally to account for tectonic deformation.

The modelling results show that during compressive

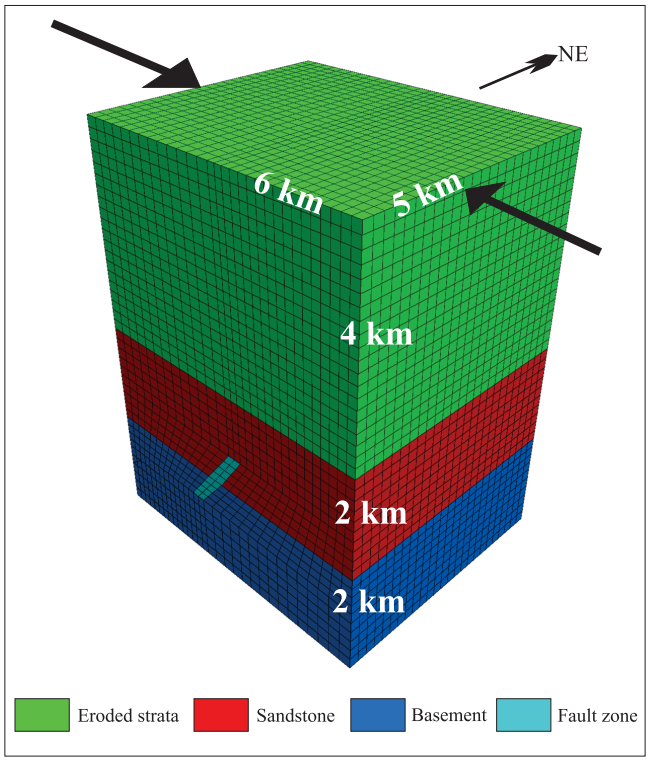

Figure 12. 3D view of the initial model used for numerical modelling of fluid flow in response to mechanical compression.

deformation, fluid migrates up the fault (Fig. 13), which is consistent with the results of Cui et al. (2012). This is due to the rapid increase of pore pressure in the low-permeability basement, the fault zone being an area of dilation and low fluid pressure relative to the surrounding basement rocks. The results of different models incorporating faults with different dip angles show that flow patterns are generally the same amongst the models. However, the model with the most shallowly dipping fault shows slightly greater flow rates than the other models. This is due to the fact that the shallowly dipping fault undergoes more dilation because its orientation is closest to the direction of the maximum principal stress (horizontal and SE-NW). The model with offset on the fault also shows a slightly greater flow rate – suggesting an increase in dilation controlled by differences in properties between units. The fault zones represent the most significant loci of shear strain in all models. As expected, the dip of the fault also strongly controls the orientation of the high strain zone, which propagates into the sandstone (Fig. 13).

Summary and implications for exploration

A 3D model of the sub-Athabasca unconformity has been constructed using publicly available geological and drillhole data. Faults have been identified primarily using basement geophysical signatures, and also from publically available data (Card et al., 2010). Three dominant sets of faults, inferred to be sub-vertical, were identified on this basis: NE, NW, and NNW, in chronological order from oldest to youngest. Numerous dominantly northeast-trending ridges and valleys have been identified in the sub-Athabasca unconformity surface. These features are interpreted to be the products of the combined action of three main factors: 1) pre-Athabasca group ductile faulting and alteration; 2) differential weathering and erosion; and 3) post-Athabasca fault reactivation, localized in pre-existing, graphite-rich ductile shear zones (Györfi et al., 2007; Jefferson et al., 2007; Ramaekers et al., 2007; Tourigny et al., 2007; Yeo et al., 2007). Although unconformity topographic features immediately adjacent to uranium deposits may be positive (ridges) or negative (valleys) (e.g. Harvey and Bethune, 2007; Kerr, 2010; Marlatt et al., 1992), they are all related to structures (Jefferson et al., 2007). These topographic features as well as structures are also spatially associated with the regional distribution of EM conductors, clay alteration patterns of the overlying Athabasca Group (e.g. Earle and Sopuck, 1989) and uranium enrichment (Jefferson et al., 2007). This implies that basement paleotopography may have played an important role in controlling and perhaps localizing fluid flow related to mineralization (e.g. Harvey and Bethune, 2007), and therefore accurate modelling of the unconformity surface may be used to define fertile areas of uranium deposits.

The basin-scale numerical modelling results indicate that fluid pressures in the Athabasca Basin were close to hydrostatic values throughout its development, and that thermal convection cells may have been well developed in the lower part of the basin, particularly below the Wolverine Point Formation aquitard, as well as in the upper part of the basin (if high permeability is assumed for the strata now eroded). These results, when compared with basin-wide geochemical data that indicate significant differences in chemical composition between the Wolverine Point Formation and the underlying strata (Chu et al., 2015; Wright and Potter, 2014), suggest that the highly permeable lower part of the Athabasca Basin experienced extensive chemical changes due to large-scale fluid circulation. These results also indicate that if fluid convection is limited to the high-permeability strata below the Wolverine Point Formation, individual convection cells are likely less than 2 km, although the convection cell size may be increased if the upper part of the basement has permeability comparable to those of the covering strata. If individual convection cells are considered as potential mineralization centres, the spacing between these centres may be just a few kilometers. This is of interest for uranium exploration within individual districts.

Local-scale numerical modelling of fluid flow indicates that the location and spacing of basement faults influences thermally driven fluid convection. Fault controls the initial position of the convection, and isolated faults generally coincide with upwelling flow, but they may also be located within a convection cell under certain configurations of fault spacing. In the latter case, fluid may flow into and out of the same fault zone. Modelling results of fluid flow due to mechanical compression suggest that fluid migrates up the fault during compression, and that the model with the most shallowly dipping fault and the model with fault offset of the unconformity show slightly greater flow rates than the other models. Collectively, these results further support the empirical model that faults crosscutting the unconformity played

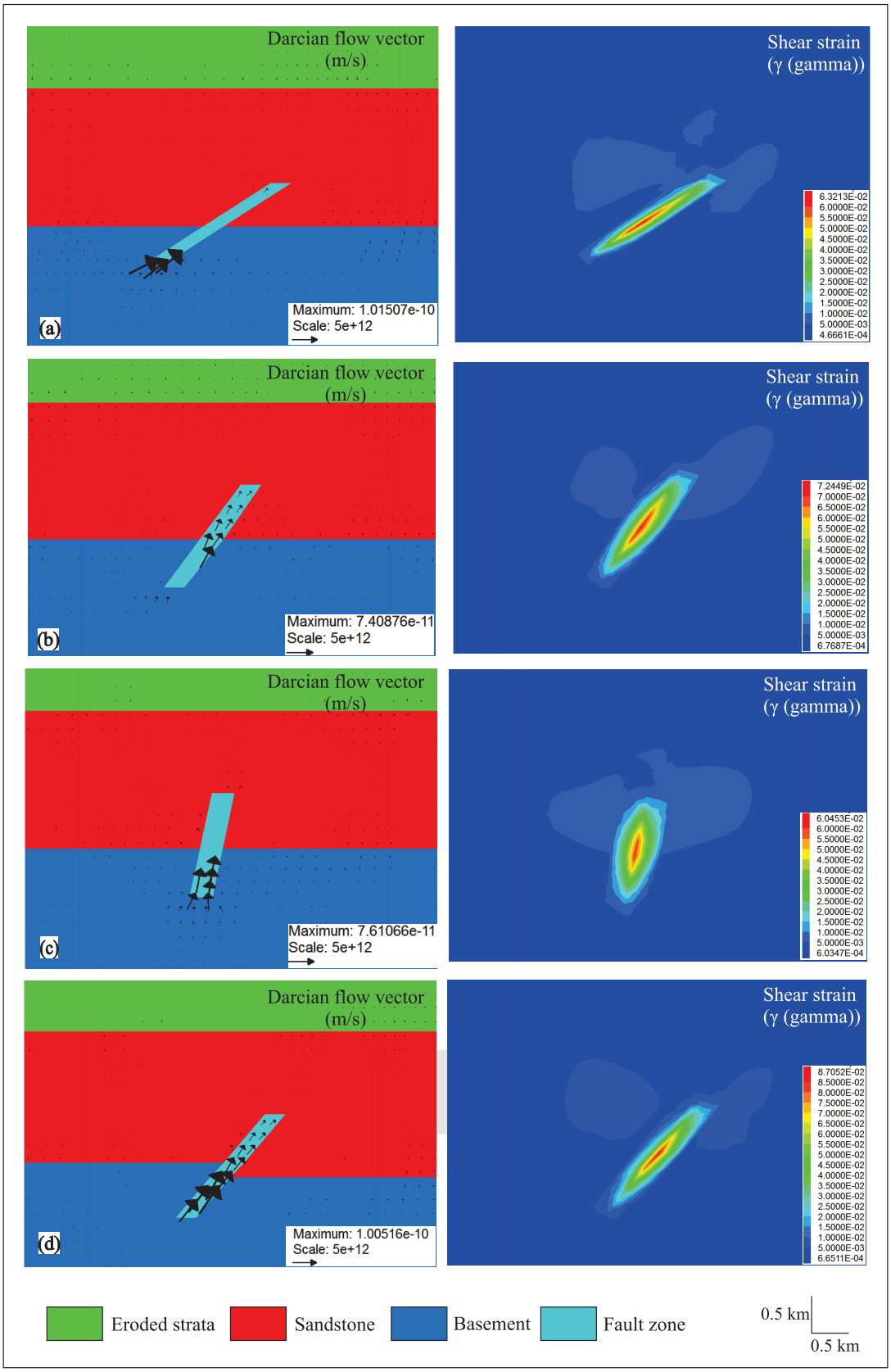

FIGURE 13. Sectional plots of fluid flow vectors (left) and shear strain development (right) for each model after 0.1% shortening. Black arrows indicate the direction of fluid flow and length of arrows indicates magnitude of Darcian fluid-flow (m/s). Shear strain is recorded by γ (gamma) values.

an important role in localizing fluid flow and uranium mineralization, either through controlling convection cell location or providing fluid flow driving forces. The various relationships between convection cells and faults (position and spacing), in addition to other constraints such as fault kinetics and orientations, may explain why some faults are more favourable for fluid-flow than others. All these factors are potentially important in determining whether a given structure may host mineralization.

Acknowledgments

Funding for this research was provided by the Targeted Geoscience Initiative 4 (TGI-4) uranium ore systems project, through a grant to K.M. Bethune and G. Chi, and in part by a NSERC-Discovery grant (to G. Chi). Access to the GoCAD licenses were kindly provided by the Saskatchewan Geological Survey. Denison Mines Corp. is thanked for logistical support and access to drill cores. The authors also wish to thank Jianwen Yang and Eric G. Potter for editorial comments and critical reviews.

References

Alexandre, P., and Kyser, T.K., 2012. Modeling of the fluid flow involved in the formation of Athabasca Basin unconformity-type uranium deposits; Joint annual meeting of the Geological Association of Canada - Mineralogical Association of Canada, Abstracts, v. 35, p. 3.

Alexandre, P., Kyser, T.K., and Polito, P., 2003. Geochronology of the Paleoproterozoic basement-hosted unconformity-type uranium deposits in northern Saskatchewan, Canada; Uranium Geochemistry 2003, International Conference, Proceedings, p. 37–40.

Alexandre, P., Kyser, T.K., Thomas, D., Polito, P., and Marlat, J., 2009. Geochronology of unconformity-related uranium deposits in the Athabasca Basin, Saskatchewan, Canada and their integration in the evolution of the basin; Mineralium Deposita, v. 44, p. 41–59.

Card, C.D., Bosman, S.A., Slimmon, W.L., Delaney, G., Heath, P., Gouthas, G., and Fairclough, M., 2010. Enhanced geophysical images and multiscale edge (worm) analysis for the Athabasca region; Sask. Ministry of Energy and Resources, Open File 2010-46.

Chi, G., Bosman, S., and Card, C., 2013. Numerical modeling of fluid pressure regime in the Athabasca basin and implications for fluid flow models related to the unconformity-type uranium mineralization; Journal of Geochemical Exploration, v. 125, p. 8–19.

Chi, G., Li, Z., and Bethune, K.M., 2014. Numerical modeling of hydrocarbon generation in the Douglas Formation of the Athabasca basin (Canada) and implications for unconformity-related uranium mineralization; Journal of Geochemical Exploration, v. 144, Part A, p. 37–48.

Chu, H., Chi, G., Bosman, S., and Card, C. 2015. Diagenetic and geochemical studies of sandstones from drill core DV10-001 in the Athabasca basin, Canada, and implications for uranium mineralization; Journal of Geochemical Exploration, v. 148, p. 206–230.

Creaser, R.A., and Stasiuk, L.D., 2007. Depositional age of the Douglas Formation, northern Saskatchewan, determined by Re-Os geochronology; in EXTECH IV: Geology and Uranium EXploration TECHnology of the Proterozoic Athabasca Basin, Saskatchewan and Alberta, (ed.) C.W. Jefferson and G. Delaney; Geological Survey of Canada, Bulletin 588, p. 341–346.

Cui, T., Yang, J.W., and Samson, I.M., 2012. Tectonic deformation and fluid flow: implications for the formation of unconformity-related uranium deposits; Economic Geology, v. 107, p. 147–163.

Cumming, G.L., and Krstic, D., 1992. The age of unconformity-associated uranium mineralization in the Athabasca Basin, northern Saskatchewan; Canadian Journal of Earth Sciences, v. 29, p. 1623–1639.

Earle, S.A.M., and Sopuck, V.J., 1989. Regional lithogeochemistry of the eastern part of the Athabasca Basin uranium province, Saskatchewan, Canada; in Uranium Resources and Geology of North America; International Atomic Energy Agency, TECDOC-500, p. 263–296.

Fayek, M., Kyser, T.K., and Riciputi, L.R., 2002. U and Pb isotope analysis of uranium minerals by ion microprobe and the geochronology of the McArthur River and Sue Zone uranium deposits, Saskatchewan, Canada; The Canadian Mineralogist, v. 40, p. 1553–1569.

Györfi, I., Hajnal, Z., White, D.J., Takács, E., Reilkoff, B., Annesley, I.R., Powell, B., and Koch, R., 2007. High-resolution seismic survey from the McArthur River region: contributions to mapping of the complex P2 uranium ore zone, Athabasca Basin, Saskatchewan; in EXTECH IV: Geology and Uranium Exploration TECHnology of the Proterozoic Athabasca Basin, Saskatchewan and Alberta, (ed.) C.W. Jefferson and G. Delaney; Geological Survey of Canada, Bulletin 588, p. 397–412.

Harvey, S.E., and Bethune, K.M., 2007. Context of the Deilmann orebody, Key Lake mine, Saskatchewan; in EXTECH IV: Geology and Uranium Exploration TECHnology of the Proterozoic Athabasca Basin, Saskatchewan and Alberta, (ed.) C.W. Jefferson and G. Delaney; Geological Survey of Canada, Bulletin 588, p. 249–266.

Hoeve, J., and Quirt, D.H., 1984. Mineralization and host rock alteration in relation to clay mineral diagenesis and evolution of the middle-Proterozoic, Athabasca Basin, northern Saskatchewan, Canada; Saskatchewan Research Council, SRC Technical Report 187, 187 p.

Itasca, 2012. FLAC3D: Fast Lagrangian Analysis of Continua in 3 Dimensions, User's Guide, version 5.0; Itasca Consulting Group Inc., Minnesota.

Jefferson, C., Thomas, D., Gandhi, S., Ramaekers, P., Delaney, G., Brisbin, D., Cutts, C., Portella, P., and Olson, R., 2007. Unconformity-associated uranium deposits of the Athabasca Basin, Saskatchewan and Alberta; in EXTECH IV: Geology and Uranium Exploration TECHnology of the Proterozoic Athabasca Basin, Saskatchewan and Alberta, (ed.) C.W. Jefferson and G. Delaney; Geological Survey of Canada, Bulletin 588, p. 23–67

Kerr, W.C., 2010. The discovery of the Phoenix Deposit; a new high-grade, Athabasca Basin unconformity-type uranium deposit, Saskatchewan, Canada; Society of Economic Geologists Special Publications, v.15, p. 703–728.

Kyser, K., Hiatt, E., Renac, C., Durocher, K., Holk, G., and Deckart, K., 2000. Diagenetic fluids in Paleo- and Mesoproterozoic sedimentary basins and their implications for long protracted fluid histories; in Fluids and Basin Evolution, (ed.) T.K. Kyser; Mineralogical Association of Canada Short Course Series, v. 28, p. 225–262.

Li, Z., Bethune, K.M., Chi, G., Bosman, S.A., and Card, C.D., 2013. Preliminary 3D modelling and structural interpretation of southeastern Athabasca Basin; Geological Survey of Canada, Open File 7426.

Li, Z., Bethune, K.M., Chi, G., Card, C.D., and Bosman, S.A., 2014a. Topographic features of the sub-Athabasca Group unconformity surface in southeastern Athabasca Basin and its relationship to uranium ore deposits; Joint annual meeting of the Geological Association of Canada - Mineralogical Association of Canada, Abstracts v.37, p. 162.

Li, Z., Chi, G., Bethune, K.M., Bosman, S., and Card, C.D., 2014b. Preliminary 3D geomodelling and simulation of coupled fluid flow and compressional deformation in the Athabasca Basin; Geological Survey of Canada, Open File 7612, one sheet.

Long, D.G.F. 2007. Topographic influences on the sedimentology of the Manitou Falls Formation, eastern Athabasca Basin, Saskatchewan; in EXTECH IV: Geology and Uranium Exploration TECHnology of the Proterozoic Athabasca Basin, Saskatchewan and Alberta, (ed.) C.W. Jefferson and G. Delaney; Geological Survey of Canada, Bulletin 588, p. 267–280.

Marlatt, J., McGill, B., Matthews, R., Sopuck, V., and Pollock, G., 1992. The discovery of the McArthur River uranium deposit, Saskatchewan, Canada; in New Developments in Uranium Exploration, Resources, Production and Demand; International Atomic Energy Agency and the Nuclear Energy Agency of the Organization for Economic Cooperation Development, IAEA-TECDOC-650, p. 118–127.

McGill, B.D., Marlatt, J.L., Matthews, R.B., Sopuck, V.J., Homeniuk, L.A., and Hubregtse, J.J., 1993. The P2 north uranium deposit, Saskatchewan, Canada; Exploration and Mining Geology, v. 2, p. 321–331.

Raffensperger, J.P., and Garven, G., 1995. The formation of unconformity-type uranium ore-deposits. 1. Coupled groundwater-flow and heat-

transport modeling; American Journal of Science, v. 295, p. 581–636.

Rainbird, R.H., Stern, R.A., Rayner, N., and Jefferson, C.W., 2007. Age, provenance, and regional correlation of the Athabasca Group, Saskatchewan and Alberta, constrained by igneous and detrital zircon geochronology; in EXTECH IV: Geology and Uranium Exploration TECHnology of the Proterozoic Athabasca Basin, Saskatchewan and Alberta, (ed.) C.W. Jefferson and G. Delaney; Geological Survey of Canada, Bulletin 588, p. 193–209.

Ramaekers, P., Jefferson, C.W., Yeo, G.M., Collier, B., Long, D.G.F., Drever, G., Mchardy, S., Jiricka, D., Cutts, C., Wheatley, K., Catuneanu, O., and Bernier, S., 2007. Revised geological map and stratigraphy of the Athabasca Group, Saskatchewan and Alberta; in EXTECH IV: Geology and Uranium Exploration TECHnology of the Proterozoic Athabasca Basin, Saskatchewan and Alberta, (ed.) C.W. Jefferson and G. Delaney; Geological Survey of Canada, Bulletin 588,. 155–192.

Stasiuk, L.D., Fowler, M.G., Jiricka, D., Mossisson, D., Sopuck, V., Wheatley, K., Wilson, N.S., and Zaluski, G., 2001. Preliminary investigation into organic petrology and organic geochemistry of Proterozoic Douglas Formation shales and Athabasca Group sandstones distal and proximal to uranium mineralization, Athabasca Basin, Saskatchewan; in Summary of Investigations 2001, Saskatchewan Geological Survey, Saskatchewan Energy and Mines, Miscellaneous Report 2001-4.2, vol. 2, p. 224–239.

Tourigny, G., Quirt, D.H., Wilson, N.S.F., Wilson, S., Breton, G., and Portella, P., 2007. Geological and structural features of the Sue C uranium deposit, McClean Lake area, Saskatchewan; in EXTECH IV: Geology and Uranium Exploration TECHnology of the Proterozoic Athabasca Basin, Saskatchewan and Alberta, (ed.) C.W. Jefferson and G. Delaney; Geological Survey of Canada, Bulletin 588, p. 229–247.

Wright, D.M. and Potter, E.G., 2014. Regional surface rock geochemistry, Athabasca Basin. Saskatchewan; Geological Survey of Canada, Open File 7614, 33 pages, doi:10.4095/293915.

Yeo, G.M., and Delaney, G., 2007. The Wollaston Supergroup, stratigraphy and metallogeny of a Paleoproterozoic Wilson cycle in the Trans-Hudson Orogen, Saskatchewan; in EXTECH IV: Geology and Uranium Exploration TECHnology of the Proterozoic Athabasca Basin, Saskatchewan and Alberta, (ed.) C.W. Jefferson and G. Delaney; Geological Survey of Canada, Bulletin 588, p. 89–118.

The Otish Basin: Basin Evolution and Formation of the Camie River Uranium Deposit, Quebec

Dejan Milidragovic[1], Marion Lesbros-Piat-Desvial[1], Julia J. King[1], Georges Beaudoin[1], Mike A. Hamilton[2], and Robert A. Creaser[3]

1. Département de géologie et de génie géologique, Université Laval, 1065 avenue de la Médecine, Québec, Québec, G1V 0A6

2. Jack Satterly Geochronology Lab, Department of Earth Sciences, University of Toronto, 22 Russell Street, Toronto, Ontario, M5S 3B1

3. Department of Earth and Atmospheric Sciences, 1-26 Earth Sciences Building, University of Alberta, Edmonton, Alberta, T6G 2E3

Abstract

The Otish Basin of central Québec hosts over thirty uranium prospects, including the Camie River prospect that is located near the unconformable contact between the graphite-bearing, metamorphic basement of Archean age and the overlying basinal sedimentary rocks of the Otish Supergroup. The maximum age of the basin, constrained by the age of the unconformably-underlying Mistassini dyke swarm, is 2515 ± 3 Ma. Following the deposition of the Otish Supergroup, the basin was intruded by the Otish Gabbros, a suite of olivine-tholeiitic dykes and sills of near-liquid compositions (Group 1) and cumulate rocks (Group 2). Uranium-lead zircon ages from the Otish Gabbros indicate the minimum age of the Otish Basin is ca. 2.17 Ga. The Otish Basin was also intruded by the Matoush dyke, interpreted to be younger than the Otish Gabbros. The least altered samples of the Matoush dyke have mineralogy and trace element systematics, such as highly fractionated REE patterns, similar to lamprophyric rocks and are distinct from the tholeiitic to weakly trace element-enriched Otish Gabbros. This, therefore, indicates that the Otish Basin was affected by at least two igneous events.

The uranium mineralization formed after the peak diagenetic alteration of the Otish Supergroup. During peak diagenetic conditions, early albitic sandstone cement was largely replaced by K-feldspar. The feldspathic cement was subsequently partially replaced by a green muscovite alteration. The increase in Na_2O concentrations of the feldpsathic-cemented sandstones towards the base of the sedimentary sequence is noteworthy. Uraninite and brannerite are the principal uranium minerals at the Camie River prospect. Molybdenite grains, intergrown with uraninite, yield a Re-Os model age of 1724 ± 4.9 Ma that is indistinguishable from the previously published uraninite ages. The age of mineralization is significantly younger than the age of the Otish Gabbros, indicating that the uranium mineralization postdates sedimentation by ≥450 m.y. The overlapping Sm-Nd isotopic ages from Otish Gabbros suggest the main uranium mineralization was locally accompanied by resetting of the Sm-Nd system and LREE mobility in the gabbros. The age of mineralization in the Otish Basin is similar to the age of polymetallic mineralization of the Huronian Supergroup, suggesting the ca. 1.7 Ga hydrothermal activity may have been a regional phenomenon affecting the southern Superior Province.

Introduction

The Paleoproterozoic Otish Basin of central Québec hosts over thirty uranium prospects (Gatzweiler, 1987), many of which remain poorly understood and underexplored. Globally, Proterozoic sedimentary basins host several world-class uranium deposits (e.g. Ranger and Jabiluka deposits in MacArthur Basin, Australia and Cigar Lake and McArthur River deposits in Athabasca Basin, Canada), providing clear impetus for a better understanding of the style and mechanisms of uranium-enrichment in the Otish Basin. This report primarily examines the Camie River prospect (7.83 wt. % U_3O_8 over 1 m, Gatzweiler, 1987; 1 wt. % U_3O_8 over 15 m with a maximum 13.6 wt. % U_3O_8 over 0.5 m; Aubin, 2011), whose location along the regional unconformity between the basal Otish Supergroup sediments and the underlying metamorphosed Archean volcano-sedimentary rocks (Fig. 1) is consistent with unconformity-related uranium systems (Gatzweiler, 1987; Beyer et al., 2012). New geochronological and geochemical data, summarized in this report, provide additional constraints on the timing of formation and evolution of the Otish basin, whereas revised mineral parageneses, whole-rock geochemistry and mineral chemistry of the hydrothermally-altered rocks that host the uranium minerals at the Camie River prospect establish the spatial and temporal relationships between alteration and uranium mineralization.

Geological Background

The Otish Basin is located at the southeastern margin of the Archean Superior Province, just north of the Grenville Tectonic Front (Fig. 1). The 150 by 50 km basin is host to the Otish Supergroup, a ca.1500 m thick, predominantly clastic, sedimentary sequence composed of conglomerate and sandstone of the Indicator Group, and sandstone, argillaceous sandstone, minor conglomerate and dolostone of the conformably overlying Peribonca Group (Chown and Caty, 1973; Gatzweiler, 1987; Genest, 1989; Beyer et al., 2012). The Otish Supergroup unconformably overlies an Archean basement, which consists of high-grade metamorphic (Epervanche Complex) and volcano-sedimentary (Tichegami Group) rocks, cut by younger felsic intrusions. The Archean basement is intruded by the northwest-trending Mistassini

Milidragovic, D., Lesbros-Piat-Desvial, M., King, J.J., Beaudoin, G., Hamilton, M.A., and Creaser, R.A., 2015. The Otish Basin: basin evolution and formation of the Camie River uranium deposit, Quebec, *in* Targeted Geoscience Initiative 4: unconformity-related uranium systems, (ed.) E.G. Potter and D.M. Wright; Geological Survey of Canada, Open File 7791, p. 115–122. doi:10.4095/295776

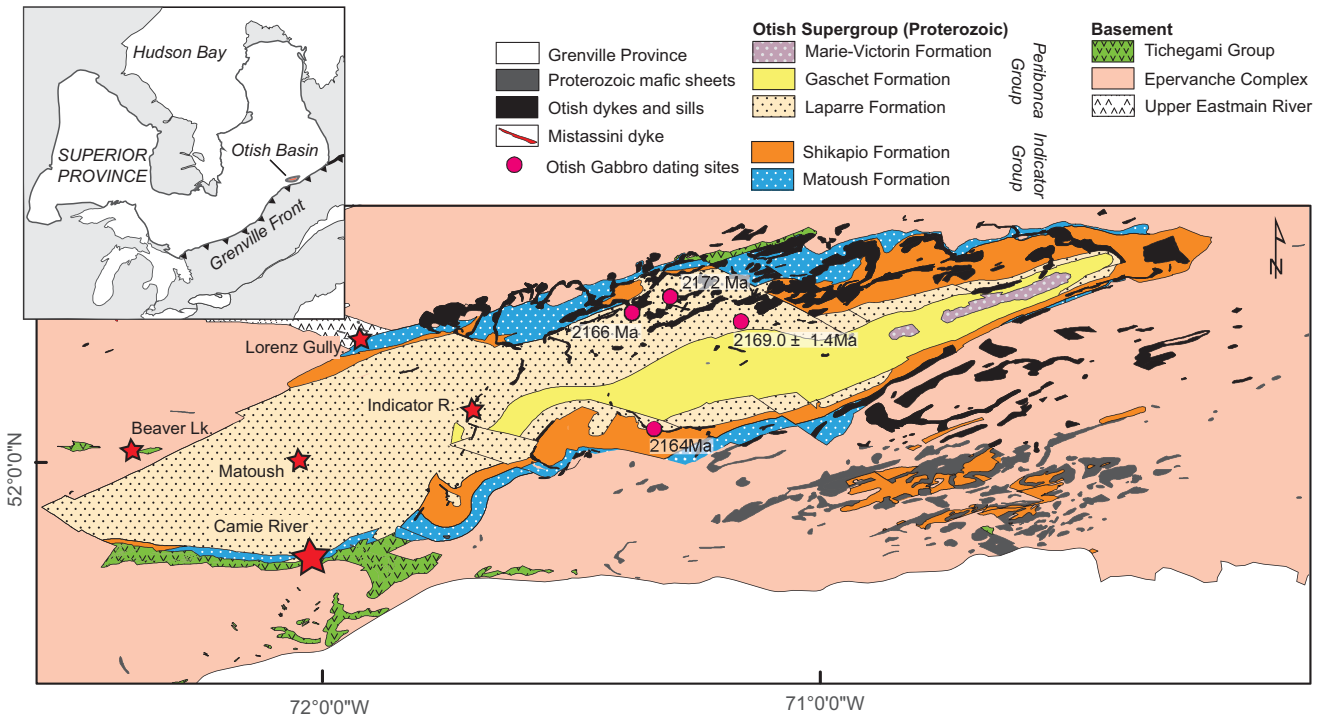

Figure 1. Geological map of the Otish Basin (modified from Lesbros-Piat-Desvial, 2014), showing select uranium showings (stars). Inset: location of Otish Basin in relation to the Superior Province.

dyke swarm, dated at 2515 ± 3 Ma (U-Pb baddeleyite; Hamilton, 2009). As the Mistassini dykes do not intrude the overlying Otish Basin sedimentary rocks, their age defines the maximum age of the Otish Supergroup.

The Otish Supergroup was intruded by dykes and sills of the Otish Gabbro suite (Fahrig and Chown, 1973; Chown and Archambault, 1987). Based on K-Ar results (1465 Ma; Wanless et al., 1965) and Sm-Nd age determinations (1730 ± 10 Ma and 1710 ± 30; C. Brooks in Ruhlmann et al., 1986; Gatzweiler, 1987; Höhndorf et al., 1987), the Otish Gabbros were long thought to have been emplaced during the period 1750–1710 Ma. This estimate is significantly younger than the more recent U-Pb baddeleyite age of 2169 ± 1.4 Ma for an upper Otish Gabbro sill presented by Hamilton and Buchan (2007). Late Paleoproterozoic U-Pb ages, indistinguishable from the ca. 1730 Ma Sm-Nd age reported by Gatzweiler (1987) and Höhndorf et al. (1987), have also been obtained from uraninite at the Camie River (1723 ± 16 Ma; Höhndorf et al., 1987; 1721 ± 20 Ma; Beyer et al., 2012) and Lorenz Gully (1717 ± 20 Ma; Höhndorf et al., 1987) prospects. The latter age coincidence led Beyer et al. (2012) to propose that the intrusion of the Otish Gabbros promoted the circulation of U-rich basinal brines that resulted in formation of the Camie River deposit.

During the Mesoproterozoic Grenville Orogeny (ca. 1.09–0.98 Ga; Hynes and Rivers, 2010), the Otish Basin and proximal basement rocks developed both dextral and sinistral strike-slip faults. The northwestern part of the basin underwent brittle deformation and sub-greenschist facies metamorphism limited to fault zones, whereas the southeastern part of the basin experienced ductile deformation and increasing regional metamorphic grade from greenschist to amphibolite facies close to the Grenville Front (Chown, 1979; 1984).

Geology of the Camie River prospect

Uranium mineralization at the Camie River prospect is dominated by uraninite, variably altered to brannerite and coffinite (Ruzicka and LeCheminant, 1984; Gatzweiler, 1987; Höhndorf et al., 1987; Beyer et al., 2012). According to Gatzweiler (1987), Beyer et al. (2012), and Lesbros-Piat-Desvial (2014), the high-grade mineralization is mainly hosted by sub-vertical graphitic schists ± massive sulphides that coincide with reverse faults that offset the unconformity between the Otish Supergroup (Matoush Formation) and the underlying Archean Hippocampe Belt (Tichegami Group). Mineralization is also hosted by faulted fluviatile sandstones and conglomerates of the Matoush Formation, near basement wedges (Lesbros-Piat-Desvial, 2014). As reported by Gatzweiler (1987) and Höhndorf et al. (1987), the uranium mineralization is polymetallic with enrichments in Mo, Cu, Co, Ni, As, Se, Nb, V, Ag and Au (± Th) that coincide with a zoned, mushroom-shaped alteration halo composed of an inner Fe-Mg chlorite and Fe-dolomite zone, and an outer albite, chlorite and pyrite zone.

Mineral paragenesis of the basement rocks at the Camie River prospect

The study of the Camie River prospect is based on the description of samples from 15 mineralized (n =6) and non-mineralized (n =9) diamond drill-holes. Sample details, such as the locations of the drill-holes and depths from which the

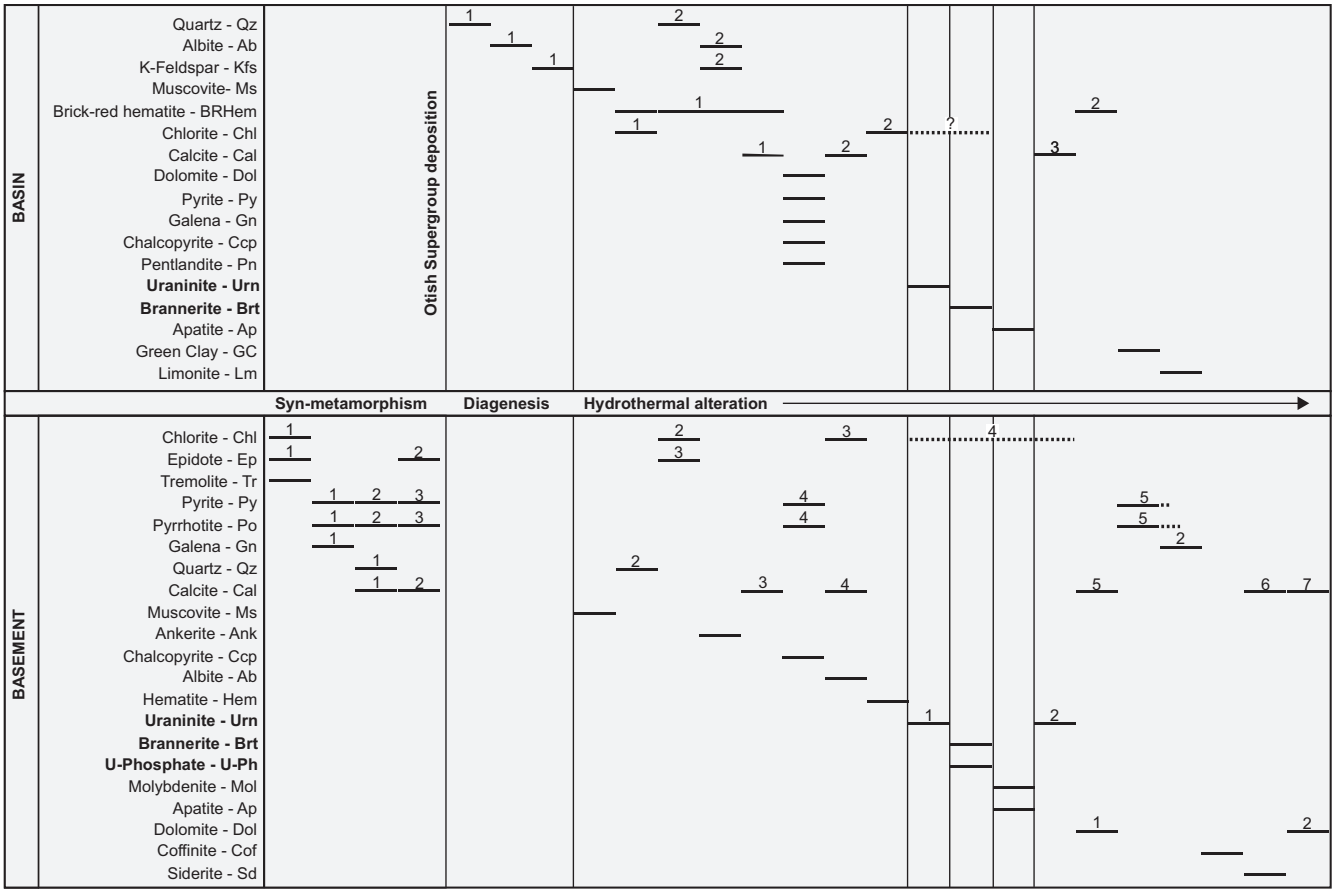

Figure 2. Paragenetic sequence of minerals associated with metamorphism, diagenesis and hydrothermal alteration at the Camie River prospect. Numbers indicate the different generations of a mineral. Vertical lines into basin and basement paragenesis indicate hydrothermal alteration and mineralization events which are recognized to have synchronously affected both sedimentary and basement rocks (Lesbros-Piat-Desvial, 2014).

samples were obtained, are presented in Lesbros-Piat-Desvial (2014). At the Camie River prospect, basement (Tichegami Group) and basin sedimentary rocks (Otish Supergroup) have been affected by several stages of hydrothermal alteration and are cut by several types of veins (Beyer et al., 2012; Lesbros-Piat-Desvial, 2014; Fig. 2). The basement rocks are moderately to strongly chloritized (*Chl1*) and contain coarse-grained pyrite (*Py1*), pyrrhotite (*Po1*), and minor galena (*Gn1*). The basement rocks are cut by numerous, centimeter-scale, quartz (*Qz1*) and calcite (*Cal1*) veins parallel to foliation, which contain disseminated pyrite (*Py2*) and pyrrhotite (*Po2*). The *Qz1* quartz and *Cal1* calcite veins are cut by later calcite (*Cal2*) and/or epidote (*Ep2*) veins that contain minor disseminated pyrite (*Py3*) and pyrrhotite (*Po3*).

After basement erosion and deposition of Otish Supergroup, pervasive coarse- to fine-grained muscovite alteration affected the top of the Tichegami Group down to several meters where the altered basement rocks appear bleached. The muscovite-altered basement rocks are cut by quartz veins (*Qz2*), followed by chlorite and epidote veins (*Chl2 and Ep3*, respectively). *Chl2* chlorite and *Ep3* epidote veins are cut by rare ankerite veins, themselves cut by later calcite veins (*Cal3*). Pyrite (*Py4*), pyrrhotite (*Po4*) and minor chalcopyrite fill fractures in previous *Cal3* calcite and *Ep3* epidote veins.

In basement rocks, uranium mineralization comprises a first generation of disseminated Pb-rich uraninite (*Urn1*) that is replaced by brannerite low in Ce and Fe, but rich in U, Pb, Si and Nb. Brannerite contains abundant inclusions of *Urn1* uraninite and few inclusions of galena (*Gn1*). *Urn1* uraninite is also replaced by an unidentified uraniferous phosphate that contains rare *Gn1* galena inclusions. The uraniferous phosphate is replaced by rare apatite. Disseminated and euhedral *Urn1* uraninite (< 3 μm) is intergrown with molybdenite, forming irregular aggregates and veins. Fine-grained (< 10 μm), euhedral molybdenite crystals are commonly cemented by galena (*Gn2*). Molybdenite is moulded by a second generation of Pb-rich uraninite (*Urn2*).

The uranium mineralization is cut by carbonate veins (*Dol1* and *Cal5*; < 10 cm), which are only found in rocks containing uranium minerals. *Gn2* galena cements fractures in disseminated pyrite (*Py5*) and pyrrhotite (*Po5*) inside *Dol1* dolomite and *Cal5* calcite veins. In *Dol1* dolomite veins, late and minor coffinite replaces and fills fractures in *Po5* pyrrhotite and *Gn2* galena. Uranium minerals and molybdenite are also cut by small *Py5* pyrite and siderite veins. The latest mineral phases observed in basement rocks

are carbonate veins: calcite (*Cal6*) and siderite, and finally calcite (*Cal7*) and dolomite (*Dol2*).

Mineral paragenesis of the basin sedimentary rocks at the Camie River prospect

In the Otish Basin sedimentary rocks, early diagenetic quartz (*Qz1*) is rare and forms overgrowths on detrital quartz grains. It is almost completely replaced by orange/pink-coloured feldspathic cement composed of two feldspars: (1) early albite (*Ab1*) progressively replaced by (2) later potassic feldspar (*Kf1*). The early diagenetic quartz (*Qz1*) cement and the feldspathic (*Ab1* and *Kf1*) cement are replaced by the same coarse- to fine-grained green muscovite observed in the basement rocks. In basin sedimentary rocks, intergrown muscovite and illite form pore-filling aggregates of irregular, platy crystals or minute flakes. The feldspathic and muscovite alteration types appear to be the two principal types of pervasive hydrothermal modification of the sedimentary rocks, forming three zones of hydrothermal alteration from the bottom to the top of the stratigraphic sequence (lower, interdigitation and upper zones; Fig. 3). The muscovite alteration is cut by narrow (< 5 mm) chlorite veins (*Chl1*) associated with moderate brick-red hematite alteration (*BRHem1*), more commonly located near fracture zones. Rare quartz veins (*Qz2*; <10 cm) are associated with *BRHem1* brick-red hematite alteration, as well as paragenetically later albite (*Ab2*), K-feldspar (*Kfs2*) and calcite (*Cal1*) veins. However, the *BRHem1* brick-red hematite alteration often occurs isolated from other minor alteration and veins.

In the basin sedimentary rocks, uranium mineralization and fractured zones commonly contain narrow dolomite veins with disseminated, euhedral, pyrite, and with fractures cemented by galena with minor chalcopyrite and pentlandite. Dolomite in veins is partly replaced by calcite (*Cal2*). Fractured zones also contain a spatially associated chlorite alteration (*Chl2*). In uranium-mineralized basin sedimentary rocks, disseminated, Pb-rich uraninite (*Urn1)*, similar to that found in the basement rocks, is progressively replaced by Nb-rich brannerite that is itself replaced by rare apatite.

The uranium mineralization is cut by small calcite veins (*Cal3*), which are themselves cut by brick-red hematite veins (*BRHem2*). The brick-red hematite veins (*BRHem2*) are cut by later green clay veins. In the basin sedimentary rocks, the paragenetic sequence ends with limonite in veins and limonite alteration. Limonite weathers the Otish Supergroup rocks over several meters below the current erosion surface, and infiltrates deeper in fractured zones.

Lithogeochemistry of the Camie River prospect

Forty-one non-mineralized (15 feldspathic and 26 muscovite-altered) sandstone and conglomeratic sandstone samples from fourteen diamond drill-holes at the Camie River prospect, in addition to nine (5 muscovite and 4 "least-altered") sandstone and conglomeratic sandstone samples from a diamond drill-hole (OTS-01) ~18 km NW of the Camie River prospect, were analyzed for major and trace elements.

The least-altered sandstones from OTS-01 and feldspathic sandstones from Camie River have relatively low Al_2O_3 and K_2O, but higher SiO_2 contents, compared to the muscovite-altered sandstones. The feldspathic sandstones at the Camie River prospect are characterized by the lowest LOI values (≤0.5 wt. %) and highest Na_2O concentrations. Notably, Na_2O concentrations in the feldspathic sandstones increase from 1.0 wt. %, 125 m above the unconformity, to 3.4 wt. % at the unconformity and near the uranium mineralization (Fig. 4). In contrast, the least-altered and muscovite-altered sandstones have relatively high LOI values (≥ 1 wt. %) and uniformly low Na_2O contents (<0.5 wt. %).

In order to characterize feldspathic and muscovite alteration at the Camie River prospect, the Grant (1986) isocon method was applied using the average of three lithochemically similar "least-altered" sandstones from the diamond drill hole OTS-01. Relative to the "least-altered" sandstones,

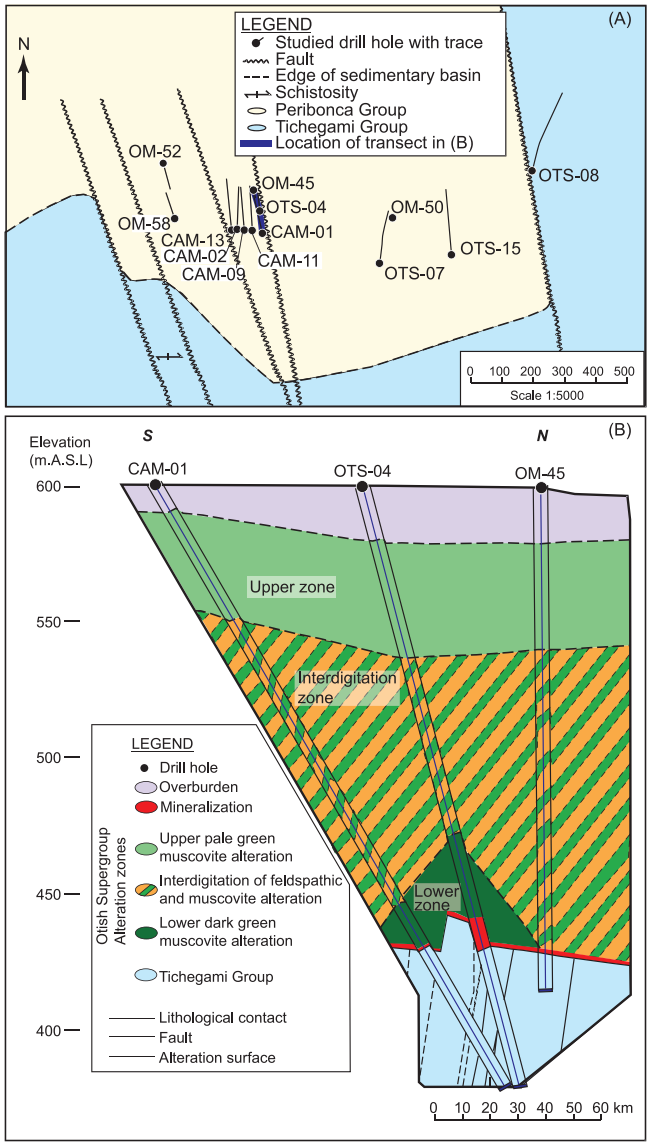

Figure 3. (A) Map of the Camie River prospect, showing the locations of 14 out of 15 drill-holes, sampled as part of this study (modified from Aubin, 2011). **(B)** Schematic cross-section, showing the distribution of the principal types of alteration (feldspathic and muscovite) in the sedimentary rocks of the Camie River prospect, from Lesbros-Piat-Desvial (2014).

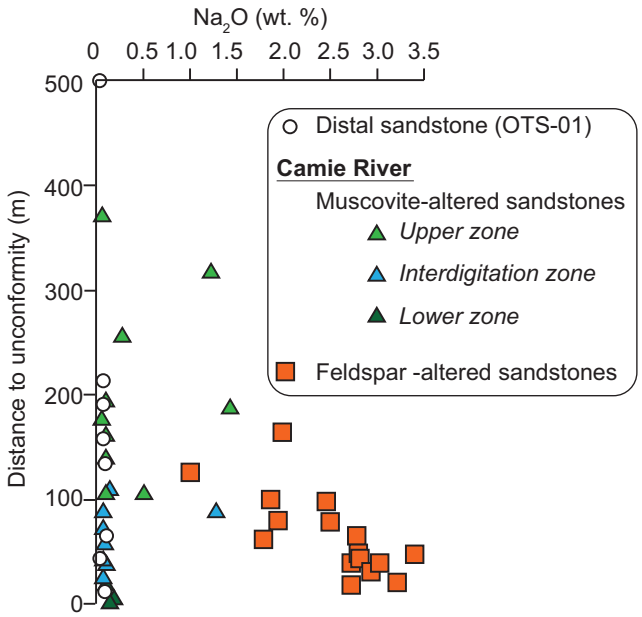

Figure 4. Na_2O concentrations (wt. %) in the sandstones from Camie River and OTS-01 versus distance to the unconformity (modified from Lesbros-Piat-Desvial, 2014).

the non-mineralized, altered sandstones from Camie River and OTS-01 are enriched in the heavy rare earth elements (HREE) and yttrium. The well-defined linear array of HREE (+Y) in the isocon plots, suggests the immobility of these elements during alteration and diagenesis. Applying the isocon method suggests that the altered sandstones experienced mass losses of at least 30% (Grant, 1986). This mass loss was likely accomplished through a combined increase in porosity and decrease in rock density. The feldspathic sandstones at the Camie River prospect show a mass loss of about 75%, higher than muscovite-altered sandstones from the upper (about 30% mass loss) and interdigitation (about 40% mass loss) alteration zones, but close to that from the lower alteration zone (about 80%). The muscovite-altered sandstones from Camie River show an increasing mass loss with depth. In comparison, the muscovite-altered sandstones from OTS-01 show a mass loss of about 50%.

Age of molybdenite mineralization at Camie River prospect

Metal-free crushing followed by conventional magnetic and gravity separation techniques (c.f. Selby et al., 2003) were used to isolate molybdenite from the uraninite-bearing sample 8570 (U ~95,500 ppm, Mo ~13,700 ppm), which was collected from drill-hole CAM-11 (Fig. 3) at a depth of ~197 m. The mineralized sample is hosted within a graphitic metapelite of the Tichegami Group. Molybdenite is disseminated with a typical layered texture, and intergrown with *Urn1* uraninite (Fig. 5). Duplicate analyses of molybdenite at University of Alberta, using the methods described by Selby and Creaser (2004) and Markey et al. (2007), yield a Re-Os model age of 1724 ± 4.9 Ma (Lesbros-Piat-Desvial, 2014). The Re-Os model age is indistinguishable from the U-Pb uraninite (*Urn1*) ages of 1723 ± 16 Ma and 1721 ± 20 Ma

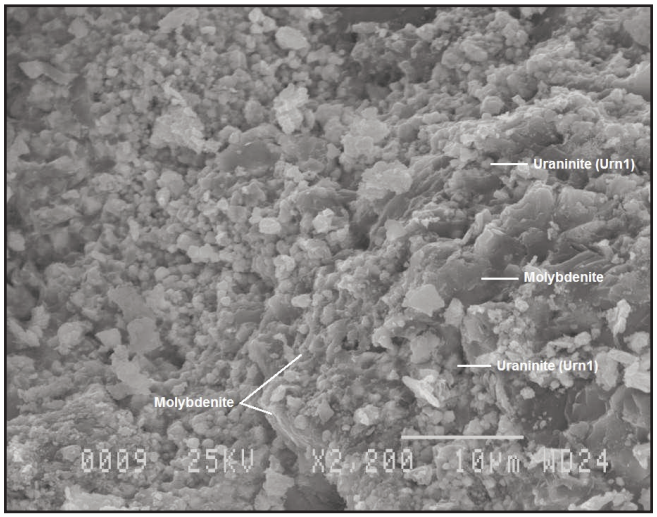

Figure 5. Secondary electron (SE) image of sample 85780, which contains 1724 ± 4.9 Ma molybdenite intergrown with uraninite.

reported by Höhndorf et al. (1987) and Beyer et al. (2012), respectively.

Age and evolution of the Otish Basin

Petrology and age of the Otish Gabbros

The Otish Gabbro dykes and sills, which intrude the Otish Basin, provide an important constraint on the age of the basin. Previous age determinations (Gatzweiler, 1987; Höhndorf et al., 1987; Hamilton and Buchan, 2007) suggest: 1) one or more episodes of gabbro emplacement with the ca. 1.73 Ga episode broadly coinciding with uranium mineralization in the western Otish Basin (Beyer et al., 2012), or 2) basin-wide thermal disturbance and resetting of the Sm-Nd isotopic system that accompanied hydrothermal activity and uranium mineralization.

The bulk of the exposed Otish Gabbro outcrops consist of three sills that dip shallowly (≤15°) to the south (Fig. 1). The sills, Novet (basal), Margat (middle), and Conflans (uppermost), terminate along northeast-trending dykes and are discontinuous throughout the Otish Basin (Fahrig and Chown, 1973; Chown and Archambault, 1987). The sills display rhythmic layering and cumulate textures, and range in thickness from <300 m to >500 m. The dykes have variable northeast to northwest strikes, and range in width from 30–200 m. Both dykes and sills are plagioclase and clinopyroxene-dominated, display variable grain size and textures, and are weakly to strongly altered. Ubiquitous saussuritized plagioclase and abundance of chlorite, epidote, actinolite, and sericite indicate greenschist-facies metamorphic conditions. Olivine was the earliest mineral to crystallize, as indicated by the presence of subhedral to resorbed olivine crystals, partially to fully enclosed by plagioclase and clinopyroxene.

The Otish Gabbros were subdivided into two geochemical groups based on differences in their major and incompatible trace element contents (Fig. 6). Samples belonging to both groups have been collected from the same sill, suggesting that the geochemical variations do not reflect multiple

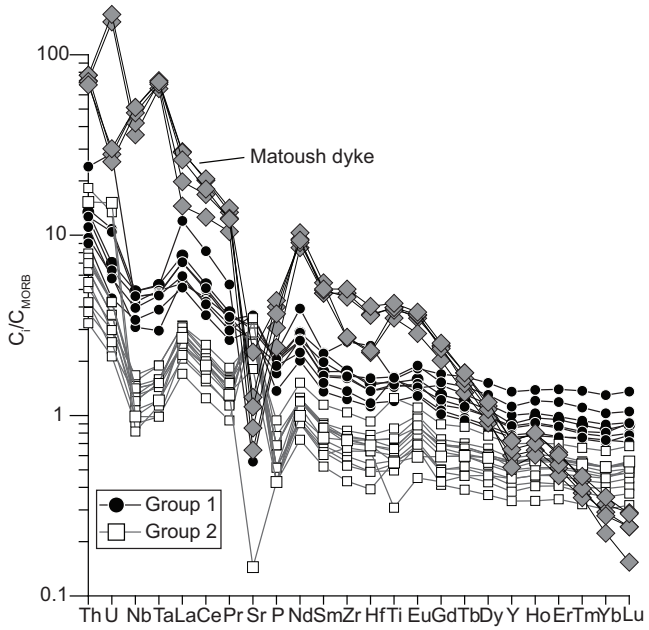

Figure 6. MORB-normalized (Sun and McDonough, 1989) trace element abundances of Otish Gabbro samples examined in this study, plotted by group. Also shown are the compositions of 5 least-altered samples of the subsurface Matoush dyke.

episodes of intrusion. Group 1 Otish Gabbros are characterized by SiO_2 (48–56 wt. %) contents that overlap, but are lower overall than those of the Group 2 gabbros (SiO_2 =50–53 wt. %). In contrast, FeO^{TOT} (11–16 wt. %) and TiO_2 (1.6–2.2 wt. %) have lower overall abundances in the Group 1 gabbros than in the Group 2 gabbros (FeO^{TOT} =8–15 wt. %, TiO_2 =0.4–1.6 wt. %). The most striking difference between the two groups is their trace element profiles. Group 1 gabbro samples are characterized by higher absolute abundances of all incompatible trace elements, except for Sr, than Group 2 samples (Fig. 6). The geochemical differences between the Group 1 and Group 2 Otish gabbros are ascribed to the effects of crystal accumulation (Milidragovic et al., 2014). Mass-balance modelling of trace elements suggests that the Group 2 gabbros are crystal cumulates formed by physical addition of plagioclase and clinopyroxene to Group 1 gabbros, which may approximate liquid compositions.

Samples dated at the University of Toronto as a part of this study include both Group 1 and Group 2 compositions, the locations of which are shown on Figure 1. Baddeleyite crystals from the Novet (Group 1) and Margat (Group 2) sills yield isotope dilution - thermal ionization mass spectrometry (ID-TIMS) U-Pb crystallization ages of 2172 and 2166 Ma, respectively, consistent with a previous determination on the uppermost (Conflans) sill at 2169.0 ± 1.4 Ma (Hamilton and Buchan, 2007; *submitted*). Another Otish Gabbro sample, representing an irregular satellite dyke in the south-central part of the basin has yielded an emplacement age of 2164 Ma, based on U-Pb baddeleyite dating. The geochemical and geochronological constraints from the Otish Gabbro dykes and sills indicate that they were emplaced as a result of a principal magmatic pulse ca. 2165–2170 Ma. Furthermore, these results constrain the age of the Otish Basin deposition to ca. 2515–2165 Ma and suggest that uranium mineralization postdates the basin formation by >450 million years.

The Matoush Dyke

At the Matoush deposit, uranium mineralization is spatially associated with the subsurface Matoush dyke, a 0.5–3.0 m wide intrusion that follows the northeast-striking Matoush Fault, northeast of the Camie River deposit (Fig. 1; Alexandre et al., 2014). The least-altered samples from the Matoush dyke are characterized by a fine-grained, biotite-phyric texture. Rare large (>0.5 mm) polygonal crystals, composed of calcite-dolomite cores and rims of serpentine, have prismatic grain terminations and display "tracks" of fine-grained magnetite, suggesting they may be pseudomorphs after olivine. The groundmass of the least-altered samples of the Matoush dyke is dominated by serpentine and carbonate, with the more altered samples containing increased carbonate contents.

The strongly fractionated trace element profile of the Matoush dyke samples reflects both a strong enrichment in LREE and depletion in HREE relative to MORB (Fig. 6). Furthermore, in contrast to the Otish Gabbros, the Matoush dyke shows an enrichment in HFSE relative to similarly compatible REE. The strongly fractionated REE profiles, the highly enriched LREE, and elevated concentrations of the HFSE suggest an alkaline affinity for the Matoush dyke, and resemble ultramafic lamprophyres and kimberlites (Rock, 1991; Tappe et al., 2004).

Geophysical imaging (J. Lafontaine, pers. comm.) suggests that the Matoush dyke cross-cuts an Otish Gabbro dyke and is therefore likely ≤2170 Ma. Given this relationship, it is possible that intrusion of Matoush-related magmas promoted circulation of uranium-rich brines and precipitation of uranium-minerals, as previously suggested for the Otish Gabbro by Beyer et al. (2012). Efforts to date the crystallization age of the Matoush dyke directly via U-Pb methods are in progress.

Implications for uranium exploration

The temporal relationship between the uranium mineralization in the Otish Basin and the host rocks differs from other major sedimentary basin-hosted Proterozoic uranium districts. The U-Pb and Re-Os ages of uraninite and molybdenite at the Camie River deposit postdate the minimum age of the Otish Basin by ≥450 m.y., significantly exceeding the characteristic time-gap of other major uranium mineralization events in the Proterozoic. For instance, the primary ca. 1590 Ma uranium mineralization in the Athabasca Basin (Alexandre et al., 2009) occurred approximately 150 m.y. after the formation of the basin (ca. 1740 Ma; Orell et al., 1999; Rainbird et al., 2007), and even overlaps deposition of the uppermost units (1541 ± 13 Ma; Creaser and Stasiuk, 2007). Similarly, the ca. 1680 Ma age of mineralization at the Jabiluka uranium deposit was synchronous with diagenesis of the basin-filling Kombolgie Subgroup following basin formation at ca. 1822 Ma (Sweet et al., 1999; Polito et al., 2005; 2011). These observations make the uranium mineralization of the Otish Basin unique and highlight the neces-

sity for better understanding of the basin's post-digenetic tectonothermal history, namely ca. 1.72 Ga. Hydrothermal activity of similar age (ca. 1.7 Ga) has also resulted in the polymetallic vein mineralization (including U) in the ca. 2.45–2.22 Ga Huronian Supergroup in the southern Superior Province (Potter and Taylor, 2010 and references therein). The hydrothermal activity included both regional K- (1728–1688 Ma; Fedo et al., 1997) and Na- (1700 ±2 Ma; Schandl et al., 1994) metasomatism, and the emplacement of the polymetallic calcite-quartz veins (ca. 1675 Ma; Potter & Taylor, 2009). Fedo et al., (1997) and Potter and Taylor (2010) ascribed the ca. 1.7 Ga hydrothermal activity to the waning stages of the Penokean Orogeny. Establishing the age of the Matoush dyke, thus, appears to be critical to understanding the sequence of geological events that led to uranium mineralization in the Otish basin, and to evaluating the regional extent of ca. 1.7 Ga hydrothermal activity along the southern margin of the Superior Province.

Conclusions

1. This report demonstrates that the age of the Otish Basin is older than previously thought. The maximum age of the Otish Basin is defined by the age of the unconformably underlying ca. 2515 Ma Mistassini dyke swarm (Hamilton, 2009). The minimum age of the basin corresponds to the emplacement age of the Otish Gabbro suite (ca. 2170 Ma). The younger (ca. 1730 Ma) Sm-Nd isotopic age of the Otish Gabbro suite is ascribed to later isotopic resetting and LREE remobilization.
2. A younger igneous event, which followed the emplacement of the Otish Gabbros, is inferred based on the mineralogy and geochemistry of the subsurface Matoush dyke. The Matoush dyke has lamprophyric affinity.
3. Re-Os dating of molybdenite intergrown with uraninite (*Urn1*) confirms the previous interpretations of the age of the main uranium mineralization event ca. 1720 Ma, which postdates the formation of the Otish basin by ≥ 450 M.y.
4. Uranium + Mo + Cu + Co + Ni + As + Se + Nb + V + Ag + Au ± Th mineralization at the Camie River prospect postdates the early and peak diagenetic Na- and K- feldspathic and muscovite alteration of the basin sedimentary rocks, and is focussed along the unconformable contact between the Paleoproterozoic Otish Supergroup (Matoush Formation) and the Archean Basement. Sandstones proximal to the unconformable contact and uranium mineralization show elevated Na_2O concentrations (> 1 wt. %)

Acknowledgments

Funding for this research was provided by contributions from Cameco Corporation and a grant to G. Beaudoin through the Targeted Geoscience Initiative 4 (TGI-4) uranium ore systems project of Natural Resources Canada. Constructive peer-reviews by S. Beyer and E.G. Potter improved the quality of the manuscript.

References

Alexandre, P., Kyser, K., Thomas, D., Polito, P., and Marlat, J., 2009. Geochronology of unconformity-related uranium deposits in the Athabasca Basin, Saskatchewan, Canada and their integration in the evolution of the basin; Mineralium Deposita, v. 44, 41–59.

Alexandre, P., Peterson, R.C., Kyser, K., Layton-Matthews, D., and Joy, B., 2014. High-Cr minerals from the Matoush Uranium deposit in the Otish Basin, Quebec, Canada; The Canadian Mineralogist, v. 52, p. 61–75.

Aubin, A., 2011. The Camie-Beaver and Otish South projects and the uranium potential of the Otish sedimentary basin; Symposium Mines Baie-James, May 31, 2011, Abstracts, p.10.

Beyer, S.R., Kyser, K., Hiatt, E.E., Polito, P.A., Alexandre, P., and Hoksbergen, K., 2012. Basin evolution and unconformity-related Uranium mineralization: The Camie River U prospect, Paleoproterozic Otish Basin, Quebec; Economic Geology, v. 107, p. 401–425.

Chown, E.H., 1979. Structure and metamorphism of the Otish Mountain area of the Grenvillian Foreland Zone, Québec: summary; Geological Society of America Bulletin, v. 90, p. 13–15.

Chown, E.H., 1984. Mineralization Controls in the Aphebian formations, Chibougamau; Mistassini and Otish areas; Canadian Institute of Mining and Metallurgy, Special Volume 34, p. 229–243.

Chown, E.H. and Archambault, G., 1987. The transition from dyke to sill in the Otish Mountains, Quebec; relations to host-rock characteristics; Canadian Journal of Earth Sciences, v. 24, p. 110–116.

Chown, E.H. and Caty, J.L., 1973. Stratigraphy, petrography, and paleocurrent analysis of the Aphebian clastic formations of the Mistassini-Otish Basin; Geological Association of Canada, Special Paper 12, p. 49–71.

Creaser, R.A. and Stasiuk, L.D., 2007. Depositional age of the Douglas Formation, northern Saskatchewan, determined by Re-Os geochronology; in EXTECH IV: geology and uranium EXploration TECHnology of the Proterozoic Athabasca Basin, Saskatchewan and Alberta, (ed.) C.W. Jefferson and G. Delaney; Geological Survey of Canada Bulletin, v. 588, p. 341–346.

Fahrig, W.F. and Chown, E.H., 1973. The Paleomagnetism of the Otish gabbro from north of the Grenville Front, Quebec; Canadian Journal of Earth Sciences, v. 10, p. 1556–1564.

Fedo, C.M, Young, G.M, Nesbitt, H.W. and Hanchar, J.M., 1997. Potassic and sodic metasomatism in the Southern Province of the Canadian Shield: evidence from the Paleoproterozoic Serpent Formation, Huronian Supergroup, Canada; Precambrian Research, v. 84, p. 17–36.

Gatzweiler, R., 1987. Uranium mineralization in the Proterozoic Otish Basin, central Quebec, Canada; Berlin-Stuttgart, Gebrüder Borntraeger, Monograph Series on Mineral Deposits 27, p. 27–48.

Genest, S., 1989. Histoire géologique du Bassin d'Otish, Protérozoïque Inférieur (Québec); Ph.D. thesis, Université De Montréal, Montréal, Québec, 329 p.

Grant, J.A., 1986. The isocon diagram - a simple solution to Gresens' equation for metasomatic alteration; Economic Geology, v. 81, p. 1976–1982.

Hamilton, M.A., 2009. Datation isotopique (U-Pb) d'un diabase de l'essaim de dykes Mistassini, Québec - U-Pb isotopic dating of a diabase dyke of the Mistassini swarm, Québec; Ministère des Ressources Naturelles et de la Faune, Québec, GM 65972, 13 p.

Hamilton, M.A. and Buchan, K.L., 2007. U-Pb baddeleyite age for Otish Gabbro: Implications for correlation of Proterozoic sedimentary sequences and magmatic events in the eastern Superior Province; Joint Annual Meeting of the Geological Association of Canada – Mineralogical Association of Canada, Abstracts, v. 32, p. 35.

Hamilton, M.A. and Buchan, K.L., *submitted*. A 2169 Ma U-Pb baddeleyite age for the Otish Gabbro, Quebec: Implications for correlation of Proterozoic magmatic events and sedimentary sequences in the eastern Superior Province; Submitted to Canadian Journal of Earth Sciences, Nov. 2014.

Höhndorf, A., Bianconi, F., and Von Pechmann, E., 1987. Geochronology and metallogeny of vein-type uranium occurrences in the Otish Basin area, Quebec, Canada; in Metallogenesis of Uranium Deposits: Proceedings of a Technical Committee Meeting on Metallogenesis of Uranium Deposits, Vienna, IAEA, p. 233–260.

Hynes, A.J. and Rivers, T., 2010. Protracted continental collision – evidence from the Grenville Orogen; Canadian Journal of Earth Sciences, v. 47, p. 591–620.

Lesbros-Piat-Desvial, M., 2014. Hydrothermal alteration and uranium min-

eralization at the Camie River prospect (Otish Basin, Québec); M.Sc. thesis, Université Laval, Québec City, Québec, 130 p.

Markey, R.J, Stein, H.J, Hannah, J.L., Selby, D. and Creaser, R.A., 2007. Standardizing Re-Os geochronology: a new molybdenite reference material (Henderson, USA) and the stoichiometry of Os salts; Chemical Geology, v. 244, p. 74–87.

Milidragovic, D., King, J.J., Beaudoin, G., and Hamilton, M.A., 2014. Petrology and geochemistry of the Otish Gabbros and comparison to ca. 2.17 Ga mafic dyke swarms of the Superior Province; Joint Annual meeting of the Geological Association of Canada – Mineralogical Association of Canada, Abstracts v.37, p.188-189.

Orrell, S.E., Bickford, M.E. and Lewry, J.F., 1999. Crustal evolution and age of thermotectonic reworking in the western hinterland of Trans-Hudson orogen, northern Saskatchewan; Precambrian Research, v. 95, p. 187–223.

Polito, P.A., Kyser, T.K., Thomas, D., Marlatt, J., and Drever, G., 2005. Re-evaluation of the petrogenesis of the Poterozoic Jabiluka unconformity-related uranium deposit, Northern Territory, Australia; Mineralium Deposita, v. 40, p. 257–288.

Polito, P.A., Kyser, T.K., Alexandre, P., Hiatt, E.E. and Stanley, C.R., 2011. Advances in understanding the Kombolgie Subgroup and unconformity-related uranium deposits in the Alligator Rivers Uranium Field and how to explore for them using lithogeochemical principles; Australian Journal of Earth Sciences, v. 58, p. 453–474.

Potter, E.G. and Taylor, R.P., 2009. The lead isotope composition of ore minerals from precious metal-bearing, polymetallic vein systems in the Cobalt Embayment, Northern Ontario: metallogenic implications; Economic Geology, v. 104, p. 869–879.

Potter, E.G. and Taylor, R.P., 2010. The stable and radiogenic isotopic atributes of precious-metal-bearing polymetallic veins from the Cobalt Embayment, Northern Ontario, Canada: genetic and exploration implications; The Canadian Mineralogist, v. 48, p. 391–414.

Rainbird, R.H., Stern, R.A., Rayner, N., and Jefferson, C.W., 2007. Age, provenance, and regional correlation of the Athabasca Group, Saskatchewan and Alberta, constrained by igneous and detrital zircon geochronology; in EXTECH IV: geology and uranium EXploration TECHnology of the Proterozoic Athabasca Basin, Saskatchewan and Alberta, (ed.) C.W. Jefferson and G. Delaney; Geological Survey of Canada Bulletin, v. 588, p. 193–210.

Rock, N.M.S., 1991. Lamprophyres; Blackie & Son, Glasgow, 285 pp.

Ruhlmann, F., Raynal, M., and Lavoie, S., 1986. Un exemple de métasomatisme alcalin albite-uranium dans le basin des Monts Otish, Québec; Canadian Journal of Earth Sciences, v. 23, p. 1742–1752.

Ruzicka, V. and LeCheminant, G.M., 1984. Uranium deposit research; in: Current Research, Part A, Geological Survey of Canada, Paper 84-1A, p. 39–51.

Schandl, E.S, Gorton, M.P. and Davis, D.W., 1994. Albitization at 1700 ±2 Ma in the Sudbury-Wanapitei Lake area, Ontario: implications for deep-seated alkalin magmatism in the Southern Province; Canadian Journal of Earth Sciences, v. 31, p. 597–607.

Selby, D. and Creaser, R.A., 2004. Macroscale NTIMS and microscale LA-MC-ICP-MS Re-Os isotopic analysis of molybdenite: Testing spatial restrictions for relaible Re-Os age determinations, and implications for the decoupling of Re and Os within Molybdenite; Geochimica et Cosmochimica Acta, v. 68, p. 3897–3908.

Selby, D., Creaser, R.A, Heaman, L.M. and Hart, C.J.R., 2003. Re-Os and U-Pb geochronology of the Clear Creek, Dublin Gulch, and Mactung deposits, Tombstone Gold Belt, Yukon, Canada: absolute timng relationships between plutonism and mineralization; Canadian Journal of Earth Sciences, v. 40, p. 1839–1852.

Sun, S. and McDonough, W.F., 1989. Chemical and isotopic systematics of oceanic basalts: implications for mantle composition and processes; in Magmatism in the ocean basins, (ed.) A.D. Saunders and M. Norry; Geological Society of London Special Publication 42, p. 313–345.

Sweet, I.P., Brakel, A.T. and Carson, L., 1999. The Kombolgie Subgroup - a new look at an old 'formation'; AGSO Research Newsletter, v. 30, p. 26–28

Tappe, S., Jenner, G.A., Foley, S.F., Heaman, L., Besserer, D., Kjarsgaard, B.A., and Ryan, B., 2004. Torngat ultramafic lamprophyres and their relation to the North Atlantic Alkaline Province; Lithos, v. 76, 491–518.

Wanless R K, Stevens, R.D., Lachance, G.R., and Rimsaite, R.Y.H., 1965. Age determinations and geological studies, Part I: Isotope ages; Geological Survey of Canada, Report 5, Paper 64-17, pt. 1, 126 p.